CHAPTER 1

THE FACILITY

Chapter 1 - Valid Pages
Rev. 1 5/1/2012

i	Rev. 0 7/1/2004
ii	Rev. 0 7/1/2004
1	Rev. 0 7/1/2004
2	Rev. 1 5/1/2012
3	Rev. 0 7/1/2004
4	Rev. 0 7/1/2004
5	Rev. 1 5/1/2012

TABLE OF CONTENTS

LIST OF TABLES

THIS PAGE INTENTIONALLY LEFT BLANK

1 THE FACILITY

1.1 Introduction

This safety analysis report supports an application to the U.S. Nuclear Regulatory Commission (NRC) by Oregon State University for the utilization of a TRIGA®-fueled research reactor. The reactor is owned and operated by Oregon State University for the purpose of performing neutron irradiation services for a wide variety of scientific applications. The reactor is known as the Oregon State TRIGA® Reactor (OSTR).

This document addresses only the safety issues associated with the operation of the OSTR. This document reflects experience with the operation and performance of the reactor systems, radiation surveys, and personnel exposure histories related to the operation of the OSTR.

1.2 Summary and Conclusions on Principal Safety Considerations

Analysis of possible accident scenarios is included in Chapter 13. As a TRIGA®-fueled reactor, the primary safety features stem from the use of a fuel with a strong negative temperature confinement which limits the steady-state and peak power achievable, thus preventing fuel damage from credible reactivity accidents. Ejection of the transient rod from the core when the core is operating at the power level scram point will not result in fuel damage. Since experiments are limited to less reactivity worth than the transient rod, experiment failure cannot result in more severe transients. In addition, the licensed operating power level of 1.1 MW results in a decay heat potential in the fuel small enough that loss of reactor water does not result in fuel damage.

For the maximum hypothetical accident where the fuel cladding is removed, the reactor water disappears, and no confinement building exists, the resulting estimated doses to occupational workers and the general public are well within the annual limits given in 10 CFR 20.

1.3 General Description of the Facility

The Oregon State University (OSU) Radiation Center complex is an approximately 47,000-square foot facility located at the northeast corner of 35th Street and Jefferson Way in Corvallis, Oregon. The complex is comprised of three buildings. The TRIGA® reactor is located in a four-story building, which is called the Reactor Building, on the north side of the Radiation Center. The Reactor Building contains primarily the main Reactor Bay, the Reactor Control Room, space for reactor mechanical equipment, two research laboratories, office space for the Reactor Operations Staff, and a small conference room.

The Advanced Thermal Hydraulics Research Laboratory (ATHRL) is a high-bay facility attached to the east side of the Reactor Building; however, there is no access between these two buildings. The ATHRL houses experimental test loops. The Radiation Center Building houses classrooms, offices, a wide variety of radioisotope laboratories, a cobalt-60 irradiation facility, a large inventory of nuclear instrumentation useful for research applications as well as for radiation protection, and a number of supporting facilities. Access to the Reactor Building from the Radiation Center may be made through two secure locations.

The OSTR is a light-water-cooled, graphite-reflected reactor using uranium-zirconium hydride fuel elements. These fuel elements are placed in a circular grid with 16 feet of water over the top of the core. The reactor has an authorized maximum steady-state thermal power of 1.1 MW and may be pulsed to a peak power of over 2,000 MW.

The OSTR is owned and operated by Oregon State University under the NRC License Number R-106 (Docket Number 50- 243). It is used for teaching, research, public service, and radionuclide production. Nuclear Engineering students perform a number of tests and experiments using the reactor in order to reinforce their class work on reactor theory. Researchers use the beamports, the rotating rack, the pneumatic transfer system, the cadmium-lined irradiation tube, the in-core irradiation tube, and the thermal column for experiments involving neutron irradiation. Radionuclides are produced for both research and class applications, particularly classes in nuclear reactor chemistry, radiotracer techniques, and other phases of radiochemistry. Although outside agencies and institutions are regularly accommodated, a significant percentage of the reactor's users come from OSU and other schools within the Oregon University System.

Significant features of the reactor include:

- three standard control rod and drive systems;
- one transient control rod and drive system; and
- numerous irradiation facilities including an In-Core Irradiation Tube, a Cadmium-Lined In-Core Irradiation Tube, a pneumatic transfer system, Sample Holding Dummy Fuel Elements, a Rotating Rack, four Beamports, a Central Thimble, a Thermal Column, and a Thermalizing Column.

1.4 Shared Facilities and Equipment

The OSTR is an integral part the Radiation Center, and thus shares walls, water supplies, sewage, and main electrical supply. The ventilation system, electrical distribution, water distribution, and heating are all separate.

1.5 Comparison with Similar Facilities

The design of the OSTR is similar to those of approximately 50 TRIGA®-type reactors currently operating world-wide. Three facilities that are nearly identical to the OSTR include the U.S. Geological Survey Center - Denver, University of Texas - Austin, and Penn State University. Since most of these reactors have been in operation for more than twenty years, considerable operational information is available and their characteristics are well documented.

1.6 Summary of Operations

The OSTR is a unique and valuable tool for a wide variety of research applications and serves as an excellent source of neutrons and/or gamma rays. The OSTR has a number of irradiation facilities providing a wide range of neutron flux levels and neutron flux qualities, which are sufficient to meet the needs of most researchers. The reactor is normally operated between 4 and 7 hours a day during the 5-day work week, with the most usual power level being 1 MW. The average energy output per year is approximately 45 MWd. As an indication of operating tempo, operational statistics for reporting year 2003 are given in Table 1-1. Based on the analysis presented in this SAR, there are no limitations on the operating schedule.

Table 1-1 Operating Statistics for Reporting Year 2003

Operation Data	Annual Value
MWh	1,025
MWd	42.7
Number of pulses	10
Hours reactor critical	1,100
Hours reactor at full power	1,023
Number of irradiation requests	215
Number of samples irradiated	2,000

1.7 Compliance With the Nuclear Waste Policy Act of 1982

In accordance with U.S. Department of Energy (DOE) contract DE-AC07-76ER01953 the DOE shall retain title to the fuel and the DOE is obligated to take the spent fuel and/or high level waste for storage or reprocessing.

1.8 Major Facility Modifications and History

The initial construction of the OSU Radiation Center was completed in 1964. The second phase of the facility was completed in 1967 with the addition of the OSTR. Since then, additional space for teaching, computing, and offices was added to accommodate the rapidly-expanding Nuclear Engineering program. More recent additions have been the Advance Plant Experiment

(APEX) and the Advanced Thermal Hydraulics Research Laboratory (ATHRL). The current Radiation Center Complex is approximately 47,000 square feet.

A brief chronology of the key dates and events in the history of the OSU Radiation Center and the TRIGA® reactor is given below.

June 1964	Completion of the first phase of the Radiation Center, consisting of 32,397 square feet of office and laboratory space, under the direction of founding Director, C. H. Wang
July 1964	Transfer of the 0.1 W AGN 201 reactor to the Radiation Center. This reactor was initially housed in the Department of Mechanical Engineering and first went critical in January, 1959
September 1965	Initial request for construction permit submitted
August 1966	Issuance of the construction permit (CPRR-93) for the OSTR
October 1966	Completion of the second phase of the Radiation Center, consisting of 9,956 square feet of space for the TRIGA® reactor and associated laboratories and offices.
March 1967	Issuance of the operating license (R-106) for the OSTR
March 1967	Initial criticality of the OSTR. The reactor was licensed to operate at a maximum steady-state power level of 250 kW and was fueled with 20% enriched fuel
October 1967	Formal dedication of the Radiation Center
August 1969	OSTR licensed to operate at a maximum steady-state power of 1 MW, but could do so only for short periods of time due to lack of cooling capacity
June 1971	OSTR cooling capacity upgraded to allow continuous operation at 1 MW
April 1972	OSTR Site Certificate issued by the Oregon Energy Facility Siting Council
December 1974	AGN-201 reactor permanently shut down
March 1976	Completion of 1,600 square feet of additional space to accommodate the rapidly expanding nuclear engineering program

July 1976	OSTR refueled with 70% enriched FLIP fuel
July 1977	Completion of a second 1,600 square feet of space to bring the Radiation Center complex to a total of 45,553 square feet
July 1980	AGN-201 reactor decommissioned and space released for unrestricted use
June 1982	Shipment of the original 20% enriched OSTR fuel to Westinghouse Hanford Company
December 1988	AGN-201 components transferred to Idaho State University for use in their AGN-201 reactor program
December 1989	OSTR licensed power increased to 1.1 MW
June 1990	Installation of a 7000 Ci ^{60}Co Gammacell irradiator
March 1992	25th anniversary of the OSTR initial criticality
August 1994	APEX inauguration ceremony
January 1999	Installation of the Argon Production Facility in the OSTR
April 1999	Completion of ATHRL facility brings the Radiation Center complex to a total of 47,198 square feet
October 2004	Neutron Radiography Facility completed
December 2008	OSTR converted to LEU fuel
February 2009	PGNAA Facility completed
June 2010	ANSEL Facility construction completed

CHAPTER 2

SITE CHARACTERISTICS

Chapter 2 - Valid Pages
Rev. 1 5/1/2012

i	Rev. 0 7/1/2004
ii	Rev. 0 7/1/2004
1	Rev. 0 7/1/2004
2	Rev. 0 7/1/2004
3	Rev. 0 7/1/2004
4	Rev. 0 7/1/2004
5	Rev. 0 7/1/2004
6	Rev. 0 7/1/2004
7	Rev. 0 7/1/2004
8	Rev. 0 7/1/2004
9	Rev. 0 7/1/2004
10	Rev. 0 7/1/2004
11	Rev. 0 7/1/2004
12	Rev. 0 7/1/2004
13	Rev. 0 7/1/2004
14	Rev. 0 7/1/2004
15	Rev. 0 7/1/2004

TABLE OF CONTENTS

2 SITE CHARACTERISTICS

LIST OF FIGURES

LIST OF TABLES

2 SITE CHARACTERISTICS

This chapter describes the site characteristics for the vicinity of the OSTR and Radiation Center on the Oregon State University campus and their relation to the safety and operation of the University's TRIGA® reactor.

The conclusion reached in this chapter and throughout this document is that the selected site is well-suited for the OSTR when considering the relatively benign operating characteristics of the reactor, including the Maximum Hypothetical Accident (MHA).

This is consistent with the conclusions reached for the other 50 TRIGA® reactors operating throughout the world. Many of them are located on university campuses, in hospitals, and other highly populated areas.

2.1 Geography and Demography

2.1.1 Site Location and Description

Oregon State University's TRIGA® reactor (OSTR) is located in Corvallis, Oregon. Corvallis is located approximately 50 miles from the Oregon Coast and 35 miles from Salem, the state capital.

2.1.1.1 Specification and Location

The OSTR is located on the far west end of the Oregon State University campus and west of downtown Corvallis. The latitude and longitude of the OSTR is 44º 33' 54" by 123º 17' 22". Corvallis and Oregon State University lie in Benton County in the Willamette Valley. Corvallis lies 5 miles from Philomath, Oregon; 13 miles from Albany, Oregon; 35 miles from Salem, Oregon; and 45 miles from Eugene, Oregon. The reactor is located approximately 400 yards northeast of Oak Creek and 1.5 miles west of the Willamette River. Good Samaritan Hospital is located approximately 3.5 miles to the northeast.

2.1.1.2 Boundary and Zone Area Maps

Figures 2.1 and 2.2 illustrate the location of the OSTR with respect to the State of Oregon and the OSU campus.

2.1.1.3 Population Distribution

The OSTR is located in Corvallis, Oregon. Metropolitan Corvallis has a population of 49,332 (Ref. 2.1), which has increased by 9% over the ten preceding years. The city of Philomath, located 5 miles from the OSTR has a population of 3,838 (2000 census), which

Figure 2.1 Map of Oregon

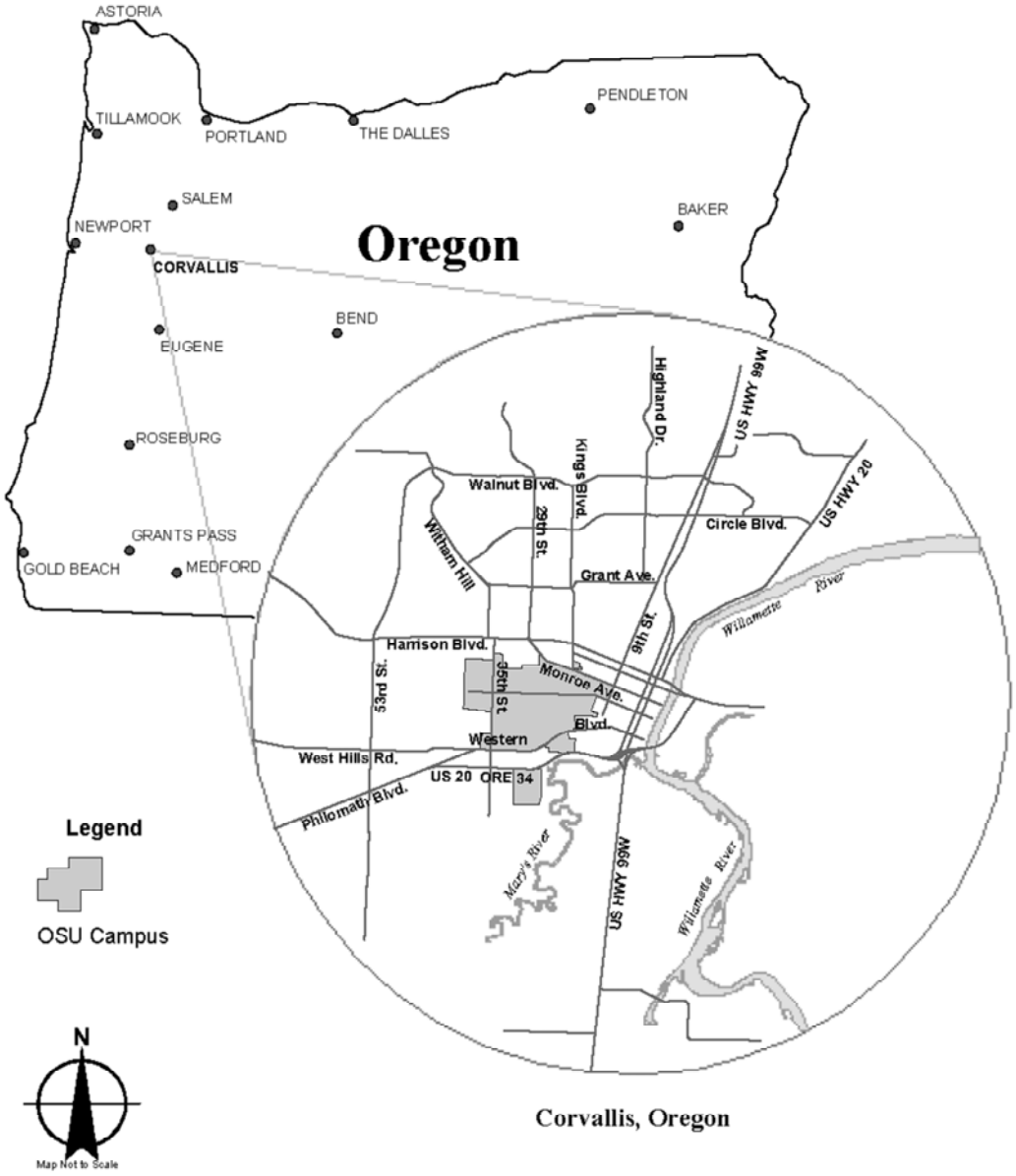

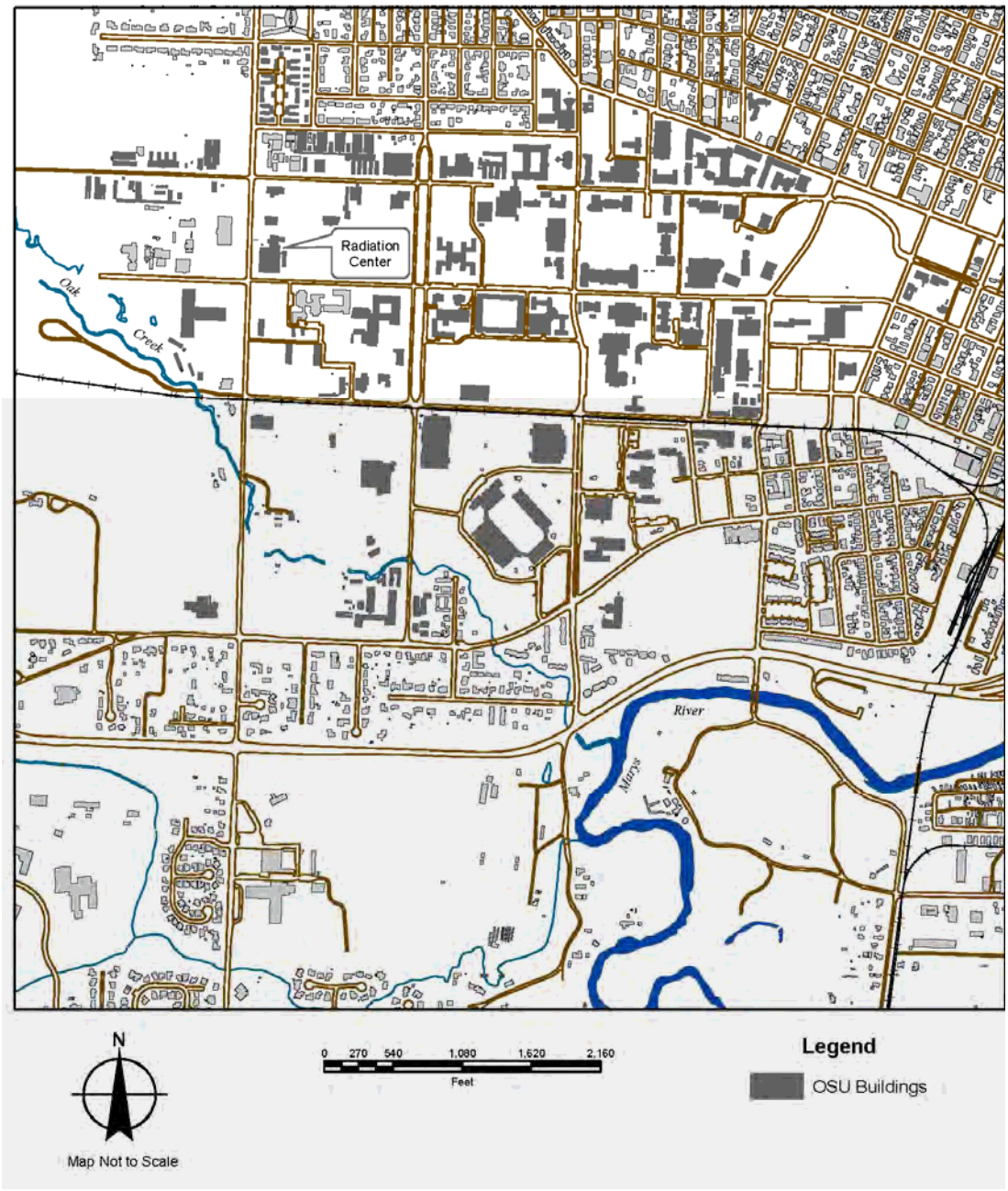

Figure 2.2 Campus Map

has increased 22% over the ten preceding years (Ref. 2.1). The population of Corvallis resides primarily to the north-northeast and south of the OSTR. The total population in all of Benton County is 78,153 (Ref. 2.1). Oregon State University has a population (student and employees) of approximately 23,000 people.

The nearest Oregon State University dormitory, Sackett Hall, is located approximately 1,300 feet to the east of the OSTR. Sackett Hall has 3 floors, and has a capacity of 311 residents including university employees. Reed Hall is directly across from Sackett Hall approximately the same distance from the OSTR. It has a capacity of 54 residents. The typical capacity for all of the residence halls on the Oregon State University campus is 3,500 students (Ref. 2.2*)*. This number of residents only applies during the school year which occurs from late September to early June.

2.2 Nearby Industrial, Transportation, and Military Facilities

2.2.1 Locations and Routes

Figure 2.2 shows the railway near the OSTR. The rail line is located approximately 1200 feet to the south of the Radiation Center. The reactor building is located on the north side of the Radiation Center. Based on the distance and the location of the reactor building on the opposite side of the Radiation Center from the rail line, shipments on the rail line do not likely pose a threat to the reactor facility. With the exception of a single rail car a year, all transport on the rail spur involves lumber.

There are no refineries, chemical plants, mining facilities, manufacturing facilities, water transportation routes, fuel storage facilities, military facilities, or rail yards located near the OSTR.

2.2.2 Air Traffic

Six miles south of the OSTR and approximately 5 miles south of downtown Corvallis lies Corvallis Municipal Airport. This small airport has a main runway in the north/south direction (170-350) which is 5,900 feet by 150 feet and is made of asphalt and has a weight limit for double-tandem wheeled aircraft of 75 tons (150,000 lbs). The secondary east/west general aviation runway (90-270) is 3,545 feet by 75 feet. There is no control tower at the airport, but the airport does offer approach lights and ILS instrument approach to its primary runway. The airport averages 106 aircraft operations per day and has 142 aircraft based on it, 115 of which are single engine aircraft (Ref. 2.3). The major airport in Oregon is Portland International Airport (PDX), located approximately 80 miles to the north of the OSTR. The runways at PDX run east/west. Mahlon Sweet Field Airport is located 7 miles northwest of Eugene and located approximately 35 miles from the OSTR. This airport averages 263 aircraft per day, with a maximum weight of 150 tons (300,000 lbs) for a double-tandem wheeled aircraft (Ref. 2.3). This is a controlled airfield with four runways, the primary runway running north/south. There are 173 aircraft based on Mahlon Sweet Field, 131 of which are single engine aircraft.

2.2.3 Analysis of Potential Accidents at Facilities

Local buildings around the OSTR include Oregon State University's Hazardous Waste Facility, the Environmental Protection Agency's Western Ecology Division, Oregon State's Forestry Building, and the O.H. Hinsdale Wave Laboratory.

2.2.3.1 Hazardous Materials Building

The Oregon State University Hazardous Waste Facility is located 100 feet to the north of the OSTR. The facility processes all hazardous waste that is produced in the Oregon State University campus laboratories, including chemistry products, radioactive waste, medical waste, and paint supplies. In 2001, the facility handled approximately 60,000 pounds of waste, 80% of which was in the form of a liquid solvent. This facility stores and packages these wastes for transportation to either a permanent storage location or a destruction facility. Radioactive wastes that are typically stored in this facility contain radiotracers such as ^{3}H, ^{14}C, and ^{32}P and are usually mCi quantities or less.

An outside contractor provides transportation from the facility on an average of twice per week. Hazardous materials are stored on an 80-day cycle (i.e., wastes are never stored in the facility for more than 80 days) at which point they are transferred to a waste broker. The materials are stored in various containers from 10 to 55 gallons in volume. The maximum inventory of volatile organic fluids with low flash points may reach 150 gallons and they are usually diluted into an aqueous solution. Radioactive materials are usually stored on a 180-day cycle at which point they are transferred to a waste broker.

The facility has 3 bays, which are all classified as separate buildings and are connected by sealing fire doors. Each building has an 8-hour burn-through rate to the connected building. All air vents exiting the buildings are monitored and alarmed. Each building has a floor drain with an overflow trench which empties into a 120-gallon, below-grade tank. The mixing station has a blow-out wall that will release at 110 pounds of force. This blow-out wall faces east, away from the OSTR. All of the buildings are also equipped with interior and exterior fire sprinklers.

This facility does not pose a significant threat of accident to the OSTR because of its distance from the reactor, the small quantity of hazardous materials stored, the design, and the building security.

2.2.3.2 EPA Western Ecology Division

The Environmental Protection Agency's Western Ecology Division is located one block west of the OSTR. Included in this facility are a variety of laboratories, plant and animal research facilities, a library, a computer center, and offices. This facility poses no threat to the OSTR.

2.2.3.3 Oregon State's Forestry Building

The forestry building is located one block southeast of the OSTR. It houses the administration office, the forestry dean, accounting offices, and classrooms. There are also offices for the United States Forestry Service. This building also poses no threat to the OSTR.

2.2.3.4 O.H. Hinsdale Wave Research Lab

The O. H. Hinsdale Wave Research Lab is located one block southwest of the OSTR. The building features 3 different wave basins and a control room. This facility poses no threat to the OSTR.

2.3 Meteorology

2.3.1 General and Local Climate

The Willamette Valley is located between the Cascade Mountains and the Coastal Mountain Range. The climate is considered very mild, characterized by cool, wet winters and warm, dry summers. A rain shadow is created over the Willamette Valley by the Coastal Range, which reduces the rainfall totals and coastal winds.

2.3.1.1 Humidity

Relative humidity is highest during early morning hours, and is generally 80-100% throughout the year. During the afternoon, humidity is generally lowest, ranging from 70-80% during January to 30-50% during summer (Ref. 2.4).

2.3.1.2 Wind Stability

Wind rose data is readily available for first order stations (operated by the National Weather Service and fully-instrumented), the closest being Eugene, 45 miles south, and Salem, 35 miles northeast. Annual average data from these two stations taken from 1961 to 1990 are shown in Figures 2.3 and 2.4, respectively (Ref. 2.4).

2.3.1.3 Temperatures

Temperature values for the Corvallis area are shown in Table 2-1. Values are taken from 1971 to 2000. Monthly averages and daily extremes are given for each month. The normal minimum daily temperature extreme is 33.6°F in January and the normal maximum daily temperature extreme is 82.4°F in August. Extreme temperatures have ranged from –7°F to 108°F (Ref. 2.4).

Table 2-1 Monthly Temperatures (Ref. 2.4)

	Monthly Normals (°F)			Daily Extremes (°F)	
Month	Maximum	Minimum	Mean	Maximum	Minimum
Jan	47	33.6	40.3	64	9
Feb	51	35.4	43.2	68	7
Mar	56.1	37.6	46.9	76	12
Apr	60.7	39.9	50.3	83	27
May	67.1	44	55.6	96	28
Jun	73.4	48.5	61	102	33
Jul	81.2	51.8	66.5	103	38
Aug	82.4	51.5	67	108	37
Sep	77.1	48.2	62.7	103	27
Oct	65.4	41.8	53.6	92	25
Nov	52.9	38	45.5	72	15
Dec	46.4	33.8	40.1	66	-7
Annual	63.4	42	52.7	108	-7

2.3.1.4 Precipitation

Precipitation values, also taken from 1971 to 2000 are shown in Table 2-2. The normal precipitation for the Corvallis area is 43.6 inches per year, with a maximum of 73.21 inches in 1996 and a minimum of 27.15 inches in 1985. The maximum monthly rainfall was 18.28 inches, which fell in November of 1973. Very little precipitation falls as snow.

Table 2-2 Monthly Rainfall in Inches (Ref. 2.4)

	Jan	Feb	Mar	Apr	May	Jun	Jul	Aug	Sep	Oct	Nov	Dec	Annual
Mean	6.5	5.7	4.6	3	2.3	1.5	0.6	0.7	1.5	3	6.9	7.4	43.6
Max	11.59	13.63	8.87	11.42	5.8	4.34	2.55	2.67	3.58	7.21	18.28	17.11	73.21
Min	0.25	1.65	1.04	1.02	0	0.29	0.01	0	0	0.14	1.03	1.47	27.15
S.D.	3.1	3	1.8	1.5	1.3	0.9	0.6	0.8	1.2	1.7	3.8	3.8	10.1

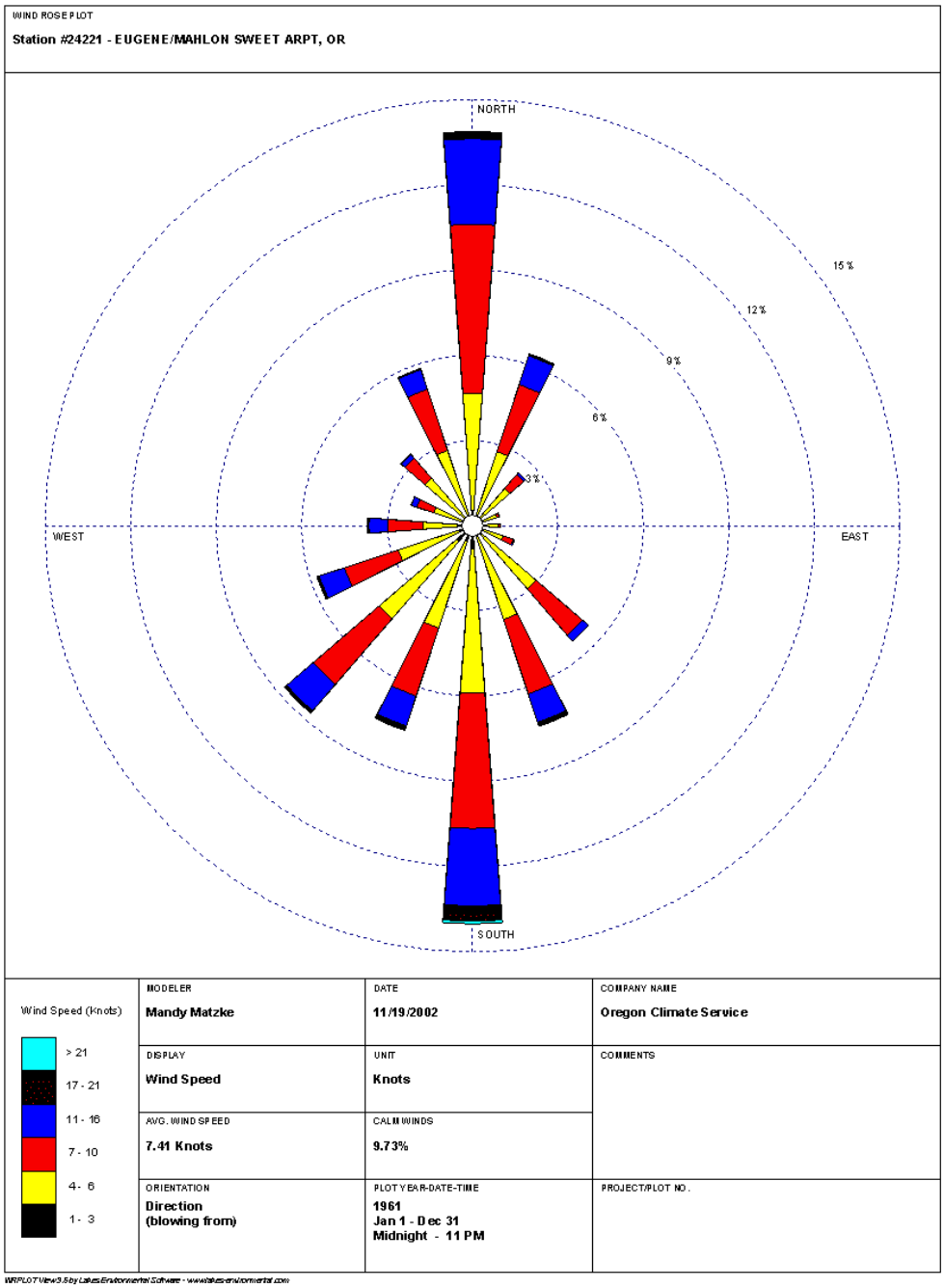

Figure 2.3 Eugene Wind Rose (Annual Average) Ref. 2.4

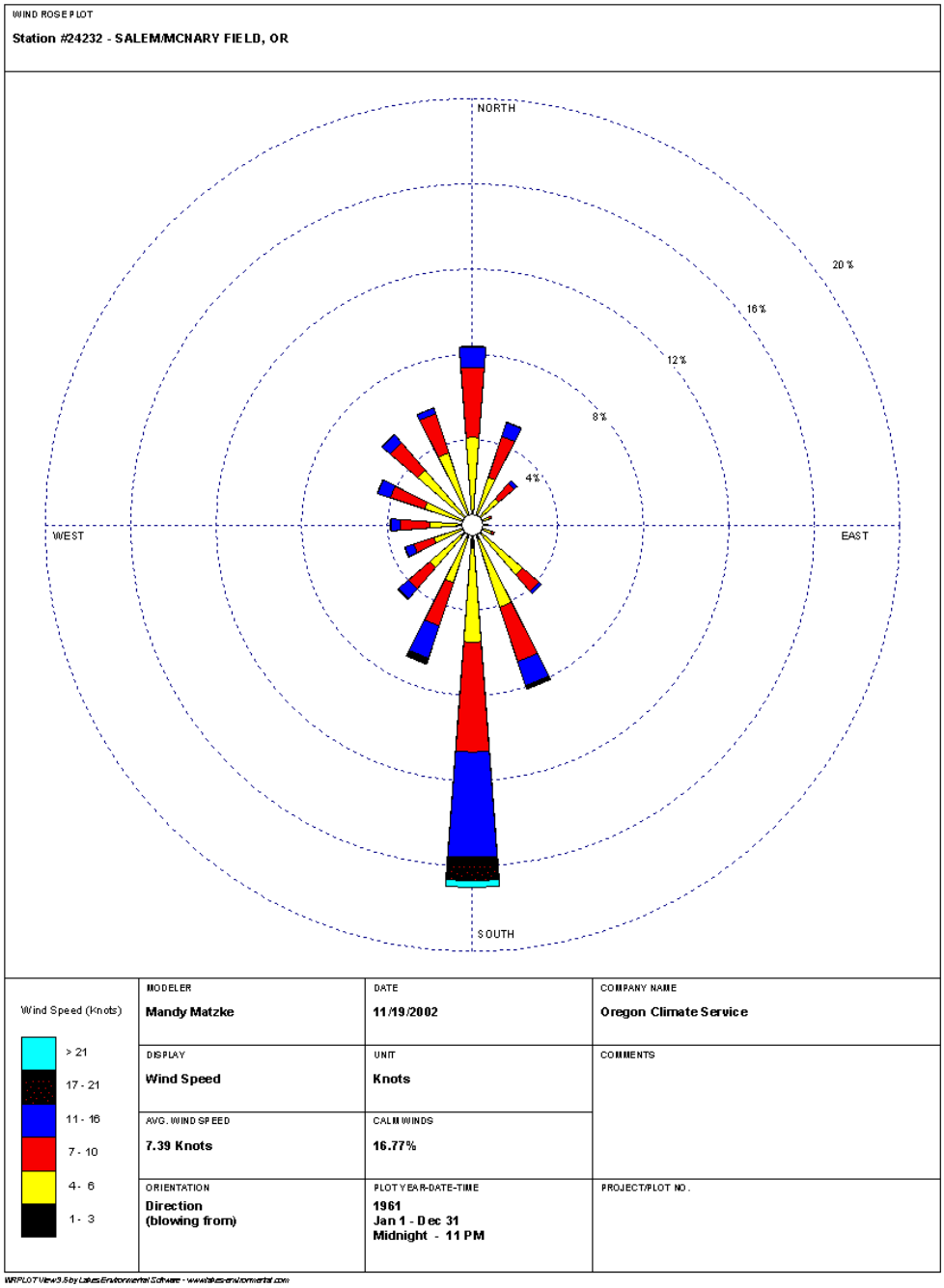

Figure 2.4 Salem Wind Rose (Annual Average) Ref. 2.4

2.3.1.5 Severe Weather Phenomena

Tornadoes in Oregon are quite infrequent due to the mild climate. Between the years 1887 and 1996 there have been only two tornadoes which have measured as an F2 on the Fujita scale. Tornadoes of this magnitude have wind speeds between 113 and 157 mph and have the ability to tear roofs off some buildings, damage trees and mobile homes, and light objects are blown about. These occurred in 1993 at Newberg, OR and in 1968 at an unpopulated forest area in northeast Oregon. In the same 100-year period, only 69 tornadoes were reported in the entire state of Oregon, most of them being of the classification F0, or a gale wind tornado, with wind speeds reaching up to 72 mph.

Only 8 of these 69 tornadoes occurred within a 50-mile radius of the OSTR (Ref. 2.5 & 2.6). Because of the low frequency and severity, tornadoes do not represent a significant hazard to the OSTR.

2.4 Hydrology

2.4.1 River Flooding

The only two waterways near the OSTR are Marys River and Oak Creek. The Marys River is located approximately 5,000 feet from the OSTR. Oak Creek is located approximately 1,200 feet from the OSTR. Oak Creek flows into Marys River which subsequently flows into the Willamette River on the east side of Corvallis. The 100-year flood plain for these two waterways is shown in Figure 2.5. The OSTR is not located in either flood plain.

2.4.2 Seismically-Induced Flooding

There are no lakes or dams near the OSTR and, therefore, seismically-induced flooding due to dam failure or seiches is not a risk to the OSTR. Tsunamis are of little concern as well, as the OSTR is located 50 miles from the coastline.

2.5 Geology, Seismology, and Geotechnical Engineering

2.5.1 Regional Geology

Western Oregon geology consists of two primary tectonic plates: the Juan de Fuca Plate, which is located off the Oregon coast and the North American Plate, which lies under all of Oregon. The Juan de Fuca plate is being subducted beneath the North American Plate and the subduction zone, known as the Cascadia Subduction Zone, runs south from Vancouver Island in British Columbia, to Northern California. No great subduction zone event has occurred in Oregon during the 150 years of recorded earthquakes (Ref. 2.7).

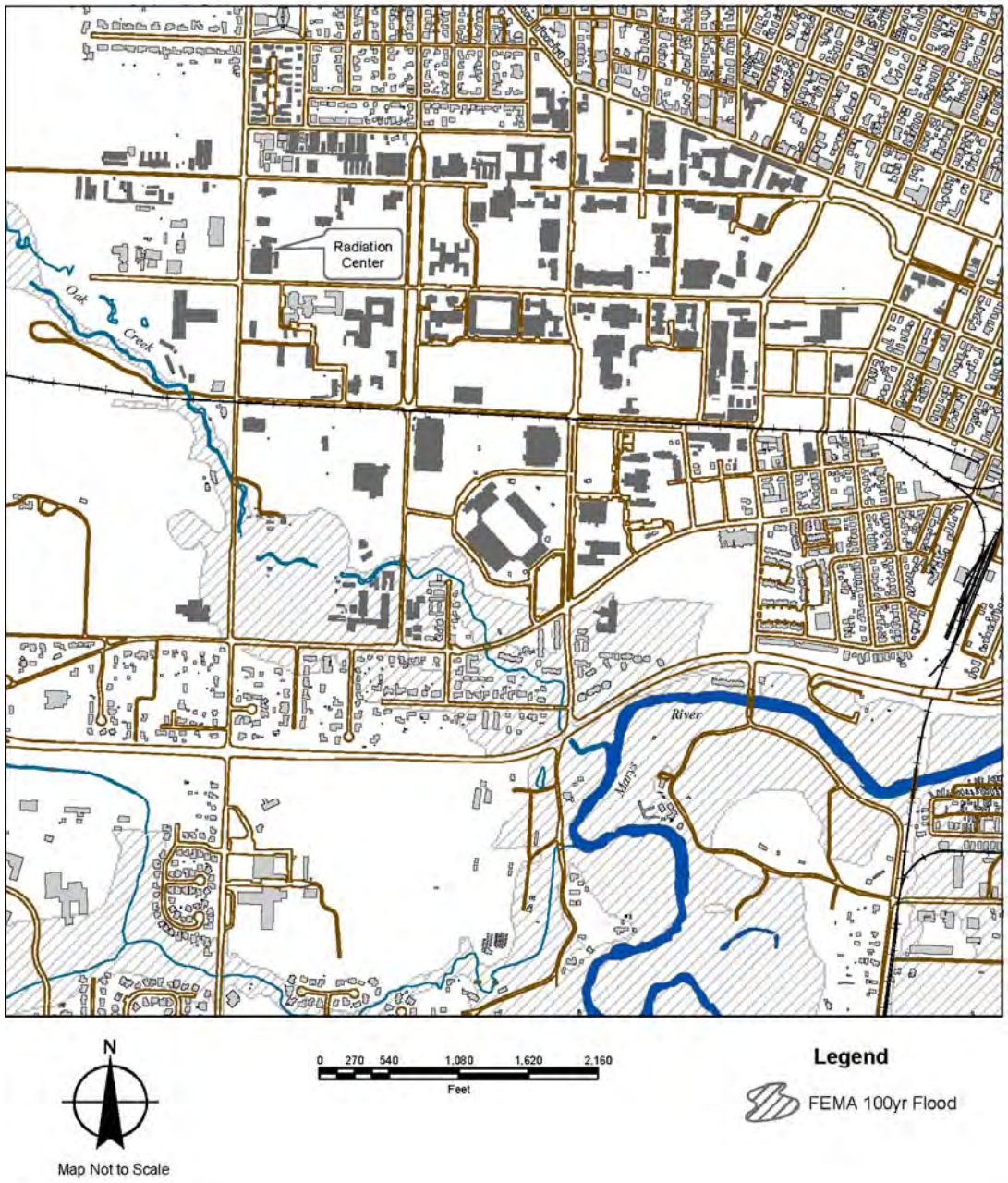

Figure 2.5 OSU Campus 100-year Flood Plain

2.5.2 Site Geology

There are two major fault zones within 5 miles of the OSTR: The Corvallis Fault and the Owl Creek Fault.

2.5.2.1 Corvallis Fault

The Corvallis Fault is located 1.5 miles northwest of the OSTR and is approximately 34 miles long, running northeast. Faulting has been ongoing since the Eocene period with the most recently detectable movement occurring before 28,500 years ago (Ref. 2.8).

2.5.2.2 Owl Creek Fault

The Owl Creek Fault is located 3 miles east of Corvallis and shows Pleistocene period movement, between 10,000 and 30,000 years ago. The fault line is approximately 9 miles long (Ref. 2.8).

2.5.2.3 Faults within 10 miles

There are many other old concealed faults that are located around Corvallis including Bald Hill, Calopooia River, Kings Valley, Lebanon and East Albany faults. None of these show any evidence of movement in the last 1.8 million years (Ref. 2.8).

2.5.3 Seismicity

All recorded earthquakes within 50 miles of the OSTR in the past 150 years have been crustal earthquakes. Only 3 earthquakes of Richter Local Magnitude (M_L) 6 have even been felt in Oregon. Most of the major earthquakes have fallen in the M_L 4 to 5 range. Table 2-3 shows all of the M_L>3.5 earthquakes that have occurred within a 50-mile radius of the OSTR (Refs. 2.9 and 2.10).

Table 2-3 Historic Earthquakes Within 50 miles of Corvallis

Year	Month	Day	Hour	Minute	Latitude	Longitude	Depth (km)	Magnitude
1956	May	18	3	41	45	124	Unknown	3.7
1961	August	19	4	56	44.7	122.5	Unknown	4.5
1962	September	5	5	37	44.5	122.9	Unknown	3.5
1963	March	7	23	53	44.9	123.5	47.0	4.6
1993	March	25	13	34	45.0	122.6	20.6	5.6
1993	June	8	00	01	45.0	122.6	20.2	3.7
1995	Feb	8	9	10	45.1	122.7	31.7	3.6

Distant earthquakes that were felt in the city of Corvallis include the following, with the modified Mercalli intensity of the earthquake at the epicenter in parentheses: the 2001 Nisqually Earthquake (II-III); the 1993 Klamath Falls Earthquake (IV); the 1993 Scotts Mills Earthquake (IV); the 1962 Portland Earthquake (I-IV); and the 1873 Crescent City Earthquake (V) (Refs. 2.11, 2.12, 2.13, 2.14). None of these earthquakes, however, caused any damage in the city of Corvallis.

2.5.4 Maximum Earthquake Potential

The Cascade Range is the primary geological structure in the area of Corvallis, running north-south in central Oregon into northern California and Washington. With the exception of Mt. St. Helens, volcanoes in the Cascade Range are all at normal levels of background seismicity. In Oregon, these include Mount Hood, Mount Jefferson, Three Sisters, Newberry, and Crater Lake. The USGS monitors the major volcanoes in the Cascade Range of northern California, Oregon, and Washington. Mt. Hood, considered the most active of the volcanoes in Oregon, last erupted in the 1790s. As of 1999, the largest of the earthquakes at Mt. Hood was a magnitude 4.0 in 1974 (Ref. 2.13).

2.5.5 Vibratory Ground Motion

Devco Engineering performed a peak bedrock accelerations analysis of the site of the OSTR in April of 2003 based on maps available from the USGS website as well as maps prepared for ODOT by Geomatrix in 1995 (Ref. 2.7 and 2.8). These estimated bedrock accelerations are given for earthquakes with 10%, 5% and 2% probability of being exceeded in 50 years. These probabilities correspond to approximate return periods of 500, 1,000, and 2,500 years and are shown in Table 2-4. These numbers can also be seen in the USGS map of peak acceleration in Figure 2.6. The values of the maximum accelerations are measured in terms of g, or the acceleration due to gravity. Values are given as a percentage of this acceleration. Acceleration due to gravity is 980 cm s^{-2} so a value of .19 g corresponds to .19 x 980 cm s^{-2}, which is a value of 186 cm s^{-2}.

Table 2-4 Maximum Acceleration for the Corvallis Area as Determined by Geomatrix and USGS

Literature Source	500-year return	1,000-year return	2,500-year return
Geomatrix 1995	.19g	.27g	.37g
USGS 2003	.18g	.26g	.38g

The landslide hazard for the OSTR area and the general Corvallis area is classified as low on a scale of low to very high. The topography of the area contains between a 0 and 5% slope.

2.5.6 Surface Faulting

Subsurface soil conditions near the OSTR include 10 feet of medium stiff, low plasticity, clayey silt. Undrained shear strength compression tests show shear strengths ranging from 1,400 to 1,600 psf. Below 10 feet, the soil turns to very stiff, silty clay. Below 20 feet, the soil becomes sand and gravel until it turns to very stiff clay with silt scattered throughout. The potential for ground rupture at the Radiation Center is considered very low due to the lack of known faulting below the site (Ref. 2.7).

2.5.7 Liquefaction Potential

The OSTR site is underlain with between 20 and 24 feet of medium-stiff to stiff, low plasticity, clayey silt to silty clay. The stiff, cohesive soil profile does not lend itself to liquefaction and is, therefore, not a significant concern to the OSTR (Ref. 2.7).

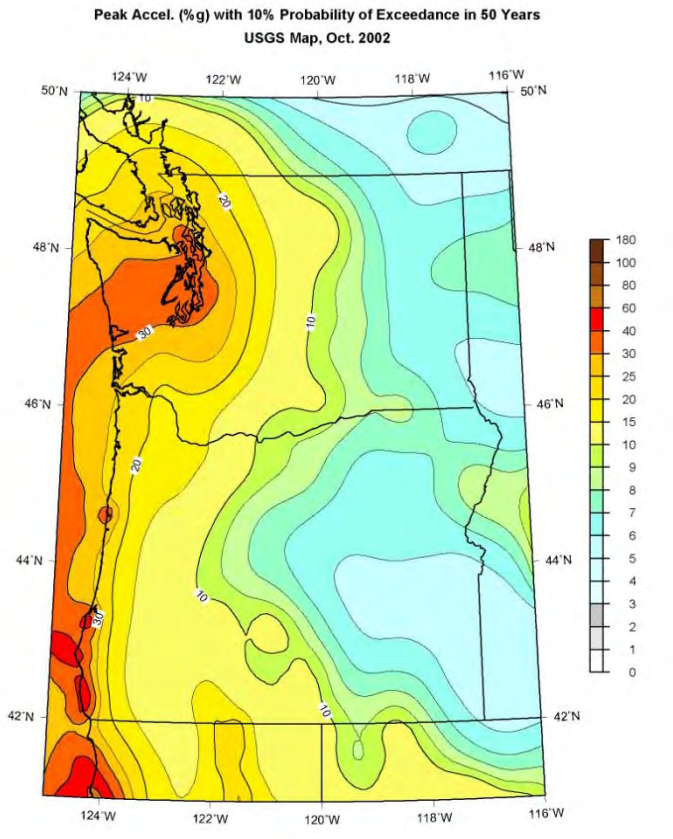

Figure 2.6 Peak Acceleration (%g) with 10% Probability of Exceedance in 50 Years

2.6 References

2.1 U.S. Census Bureau, *United States Census 2000*.

2.2 University Housing and Dining Services, 2001, *Utilization of Housing Capacity*.

2.3 AIRNAV.LLC, *Corvallis Municipal Airport*, Morganville, NJ, 2002.

2.4 Oregon Climate Services, www.ocs.orst.edu, July 2003.

2.5 Taylor, Bohman, Foster, *History of Tornadoes in Oregon*, Oregon State University, August 1996.

2.6 National Oceanic and Atmospheric Administration, www.noaa.gov, July 2003.

2.7 Devco Engineering, *OSU Radiation Center Modifications*, April 11, 2003.

2.8 Geomatrix Consultants, 1995, *Final report: Seismic Design Mapping, State of Oregon*: Prepared for Oregon Department of Transportation, Salem Oregon, Personal Services Contract 11688, January, 1995.

2.9 Johnson, Scofield, Madin, 1994, *Earthquake Database for Oregon, 1833 through 1993: Oregon Department of Geology and Mineral Industries*.

2.10 PNSN, 2002, Pacific Northwest Earthquake Catalog Search, 1970 to Present: www.geophys.washington.edu/SEIS/PNSN/CATDAT/catalog.html, University of Washington, Pacific Northwest Seismograph Network.

2.11 Black, G.L., 1996, *Earthquake Intensity Maps for the March 25, 1993, Scotts Mill, Oregon Earthquake: Oregon Geology*, v. 58, no. 2, p. 35-41.

2.12 Madin, Preist, Mabey, Malone, Yelin, Meier, 1993, *1993 Scotts Mills Earthquake-Western Oregon's Wake Up Call: Oregon Geology*, v. 55, no. 3, p. 51-58.

2.13 USGS, 2001, *US Geological Survey*, www.usgs.gov.

2.14 Wong, Bott, 1995, *A Look Back at Oregon's Earthquake History, 1841-1994:* Oregon Geology, v. 57, no. 6, p. 125-139.

CHAPTER 3

DESIGN OF STRUCTURES, COMPONENTS, EQUIPMENT AND SYSTEMS

Chapter 3 - Valid Pages
Rev. 1 5/1/2012

i	Rev. 0 7/1/2004
ii	Rev. 0 7/1/2004
1	Rev. 0 7/1/2004
2	Rev. 1 5/1/2012
3	Rev. 1 5/1/2012
4	Rev. 0 7/1/2004

TABLE OF CONTENTS

THIS PAGE INTENTIONALLY LEFT BLANK

3 DESIGN OF STRUCTURES, COMPONENTS, EQUIPMENT AND SYSTEMS

3.1 Design Criteria

The OSTR was built in 1966-67. The original reactor installation used fuel and components manufactured by General Atomics (GA), and the specifications to which structures were built were those stated by GA. Specific design criteria were not stated. All building modifications and equipment additions were in conformance with the building codes in existence at the time.

Accident analyses presented in Chapter 13 show that under credible accident conditions, the safety limit on the temperature of the reactor fuel will not be exceeded. Consequently, there would be no fission product release that would exceed 10 CFR 20 allowable radiation levels.

When the OSTR was upgraded to 1 MW in 1976, the principal design criterion was to assure the facility could withstand loss of pool water and any other credible accident with no hazard to the public, without reliance on engineered safety systems. This criterion was met by selecting stainless steel clad TRIGA® fuel with its well-documented characteristics (Ref. 3.1). The design criteria creating this negligible safety risk are the result of the fuel composition and cladding, not of specific features provided in the equipment and building that surrounds the reactor. The accidents described in Chapter 13 conservatively demonstrate that instrumented shutdown actions and building confinement are not necessary to ensure that radiological doses will not exceed allowable limits.

The basic parameter that allows the OSTR to operate safely during either steady-state or transient conditions is the prompt negative temperature coefficient of reactivity ($-\alpha_T$). The fuel-moderator material (U-ZrH) was created such that if all the available excess reactivity were suddenly inserted into the core, the resulting fuel temperature would automatically cause the power excursion to terminate before any core damage resulted (Ref. 3.2). The rise in temperature of the hydride increases the probability that a thermal neutron in the fuel element will gain energy from an excited state of an oscillating hydrogen atom in the lattice. As the neutrons gain energy from the ZrH, their mean-free-path is increased. Since the average chord length in the fuel element is comparable with a mean-free-path, the probability of escape from the fuel element before capture is increased. In the water, where the temperature remains relatively constant, the neutrons are rapidly rethermalized so that the capture and escape probabilities are relatively insensitive to the energy when the neutrons enter the water. The heating of the moderator mixed with the fuel thus causes the spectrum to harden more in the fuel than the water. As a result, there is a temperature-dependent disadvantage factor for the unit cell in the core that decreases the ratio of absorptions in the fuel to total-cell absorptions as the fuel element temperature is increased. This change in disadvantage factor brings about a shift in the core neutron balance, gives a loss of reactivity, and is termed the cell effect (Ref. 3.3).

Routine steady-state power operation is performed with the transient, shim, and regulating rods partially withdrawn. As shown in Chapters 4 and 13, the most rapid possible reactivity insertion rates are adequately compensated for by the negative temperature reactivity coefficient of $-1¢\ °C^{-1}$ (7E-4 $\Delta k/k/°C$).

The transient-rod system is specially designed for rapid reactivity insertion. Accidental actuation of the transient rod system may cause a reactivity accident in the sense that it was not planned. However, rapid reactivity additions constitute the normal pulse mode and the maximum reactivity change and the rate of addition are limited by the design of the system (i.e., upper limit switch and bracket).

Natural convection cooling is adequate to dissipate core heat. Many years of operations with TRIGA® reactors have shown that natural convection will provide adequate flow for the removal of heat after several hours of maximum steady-state operation.

3.2 Meteorological Damage

The OSTR reactor core is protected from damage by high winds or tornadoes by virtue of the thick reinforced concrete structure surrounding the reactor tank. The superstructure of the OSTR has been designed for area wind, rain, snow, and ice loads. The OSTR has endured approximately 40 years of local weather conditions with no meteorological damage. Hurricanes, tsunamis, and seiches do not occur in the Corvallis area.

Only a small number of tornadoes, one every few years, have been reported in Oregon. Based on the small probability of occurrences, postulated low intensity, intermittent reactor operation and low fission-product inventory, no criteria for tornadoes have been established for the OSTR structure.

3.3 Water Damage

As discussed in Chapter 2, flooding is not expected at the OSTR site. The OSTR is located comfortably outside the projected 100-year flood plains for nearby rivers and streams. However, even if flooding occurred, reactor safety would not be an issue since the core is located in a water pool.

3.4 Seismic Damage

The Oregon Structural Specialty Code (OSSC 1998) classifies Corvallis, Oregon as Seismic Zone 3. The OSTR was designed and constructed in accordance with Uniform Building Code (UBC 1964) Zone 3 seismic intensity requirements. Meeting these requirements will ensure that the reactor can be returned to operation without structural repairs following any earthquake likely to occur during the plant lifetime.

Unfortunately, because the accelerations listed in Table 2-4 are peak ground accelerations and accelerations of the 1964 UBC method are building design level accelerations, one cannot do a direct comparison. The 1964 UBC does not have a method to calculate peak ground accelerations to compare to Table 2-4, but the building design level forces can be calculated using 2006 IBC criteria to provide a basis of comparison with the 1964 UBC method (Ref. 3.4).

The criteria calculated using the 1964 UBC results in a building design level acceleration. Design level acceleration is a scaled form of acceleration that includes methods to account for the building response characteristics. This scaling is intended to give forces that are comparable with those observed in actual events and testing. The different Codes have used methods of different sophistication for this scaling. The 1964 method was very rudimentary, while the most recent 2006 IBC methods are more sophisticated and include factors to account for soil response characteristics and the hazard to the public of the building occupancy which were not in the 1964 method.

The 1964 UBC method is a single prescriptive formula that results in an acceleration that is intended for use in building element design. The seismic response characteristics of the structure and empirically observed behavior are built into the formulas. The maps included in the 1964 UBC indicate the area in zone 2 (zones ranged from 0 to 3, with 3 being the zone of highest seismic concern), however zone 3 was conservatively used. The resulting building design level was calculated to be 0.2W. Using the 2006 IBC and corresponding site specific data now available, the design level acceleration was calculated to be 0.14W. Although the 2006 IBC value is lower and also more representative, it is still difficult to directly compare these values.

The likelihood of significant seismic events, discussed in detail in Chapter 2, is low. Furthermore, failure of the reactor tank and loss of the coolant in the event of a very large earthquake have been considered in Chapter 13 and the consequences found acceptable from the standpoint of public safety.

3.5 Systems and Components

3.5.1 Control Rod Drives

The control rod drive assemblies for all control rods are mounted on the reactor bridge structure. The OSTR has three different drive systems.

Two of the shim rods, specifically the shim and safety rods, have electrically-driven rack-and-pinion drives consisting of a two-phase reversible motor, a magnet rod-coupler, a rack-and-pinion gear system, an electromagnet and armature, a dashpot assembly, control rod extension shaft, and a potentiometer used to provide rod position indication. These drives are standard TRIGA® drive mechanisms manufactured by GA. Limit switches are provided to indicate the up and down positions of the magnet and the down position of the rod. The nominal drive speed for these two rods is 18 inches min^{-1}. During a scram, the control rod, rod extension, and magnet armature are detached from the electromagnet and, thus, drop by gravity. The dashpot assembly slows the rate of insertion near the bottom to limit deceleration forces.

The regulating rod is similar to the shim and safety rods except a stepping motor and reduction gear are used in place of the reversible motor. The nominal drive speed for the regulating rod is 24 inches min^{-1}. The stepping motor speed is adjustable with a maximum rod speed of 42 inches min^{-1}. The ability to change the rod drive speed is administratively-controlled and access to the area is limited to authorized personnel only.

The transient rod drive mechanism is a single-acting pneumatic cylinder manufactured by GA. Compressed air drives a piston (attached to the transient rod though a connecting rod assembly) against the top of a cylinder. The cylinder holding the piston can move up and down by virtue of a motor-driven worm gear engaged with a ball nut assembly. A potentiometer attached to the worm drive provides rod position indication. Limit switches provide indication when the cylinder is fully-up or fully-down.

3.5.2 Ventilation System

Although there are no required engineered safety features for this reactor due to its low operating power and good fission product retention in the fuel, a controlled ventilation system acts to reduce the consequences of fission products released from the fuel or other experimental facilities. Automatic shutdown of the ventilation system confines the free air volume of the reactor building during emergency conditions. Remote monitoring of the conditions within the reactor building can be conducted. The ventilation system is specifically described in Chapter 9.

3.5.3 Confinement

Based on radioactivity release calculations given in Chapter 13, the reactor building is not required to provide a containment function. No special seals for doors or lines which penetrate the walls are provided. All doors are normally closed and locked while operating for security and airflow considerations.

3.6 References

3.1 Safety Analysis Report for the Torrey Pines TRIGA® Mark III Reactor, GA-9064, January 5, 1990.

3.2 The U-ZrH_x Alloy: Its Properties and Use in TRIGA® Fuel, GA-E-117-883, 1980.

3.3 Simnad, M.T., Fabian, C.F. and West, G.B., Fuel Elements for Pulsed TRIGA® Research Reactors; Nuclear Technology 28:31-56; 1976.

3.4 DEVCO Engineering, Seismic Acceleration Considerations for Beam Hall at Radiation Center, July 20, 2007.

CHAPTER 4

OREGON STATE TRIGA® REACTOR

Chapter 4 - Valid Pages
Rev. 1 5/1/2012

i	Rev. 1 5/1/2012	27	Rev. 1 5/1/2012	57	Rev. 1 5/1/2012
ii	Rev. 1 5/1/2012	28	Rev. 1 5/1/2012	58	Rev. 1 5/1/2012
iii	Rev. 1 5/1/2012	29	Rev. 1 5/1/2012	59	Rev. 1 5/1/2012
iv	Rev. 1 5/1/2012	30	Rev. 1 5/1/2012	60	Rev. 1 5/1/2012
1	Rev. 1 5/1/2012	31	Rev. 1 5/1/2012	61	Rev. 1 5/1/2012
2	Rev. 1 5/1/2012	32	Rev. 1 5/1/2012	62	Rev. 1 5/1/2012
3	Rev. 1 5/1/2012	33	Rev. 1 5/1/2012	63	Rev. 1 5/1/2012
4	Rev. 1 5/1/2012	34	Rev. 1 5/1/2012	64	Rev. 1 5/1/2012
5	Rev. 1 5/1/2012	35	Rev. 1 5/1/2012	65	Rev. 1 5/1/2012
6	Rev. 1 5/1/2012	36	Rev. 1 5/1/2012	66	Rev. 1 5/1/2012
7	Rev. 1 5/1/2012	37	Rev. 1 5/1/2012	67	Rev. 1 5/1/2012
8	Rev. 1 5/1/2012	38	Rev. 1 5/1/2012	68	Rev. 1 5/1/2012
9	Rev. 1 5/1/2012	39	Rev. 1 5/1/2012	69	Rev. 1 5/1/2012
10	Rev. 1 5/1/2012	40	Rev. 1 5/1/2012	70	Rev. 1 5/1/2012
11	Rev. 1 5/1/2012	41	Rev. 1 5/1/2012	71	Rev. 1 5/1/2012
12	Rev. 1 5/1/2012	42	Rev. 1 5/1/2012	72	Rev. 1 5/1/2012
13	Rev. 1 5/1/2012	43	Rev. 1 5/1/2012	73	Rev. 1 5/1/2012
14	Rev. 1 5/1/2012	44	Rev. 1 5/1/2012	74	Rev. 1 5/1/2012
15	Rev. 1 5/1/2012	45	Rev. 1 5/1/2012	75	Rev. 1 5/1/2012
16	Rev. 1 5/1/2012	46	Rev. 1 5/1/2012	76	Rev. 1 5/1/2012
17	Rev. 1 5/1/2012	47	Rev. 1 5/1/2012	77	Rev. 1 5/1/2012
18	Rev. 1 5/1/2012	48	Rev. 1 5/1/2012	78	Rev. 1 5/1/2012
19	Rev. 1 5/1/2012	49	Rev. 1 5/1/2012	79	Rev. 1 5/1/2012
20	Rev. 1 5/1/2012	50	Rev. 1 5/1/2012	80	Rev. 1 5/1/2012
21	Rev. 1 5/1/2012	51	Rev. 1 5/1/2012	81	Rev. 1 5/1/2012
22	Rev. 1 5/1/2012	52	Rev. 1 5/1/2012	82	Rev. 1 5/1/2012
23	Rev. 1 5/1/2012	53	Rev. 1 5/1/2012	83	Rev. 1 5/1/2012
24	Rev. 1 5/1/2012	54	Rev. 1 5/1/2012	84	Rev. 1 5/1/2012
25	Rev. 1 5/1/2012	55	Rev. 1 5/1/2012	85	Rev. 1 5/1/2012
26	Rev. 1 5/1/2012	56	Rev. 1 5/1/2012	86	Rev. 1 5/1/2012

TABLE OF CONTENTS

4 OREGON STATE TRIGA® REACTOR

LIST OF FIGURES

LIST OF TABLES

THIS PAGE INTENTIONALLY LEFT BLANK

4 OREGON STATE TRIGA® REACTOR

4.1 Summary Description

The OSU reactor is a standard design nominal 1-MW (licensed 1.1-MW), natural-convection-cooled TRIGA® pool reactor with the graphite reflector providing accommodation to four beamports (three radial and one tangential), a thermal column, and a pool irradiation facility. The reactor core is located near the bottom of a water-filled aluminum tank 6½ feet in diameter and about 20½ feet deep. For personnel shielding, the tank is shielded radially by a minimum of 8 feet 2 inches of ordinary concrete with a density of 2.3 g/cm^3, 1½ feet of water, 2 inches of lead, and 10.2 inches of graphite. The approximately 16 feet of water above the core provides adequate shielding at the top of the tank. The control rod drives are mounted at the top of the tank on a bridge structure spanning the diameter of the tank. The reactor can be operated in a steady-state mode by either manual or automatic control. The reactor can also be operated in square-wave and pulse mode.

The OSU reactor was originally taken critical with TRIGA® Standard fuel from 1967 through 1974, then fueled with Fuel Life Improvement Program (FLIP) TRIGA® fuel rods from 1974 through 2008, and now operates with low enriched uranium 30/20 fuel. Detailed data on TRIGA® fuel rods are given in Table 4-1 below.

Table 4-1 Characteristics for LEU 30/20 Fuel

Fuel Type	LEU 30/20
Uranium content [mass %]	30
U-235 enrichment [mass % U]	19.75
Erbium content [mass %]	1.1
Fuel alloy inner diameter [mm]	6.35
Fuel alloy outer diameter [mm]	36.449
Fuel alloy length [mm]	381
Cladding material	Type 304 SS
Cladding thickness [mm]	0.508
Cladding outer diameter [mm]	37.465

TRIGA® fuel is characterized by inherent safety, high fission product retention, and the demonstrated ability to withstand water quenching with no adverse reaction from temperatures to 2,102°F (1150°C). The inherent safety of this TRIGA® reactor has been demonstrated by the extensive experience acquired from similar TRIGA® systems throughout the world. This safety arises from the strongly negative prompt temperature coefficient that is characteristic of uranium-zirconium hydride fuel-moderator elements used in TRIGA® systems. As the fuel temperature increases, this coefficient immediately compensates for reactivity insertions. This results in a mechanism whereby reactor power excursions are terminated quickly and safely. The analyses that follow establish the safety limits for operation of the OSTR.

4.2 Reactor Core

The OSTR utilizes solid fuel elements, developed by General Atomics (GA), in which the zirconium hydride moderator is homogeneously combined with enriched uranium. The unique feature of these fuel-moderator elements is the prompt temperature coefficient of reactivity, which gives the TRIGA® reactor its built-in safety by automatically limiting the reactor power to a safe level in the event of a power excursion. The reactor core consists of a lattice of cylindrical stainless-steel-clad U-$ZrH_{1.6}$ fuel-moderator elements and aluminum-clad graphite dummy elements. The fuel-moderator elements have 3.5-inch-long graphite end sections that form the top and bottom reflector. Water occupies about one-third of the core volume.

Neutron reflection in the radial direction is provided by 10.2 inches of graphite in an aluminum container. The height of the graphite in the reflector is about 22 inches. Also in this container, at the outer perimeter, is 2 inches of lead which acts as a thermal shield to protect the concrete structure from excessive nuclear heating, and also contributes to reducing the dose outside the concrete shield.

The core components are contained between top and bottom aluminum grid plates. The top grid plate has 126 positions for fuel elements and control rods arranged in six concentric rings around a central thimble (used for high flux irradiations).

The power level of the TRIGA® reactor is accurately controlled with four control rods: a regulating rod, a shim rod, a safety rod, and a transient rod.

Four instrumentation channels monitor and indicate the reactor neutron flux and power level on the console. The bulk water temperature and the reactor tank outlet and inlet water temperatures are indicated on the console. The water conductivity, measured at the inlet and outlet of the demineralizer, is displayed on a panel near the console. In addition, primary reactor water is routinely monitored to identify any significant increase in radioactivity.

The reactor core is cooled by natural convection of the demineralized water in the reactor pool. A diffuser nozzle on the reactor tank inlet provides water discharge at a high velocity above the core. This water circulation pattern reduces the dose rate at the pool surface resulting from the ^{16}N formed in the coolant water as it passes through the core.

4.2.1 Reactor Fuel

The active part of each fuel-moderator element, shown in Fig. 4.1, is approximately 1.5 inches in diameter and 15 inches long. TRIGA® fuel is a solid, homogeneous mixture of uranium-zirconium hydride alloy containing from about 8½ wt% to 45 wt% of uranium enriched from 20% to 70% in ^{235}U. The hydrogen-to-zirconium atom ratio is approximately 1.7 to 1.0. To facilitate hydriding, a 0.19-inch diameter hole is drilled through the center of the active fuel section; a zirconium rod is inserted in this hole after hydriding is complete.

Each element is clad in 0.020 inches of stainless steel, and all closures are made by heliarc welding. Two 3.5-inch sections of graphite are inserted in this can, one above and one below the fuel, to serve as top and bottom reflectors for the core. Stainless steel end fixtures are attached to both ends of the can, making the overall length of the fuel-moderator element approximately 28.4 inches.

The lower end fixture supports the fuel-moderator element on the bottom grid plate. The upper end fixture consists of a knob for attachment of the fuel handling tool and a triangular spacer, which permits cooling water to flow through the upper grid plate. The total weight of a fully loaded fuel element is about 7 pounds.

An instrumented fuel-moderator element has three thermocouples embedded in the fuel. The sensing tips of the fuel element thermocouples are located halfway between the outer radius and the vertical centerline at the center of the fuel section and 1 inch above and below the horizontal center. The thermocouple leadout wires pass through a seal contained in a stainless steel tube welded to the upper end fixture. This tube projects about 3 inches above the upper end of the element and is extended by two 10-foot lengths of tubing connected by unions to provide a watertight conduit carrying the leadout wires above the water surface in the reactor pool. In other respects, the instrumented fuel-moderator element is identical to the standard element.

The specific characteristics that make TRIGA®-type fuels uniquely suited for use in extremely safe research-type reactors are covered in detail later in this chapter. A summary of the characteristics is given below [Ref. 4.1 and Ref. 4.2]:

- $ZrH_{1.6}$ is single phase up to 1,200°F (649°C) [delta phase region];
- low hydrogen equilibrium disassociation pressure at normal fuel temperatures;
- high hydrogen retention;
- high heat capacity;
- low thermal expansion coefficient;
- relatively low reactivity in water;
- high fission product retention;
- very large negative prompt temperature coefficient of reactivity;
- high burnup possible by addition of burnable poison; and
- high loading of uranium possible with insignificant change in fuel material properties.

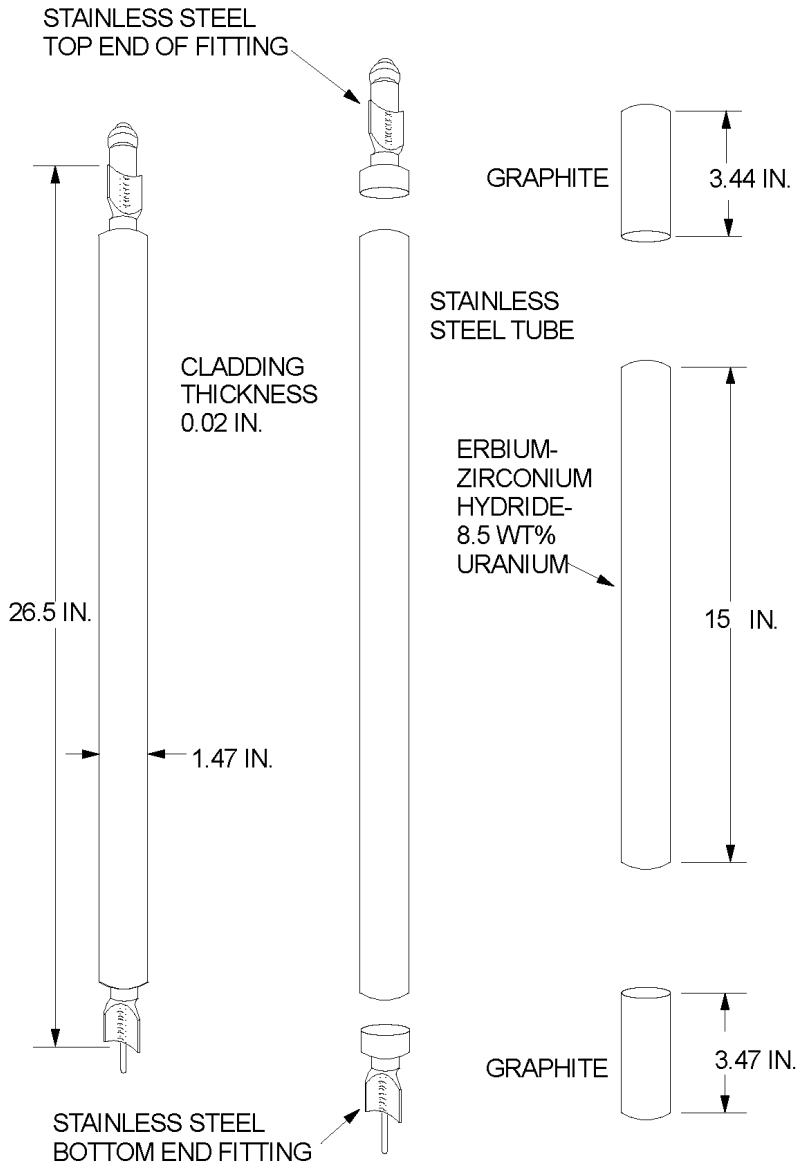

Figure 4.1 Typical TRIGA® Fuel Element Assembly

4.2.1.1 TRIGA® Fuel Development

The development and use of U-ZrH fuels for the TRIGA® reactor began at GA in 1957 and continues today. Over 6,000 fuel elements of 7 distinct types have been fabricated for the 60 TRIGA® research reactors in various countries around the world. The earliest of these has now passed 40 years of operation. U-ZrH fuel has exhibited unique safety features including a large

negative prompt temperature coefficient of reactivity, high fission product retentivity, chemical stability when quenched from high temperatures in water, and dimensional stability over large swings of temperature. The first TRIGA® reactor to be exported was for the U.S. exhibit at the Second Geneva Conference on the Peaceful Uses of Atomic Energy in 1958.

The standard TRIGA® fuel contains 8.5 wt% uranium (20% enriched) as a fine metallic dispersion in a zirconium hydride matrix. The H/Zr ratio is nominally 1.6 (in the face-centered cubic delta phase). The equilibrium hydrogen dissociation pressure is governed by the composition and temperature. For U-$ZrH_{1.6}$, the equilibrium hydrogen pressure is 1 atm at about 1,400°F (760°C). The single-phase, high-hydride composition eliminates the problems of density changes associated with phase changes and with thermal diffusion of the hydrogen.

TRIGA® fuel was developed around the concept of inherent safety. A core composition was sought which had a large negative prompt temperature coefficient of reactivity such that if all the available excess reactivity were suddenly inserted into the core, the resulting fuel temperature increase would automatically cause the power excursion to terminate before any core damage resulted. Experiments performed in the late 1950s demonstrated that zirconium hydride possessed the basic mechanism needed to produce this desired characteristic [Ref. 4.1]. Additional advantages were that ZrH has a good heat capacity, allowing construction of a reactor with a relatively small core size and high flux values due to the high-hydrogen content of the fuel rods, and could be used effectively to fabricate rugged fuel rods.

In early 1976, GA undertook the development of fuels containing up to 45 wt% uranium (3.7 g U/cc) in order to allow the use of low-enriched uranium (LEU) (under 20% enrichment) to replace the highly-enriched fuels while maintaining long core life. The 45 wt% fuel contains a relatively modest ~20 volume percent of uranium. These fuels were fabricated successfully, with the required hydrogen content and erbium loading. The structural features of the hydrated LEU fuel were similar to those of the well-proven 8.5- and 12-wt% fuels, as shown by metallographic, electron microprobe analysis, and x-ray diffraction examination. Detailed evaluations of the new LEU fuel have shown that it performs essentially identically to the older standard TRIGA® fuel [Ref. 4.1].

Nuclear design and analytical studies have shown that the prompt temperature coefficient for the 20-wt% uranium fuel is essentially the same as that for standard fuel over the temperature range of interest [68° to 1,292°F (20° to 700°C)] and greater than that for the FLIP fuel which it replaces. The prompt temperature coefficient for the more highly-loaded LEU fuel shows a small temperature dependence, whereas the coefficient is relatively constant for standard fuel. The value of the prompt temperature coefficient of reactivity is slightly lower for the 30-wt% uranium fuel compared to the highly-enriched fuel it replaces; however, it is still large and significantly higher than the prompt temperature coefficients for any other type of reactor fuel.

Inclusion of erbium burnable poison in the TRIGA® LEU fuel has enabled core lifetimes of up to 3,000 MWd to be predicted for the 30-wt% fuel. It is emphasized that this is the core life from the time of initial refueling to end of useful life.

4.2.1.2 Dissociation Pressures

The hydrogen dissociation pressures of hydrides have been shown to be comparable in the alloys containing up to 75 wt% U [Ref. 4.1]. The concentration of hydrogen is generally reported in terms of either weight percent or atoms of H/cm^3 of fuel (N_H). In the delta phase region, the dissociation pressure equilibria of the zirconium-hydrogen binary mixture may be expressed in terms of composition and temperature by the relation:

$$\log P = K_1 + \frac{\left(K_2 x 10^3\right)}{T}, \qquad (4\text{-}1)$$

where:

$K_1 = -3.8415 + 38.6433\ X - 34.2639\ X^2 + 9.2821\ X^3$,
$K_2 = -31.2982 + 23.5741\ X - 6.0280\ X^2$,
P = pressure, atm,
T = temperature, K, and
X = hydrogen-to-zirconium atom ratio.

The higher-hydride compositions (H/Zr>1.5) are single-phase (delta or epsilon) and are not subject to thermal phase separation on thermal cycling. For $ZrH_{1.6}$, the equilibrium hydrogen dissociation pressure is 1 atm at about 1,400°F (760°C). The absence of a second phase in the higher hydrides eliminates the problem of large volume changes associated with a phase transformation at approximately 1,000°F (540°C) in the lower hydride compositions. Similarly, the absence of significant thermal diffusion of hydrogen in the higher hydrides precludes concomitant volume change and cracking. The clad material of stainless steel or nickel alloys provides a satisfactory diffusion barrier to hydrogen at long-term (several years) sustained cladding temperatures below about 570°F (300°C).

4.2.1.3 Hydrogen Migration

Under nonisothermal conditions, hydrogen migrates to lower-temperature regions from higher-temperature regions. The equilibrium dissociation pressure obtained when the redistribution is complete is lower than the dissociation pressure before redistribution. The dimensional changes of rods resulting from hydrogen migration are of minor importance in the delta and epsilon phases.

4.2.1.4 Hydrogen Retention

The rates of hydrogen loss through 250-μm-thick stainless steel cladding are low at cladding temperatures characteristic of TRIGA® fuel elements. A 1% loss of hydrogen per year occurs at about 930°F (500°C) clad temperature [Ref. 4.1].

4.2.1.5 Density

The density of ZrH decreases with an increase in the hydrogen content. The density change is quite high up to the delta phase (H/Zr = 1.5) and then changes little with further increases in hydrogen. The bulk density of massively-hydrided zirconium is reported to be about 2% lower than the results from x-ray defraction analysis [Ref. 4.1].

For TRIGA® fuel with a hydrogen-to-zirconium atom ratio of 1.6, the following relationships for the uranium density, $\Delta_{U(A)}$, and weight fraction, ^{w}U, in the U-$ZrH_{1.6}$ alloy apply:

$$\rho u_{(A)} = \frac{^{w}U}{0.177 - 0.125\ ^{w}U}, \text{ and} \tag{4-2}$$

$$^{w}U = \frac{0.177\rho_{u(A)}}{1 + 0.125\rho_{u(A)}} \tag{4-3}$$

The relationship between the uranium density and the volume fraction of uranium in the alloy is given by:

$$\rho_{u(A)} = 19.07 V_f^{U(A)} \tag{4-4}$$

where:

$V_f^{U(A)}$ = volume fraction of uranium in the U-$ZrH_{1.6}$ alloy. The calculated density for the LEU 30/20 fuel containing 30 mass % uranium, enriched to 19.75 mass % U-235, and 1.1 mass % natural erbium is 7.18 g/cm^3.

4.2.1.6 Thermal Conductivity

Thermal conductivity measurements have been made over a range of temperatures. A problem in carrying out these measurements by conventional methods is the disturbing effect of hydrogen migration under the thermal gradients imposed on the specimens during the experiments. This has been minimized at GA by using a short-pulse heating technique to determine the thermal diffusivity and hence to permit calculation of the thermal conductivity.

Data from the thermal diffusivity measurements taken by General Atomics along with the best available data for density and specific heat showed that the thermal conductivity is both independent of temperature and uranium content. Thermal conductivity is given below in Equation (5) [Ref. 4.8-4.9].

$$K(T)_{HEU,LEU-FUEL} = 0.18 \pm 0.009 \quad \text{[W/cm-°C]} \tag{4-5}$$

4.2.1.7 Volumetric Specific Heat

TRIGA® FLIP fuel has a defined volumetric heat capacity as shown in Equation (6) [Ref. 4.10].

$$\rho C_P\left(T\right)_{HEU,LEU-FUEL} = 2.04 + 4.17\text{x}10^{-3}\left(T\right) \quad \text{[W-sec/cm}^3\text{-°C]} \tag{4-6}$$

As stated in NUREG-1282, [Ref. 4.11]. "The performance of uranium-zirconium hydride fuel is substantially independent of uranium content up to 45 w% uranium. The behavior of the proposed 20- and 30-w% uranium fuels is indistinguishable from that of the currently approved 8.5-w% uranium fuel." It is thus assumed that volumetric heat capacity of the LEU fuel is similar to that of the HEU fuel.

4.2.1.8 Chemical Reactivity

Zirconium hydride has a relatively low reactivity in water, steam, and air at temperatures up to about 1,112°F (600°C). Zirconium hydride has been heated in air for extended periods of time at temperatures up to 1,112°F (600°C) with negligible loss of hydrogen [Ref. 4.1]. An oxide film forms which inhibits the loss of hydrogen.

The hydride fuel has excellent corrosion resistance in water. Bare fuel specimens have been subjected to a pressurized water environment at 570°F (299°C) and 1,230 psi during a 400-hour period in an autoclave. The average corrosion rate was 350 mg/cm^2-month weight gain, accompanied by a conversion of the surface layer of the hydride to an adherent oxide film. The maximum extent of corrosion penetration after 400 hours was less than 2 mils.

In the early phases of development of the TRIGA® fuel, water-quench tests were carried out from elevated temperatures. Fuel rods (1-inch dia) were heated to 1,470°F (800°C) and end-quenched to test for thermal shock and corrosion resistance. No deleterious effects were observed. Also, a 6-mm diameter fuel rod was heated electrically to about 1,470°F (800°C) and a rapid stream of water was sprayed on it; no significant reaction was observed. Small and large samples were heated to 1,650°F (900°C) and quenched in water; the only effect observed was a slight surface discoloration. Finely-divided U-ZrH powder was heated to 570°F (300°C) and quenched to 175°F (80°C) in water; no reaction was observed. Later, these tests were extended to temperatures as high as 2,200°F (1,200°C), in which tapered fuel rods were dropped into tapered aluminum cans in water. Although the samples cracked and lost hydrogen, no safety problems arose in these tests.

Low-enriched TRIGA® fuels have been subjected to water-quench safety tests at GA. Quench tests were performed on 20%-enriched TRIGA® fuel samples (45 wt% uranium, 53 wt% zirconium, 1 wt% erbium, 1 wt% hydrogen) to simulate cladding rupture and water ingress into the TRIGA® reactor fuel rods during operation.

These results indicate satisfactory behavior of TRIGA® fuel for temperatures to at least 2,200°F (1,200°C). Under conditions where the clad temperature can approach the fuel temperature for several minutes (which may allow formation of eutectics with the clad), the results indicate satisfactory behavior to about 1,925°F (1,050°C). This is still about 125° to 210°F (50° to 100°C) higher than the temperature at which internal hydrogen pressure is expected to rupture the clad, should the clad temperature approach that of the fuel. It should be pointed out that thermocouples have performed well in instrumented TRIGA® fuel elements at temperatures up to 1,200°F (650°C) in long-term steady-state operations, and up to 2,100°F (1,150°C) in very short-time pulse tests.

4.2.1.9 Irradiation Effects

Most of the irradiation experience to date has been with the uranium-zirconium hydride fuels used in the Space Nuclear Auxiliary Power (SNAP) Program (containing about 10 wt% uranium) and TRIGA® reactors. The presence of uranium influences the radiation effects because of the damage resulting from fission recoils and fission gases. Some significant conclusions may be drawn from the results of these experiments [Ref. 4.1]. The uranium is present as a fine dispersal (about 1 μm-dia) in the U-ZrH fuels, and hence the recoil damage is limited to small regions within the short (~10-μm) range of the fission recoils. The U-ZrH fuel exhibits high growth rate during initial operation, the so-called "offset" growth period, which has been ascribed to the vacancy-condensation type of growth phenomenon over the temperature range where voids are stable.

The swelling of the U-ZrH fuels at high burnups is governed by three basic mechanisms:

- the accommodation of solid fission products resulting from fission of ^{235}U. This growth is approximately 3% $\Delta V/V$ per metal atom % burnup. This mechanism is relatively temperature insensitive;

- the agglomeration of fission gases at elevated temperatures [above 1,300°F (750°C)]. This takes place by diffusion of the xenon and krypton to form gas bubbles; and

- a saturable cavity nucleation phenomenon which results from the nucleation and growth of irradiation-formed vacancies into voids over a certain range of temperatures where the voids are stable. The saturation growth by this mechanism was termed offset swelling. This was deduced from the rapid decrease in fuel-to-cladding)T experienced during the early part of the irradiation. The saturation was reached in approximately 1,500 hours.

Burnup tests performed by GA have shown that TRIGA® fuels may successfully be used without significant fuel degradation to burnups in excess of 50% of the contained ^{235}U.

4.2.1.10 Erbium Additions

All available evidence and extensive operating experience indicate that the addition of erbium to the U-ZrH introduces no deleterious effects to the fuel [Ref. 4.1]. Erbium has a high boiling point and a relatively low vapor pressure so that it can be melted into the uranium-zirconium uniformly. The erbium is incorporated into the fuel during the melting process. All the analyses that have been made on the alloy show that the erbium is dispersed uniformly, much as is the uranium. Erbium is a metal and forms a metallic solution with the uranium zirconium; thus there is no reason to believe that there will be any segregation of the erbium. Erbium forms a stable hydride (as stable as zirconium hydride) which also indicates that the erbium will remain uniformly dispersed through the alloy. Also, since neutron capture in erbium is an (n, α) reaction, there are no recoil products.

The LEU 30/20 fuel previously approved for use in TRIGA® reactors by NUREG-1282 contained 0.9 mass percent natural erbium, while the proposed LEU 30/20 fuel for the OSTR contains 1.1 mass percent natural erbium. However, Table 1 of NUREG-1282 bounds the erbium content from 0.0 to 1.8 wt% for nominal 20% enriched fuels under varying wt% uranium contents. The conclusion of NUREG-1282 is that fuel performance is substantially independent of uranium content up to 45 wt%. While the analysis concentrated on uranium loading, erbium loading was also varied. A reasonable conclusion can be drawn that if no performance issues were observed, fuel performance is independent of erbium content in this range as well. Additionally, in the Simnad [Ref. 4.12] paper referenced in NUREG-1282 it was concluded that, "All available evidence indicates that the addition of erbium to the U-ZrH introduces no deleterious effects to the fuel." The only anticipated effect of the increased erbium content is to decrease reactivity, the entire purpose of which is to reduce the power per element in order to increase the number of fuel elements in the core.

4.2.1.11 Prompt Temperature Coefficient of Reactivity

The basic parameter which provides the TRIGA® reactor system with a large safety factor in steady-state operation and under transient conditions is the rather constant prompt temperature coefficient of reactivity (α_T). This temperature coefficient, which is a function of the fuel composition and core geometry, allows great freedom in steady-state operation since the effect of accidental reactivity changes occurring from experimental devices in the core is minimized [Ref. 4.1].

The prompt temperature coefficient of reactivity for TRIGA® fuels is based on the neutron spectrum hardening characteristic that occurs in a zirconium hydride fuel. The spectrum hardening is caused by heating of the fuel-moderator elements. The rise in temperature of the hydride increases the probability that a thermal neutron in the fuel element will gain energy from an excited state of an oscillating hydrogen atom in the lattice. As the neutrons gain energy from the ZrH, the thermal neutron spectrum in the fuel element shifts to a higher average energy (the spectrum is hardened), and the mean free path for neutrons in the element is increased appreciably. For a standard TRIGA® element, the average chord length is comparable to a mean free path, and the probability of escape from the element before being captured is significantly increased as the fuel temperature is raised. In the water, the neutrons are rapidly rethermalized

so that the capture and escape probabilities are relatively insensitive to the energy with which the neutron enters the water. The heating of the moderator mixed with the fuel in a standard TRIGA® element thus causes the spectrum to harden more in the fuel than in the water. As a result, there is a temperature-dependent disadvantage factor for the unit cell in which the ratio of absorptions in the fuel to total cell absorptions decreases as fuel element temperature is increased. This brings about a shift in the core neutron balance, giving a loss of reactivity.

In the TRIGA® LEU fuel, the temperature-hardened spectrum is used to decrease the fuel's reactivity through its interactions with a low-energy resonance material. Thus, erbium, with its double resonance at ~0.5eV, is used in the TRIGA® LEU fuel as both a burnable poison and a material to enhance α_T. The ratio of the absorption probability to the neutron leakage probability is increased for TRIGA® FLIP and LEU fuel relative to the standard TRIGA® fuel because the ^{235}U density in the fuel rod is greater and also because of the use of erbium. When the fuel-moderator material is heated, the neutron spectrum is hardened, and the neutrons have an increasing probability of being captured by the low-energy resonance in erbium. This increased parasitic absorption with temperature causes the fuel's reactivity to decrease as the fuel temperature increases. The neutron spectrum shift pushes more of the thermal neutrons into the ^{167}Er resonance as the fuel temperature increases. As with a standard TRIGA® core, α_T is prompt because the fuel is intimately mixed with a large portion of the moderator; thus, fuel and solid moderator temperatures rise simultaneously, producing the temperature-dependent spectrum shift.

For reasons just discussed, more than 50% of α_T for a standard TRIGA® core comes from the temperature-dependent disadvantage factor, or cell effect, and ~20% each from Doppler broadening of the ^{238}U resonances and temperature-dependent leakage from the core. These effects produce a α_T of ~-1.0E-4)k/k-EC, which is essentially constant with temperature. On the other hand, for a TRIGA® LEU core, the effect of cell structure on α_T is smaller. Over the temperature range 75° to 1,300°F (23° to 700°C), about 70% of the coefficient comes from temperature-dependent changes in the parasitic absorption in the ^{167}Er in the core, and more than half of this effect is independent of the cell structure. Most of the remaining component of α_T is due to Doppler broadening of the ^{238}U resonances. Over the temperature range 75° to 1,300°F (23° to 700°C), α_T for TRIGA® LEU fuel with 20 wt% and 20% enrichment in ^{235}U is about -1.07E-4 Δk/k-°C, thus being somewhat greater than the value for standard TRIGA® fuel. The temperature coefficients of fuels containing ^{167}Er as a burnable poison are somewhat temperature dependent.

4.2.1.12 Fission Product Retention

A number of experiments have been performed to determine the extent to which fission products are retained by U-ZrH (TRIGA®) fuel. Experiments on fuel with a uranium density of 0.5 g/cm^3 (8.5 wt% U) were conducted over a period of 11 years and under a variety of conditions [Ref. 4.3]. Results prove that only a small fraction of the fission products are released, even in completely unclad U-ZrH fuel. The release fraction varies from 1.5E-5 for an irradiation temperature of 660°F (350°C) to ~10^{-2} at 1,475°F (800°C).

The experiments show that there are two mechanisms involved in the release of fission products from U-ZrH fuel, each of which is dominant over a different temperature range. The first mechanism is that of fission fragment recoil into the gap between the fuel and clad. This effect predominates in fuel at temperatures up to ~750°F (400°C); the recoil release rate is dependent on the fuel surface-to-volume ratio but is independent of fuel temperature. Above ~750°F (400°C), the controlling mechanism for fission product release from U-ZrH fuel is a diffusion-like process, and the amount released is dependent on the fuel temperature, the fuel surface-to-volume ratio, the time of irradiation, and the isotope half-life.

The results of the U-ZrH experiments, and measurements by others of fission product release from Space Nuclear Auxiliary Power (SNAP) Program fuel, have been compared and found to be in good agreement.

The fractional release, N, of fission product gases into the gap between fuel and clad from a full-size standard U-ZrH fuel element is given by:

$$\varphi = 1.5\text{E-}5 + 3.6\text{E}3e^{-\frac{1.34x10^4}{(T+273)}} \qquad (4\text{-}7)$$

where:

T = fuel temperature (0 - 1600°C). This relationship has also been found to apply to LEU TRIGA® fuels [Ref. 4.2]. The first term of this function is a constant for low-temperature release; the second term is the high-temperature portion.

The function given above applies to a fuel element which has been irradiated for a time sufficiently long that all fission product activity is at equilibrium. Actual measured values of fractional releases fall well below that calculated by the function given above. Therefore, for safety considerations, this function gives conservative values for the high-temperature release from U-ZrH fuel.

Studies in the TRIGA® reactor at GA on fission product release from fuel elements with high uranium loadings (up to 3.7 g U/cm^3, 45 wt% U) agree well with data from older similar experiments with lower U loadings. As with the lower U loadings, the release was determined to be predominantly recoil-controlled at temperatures #750°F (400°C) and controlled by a migration or diffusion-like process above 750°F (400°C). Low-temperature release appears to be independent of uranium loadings, but the high-temperature release seems to decrease with increasing weight-fractions of uranium. The correlation used to calculate the release of fission products from TRIGA® fuel remains applicable for the high uranium loaded (TRIGA® LEU) fuel as well as the 8.5-wt% U-ZrH fuel for which it was originally derived. This correlation predicts higher fission product releases than measurements would indicate up to 2,010°F (1,100°C). At normal TRIGA® operating temperatures [<1,380°F (750°C)], there is a safety factor of approximately four between predicted and experimentally determined values.

4.2.1.13 Reactor Fuel Temperature

The basic safety limit for the TRIGA® reactor system is the fuel temperature; this applies for both the steady-state and pulsed mode of operation. The TRIGA® fuel which is considered low

hydride, that with a H/Zr ratio of less than 1.5, has a lower temperature limit than fuel with a higher H/Zr ratio. The OSTR utilizes fuel with H/Zr ratios between 1.5 and 1.65 (i.e., greater than 1.5). This allows operation at a higher limit. Fig. 4.2 indicates that the higher hydride compositions are single-phase and are not subject to the large volume changes associated with the phase transformations at approximately 1,000°F (530°C) in the lower hydrides. It has been noted that the higher hydrides lack any significant thermal diffusion of hydrogen (Ref. 4.4). These two facts preclude concomitant volume changes. The important properties of delta phase U-ZrH are given in Table 4-2.

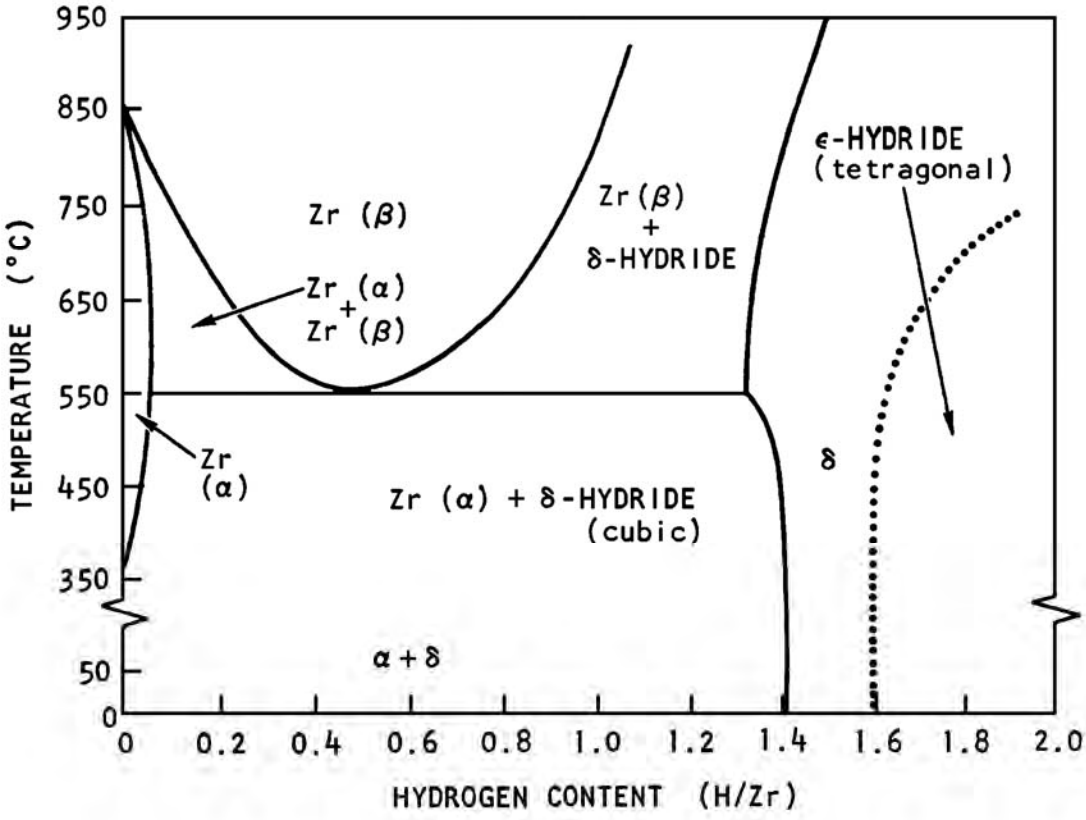

Figure 4.2 Phase Diagram of the Zirconium-Hydrogen System

Table 4-2 Physical Properties of Delta Phase U-ZrH

Thermal conductivity	200°F - 1,200°F (93°C - 650°C)	13 Btu/h - ft^2 - °F
Elastic modulus:	70°F (20°C)	9.1 x 10^6 psi
	1,200°F (650°C)	6.0 x 10^6 psi
Ultimate tensile strength to	1,200°F (to 650°C)	24,000 psi
Compressive strength	70°F (20°C)	60,000 psi
Compressive yield	70°F (20°C)	35,000 psi
Heat of formation [δH_f^0	570°F (298°C)]	37.72 kcal/g-mole

Among the chemical properties of U-ZrH and ZrH, the reaction rate of the hydride with water is of particular interest. Since the hydriding reaction is exothermic, water will react more readily with zirconium than with zirconium hydride systems. Zirconium is frequently used in contact with water in reactors, and the zirconium-water reaction is not a safety hazard. Experiments carried out at GA show that the zirconium hydride systems have a relatively low chemical reactivity with respect to water and air. These tests have involved the quenching with water of both powders and solid specimens of U-ZrH after heating to temperatures as high as 1,560°F (850°C), and of solid U-Zr alloy after heating to temperatures as high as 2,190°F (1,200°C) (Ref. 4.5). Tests have also been made to determine the extent to which fission products are removed from the surfaces of the fuel elements at room temperature. Results prove that, because of the high resistance to leaching, a large fraction of the fission products are retained in even completely unclad U-ZrH fuel.

At room temperature, the hydride is like a ceramic and shows little ductility. However, at the elevated temperatures of interest for pulsing, the material is found to be more ductile. The effect of very large thermal stresses on hydride fuel bodies has been observed in hot cell observations to cause relatively widely spaced cracks which tend to be either radial or normal to the central axis and do not interfere with radial heat flow. Since the segments tend to be orthogonal, their relative positions appear to be quite stable.

The limiting effect of fuel temperature is the hydrogen gas pressure causing cladding stress. Fig. 4.3 relates equilibrium hydrogen pressure in ZrH with varying hydrogen content as a function of temperature for three different H/Zr ratios. The main concern regarding hydrogen pressure is to ensure that the cladding ultimate strength is not exceeded by the stress caused by the pressure. The mechanisms in obtaining temperatures and pressures of concern are different in the pulsing and steady-state mode of operation, and each mechanism will be discussed separately.

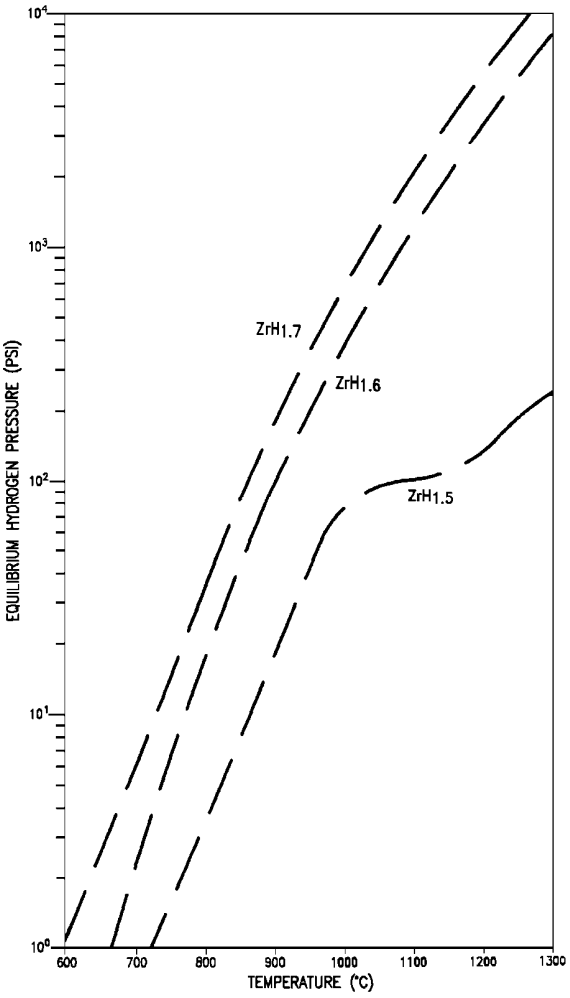

Figure 4.3 Equilibrium Hydrogen Pressure Vs.Temperature from Zirconium-Hydrogen

The OSTR fuel consists of U-ZrH with a H-Zr ratio between 1.5 and 1.65 and with the uranium being 30 wt% enriched in ^{235}U to approximately 20%. The cladding is 0.020- inch thick stainless steel and has an inside diameter of 1.43 inches. The rest of the discussion on fuel temperatures will be concerned with fuel having H/Zr ratios greater than 1.5 [i.e., single-phase and not subject to the large volume changes associated with phase transformation at approximately 985°F (530°C) in the lower hydrides]. Further, it will specifically address fuel with an H/Zr ratio of 1.7 since this is slightly higher ratio fuel than that used in the OSTR and will produce the highest clad pressure and stress for a given temperature. Fig. 4.4 shows the characteristic of 304 stainless steel with regard to yield and ultimate strengths as a function of temperature.

The stress applied to the cladding from the internal hydrogen gas pressure is given by:

$$S = \frac{\mathrm{Pr}}{t}, \tag{4-8}$$

where:

S = stress in psi,
P = internal pressure in psi,
r = radius of the stainless steel cylinder, and
t = wall thickness of the stainless steel clad.

Using the parameters given above:

$$S = \frac{P(1.43in./2)}{0.020in.} = 35.75P \tag{4-9}$$

For safety considerations, it is necessary to relate the strength of the cladding material at its operating temperature to the stress applied to the cladding due to the internal gas pressure associated with the fuel temperature. Figure 4.5 gives the ultimate cladding strength and the stress applied to the cladding as a result of hydrogen dissociation for fuel having H/Zr ratios of 1.65 and 1.7, both as a function of temperature. This curve shows that the cladding will not fail for fuel with $ZrH_{1.7}$ if both the clad and fuel temperatures are equal and below about 1,700°F (930°C). This is conservative since the cladding temperature will be below the fuel temperature. This establishes the safety limit on fuel temperature for steady-state operations. The actual steady-state peak fuel temperature at 1 MW will be below 932°F (500°C). The remainder of this section deals with the safety limit for transient operation.

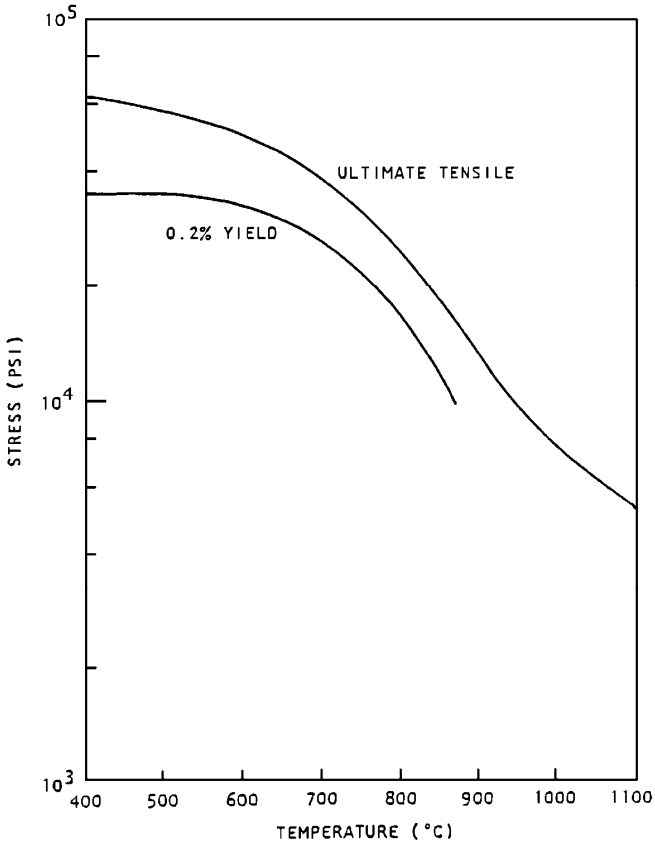

Figure 4.4 Strength of Type 304 Stainless Steel as a Function of Energy for H/2r Ratio or 1.7

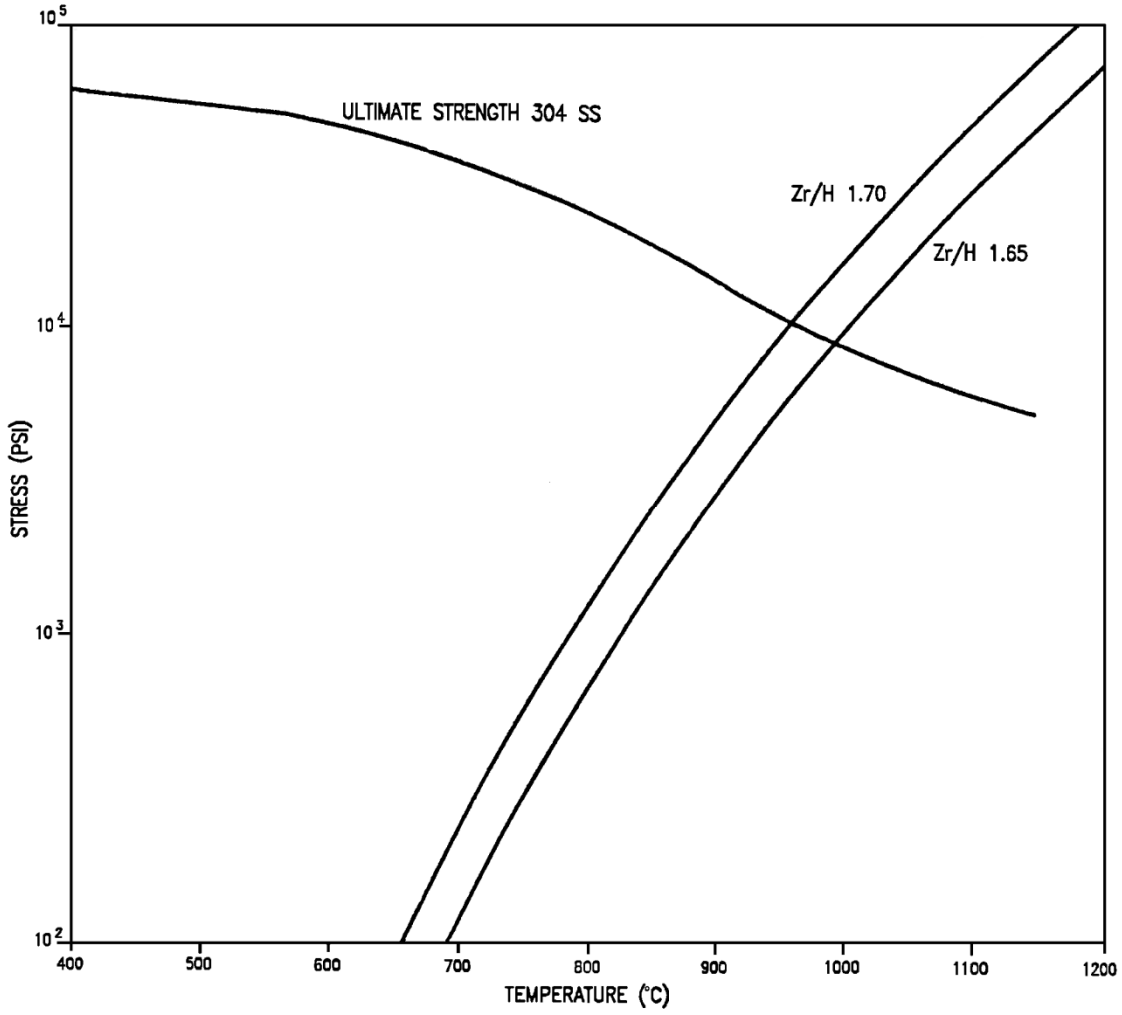

Figure 4.5 Strength and Applied Stress as a Function of Temperature, Equilibrium at Equilibrium Hydrogen Dissociation Pressure

During transient operation, it is necessary to account for the difference in fuel and cladding temperatures to establish a safety limit based on fuel temperature. Additionally, the diffusion of hydrogen reduces peak pressures from those predicted at equilibrium at the peak temperatures. The net result of these two points suggests that a higher safety limit exists for transient operation.

As can be seen from Fig. 4.4, the ultimate strength of the cladding at a temperature of 880°F (470°C) is 59,000 psi. If the stress produced by the hydrogen overpressure on the clad is less than 59,000 psi, the cladding will not be ruptured. Referring to Fig. 4.5, and considering U-$ZrH_{1.7}$ fuel with a peak temperature of 1,830°F (1,000°C), one finds the stress on the clad to be 24,000 psi. Analysis in the next section which considers diffusion will show that the actual hydrogen pressure produced in a pulse is less than the equilibrium pressure for the peak temperature. This allows a safe limit on fuel temperature to be 2,012°F (1,100°C). TRIGA® fuel with a hydrogen to zirconium ratio of at least 1.6 has been pulsed to temperatures approaching 2,100°F (1,150°C) without damage to the clad (Ref. 4.6).

4.2.1.14 Finite Diffusion Rate

To assess the effect of the finite diffusion rate and the rehydriding at the cooler surfaces, the following analysis is presented.

As hydrogen is released from the hot fuel regions, it migrates to the cooler regions and the equilibrium pressure that is obtained is characteristic of some temperature lower than the maximum. To evaluate this reduced pressure, diffusion theory is used to calculate the rate at which hydrogen is evolved and reabsorbed at the fuel surface.

Ordinary diffusion theory provides an expression describing the time dependent loss of gas from a cylinder:

$$\frac{\bar{c}-c_f}{c_i-c_f}=\sum_{n=1}^{\infty}\frac{4}{Z_n^2}\exp-\frac{Z_n^2 Dt}{r_0^2}, \tag{4-10}$$

where:

$\bar{c}, c_i, c_f$ = the average, the initial, and the final gas concentration in the cylinder, respectively;

Z_n = the roots of the Bessel function of the first kind where $J_0(x) = 0$;

D = the diffusion coefficient for the gas in the cylinder;

r_0 = the radius of the cylinder; and

t = time.

Setting the term on the right-hand side of Equation 10 equal to 6, one can rewrite Equation 10 as:

$$\bar{c}/c_i = c_f/c_i + \left(1-c_f/c_f\right)k \tag{4-11}$$

and the derivative in time is given by

$$\frac{d\left(\bar{c}/c_i\right)}{dt}=\left(1-c_f/c_i\right)\frac{dk}{dt} \tag{4-12}$$

This represents the fractional release rate of hydrogen from the cylinder, f(t). The derivative of the series in the right-hand side of Equation 10 was approximated by

$$\frac{dk}{dt}=-\left(7.339e^{-8.34\varepsilon}+29.88e^{-249\varepsilon}\right)\frac{d\varepsilon}{dt}, \tag{4-13}$$

where:

$$\varepsilon = Dt/r_0^2 .$$

The diffusion coefficient for hydrogen in zirconium hydride in which the H/Zr ratio is between 1.56 and 1.86 is given by

$$D = 0.25e^{-17800/[R(T+273)]}, \tag{4-14}$$

where:

R = the gas constant; and
T = the zirconium hydride temperature in EC.

Equation 10 describes the escape of gas from a cylinder through diffusion until some final concentration is achieved. Actually, in the closed system considered here, not only does the hydrogen diffuse into the fuel-clad gap, but also diffuses back into the fuel in the regions of lower fuel temperature. The gas diffuses through the clad at a rate dependent on the clad temperature. Although this tends to reduce the hydrogen pressure, it is not considered in this analysis. When the diffusion rates are equal, an equilibrium condition will exist. To account for this, Equation 12 was modified by replacing the concentration ratios by the ratio of the hydrogen pressure in the gap to the equilibrium hydrogen pressure, P_h/P_e. Thus,

$$f(t) = \frac{d\left(c/c_i\right)}{dt} = \left(1 - \frac{P_h(t)}{P_e}\right)\frac{dk}{dt} \tag{4-15}$$

where:

$P_h(t)$ = the hydrogen pressure, a function of time; and
P_e = the equilibrium hydrogen pressure over the zirconium hydride which is a function of the fuel temperature and H/Zr ratios.

The rate of change of the internal hydrogen pressure, in psi, inside the fuel element cladding is

$$\frac{dP_h}{dt} = \frac{14.7\, f(t) N_h}{6.02\text{E}23}\frac{22.4}{V_g}\frac{T+273}{273} \tag{4-16}$$

where:

N_h = the number of molecules of H_2 in the fuel;
T = the gas temperature (EC);
f(t) = the fractional loss rate from Equation 15; and
V_g = the free volume inside the fuel clad (liters).

For a fuel volume of 400 cm^3, the moles of H_2 available from fuel with $ZrH_{1.65}$ and $ZrH_{1.7}$ is 19.9 and 20.6 moles, respectively. The free volume is assumed to consist of a cylindrical volume, at the top of the element, 1/8 inch high with a diameter of 1.43 inches for a total of 3.3 cm^3. The temperature of the hydrogen in the gap was assumed to be the temperature of the clad. The effect of changing these two assumptions was tested by calculations in which the gap volume was decreased by 90% and the temperature of the hydrogen in the gap was set equal to the maximum fuel temperature. Neither of these changes resulted in maximum pressures different

from those based on the original assumptions although the initial rate of pressure increase was greater. For these conditions

$$P_h = A\text{E}3(T + 273)\int f(t)dt \tag{4-17}$$

where:

A = 7.29 for $ZrH_{1.65}$ and 7.53 for $ZrH_{1.7}$.

The fuel temperature used in Equation 14 to evaluate the diffusion coefficient is expressed as:

$$\begin{aligned} T(z) &= T_0 : t < 0 , \\ T(z) &= T_0 + (T_m - T_0) \cos [2.45 (z - 0.5)] ; \ t \exists 0, \end{aligned} \tag{4-18}$$

where:

T_m = the peak fuel temperature (EC),
T_0 = the clad temperature (EC),
z = the axial distance expressed as a fraction of the fuel length, and
t = the time after step increase in power.

It was assumed that the fuel temperature was invariant with radius. The hydrogen pressure over the zirconium hydride surface when equilibrium prevails is strongly temperature dependent as shown in Fig. 4.6, and for ZrH, can be expressed by:

$$P_e = 2.07\text{E}9e^{-1.974x10^{4/(T+273)}} \tag{4-19}$$

The coefficients have been derived from data developed by Johnson [Ref. 4.7]. The rate at which hydrogen is released or reabsorbed takes the form:

$$g(t,z) = \frac{\left[P_e(z) - P_h(t)\right]}{P_e(z)} f(t,z), \tag{4-20}$$

where:

f(t, z) = the derivative given in Equation 8 with respect to time evaluated at the axial position z,

$P_h(t)$ = the hydrogen pressure in the gap at time t, and

$P_e(z)$ = the equilibrium hydrogen pressure at the ZrH temperature at position z.

The internal hydrogen pressure is then

$$P_h(t) = A\text{E}3(T_0 + 273)\int_0^t \int_0^1 g(t,z)dz \tag{4-21}$$

This equation was approximated by:

$$P_h(t_i) = A\text{E}3(T_0 + 273)x\sum_{t=1}^{n}\sum\left[1 - \frac{P_h(t_{i-1)}}{P_e(z_j)}\right]1xf(t_i, z_j)\delta z\delta t\,, \qquad (4\text{-}22)$$

where:

the inner summation is over the fuel element's length increments and the outer summation is over time.

For the cases where the maximum fuel temperature is 2,100°F (1,150°C) for $ZrH_{1.65}$ and 2,020°F (1,100°C) for $ZrH_{1.7}$, the equilibrium hydrogen pressure in ZrH is 2,000 psi, which leads to an internal stress of 72,000 psi. Using Equation 14, it is found that the internal pressure for both $ZrH_{1.65}$ and $ZrH_{1.7}$ increases to a peak at about 0.3 sec, at which time the pressure is about one-fifth of the equilibrium value or about 400 psi (a stress of 14,700 psi). After this time, the pressure slowly decreases as the hydrogen continues to be redistributed along the length of the element from the hot regions to the cooler regions.

Calculations have also been made for step increases in power to peak $ZrH_{1.65}$ fuel temperatures greater than 2,100°F (1,150°C). Over a 390°F (200°C) range, the time to the peak pressure and the fraction of the equilibrium pressure value achieved were approximately the same as for the 2,100°F (1,150°C) case. Similar results were found for fuel with $ZrH_{1,7}$. Thus, if the clad remains below about 930°F (500°C), the internal pressure that would produce the yield stress in the clad (35,000 psi) is about 1,000 psi and the corresponding equilibrium hydrogen pressure is 5,000 psi. This corresponds to a maximum fuel temperature of about 2,280°F (1,250°C) in $ZrH_{1.65}$ and 2,160°F (1,180°C) in $ZrH_{1.7}$. Similarly, an internal pressure of 1,600 psi would produce a stress equal to the ultimate clad strength (over 59,000 psi). This corresponds to an equilibrium hydrogen pressure of 5 H 1,600 or 8,000 psi and a fuel temperature of about 2,370°F (1,300°C) in $ZrH_{1.65}$ and 2,260°F (1,240°C) in $ZrH_{1.7}$.

Measurements of hydrogen pressure in TRIGA® fuel elements during steady-state operation have not been made. However, measurements have been made during transient operations and compared with the results of an analysis similar to that described here [Ref. 4.1 and Ref. 4.3]. These measurements indicated that, in a pulse in which the maximum temperature in the fuel was greater than 1,830°F (1,000°C), the maximum pressure ($ZrH_{1.65}$) was only about 6% of the equilibrium value evaluated at the peak temperature. Calculations of the pressure resulting from such a pulse using the methods described above gave calculated pressure values about three times greater than the measured values.

An instantaneous increase in fuel temperature will produce the most severe pressure conditions. When a peak fuel temperature is reached by increasing the power over a finite period of time, the resulting pressure will be no greater than that for the step change in power analyzed above. As the temperature rise times becomes long compared with the diffusion time of hydrogen, the pressure will become increasingly less than for the case of a step change in power. The reason for this is that the pressure in the clad element results from the hot fuel dehydriding faster than

the cooler fuel rehydrides (takes up the excess hydrogen to reach an equilibrium with the hydrogen overpressure in the can). The slower the rise to peak temperature, the lower the pressure because of the additional time available for rehydriding.

The foregoing analysis gives a strong indication that the cladding will not be ruptured if fuel temperatures are never greater than in the range of 2,190°F to 2,280°F (1,200°C to 1,250°C), providing that the cladding temperature is less than about 930°F (500°C). However, for fuel with a $ZrH_{1.7}$, a conservative safety limit of 2,100°F (1,150°C) has been chosen for this condition. As a result, at this safety limit temperature the pressure is about a factor of 4 lower than would be necessary for cladding failure. This factor of 4 is more than adequate to account for uncertainties in cladding strength and manufacturing tolerances. As a safety limit, the peak adiabatic fuel temperature to be allowed during transient conditions is considered to be 2,012°F (1,100°C) for U-ZrH fuel with ratios up to 1.70.

Under any condition in which the cladding temperature increases above 930°F (500°C), the temperature safety limit must be decreased as the cladding material loses strength at elevated temperatures. To establish this limit, it is assumed that the fuel and the cladding are at the same temperature. There are no conceivable circumstances that could give rise to a situation in which the cladding temperatures was higher than the fuel temperature.

The use of the ultimate strength of the cladding material in the establishment of the safety limit under these conditions is justified because of the transient nature of accidents. Although the high cladding temperatures imply sharply reduced heat transfer rates to the surroundings (and consequently longer cooling times), only slight reductions in the fuel temperature are necessary to reduce the stress sharply. For a fuel with $ZrH_{1.7}$, a 70°F (40°C) decrease in temperature from 1,700°F to 1,630°F (930°C to 890°C) will reduce the stress by a factor of 2.

4.2.2 Control Rods

Three motor-driven control rods (1 regulating, 1 shim and 1 safety) and one pneumatic electro-mechanical safety transient rod control the reactor power. The transient rod, located in the C-ring, contains a solid rod of boron-carbide-impregnated graphite as a neutron poison. The transient rod assembly is about 37 inches long and is clad in a 1¼-inch O.D. aluminum tube. The borated graphite poison section is 15 inches long. The transient rod has an air-filled follower about 21 inches long. The transient rod is guided laterally in the core by a thin-walled aluminum guide tube that passes through the upper and lower grid plates and is screwed into, and supported by, the aluminum safety plate beneath the lower grid.

The fuel-followed safety, shim and regulating rods, located in the D-ring, D-ring, and C-ring, respectively, pass through, and are guided by, 1½-inch-diameter holes in the top and bottom grid plates. The rod exterior cladding is a sealed stainless steel tube approximately 43 inches long by 1d inches in diameter. A standard control rod is illustrated both withdrawn and inserted in Fig. 4.6. The upper section of the rod is graphite and the next 15 inches is the neutron absorber (graphite impregnated with powdered boron carbide). The follower section consists of 15 inches of U-$ZrH_{1.6}$ fuel, and the bottom section has 6½ inches of graphite. An aluminum safety plate attached to the shroud beneath the lower grid plate prevents the possibility of a control rod, accidentally disconnected from its drive, from dropping out of the core.

Vertical travel of the control rods is approximately 15 inches. The nominal rod worths of the transient rod, regulating rod, shim rod, and safety rod are about $4.00 (2.60% Δk/k), $2.70 (1.76% Δk/k), $2.70 (1.76% Δk/k), and $2.70 (1.76% Δk/k), respectively. That makes the total rod worth about $12.10 (7.87% Δk/k). The total excess reactivity in the core does not normally exceed $7.50 (4.88% Δk/k). The maximum possible reactivity insertion rate associated with the withdrawal of any rod except the transient rod is approximately $0.214 (0.15% Δk/k) per second.

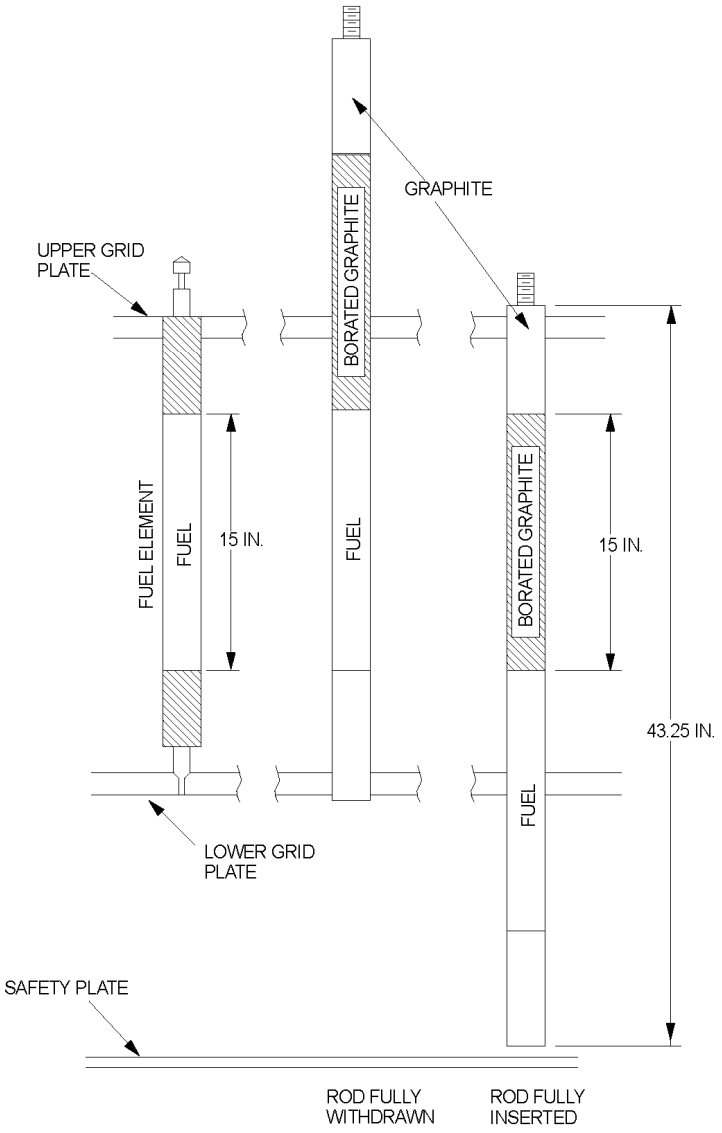

Figure 4.6 Typical Fuel-Follower-Type Control Rod Shown Withdrawn and Inserted

The transient control rod drive is mounted on a steel frame that bolts to the center channel cover plate. Two steel covers keep the mechanism clean. From zero to a maximum of 15 inches of rod

may be withdrawn from the core; however, administrative control must be exercised to restrict the travel so as not to exceed the maximum permissible step insertion of reactivity ($4.00 or 2.60% Δk/k).

A system of limit switches similar to that used with the standard control rod drives is used to indicate the position of the air cylinder and the transient rod. Two of these switches, the DRIVE UP and DRIVE DOWN switches, are actuated by a small bar attached to the bottom of the air cylinder. A third limit switch, the ROD DOWN switch, is actuated when the piston reaches its lower limit of travel. A 10-turn potentiometer driven by the motor shaft controls the position indicator on the console.

4.2.3 Neutron Moderator and Reflector

The reflector is a ring-shaped block of graphite that surrounds the core radially. The graphite is 10.2 inches thick radially, with an inside diameter of 21-5/8 inches (below the Lazy Susan) and a height of 21-13/16 inches. The graphite is protected from water penetration by a leak-tight welded aluminum can.

A "well" in the top of the graphite reflector is provided for the rotary specimen rack. This well is also aluminum-lined, the lining being an integral part of the aluminum reflector can. The rotary specimen rack is a self-contained unit and does not penetrate the sealed reflector at any point.

A 2-inch-thick lead thermal shield is located at the periphery of the reflector in the region adjacent to the water. The lead has been flame-sprayed with a molybdenum coating on the inner surface of the aluminum can to assure a good bond for the transfer to the surrounding water of the heat deposited by gamma rays in the lead.

The graphite, lead, and the outer surface of the aluminum can are pierced by an aluminum tube which forms the inner section of the piercing radial beamport. Two additional holes penetrate the graphite and lead; one for a radial beamport and one for the tangential beamport. These holes do not pierce the aluminum can. The tangential beamport terminates outside the reflector can and abuts against the graphite reflector.

4.2.4 Neutron Startup Source

A 3 Curie americium beryllium (^{241}Am-Be) neutron source is used in the OSTR core. The neutron source holder is made of aluminum, is cylindrical in shape, and has a cavity to hold the source. The source holder can be installed in any vacant fuel or graphite element location. A shoulder at the upper end of the holder supports the assembly on the upper grid plate, with the rod itself, which contains the source, extending down into the core region. The neutron source is contained in a cavity in the lower portion of the rod assembly at the horizontal centerline of the core. This cylindrical cavity is 0.981 inches in diameter and approximately 3 inches deep. The upper and lower portions are screwed together. A soft aluminum ring provides sealing against water leakage into the cavity. Since the upper end fixture of the source holder is similar to that of the fuel element, the source holder can be installed or removed with the fuel handling tool. In addition, the upper end fixture has a small hole through which one end of a stainless steel wire may be inserted to facilitate handling operation from the top of the tank.

4.2.5 Core Support Structure

The reflector assembly rests on an aluminum platform at the bottom of the tank, and provides the support for the two grid plates and the safety plate. Four lugs are provided for lifting the assembly.

The top grid plate is an aluminum plate e inches thick (d inches thick in the central region) that provides accurate lateral positioning for the core components. The plate is supported by a ring welded to the top inside surface of the reflector container and is anodized to resist wear and corrosion.

One hundred twenty six (126) holes, 1.505 inches in diameter, are drilled into the top grid plate in six circular bands around a central hole to locate the fuel-moderator and graphite dummy elements, the control rods and guide tubes, and the pneumatic transfer tube (See Fig. 4.7). A 1.505-inch-diameter center hole accommodates the central thimble. Small holes at various positions in the top grid plate permit insertion of foils into the core to obtain flux data.

A hexagonal section can be removed from the center of the upper grid plate for the insertion of specimens up to 4.4 inches in diameter into the region of highest flux; this requires prior relocation of the six fuel elements from the B ring to the outer portion of the core and removal of the central thimble.

Two generally triangular-shaped sections are cut out of the upper grid plate. Each encompasses two E and one D ring positions. When fuel elements are placed in these locations, their lateral support is provided by a special fixture. When the fuel elements and the spacer support are removed, there is room for inserting specimens up to 2.4 inches in diameter.

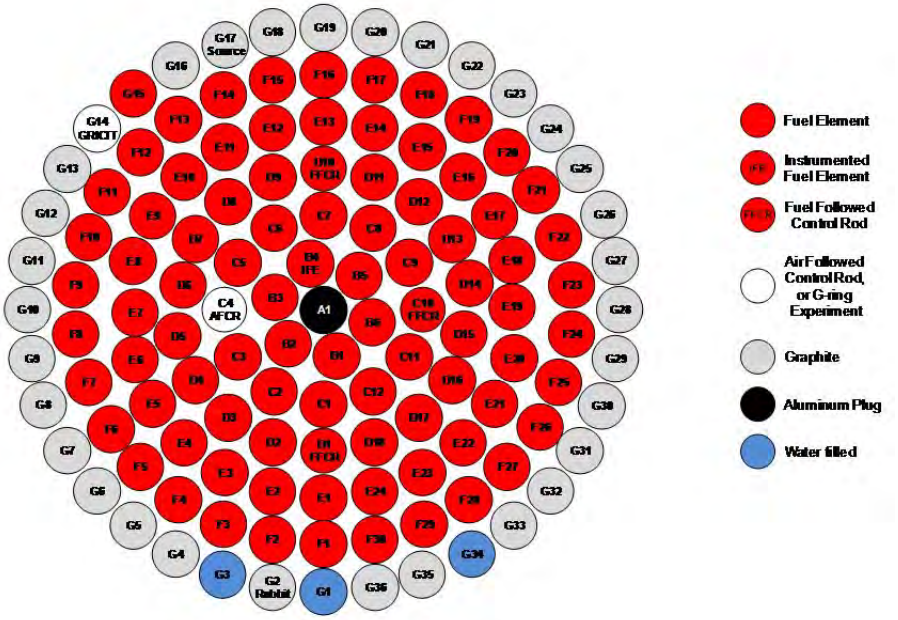

Figure 4.7 Top Grid Plate and Typical Core Configuration

Two d-inch diameter holes between the F and G rings of the grid plate locate and provide support for the source holder at alternate positions.

The differential area between the triangular-shaped spacer blocks at the top of the fuel element and the round holes in the top grid plate permit passage of cooling water through the plate.

The bottom grid plate is an aluminum plate ¾ of an inch thick which supports the entire weight of the core and provides accurate spacing between the fuel-moderator elements. Six pads are welded to a ring which is, in turn, welded to the reflector container support the bottom grid plate.

Holes in the bottom grid plate are aligned with fuel element holes in the top grid plate. They are countersunk to receive the adaptor end of the fuel-moderator elements and the adaptor end of the pneumatic transfer tube. A central hole 1.505 inches in diameter in the lower grid serves as a clearance hole for the central thimble. Eight additional 1.505-inch-diameter holes are aligned with upper grid plate holes to provide passage of fuel-follower control rods. Those holes in the bottom grid plate not occupied by control rod followers are plugged with removable fuel element adaptors that rest on the safety plate. These fuel element adaptors are solid aluminum cylinders 1.5 inches in diameter by 17 inches long. At the lower end is a fitting that is accommodated by a hole in the safety plate. The upper end of the cylinder is flush with the upper surface of the bottom grid plate when the adaptor is in place. This end of the adaptor has a hole similar to that in the bottom grid plate for accepting the fuel element lower end fitting. With the adaptor in place, a position formerly occupied by a control rod with a fuel follower will now accept a standard fuel element. The adaptor can be removed with a special handling tool.

The safety plate is provided to preclude the possibility of control rods falling out of the core. It is a ½-inch-thick plate of aluminum welded to the extension of the inner reflector liner and placed about 16 inches below the bottom grid plate.

4.3 Reactor Tank or Pool

The reactor core is located at the bottom of an aluminum tank, which is in the center of the concrete shield structure described in Section 4.4. The tank has an outside diameter of 6 feet 6 inches, a depth of 20 feet 6 inches, and a minimum thickness of 1/4 inch.

The aluminum tank was manufactured to accommodate the four beamports, the thermal column, and the thermalizing column in that the tank sections for these facilities are welded to and are an integral part of the aluminum tank.

The inner sections for the facilities have continuous welded joints, and the integrity of the joints was verified by X-ray testing, pressure testing, dye penetrant checking, and soap-bubble leak testing. For corrosion protection from the concrete, the outside of the tank is coated with an adhesive primer followed by several layers of polyethylene tape.

The reactor tank is filled with demineralized water to provide approximately 16 feet of shielding water above the top of the reflector. The tank holds about 5,000 gallons of demineralized water; however, the reactor components displace approximately 400 gallons. Therefore, the net water

volume of the tank is about 4,600 gallons. The tank water temperature is generally maintained significantly below 120°F (49°C) because of thermal stress considerations.

The top of the reactor tank is closed by hinged aluminum grating covers. A sheet of Lucite plastic is inserted into the bottom of each grating section to prevent the entry of foreign matter into the tank while still permitting visual observation of the reactor. (The plastic sheets are easily removed for cleaning.) A gap around the perimeter of the plastic and some holes in the plastic permit adequate venting of the small quantities of hydrogen gas which may be released during reactor operations. The reactor tank covers are designed to support only the weight of people who are walking and working over the reactor. Therefore, heavy equipment or isotope casks will not be placed on these tank covers.

Support for the central thimble, rotating rack irradiation facilities, control-rod drive mechanisms, and the tank covers is provided by the center channel assembly. This assembly is placed over the top of the reactor tank and consists of two structural steel channels with steel cover plates. The center channel assembly is designed to support a shielded isotope cask weighing 3½ tons, when placed over the rotating rack access opening.

4.4 Biological Shield

The steel-reinforced concrete shield structure extends about 21 feet above the reactor room floor. In elevation, the shield structure is stepped so that the shielding around the core is much thicker than the shielding above the core.

The bulk-shielding experimental tank, which is 8 feet wide by 9 feet long and 12 feet deep, is located on the west side of the lower part of the reactor structure. (The pool volume holds ~6,500 gallons of demineralized water.)

The shield structure provides about 8 feet of concrete in the radial direction from the core. The concrete shield is pierced radially by the beamports, the thermal column, and the thermalizing column.

Embedded in the concrete are small vent pipes that lead from the thermal column, thermalizing column, and each of the beamports to a manifold which is mounted on the northwest side of the shield structure. An additional vent line from the rotating rack loading tube is also attached to the manifold. An exhaust line connects the manifold to the building ventilation exhaust system. This manifold arrangement permits the purging of ^{41}Ar and other radioactive gases from the thermal column, thermalizing column, and beamports and rotating rack.

The core is shielded radially by (1) ~8 inches of graphite reflector, (2) 2 inches of lead (inside the reflector can), (3) ~1.5 feet of water, and (4) ~8 feet of concrete.

4.5 Nuclear Design

The reactor design bases are established by the maximum operational capability for the fuel elements and configuration described in this report. The TRIGA® reactor system has three major areas which are used to define the reactor design bases:

- fuel temperature,
- prompt temperature coefficient, and
- reactor power.

The ultimate safety limit is based on fuel temperature, while the strongly negative temperature coefficient of reactivity contributes to the inherent safety of the TRIGA® reactor. A limit on reactor power is set to ensure operation below the fuel temperature safety limit.

4.5.1 Critical Mass of Previous TRIGA® Reactors

Criticality was attained in the GA TRIGA® Mark I reactor with 54 standard (8.5 w% 20% enriched) TRIGA® fuel elements (1.94 kg ^{235}U) and four water-filled control rod positions. The critical mass for the Advanced TRIGA® Prototype was 75 standard TRIGA® fuel elements (2.7 kg ^{235}U) with three fuel followers and one transient rod without a follower. (Fuel followers on control rods are not counted as fuel elements.)

For the GA TRIGA® Mark III reactor, the critical mass was 56 standard TRIGA® fuel elements (2.24 kg ^{235}U) using an "A" ring element and four fuel followers. Changes in critical mass occurred with varying control rod configurations and follower materials. Tolerances in the manufacture of the fuel elements (hydrogen and uranium content) also contributed a variance of about ±3% in the critical mass of any given system.

The reflector materials around the core and the absence or presence of graphite reflector elements in empty fuel positions also affected the critical mass rather strongly. Replacing the graphite with a water reflector on the TRIGA® Mark I raised the critical mass about 25%; while placing a row of graphite reflector elements around the water-reflected core cut this difference approximately in half.

4.5.2 Critical Mass of the OSTR Using Standard 20% Enriched Fuel

Criticality of the Oregon State TRIGA® was achieved on 8 March, 1967 with 57 standard TRIGA® fuel elements and two fuel follower control rods (2.244 kg ^{235}U). Also in the core was one transient rod with an air (void) follower and 21 graphite reflector elements arranged in the "F" ring. The critical configuration resulted in a core excess of 27¢.

4.5.3 Critical Mass Final Core Loading for the Operational 70% Enriched OSTR Core

Criticality of the upgraded OSTR using Fuel Lifetime Improvement Program (FLIP) fuel was attained on 7 August, 1976 with 62 FLIP TRIGA® fuel elements and three fuel follower control rods (8.652 kg ^{235}U). The same air follower transient rod was used and the 21 graphite reflector elements were placed in the "G" ring. This critical configuration resulted in a core excess of 12¢.

The operational FLIP core was finalized on 10 August, 1976 and consisted of 82 TRIGA® FLIP fuel elements, 3 fuel follower control rods, and 21 graphite reflector elements in the "G" ring. This core configuration consisted of 11.347 kg ^{235}U with a core excess of $7.17. The total rod worth was $11.73.

4.5.4 Critical Mass and Final Core Loading for the Operational LEU 30/20 OSTR Core

The same grid plates were used in the HEU and LEU cores, so control rod locations and allowed fuel and reflector positions were unchanged. HEU fuel contained 8.5 mass percent of 70% enriched uranium, therefore each kg of fuel meat contained (1000)(0.085)(0.70) = 59.5 grams of ^{235}U. LEU fuel contains 30 mass percent of 19.75% enriched uranium, so each kg of LEU fuel meat contains (1000)(0.30)(0.1975) = 59.25 grams of ^{235}U. Although HEU fuel contained slightly more ^{235}U, it also contains more of the burnable poison erbium. The geometry of the HEU and LEU initial critical cores was also slightly different due to different placements of the fuel elements, and dissimilar arrangement of graphite reflectors. As a result, the HEU core achieved criticality with one less fuel element than the LEU core. Minimum critical data is shown in Table 4-3. The HEU initial critical configuration is shown in Fig. 4.8, and the LEU initial critical configuration is shown in Fig. 4.9.

Table 4-3 Minimum Critical Core

Fuel Type	Predicted #FE's	Measured #FE's
LEU	69	66
HEU	Not known	65

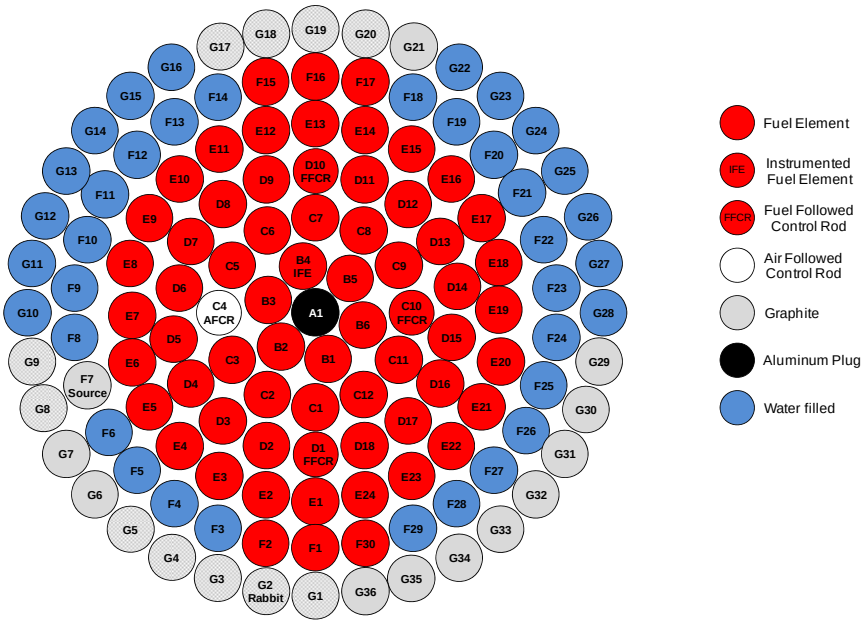

Figure 4.8 HEU Initial Critical Core Configuration

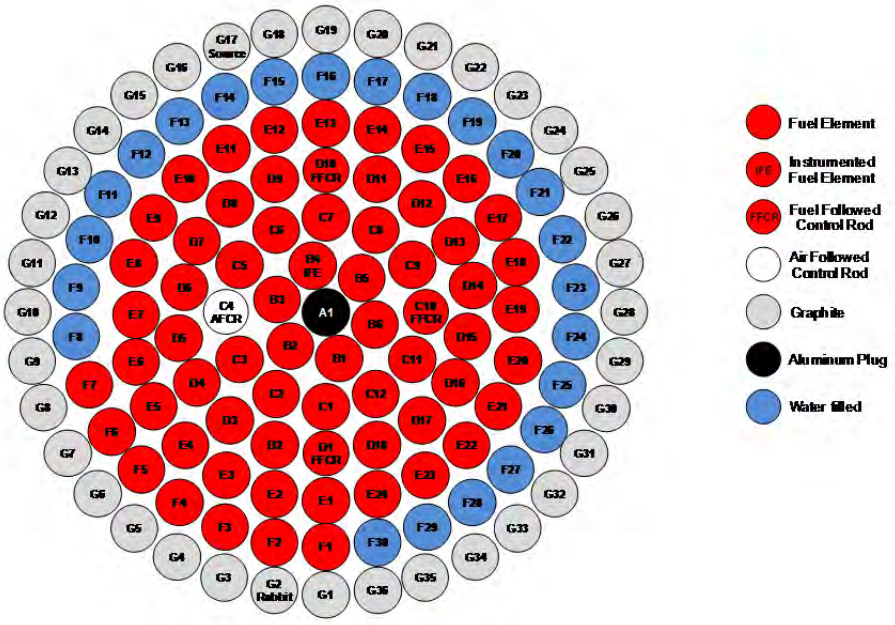

Figure 4.9 LEU Initial Critical Core Configuration

Shown in Figure 4.10, the criticality state of the LEU core was tracked using a standard 1/M plot. As expected, the criticality prediction became more accurate as the reactor became closer to critical. Using all data points, the predicted critical condition was 68.5 fuel elements. Using the last three data points, the predicted critical condition was 66.3 fuel elements. The reactor was actually taken slightly supercritical after the addition of the 66th fuel element. With all control rods fully withdrawn, the core containing 67 fuel elements had an excess reactivity of $0.48. With each subsequent 'batch' fuel addition, the reactor became closer to critical and the allowed number of fuel elements that could be added to the core between count rate measurements was decreased in accordance with the restart procedure.

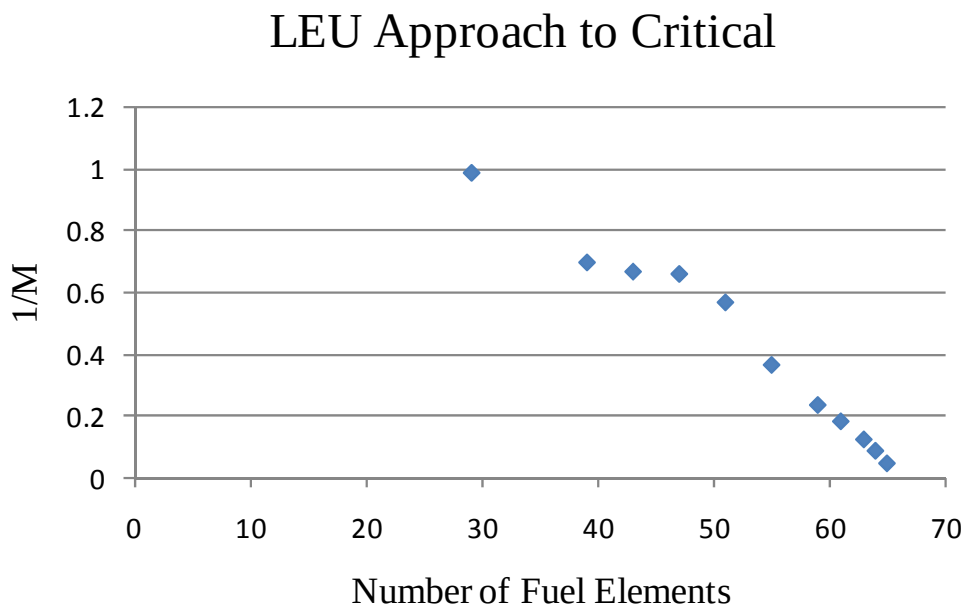

Figure 4.10 1/M plot of the LEU 30/20 fuel loading

4.5.5 Neutronics Analysis Methodology

A detailed neutronic analyses was undertaken using MCNP5 [Ref. 4.13]. MCNP5 is a general purpose Monte Carlo transport code which permits detailed neutronics calculations of complex 3-dimensional systems, and it is well suited to explicitly handle the material and geometrical heterogeneities present in the OSTR core. In the model developed to describe the OSTR, facility drawings, provided by the manufacturer at the time of construction of the facility, were used to define the geometry of the core and surrounding structures. The geometry of the standard fuel elements, instrumented fuel element (IFE), and fuel-followed control rods (FFCR) were based upon the manufacturing drawings for the assemblies.

Extensive start-up testing data is available for the original HEU FLIP core. To demonstrate the capability of MCNP5 to accurately predict core neutronic parameters, the MCNP5 model was modified to simulate core conditions present during start-up testing (the initial critical core and the initial operational core were simulated), and the calculational results of the model were compared to the experimentally determined values. The number densities for the fuel were

obtained from the fuel receipt data provided with the HEU FLIP fuel with an assumed H:Zr ratio of 1.6 and erbium loading of 1.6 mass percent natural erbium. An additional amount of erbium was added to the fuel as Er-166 (labeled "Er-16x") to account for the presence of erbium isotopes other than Er-166 and Er-167. This technique was required to accurately model the natural erbium in the fuel due to the fact that the only erbium cross sections available in MCNP5 are Er-166 and Er-167.

Thirty-eight critical cases taken from the initial calibration of the HEU FLIP control rods were modeled to establish the bias of the MCNP5 model, and it was found that the model exhibited a bias of +0.0045 $\Delta k/k \pm 0.0010$ $\Delta k/k$. During the start-up testing of the HEU FLIP core, a value of 0.0070 was used for β_{eff} to convert measured reactivity to units of dollars [$]. To be consistent with the start-up data, reactivity was converted to dollars using $\beta_{eff} = 0.0070$. In units of dollars, the bias for the beginning of life core was [+0.0045 $\Delta k/k \pm 0.0010$ $\Delta k/k$] / 0.0070 = +$0.64 ± $0.14. All reactivity values stated in this SAR are the calculated values compensated for the +0.0045 $\Delta k/k \pm 0.0010$ $\Delta k/k$ model bias.

All MCNP5 simulations of the HEU and LEU cores included an annular ring representing the rotating rack sample holder. In these models, this annulus was modeled as solid aluminum. The actual rotating rack sample holder is an aluminum shell containing mostly air or nitrogen. Calculations indicate that modeling the annulus as 100% air instead of solid aluminum reduces the model bias by 0.00095 $\Delta k/k$ ($0.13) from +0.0045 $\Delta k/k$ to +0.00355 $\Delta k/k$ (+$0.47).

4.5.6 Depletion and Reactivity

The analysis of the LEU 30/20 core was performed by modifying the MCNP5 model to reflect the new arrangement of core components within the LEU 30/20 core. Number densities for the LEU 30/20 fuel meat containing 1.1 mass percent of natural erbium were calculated by the fuel manufacturer using the NUCDEN code and are listed in Table 4.4 in addition to the number of densities for other components of the fuel element listed in Table 4.5. As was done for the HEU FLIP core, an additional amount of erbium (labeled "Er-16x") was added as Er-166 to account for erbium isotopes other than Er-166 and Er-167. This additional Er-16x was treated as non-depleting to prevent it from depleting to Er-167 which would artificially increase the magnitude of the prompt temperature coefficient. In addition to the change in the fuel alloy, the LEU 30/20 core utilizes stainless steel clad graphite reflector elements rather than the aluminum clad graphite reflector elements that were present in the HEU FLIP core. The physical dimensions of the graphite reflector elements remain the same. Only the cladding material is different.

The LEU 30/20 core has three distinct steady-state operational modes referred to as NORMAL, ICIT, and CLICIT. In the NORMAL mode, a standard fuel element is placed in grid position B-1 and there is a water-filled location in grid position F-23. In the ICIT mode, an in-core irradiation tube (ICIT) is placed in the B-1 grid position, and the standard fuel element that would otherwise be located in the B-1 position is moved to F-23. In the CLICIT mode, a cadmium-lined in-core irradiation tube (CLICIT) is placed in the B-1 grid position, and the standard fuel element that would otherwise be located in the B-1 position is moved to F-23. The arrangement of core components in the NORMAL core is shown in Fig 4.11, while the arrangement of core components in the ICIT or CLICIT core is shown in Fig. 4.12.

Table 4-4 Number Densities for the LEU 30/20 Fuel

[redacted]	Standard Fuel Elements, Instrumented Fuel Element, and Fuel-Followed Control Rod
Nuclide	Number Density [1/(barn-cm)]
H	4.9131E-02
C	1.7885E-03
Zr	3.2213E-02
Er-166	9.4400E-05
Er-16x	2.4548E-05
Er-167	6.4820E-05
U-234	8.2400E-06
U-235	1.0829E-03
U-236	1.2110E-05
U-238	4.3250E-03
Hf	1.9328E-06
Sum	8.8746E-02

Table 4-5 Physical Densities and Mass Fractions for Selected Core Components in the MCNP5 Model of the OSTR (HEU Fuel)

Material	Physical Density [g/cm^3]	Nuclide	Mass Fraction
Type 304 SS (Fuel Clad)	7.857	C-12 Natural Cr Natural Ni Natural Fe	7.993E-04 1.900E-01 1.000E-01 7.092E-01
Graphite Reflector (Fuel)	1.560*	C-12	1.0000
Graphite Segments (FFCR)	1.750	C-12	1.0000
Graphite Reflector Elements	1.620*	C-12	1.0000
Graphite Reflector (Core)	1.698	C-12	1.0000
Zr Fuel Pin	6.398	Natural Zr	1.0000
Stainless Steel + Water Mix	3.056	C-12 Natural Cr Natural Ni Natural Fe H-1 O-16	6.165E-04 1.465E-01 7.713E-02 5.470E-01 2.560E-02 2.032E-01
Pure Aluminum	2.700	Al-27	1.0000
Aluminum 6061-T6	2.700	Al-27 Natural Cr Natural Cu Natural Mg Natural Si B-10	0.9793 1.900E-03 2.800E-03 1.000E-02 6.000E-03 1.475E-06
Water	1.000	H-1 O-16	0.1119 0.8881
Air	1.29E-03	N-14 O-16	0.7671 0.2329

*Smeared density, accounting for graphite to clad gap. True physical density is 1.75 g/cm^3.

The ICIT and CLICIT configurations are used extensively in the LEU core. In the HEU core at BOL, only the NORMAL configuration was used. The ICIT was modeled as a simple air filled tube extending from 32.39 cm. above the core mid-plane to 27.86 cm. below the core mid-plane (even with the bottom of the fuel element lower graphite reflectors). The ICIT aluminum wall has an inner diameter (ID) of 3.2766 cm. and an outer diameter (OD) of 3.7465 cm. The CLICIT is modeled with the same exterior dimensions as the ICIT, but it is composed of a thin layer of cadmium sandwiched between two layers of aluminum. The inner aluminum has ID 2.88036 cm. and ID 3.1750 cm. The cadmium has ID 3.1750 cm. and OD 3.2766 cm. The outer aluminum has ID 3.2766 cm. and OD 3.7465 cm. The CLICIT model also includes thin aluminum and cadmium disks comprising the bottom of the tubes. The thickness of the cadmium disk is 0.0508 cm. The thickness of the aluminum disk is 0.0889 cm.

REBUS-MCNP5 was utilized to perform a depletion analysis of the LEU 30/20 core in the NORMAL mode [Ref. 4.25]. The depletion analysis was performed by dividing the fuel into five equal-height axial segments, with each axial segment further subdivided into three equal-volume radial rings. The depletion analysis was conducted at a core power of 1.1 MW_{th}, a fuel temperature of 327^{o}C, and a moderator temperature of 50^{o}C. The results of the depletion analysis are compared with that of the HEU FLIP core in Fig. 4.13. Based upon the depletion analysis, middle-of-life (MOL) and end-of-life (EOL) for the LEU 30/20 core were determined to be 1600 MWd and 3600 MWd, respectively. From Fig. 4.13, it can be seen that the lifetime of the LEU 30/20 core is nearly as long as the HEU FLIP core (3800 MWd), and the reactivity swing which occurs during the operation of the core due to depletion of the erbium is not nearly as pronounced for the LEU 30/20 core.

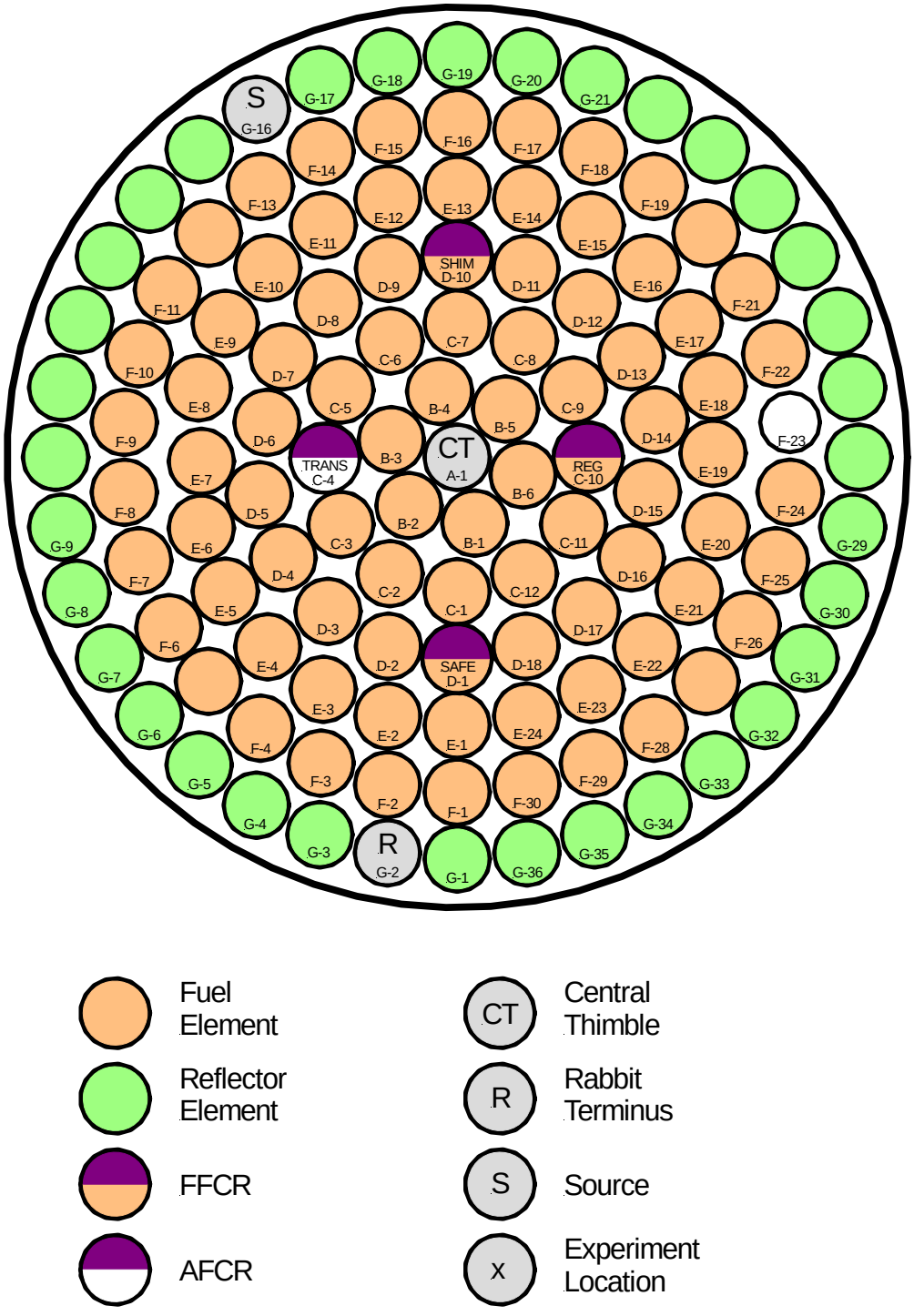

Figure 4.11 Schematic Illustration of the OSTR Upper Grid Plate Showing the Arrangement of Core Components for the LEU 30/20 Core in the NORMAL Configuration

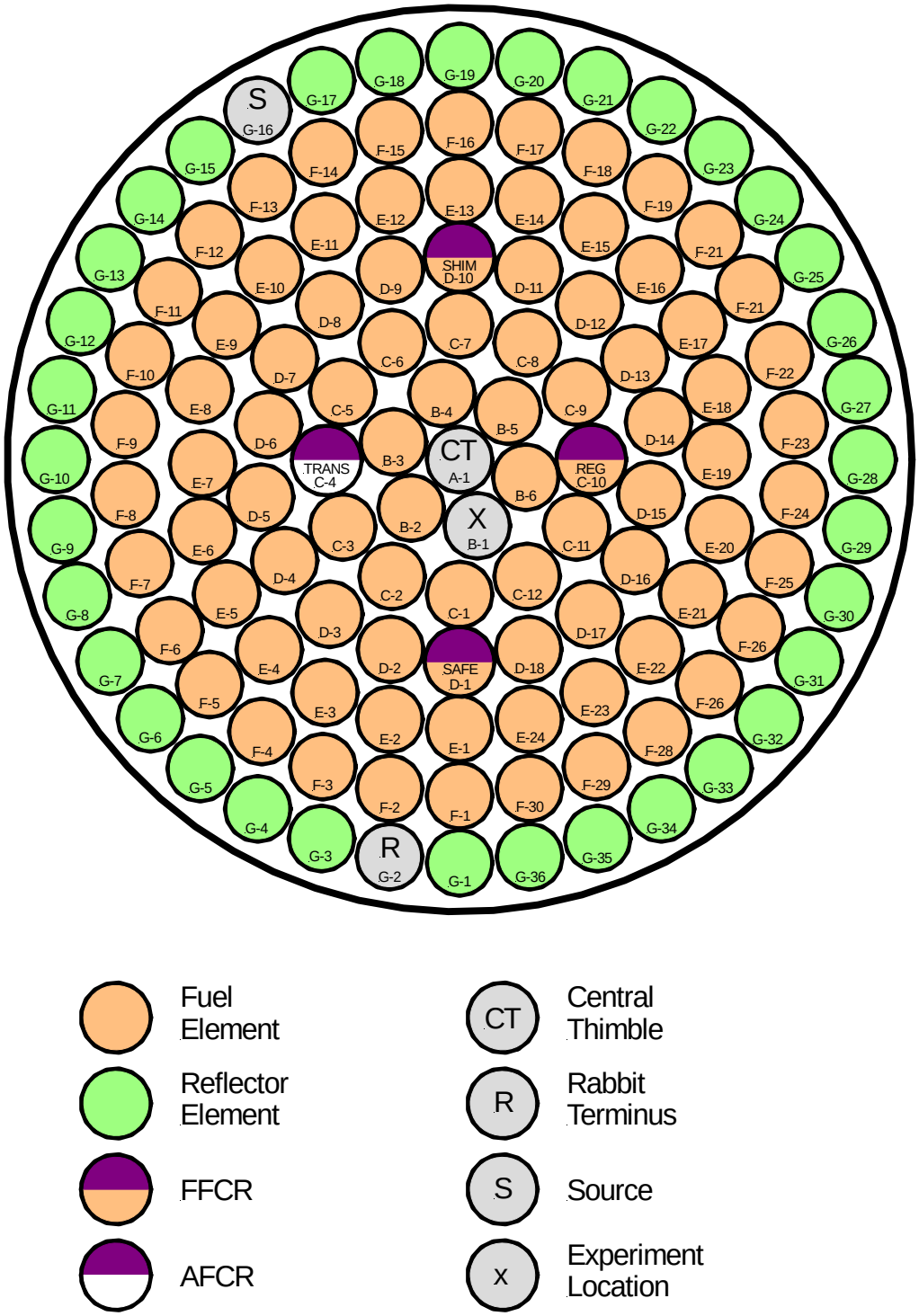

Figure 4.12 Schematic Illustration of the OSTR Upper Grid Plate Showing the Arrangement of Core Components for the LEU 30/20 Core in the ICIT or CLICIT Configuration

Operational experience with the OSTR has shown that core excess reactivity is greatest in the NORMAL mode. The excess reactivity of the LEU 30/20 core in the NORMAL configuration was calculated at various times throughout core life, and the results are presented in Table 4-5. Reactivity was converted to units of dollars using a value of β_{eff} of 0.0075. In addition, the MCNP5 model bias of 0.0045 Δk/k has been taken into account for the reported results. The $5.48 BOL core excess reactivity for the LEU 30/20 core is lower than the $7.17 that was measured at BOL for the HEU FLIP core, but it will be sufficient to permit all modes of operation while minimizing the need to alter the core configuration to accommodate the reactivity swing due to the depletion of erbium as the core is depleted.

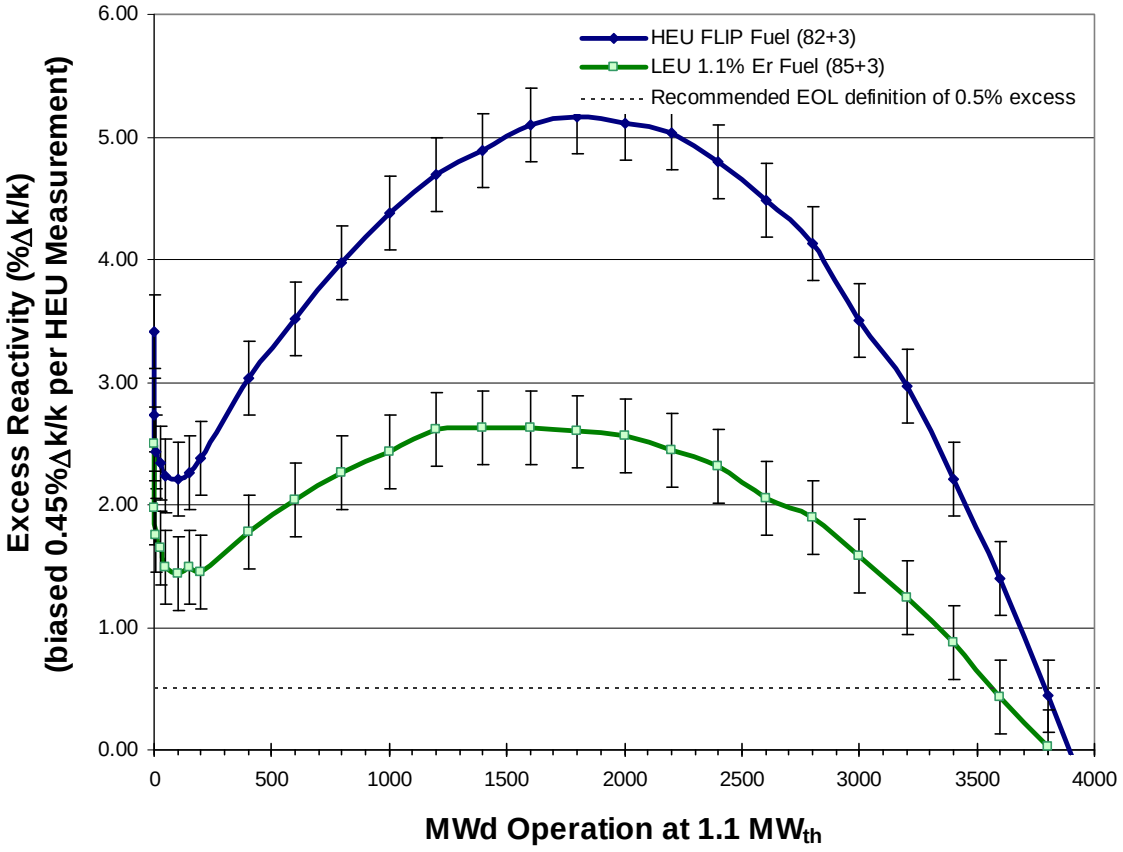

Figure 4.13 REBUS-MCNP5 Depletion Analysis Results for the LEU 30/20 Core and the HEU FLIP Core

The $5.48 value for excess reactivity was calculated assuming cold, clean conditions with no experiments in the core. Figure 4-13 shows excess reactivity at various times in core life assuming 1.1 MW_{th} operating power. The calculated power defect from 0.0 to 1.0 MW_{th} is calculated to be $2.16 for the LEU core. The calculated cold, clean BOL excess reactivity value was 2.29 %ΔK/K. This value is consistent with the values at 1.1 MW_{th} operating power if the power defect is taken into account.

$$\$5.48 - \left(\frac{1.1}{1.0}\right) * \$2.16 = \$3.10 \approx \$3.05 = 0.0229/0.0075 \qquad (4\text{-}23)$$

Table 4-6 Summary of Calculated Core Excess Reactivity for the LEU 30/20 Core at Various Times in Core Life

Time in Core Life	k_{eff} from MCNP5 Calculations	Core Excess Reactivity [$]	Measured Core Excess Reactivity [$]
BOL	1.04776 ± 0.00009	5.48 ± 0.012	7.12 ± 0.35
MOL	1.05634 ± 0.00012	6.51 ± 0.016	-
EOL	1.03384 ± 0.00012	3.76 ± 0.016	-

Control rod worth in the LEU core was measured as soon as the operational core configuration was established. Measured and predicted values of integrated control rod worth are summarized in Table 4-7. The measured and predicted control rod calibration curves for each control rod are shown in Figure 4.14 though Figure 4.17. Note that the model used to predict LEU rod curves was similar to the initial operational core configuration, but not identical. Although accuracy of the worth measurement technique has not been well characterized, it is estimated to be approximately 5% per measurement. Thus a rod calibrated with eight 'pulls' would have total integral rod worth measurement accuracy of ±14%.

Table 4-7 Summary of LEU BOL Total Integrated Rod Worth

Control Rod	Measured Rod Worth [$]	MCNP5 Predicted Rod Worth [$]
Shim Rod	2.76 ± 0.14	2.55 ± 0.16
Safety Rod	2.66 ± 0.13	2.60 ± 0.16
Regulating Rod	3.71 ± 0.19	3.36 ± 0.19
Transient Rod	2.86 ± 0.14	2.86 ± 0.15
Sum of all Rods	11.99 ± 1.68	11.37 ± 0.33

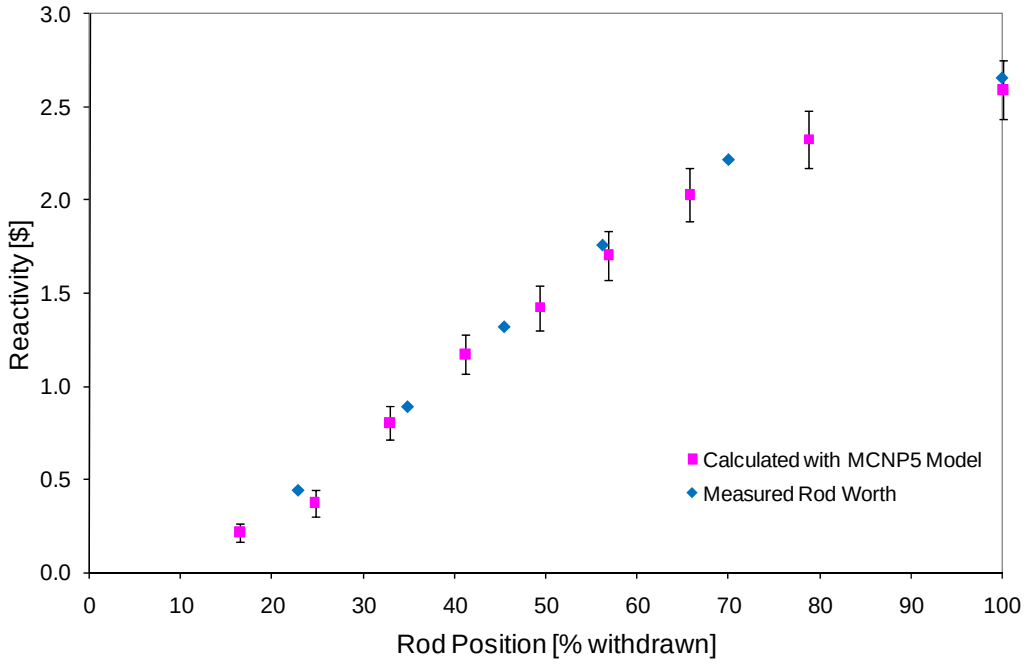

Figure 4.14 Safety Control Rod Calibration Curve

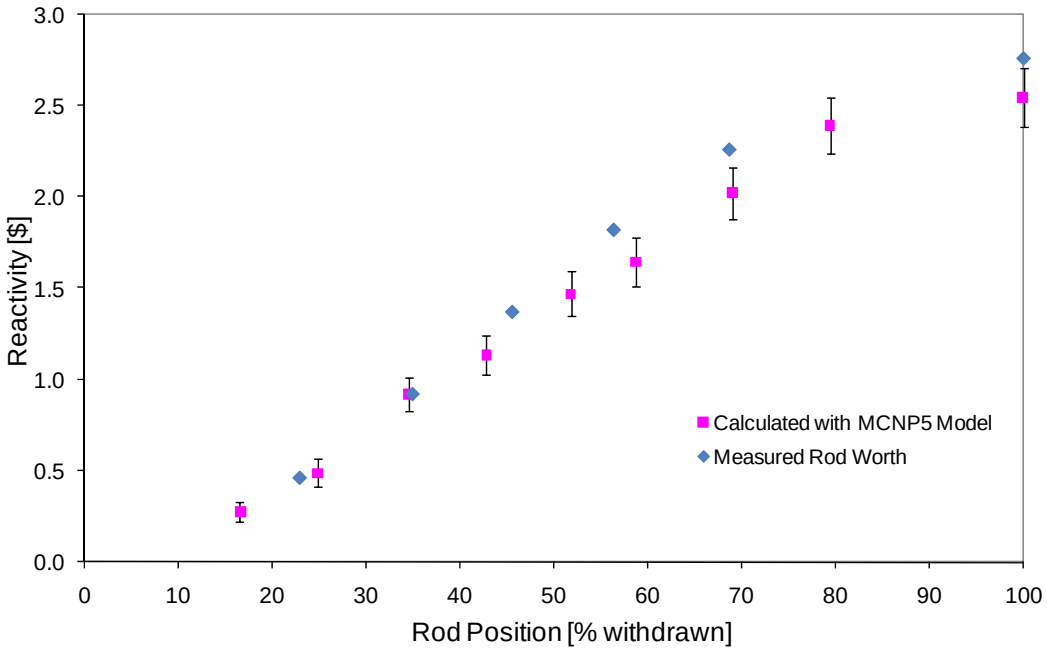

Figure 4.15 Shim Control Rod Calibration Curve

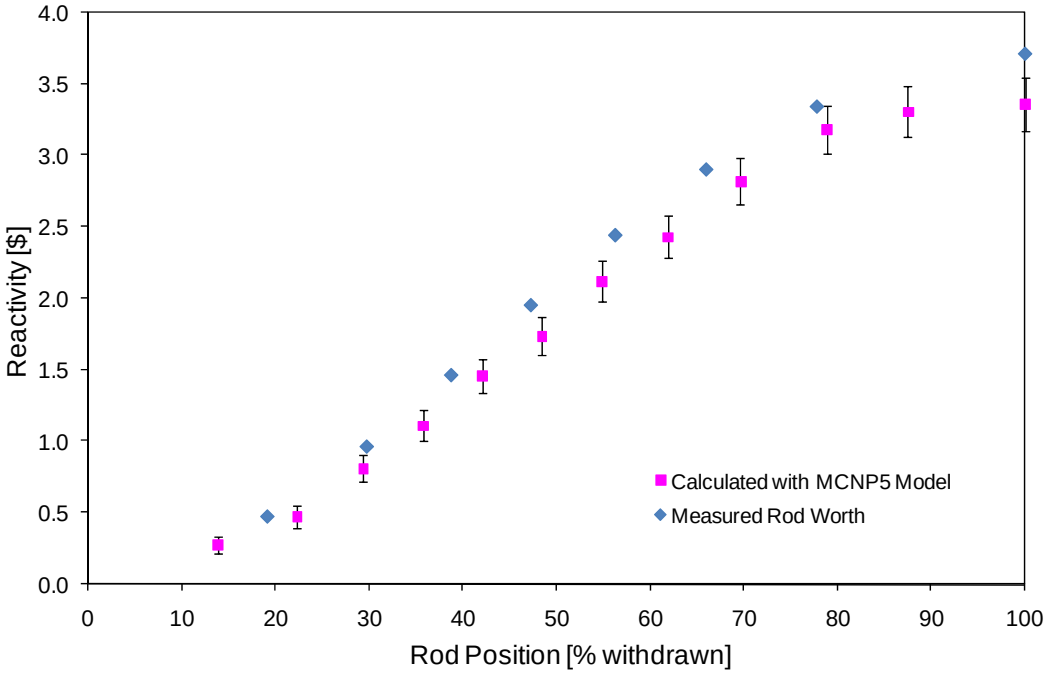

Figure 4.16 Regulating Control Rod Calibration Curve

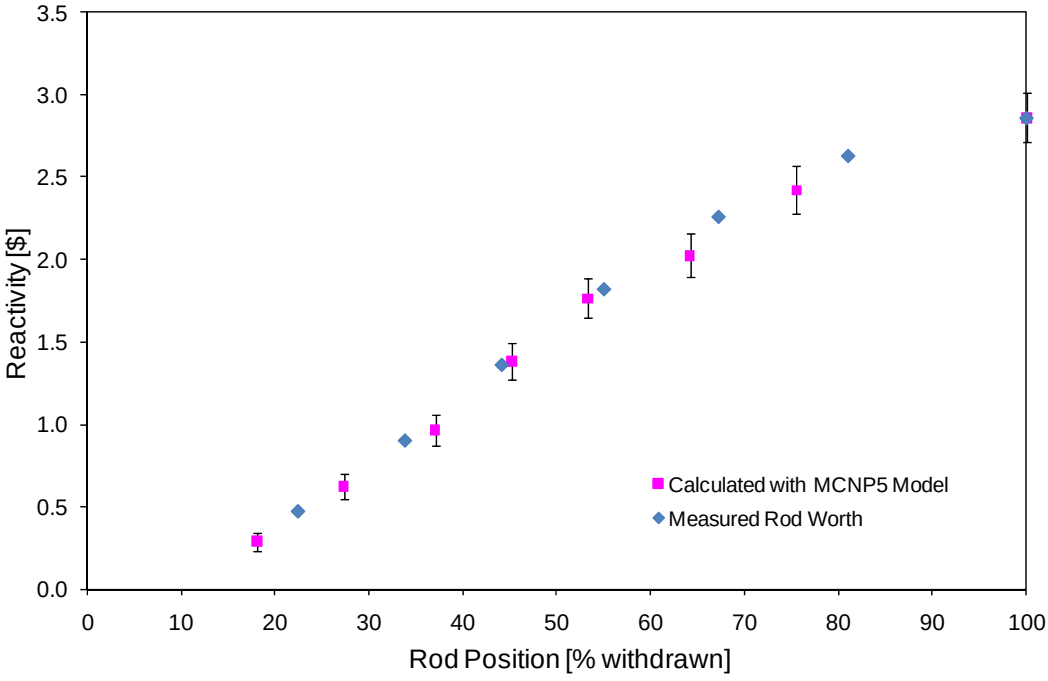

Figure 4.17 Transient Control Rod Calibration Curve

Shutdown margins for the LEU 30/20 core at various times in core life were calculated and compared to the Technical Specification required value of -$0.55. The results of the calculations are summarized in Table 4-8. Inspection of this table shows that the LEU 30/20 core meets the shutdown requirements for all rods at all times in core life with the exception of the regulating rod at MOL which has a shutdown margin of only -$0.37. Operationally, this means that there may be a need to remove one or two fuel elements from the F-ring near MOL to ensure that the regulating rod meets its required shutdown margin. Such modifications to the core will be minor in comparison to those that were necessary to accommodate the reactivity swing that was experienced with the HEU FLIP core.

Table 4-8 Summary of Shutdown Margin Calculations for the LEU 30/20 Core

Control Rod	BOL [$]	MOL [$]	EOL [$]	Measured BOL [$]
Shim Rod	-1.92 ± $0.03	-1.05 ± $0.02	-4.04 ± $0.02	-
Safety Rod	-1.90 ± $0.04	-0.97 ± $0.02	-4.00 ± $0.02	-
Regulating Rod	-1.21 ± $0.04	-0.37 ± $0.02	-3.46 ± $0.02	-1.24 ± 0.06
Transient Rod	-1.87 ± $0.04	-0.96 ± $0.02	-3.98 ± $0.02	-

4.5.7 Prompt-Neutron Lifetime

The prompt-neutron lifetime, l_p, was calculated for the LEU 30/20 core at BOL, MOL, and EOL using MCNP5 and the 1/v absorber method, whereby a small amount of boron is distributed homogeneously throughout the reactor. The calculation of l_p is as follows:

$$l_p = \frac{1}{N_{B-10}\sigma_{ao}v_o}\frac{k_{ref} - k_p}{k_p} \tag{4-24}$$

where:

k_{ref} is the eigenvalue of the original system,
k_p is the eigenvalue of the system with trace amounts of B-10,
$N_{B\text{-}10}$ = boron-10 number density [atoms/(barn-cm)],
v_o = 220,000 cm/sec, and
σ_{ao} = 3837 barns = $\sigma_a^{B\text{-}10}$ at 220,000 cm/sec.

A more accurate statement is

$$l_p = \lim_{N_{B-10}\to 0} \frac{1}{N_{B-10}\sigma_{a0}v_0}\frac{k_{ref}-k_p}{k_p} \tag{4-25}$$

Since $\frac{k_{ref}-k_p}{k_p}$ varies as a function of N_{B-10}, the expression for l_p tends to some finite value as $N_{B-10} \to 0$. Thus for appropriately small values of N_{B-10}, a linear extrapolation is justified. This theory is explained in greater detail in the RERTR Bretscher report [Ref. 4.21].

Two boron concentration data points were used for the calculations. Data points for boron concentration were selected to be sufficiently large that MCNP5 calculations with sufficient histories could be collected to ensure that the errors in the calculated k_{eff} values for the two points did not lead to unnecessary uncertainty in the value of l_p. Data points for boron concentration were selected to be sufficiently small that reactor parameters would not be significantly perturbed.

The limit as $N \rightarrow 0$ was found by perturbing the system with two different boron concentrations and then linearly extrapolating to N = 0. The boron concentrations utilized were 7.5E-8 atoms/(barn-cm) and 1.5E-7 atoms/(barn-cm). The results of the prompt-neutron lifetime calculations for the LEU core are summarized in Table 4-9.

Table 4-9 Summary of Prompt-Neutron Lifetime, l_p, Calculations for the LEU 30/20 Core at Various Times in Core Life

Time in Core Life	Prompt-Neutron Lifetime [μs]	Measured Prompt-Neutron Lifetime [μs]
BOL	22.6 ± 2.9	25.6 ± 2.6
MOL	19.0 ± 1.9	-
EOL	30.7 ± 2.8	-

4.5.8 Effective Delayed Neutron Fraction

The effective delayed neutron fraction for the LEU 30/20 core was calculated with MCNP5 by utilizing the expression

$$\beta_{eff} = 1 - \frac{k_p}{k_{p+d}} \tag{4-26}$$

where k_p is the system eigenvalue assuming fission neutrons are born with the energy spectrum for prompt neutrons, and k_{p+d} is the system eigenvalue assuming fission neutrons are born with the appropriately weighted energy spectra for both prompt and delayed neutrons. Values for the effective delayed neutron fraction of the LEU 30/20 core were calculated at various times in core life as summarized in Table 4-10. Based upon the results presented in Table 4-10, a value for the effective delayed neutron fraction of 0.0075 is a reasonable approximation of its value throughout core life and will be used in calculations in support of the LEU 30/20 core.

Table 4-10 Summary of the Calculated Effective Delayed Neutron Fraction for the LEU 30/20 Core at Various Times in Core Life

Time in Core Life	Effective Delayed Neutron Fraction	Measured Effective Delayed Neutron Fraction
BOL	0.0076 ± 0.0001	0.0080 ± 0.0004
MOL	0.0073 ± 0.0002	-
EOL	0.0075 ± 0.0002	-

4.5.9 Temperature Coefficient of Reactivity

The prompt-temperature coefficient (α_F) associated with the LEU 30/20 fuel was calculated by varying the fuel temperature while leaving other core parameters fixed. The MCNP5 model was used to simulate the reactor with all rods out at 300, 400, 600, 800, and 1200 K. The prompt-temperature coefficient for the fuel was calculated at the mid-point of the four temperature intervals, and the results were fit to a linear expression. The results are shown in Figure 4.18 and tabulated in Table 4-11. The prompt-temperature coefficient is observed to be a linear function over the given temperature range, and the magnitude of the calculated BOL and EOL prompt-temperature coefficients compare favorably with those of Simnad *et. Al* [Ref. 4.22].

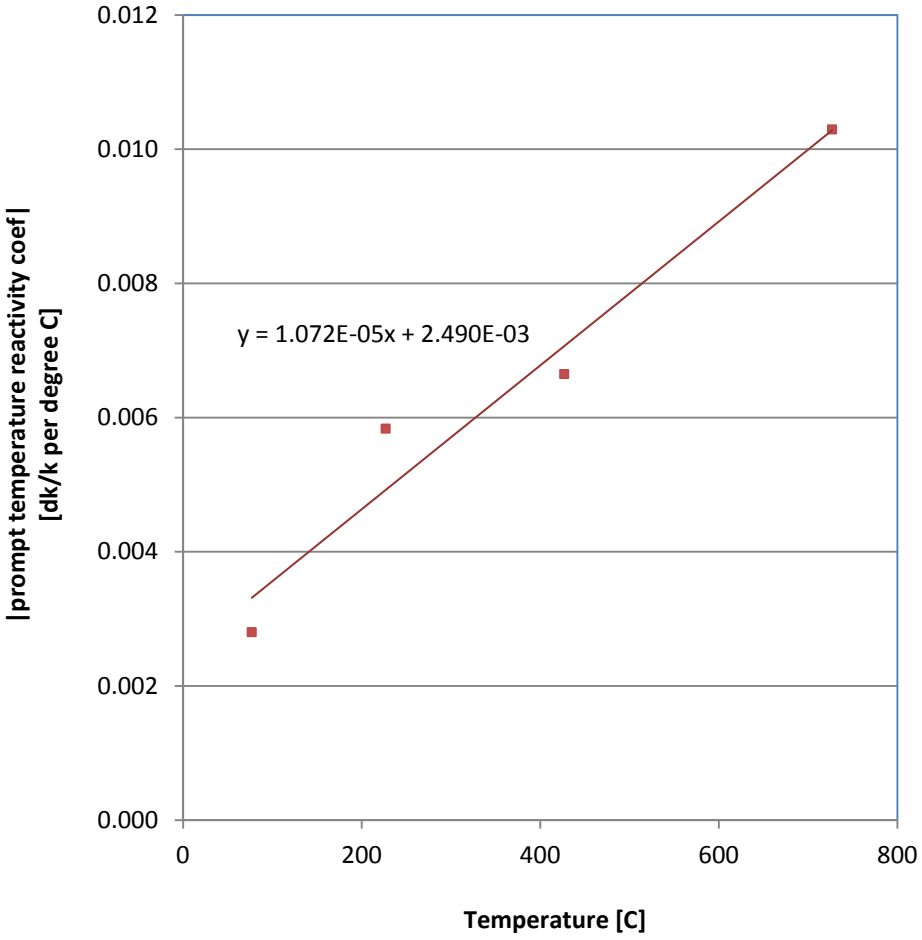

Figure 4.18 Magnitude of the Prompt-Temperature Coefficient, α_F, as a Function of Temperature for the LEU 30/20 Fuel at MOL

Table 4-11 LEU Prompt Temperature Coefficient LEU MOL

Temperature [ºC]	LEU MOL [ΔK/K per °C]	Measured LEU BOL [ΔK/K per °C]
77	-2.80E-03 ± 4.76E-05	-
227	-5.84E-03 ± 2.91E-05	5.3E-3 ± 2.0E-5
427	-6.65E-03 ± 2.99E-05	-
727	-1.03E-02 ± 1.40E-05	-

4.5.10 Void Coefficient of Reactivity

The void coefficient of reactivity for the LEU 30/20 core at BOL was calculated by introducing a void into the central region of the core by uniformly reducing the density of the liquid moderator in the central region of the core. The center of the core was chosen for two reasons: 1) it is the most likely place to develop a void during reactor operations as this is the region of maximum heat flux, and 2) it is the location with the highest neutron importance in the core, hence also the maximum void coefficient. The resultant void coefficient of reactivity at the center of the LEU 30/20 core was found to be -$0.96 ± $0.03/% void and measured to be -$0.65 ± $0.07/% void. The core average void coefficient for the LEU core was also calculated and found to be -$0.19/% void.

4.5.11 Moderator Temperature Coefficient of Reactivity

The moderator temperature coefficient of reactivity, α_m, for the LEU 30/20 core at BOL was determined by varying the moderator temperature over a temperature range from 20°C to 60°C. Within this temperature range, the calculated moderator temperature coefficient of reactivity was -0.72 ± 0.08 ¢/°C and measured to be -0.40 ± 0.40 ¢/°C.

4.5.12 Power Coefficient of Reactivity (Power Defect)

The power coefficient of reactivity and the equilibrium xenon worth for the LEU 30/20 core were estimated from the REBUS-MCNP5 depletion cases. A reactivity loss of $2.16 was observed for an increase of the moderator temperature from 27°C to 50°C coincident with a fuel temperature increase from 27°C to 327°C. The power defect was measured to be $2.41 ± $0.10. These temperatures are characteristic of reactor operation at a power of 1 MW and imply a power coefficient of reactivity of -0.22¢/kW. The equilibrium xenon worth was estimated by calculating the reactivity loss over the course of the first seven days of continuous reactor operation at 1.1 MW. During this time a reactivity loss of $0.98 was calculated, which implies an equilibrium xenon poisoning of ~$0.89 at a core power of 1MW.

4.5.13 Power Distribution

The LEU Core power distributions, as well as the intra-fuel relative power distribution (radial and axial distribution in the hot rod) are provided in Figure 4.19 through Figure 4.33. Power distribution diagrams are used to derive Hot Channel Peak Factors. Axial hot channel power profiles are used to derive Hot Channel Fuel Axial Peak Factors. Radial hot channel power profiles are used to calculate Hot Channel Fuel Radial Peak Factors. The hot channel peak factor, axial power distribution and radial power distribution are used as RELAP5-3D inputs. All peak factors for HEU and LEU cores at BOL, MOL and EOL are tabulated in Table 4.12.

Axial power distribution is affected by burnup, control rod movement and the presence of experiments in the core. Axial power distribution could also be affected by such changes as flooding of the reflector or rotating rack. Note that the OSTR core is physically small in size with a high degree of leakage and relatively large neutron mean free path. As a result the flux in the core is closely coupled and physical changes in the core will have a relatively small affect on flux distribution and hence power distribution. None of these effects, other than burnup, were explicitly modeled.

Previous analysis by GA for the Washington State University LEU core calculated axial peaking factors with all rods partially withdrawn of 1.27 for the BOL, cold critical core and 1.29 for the BOL, hot critical core [Ref. 23]. The OSU LEU BOL cores have axial peaking factors with all rods fully withdrawn of 1.22 for each of the three core configurations. These cores are not identical, but these results indicate that partially withdrawn control rods cause only a slight (~4%) increase in axial peaking factors. Note that with rods partially inserted, the power in the fuel rods close to the control rod will be suppressed, so even though the axial peak factor is slightly increased, power in nearby fuel elements will be suppressed, potentially reducing the hot rod peak factor and the net effective peak factor.

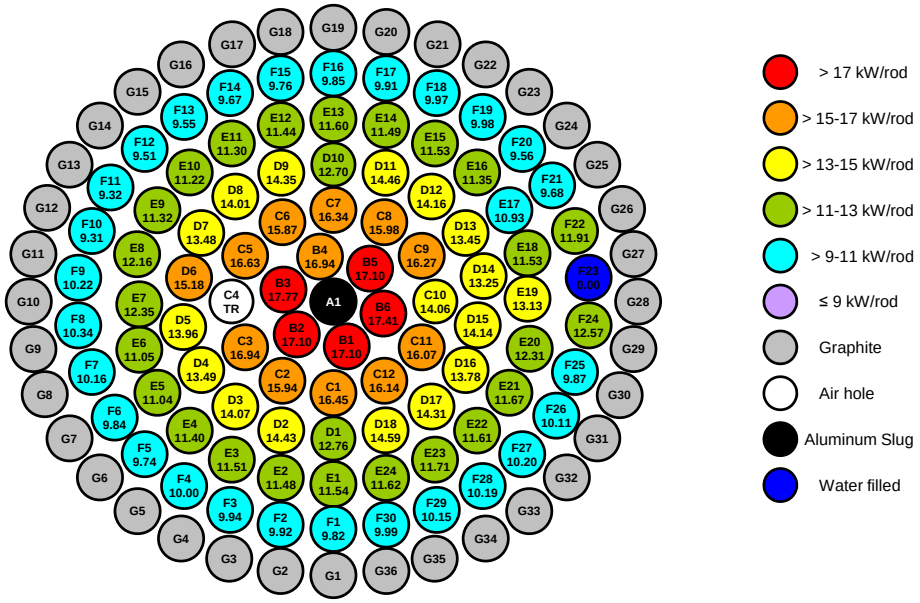

Figure 4.19 Core Power Distribution (LEU BOL NORMAL Core)

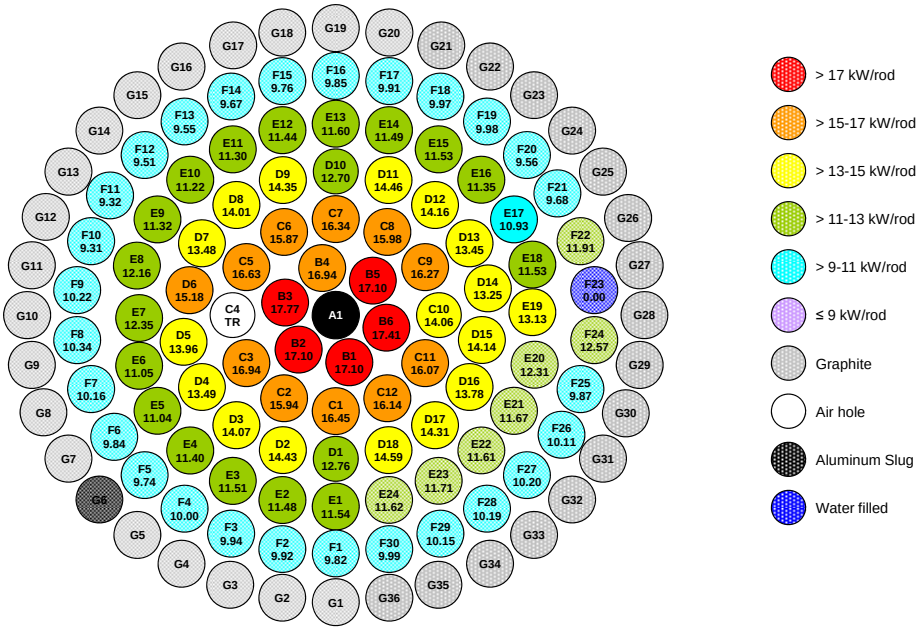

Figure 4.20 Core Power Distribution (LEU MOL NORMAL Core)

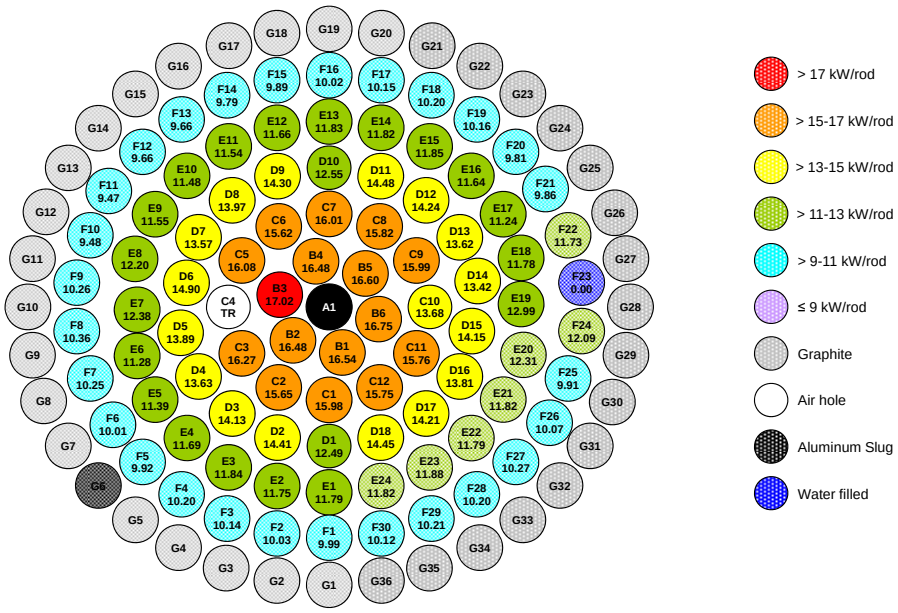

Figure 4.21 Core Power Distribution (LEU EOL NORMAL Core)

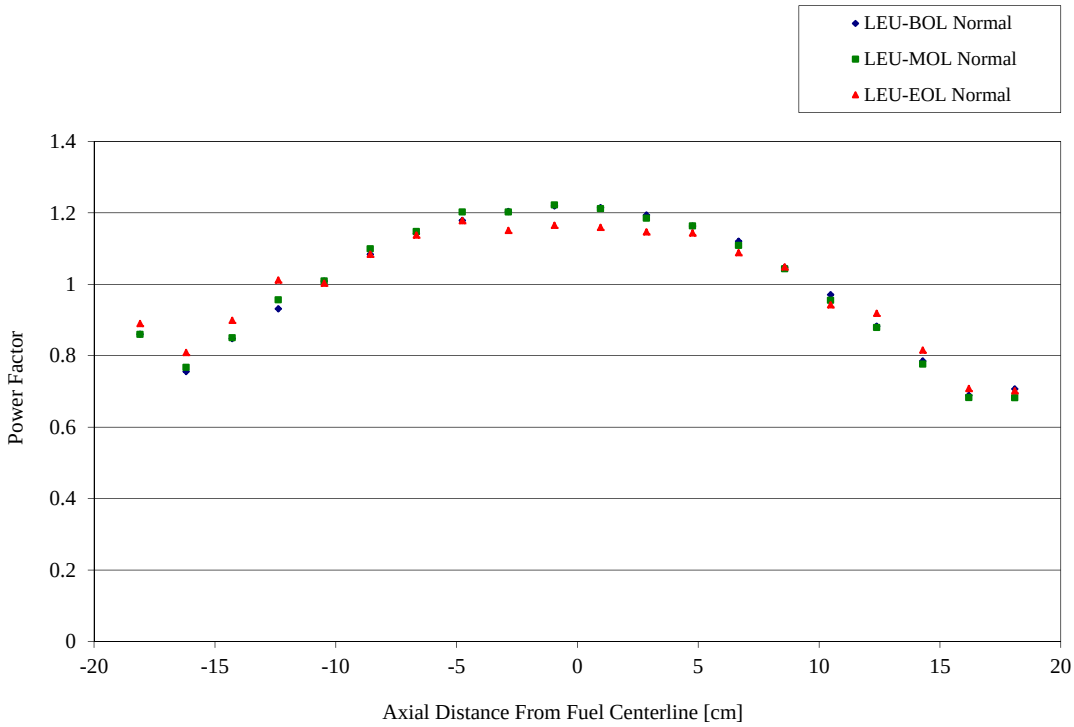

Figure 4.22 OSU LEU - Axial Power Profile vs. Distance from Fuel Centerline

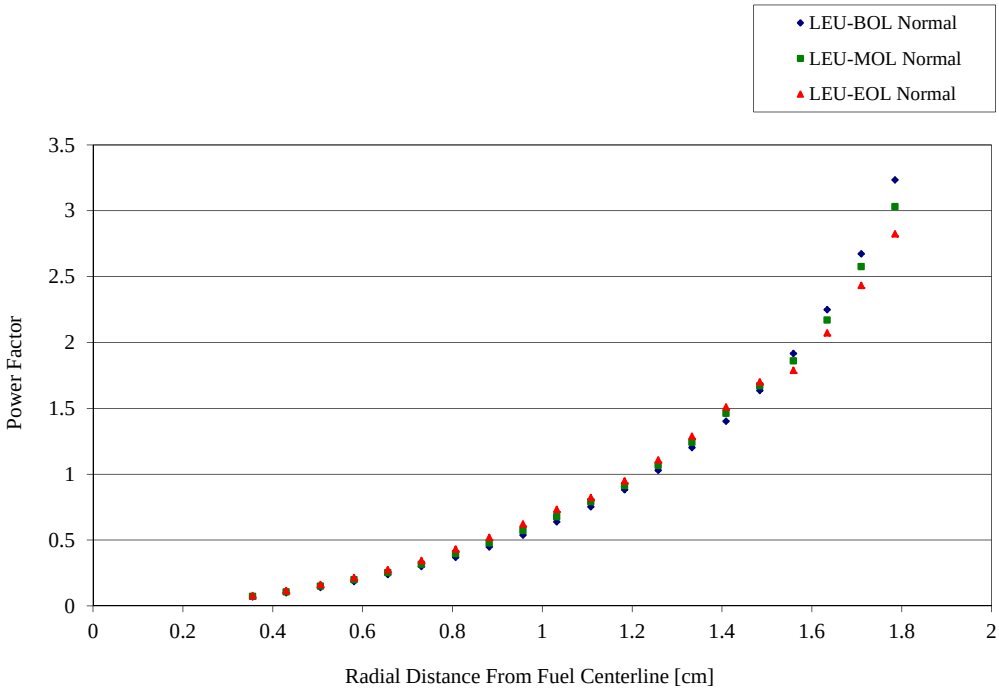

Figure 4.23 OSU LEU -Radial Power Profile vs. Distance from Fuel Centerline

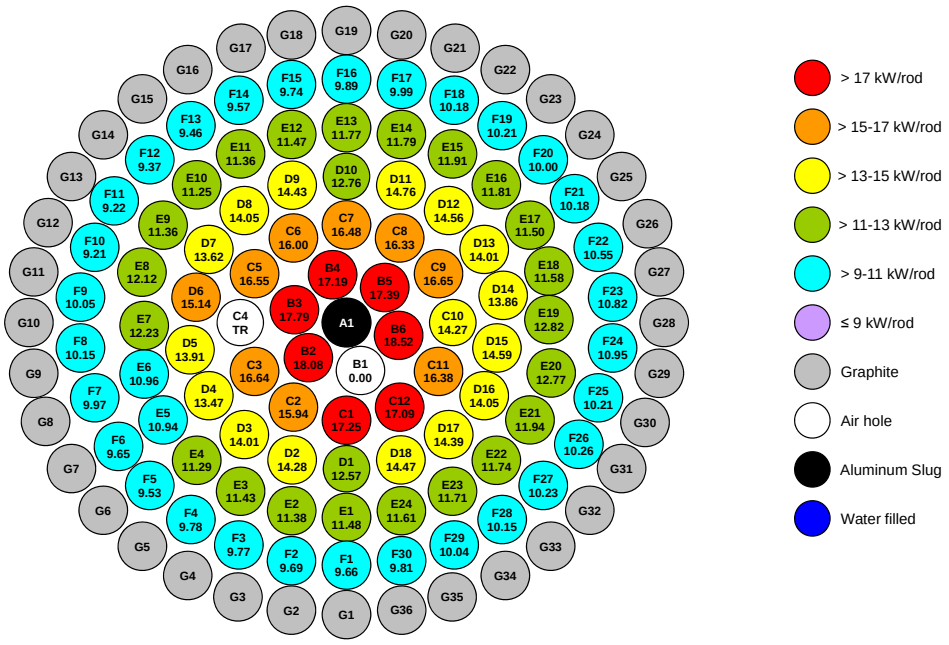

Figure 4.24 Core Power Distribution (LEU BOL ICIT Core)

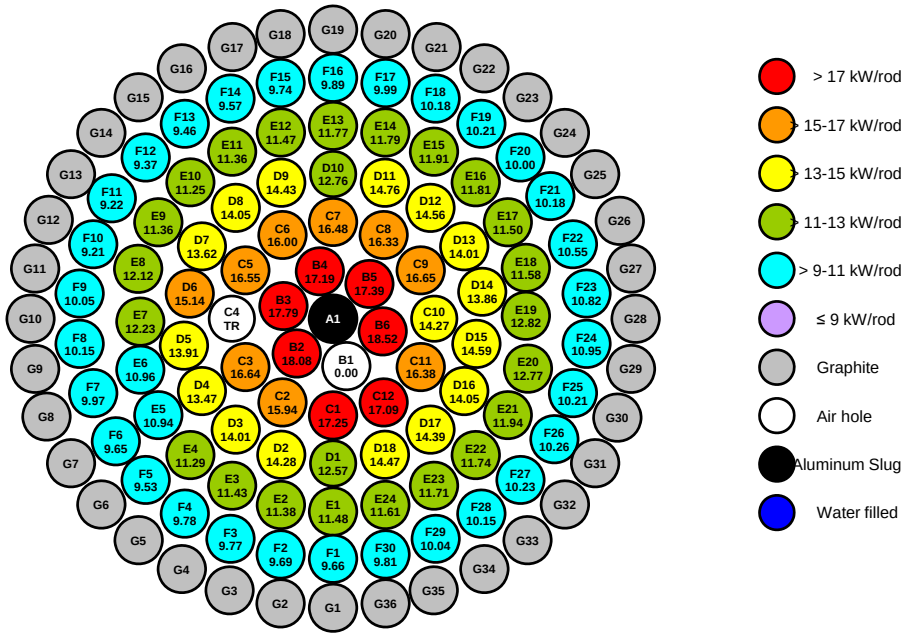

Figure 4.25 Core Power Distribution (LEU MOL ICIT Core)

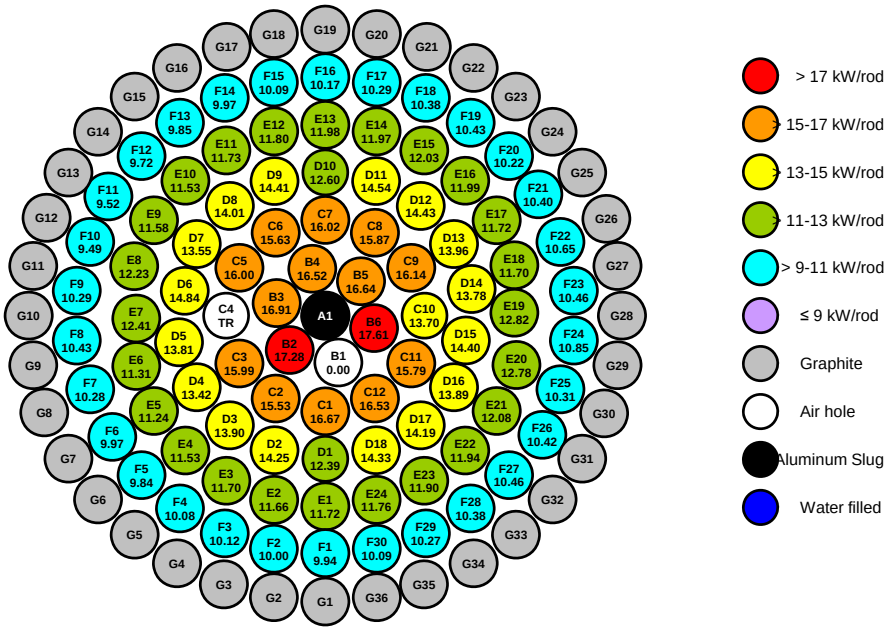

Figure 4.26 Core Power Distribution (LEU EOL ICIT Core)

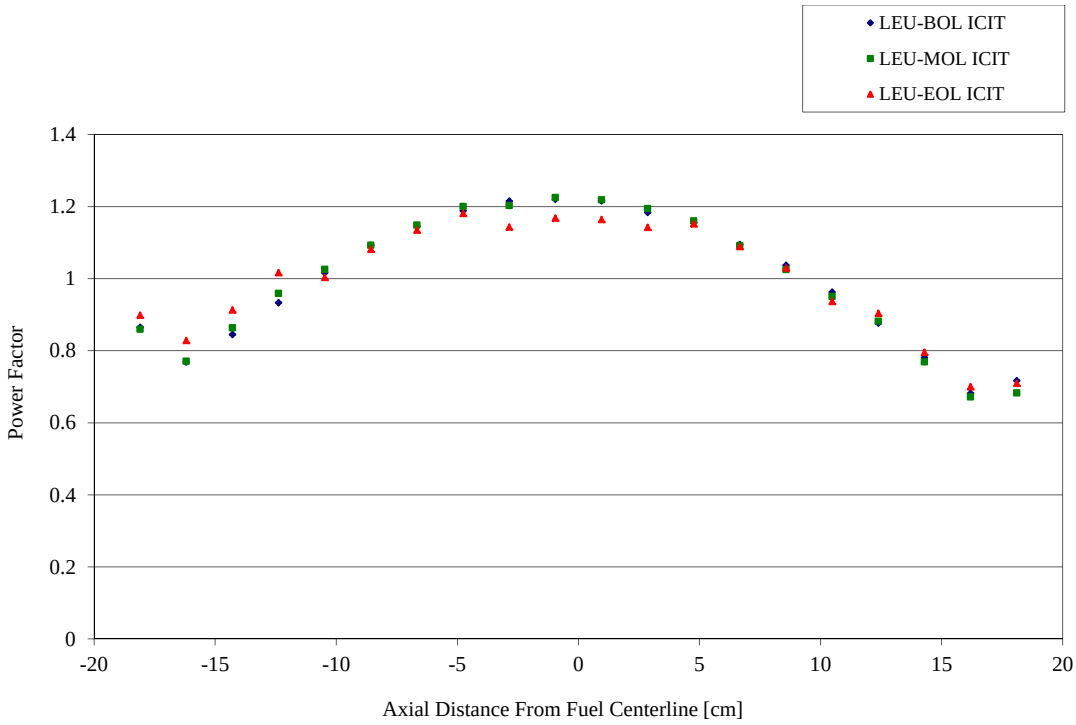

Figure 4.27 Axial Power Factor (LEU ICIT Core)

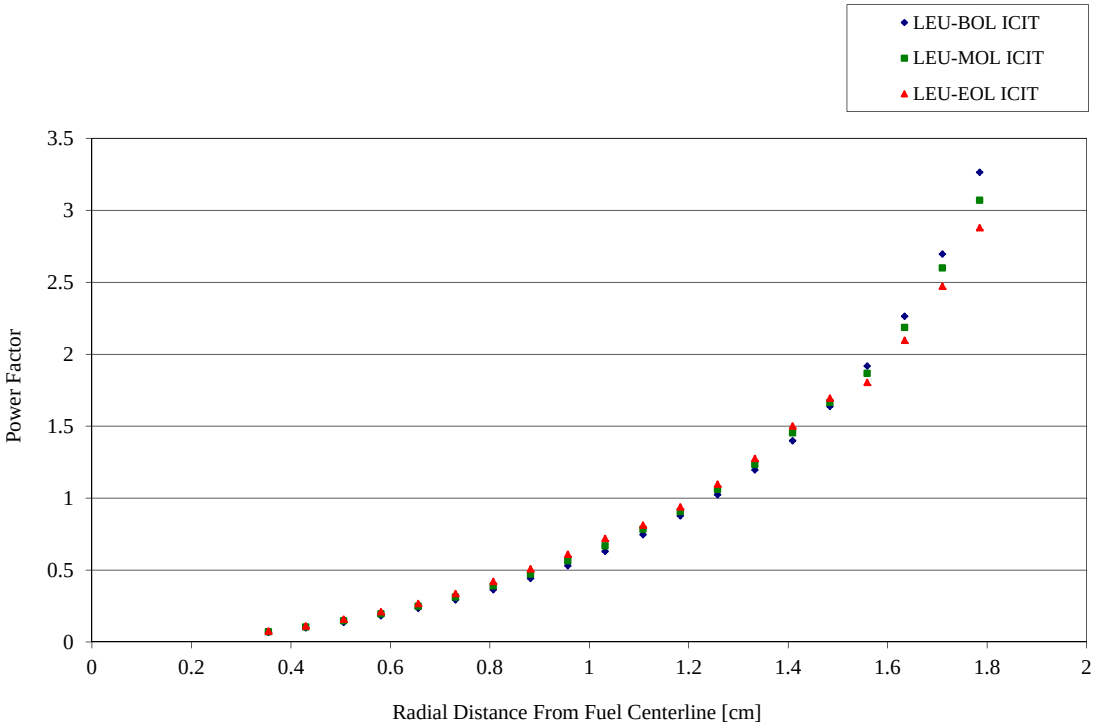

Figure 4.28 Radial Power Factor (LEU ICIT Core)

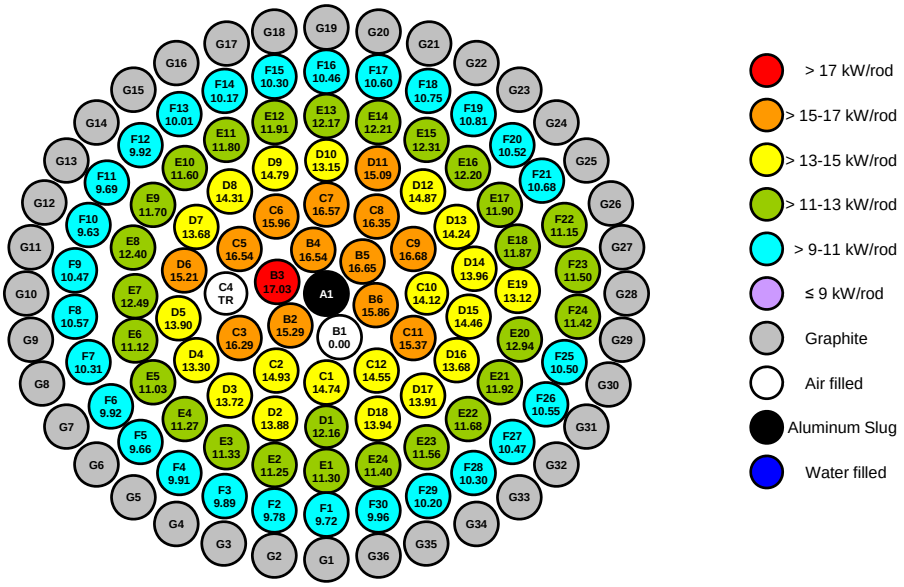

Figure 4.29 Core Power Distribution (LEU BOL CLICIT Core)

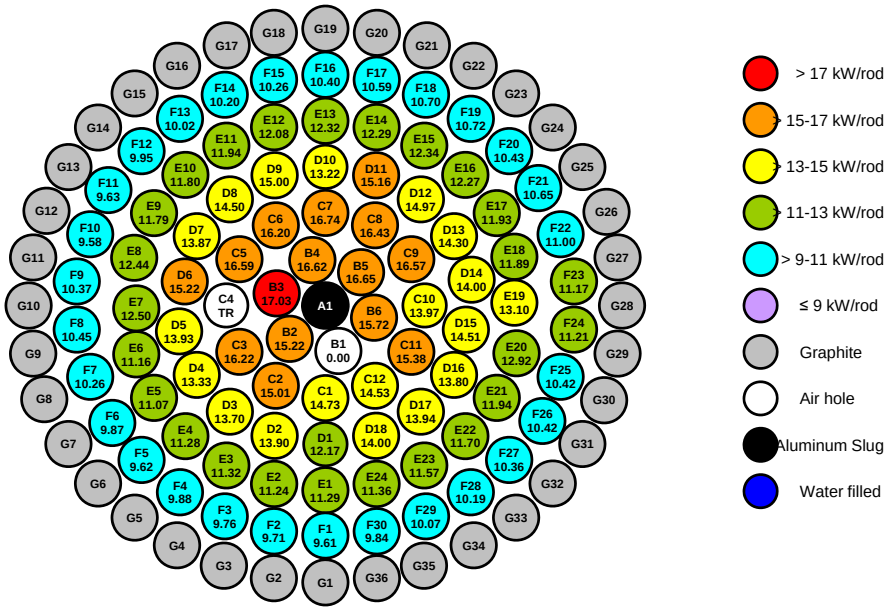

Figure 4.30 Core Power Distribution (LEU MOL CLICIT Core)

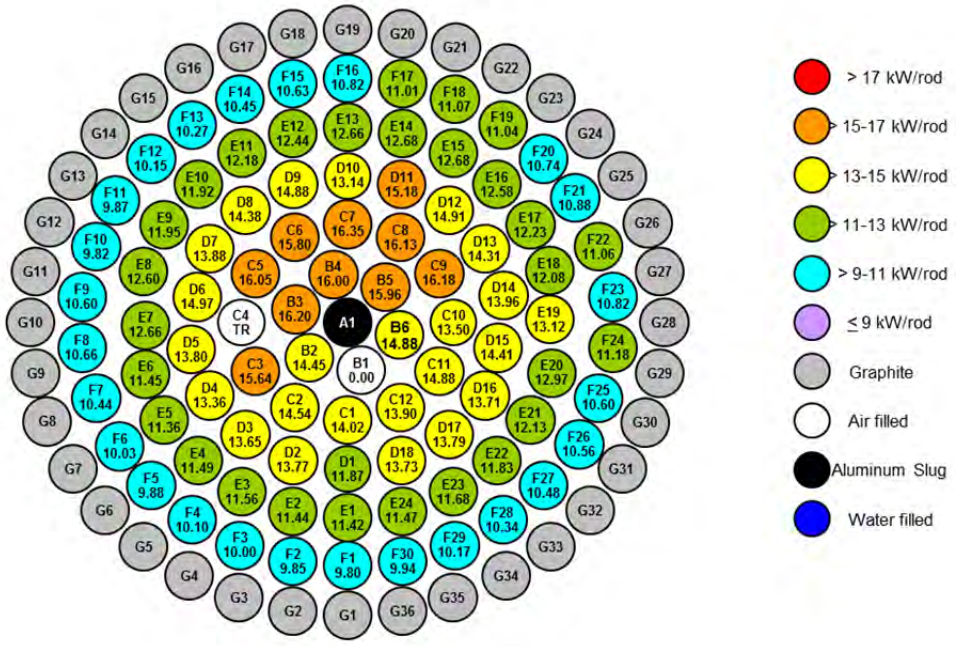

Figure 4.31 Core Power Distribution (LEU EOL CLICIT Core)

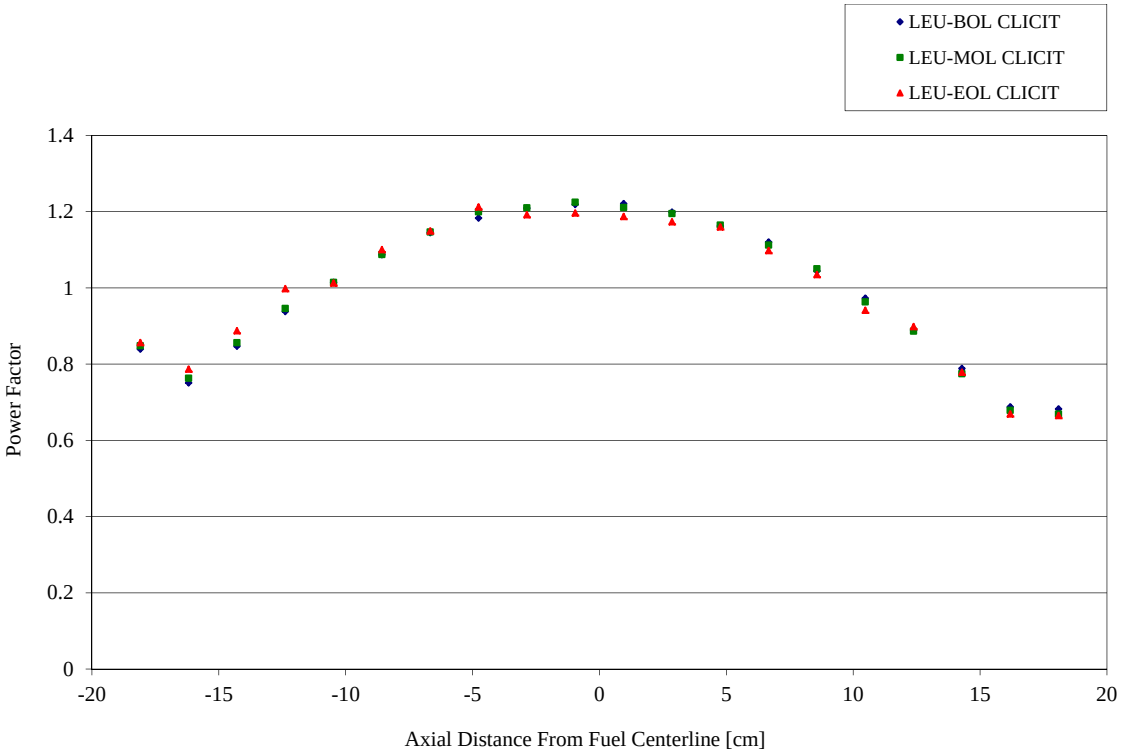

Figure 4.32 Axial Power Factor (LEU CLICIT Core)

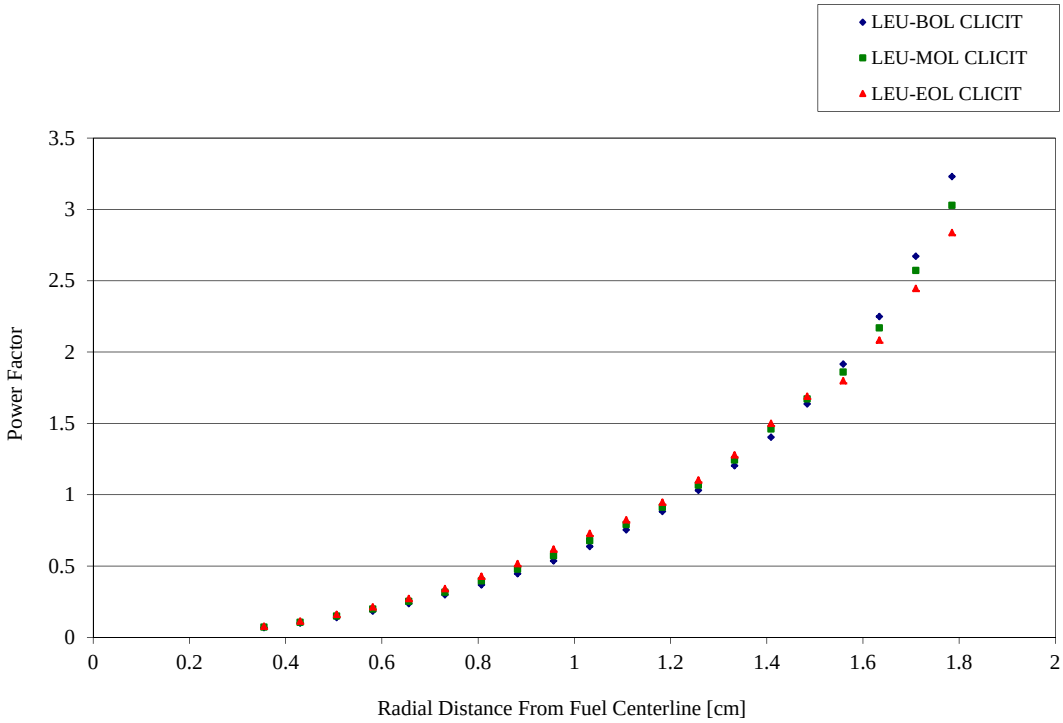

Figure 4.33 Radial Power Factor (LEU CLICIT Core)

The LEU BOL ICIT core has the highest effective power peak factor (2.817) of all the LEU cores, as shown in Table 4-12. All references and results presented for core configurations are based upon the following core life characteristics:

- LEU BOL: ~0 MWdays
- LEU MOL: ~1600 MWdays
- LEU EOL: ~3600 MWdays

For the LEU steady state cores, the ICIT configuration is analyzed in detail. The ICIT core configuration has the highest effective peak factor at BOL, MOL and EOL, and therefore it has the most uneven power distribution. The ICIT cores have the highest peak temperatures, and thus the ICIT core bounds the NORMAL and CLICIT core configurations. For the LEU cores operating in pulse mode, the ICIT core is again analyzed at each stage in life for the same reasons.

Table 4-12 Hot Rod Power Summary

Hot Rod Power Summary						
	Hot Rod Location	Hot Rod Thermal Power [kW]*	Hot Rod Peak Factor [P_{max}/P_{avg}]	Hot Rod Fuel Axial Peak Factor [P_{max}/P_{avg}]	Hot Rod Fuel Radial Peak Factor [P_{max}/P_{avg}]	Effective Peak Factor
HEU-BOL NORMAL Core	B3	18.02	1.393	1.236	1.498	2.579
HEU-MOL NORMAL Core	B6	18.37	1.420	1.209	1.074	1.844
HEU-EOL NORMAL Core	B6	16.48	1.273	1.234	1.280	2.011
LEU-BOL ICIT Core	B6	18.47	1.477	1.221	1.562	2.817
LEU-BOL CLICIT Core	B3	17.03	1.362	1.221	1.536	2.554
LEU-BOL NORMAL Core	B3	17.77	1.422	1.219	1.538	2.666
LEU-MOL ICIT Core	B6	18.52	1.482	1.225	1.434	2.603
LEU-MOL CLICIT Core	B3	17.03	1.363	1.225	1.406	2.348
LEU-MOL NORMAL Core	B3	17.80	1.424	1.222	1.409	2.452
LEU-EOL ICIT Core	B6	17.61	1.409	1.181	1.304	2.170
LEU-EOL CLICIT Core	C7	16.35	1.308	1.212	1.275	2.021
LEU-EOL NORMAL Core	B3	17.02	1.362	1.178	1.267	2.033

* Hot rod thermal power corresponds to core power of 1.1 MW_t.

4.5.14 Effects of Fresh Fuel on Power Distribution

Due to the presence of erbium, fresh fuel acts as a poison with respect to reactivity when replacing a partially burned fuel rod. As a fuel rod is burned, the erbium is consumed faster than the U-235 so the ratio of erbium to U-235 number densities is higher in fresh fuel than in burned fuel. MCNP calculations were run in order to quantify the effect of inserting fresh fuel into a MOL or EOL core. The ICIT core configuration has the highest effective peak factor at all stages of core life, so this core was selected for analysis. Five separate MCNP calculations were performed using the LEU MOL ICIT core. For each run, one of the B-ring fuel elements was replaced with a fresh fuel element. Five similar MCNP runs were also performed using the LEU EOL ICIT core configuration.

Table 4-13 shows the effect of inserting fresh fuel on the power generated in the swapped element. The 'reference' column shows power in the element prior to replacement with fresh fuel. The 'fresh' column shows power in the element after replacement. Note that for the ICIT core, the B-1 position does not contain fuel.

Table 4-13 Power per Element (Swapped Element)

	LEU MOL ICIT		LEU EOL ICIT	
Position	reference (kW)	fresh (kW)	reference (kW)	fresh (kW)
B2	18.08	16.94	17.28	15.06
B3	17.79	16.84	16.91	15.00
B4	17.19	16.12	16.52	14.40
B5	17.39	16.49	16.64	14.50
B6	18.52	17.47	17.61	15.44

Although power in the swapped element is reduced, power in other elements increases to maintain overall core power at 1100kW. The peak power, and hence the effective peak factor is actually higher in each perturbed core than in the original core. The highest power seen in the perturbed LEU MOL ICIT core is 19.55 kW. The highest power seen in the perturbed LEU EOL ICIT core is 19.88 kW. The peak power seen in each perturbed core is shown in Table 4-14, Power per Element (Peak Element). It can be seen from Table 4-14 that replacing any B-ring fuel element in the LEU MOL ICIT or LEU EOL ICIT core results in an increase in the maximum power generated in a single rod over the base (unperturbed) case.

Table 4-14 Power per Element (Peak Element)

	LEU MOL ICIT		LEU EOL ICIT	
Swapped Element	Peak Position	Peak Power (kW)	Peak Position	Peak Power (kW)
None	B6	18.52	B6	17.61
B2	B6	19.35	B6	19.73
B3	B6	19.55	B6	19.88
B4	B6	19.32	B6	19.84
B5	B6	19.42	B6	19.56
B6	B2	18.95	B3	19.31

Thermal hydraulic analysis of the hot channel was based on the assumption that the hot channel is triangular (or hexagonal), and is bordered on all three sides by a fuel rod generating power equal to the hottest rod in the core under analysis. In actuality, flow channels in the hottest regions of the core (inside the D-ring) are either approximately square or triangular, and are bordered by elements of differing powers. If we calculate the average power level in each flow channel inside the D-ring, we find that the power in the theoretical hot channel, which was assumed to be bounding, is slightly lower than the hottest channel in the perturbed core. The theoretical hot channel analyzed in this SAR assumes a power of 18.52 kW in each neighboring fuel element (as seen in the LEU MOL ICIT core). The highest average in any perturbed core flow channel is 18.79 kW which occurs in the square channel bordered by positions B2, B3, C3 and C4. This is an increase of 1.5% over the previous bounding limit, and is unlikely to significantly impact MDNBR or maximum pulse temperature. The average power level in the hottest channel of each core is shown in Table 4-15, Hot Channel Average Power. It should be noted that with the exception of the LEU EOL ICIT channel bordered by B3/C4/C5, each of

these hot channels is actually a square channel, but is only heated by three adjacent elements, and thus the true mathematical average power of the four surrounding structures is actually significantly less than the mathematical average power of the three adjacent heated structures. If this phenomenon is taken into account for all heated channels in each perturbed core, then the average power of each subchannel is less than 18.52 kW in all cases.

Table 4-15 Hot Channel Average Power

LEU MOL ICIT Core			
Swapped Element	Hot Channel		
	Bordered by	Heated by	Avg. Power (kW)
None	B6	B6	18.52
B2	B1/B6/C11/C12	B6/C11/C12	17.96
B3	B1/B6/C11/C12	B6/C11/C12	18.08
B4	B2/B3/C3/C4	B2/B3/C3	18.27
B5	B2/B3/C3/C4	B2/B3/C3	18.27
B6	B2/B3/C3/C4	B2/B3/C3	18.40
LEU EOL ICIT Core			
Swapped Element	Hot Channel		
	Bordered by	Heated by	Avg. Power (kW)
None	B6	B6	17.61
B2	B3/C4/C5	B3/C5	18.36
B3	B1/B6/C11/C12	B6/C11/C12	18.35
B4	B2/B3/C3/C4	B2/B3/C3	18.79
B5	B2/B3/C3/C4	B2/B3/C3	18.78
B6	B2/B3/C3/C4	B2/B3/C3	18.73

Since DNBR is generally considered to be a local phenomenon strongly dependent on heat flux, it is appropriate to examine the impact of peak power in any single rod. As shown above, the highest powered element in any perturbed core is 19.88 kW (LEU EOL ICIT core, B6 position with the B3 element replaced with fresh fuel). In section 4.6.7, LEU End of Life ICIT Core Analysis, we conclude that under our conservative assumptions, MDNBR in the hot channel will reach a value of 2.0 at approximately 20.0 kW hot channel steady state power. A steady state fuel element power of 19.88 kW is thus acceptable. Additionally, in the LEU MOL ICIT core, the maximum perturbed core element power of 19.55 kW is below the 19.85 kW power that would produce a MDNBR ratio of 2.0 in that core.

4.6 Thermal Hydraulic Methodology

The TRIGA® system operating with cooling provided by natural convection water flow around the fuel elements was analyzed. The predicted steady state thermal-hydraulic performance of the OSU HEU core at Beginning of Life operating conditions is determined for the reactor operating at 1.1 MW with a water inlet temperature of 49°C. This analysis is conservative since the maximum license power of the OSTR is 1.1 MW, but the reactor is operated at 1.0 MW with a

high power SCRAM at 1.06 MW. Per the Technical Specifications, the maximum pool temperature is 49°C. Operational data are used for the benchmark comparisons. The maximum power fuel rod and maximum power heated subchannel were analysed under steady-state and transient conditions. The RELAP5-3D computer code [Ref. 4.14] was used to determine the natural convection flow rate, fuel centerline temperature profile, clad temperature profile, axial temperature profile and radial fuel temperature distribution. The power in the hottest rod at which critical heat flux is predicted to occur was calculated with the aid of the RELAP5-3D code. The code was used to calculate coolant flow rate as a function of rod power. The Bernath correlation and the 2006 Groeneveld critical heat flux tables were used to determine the Departure from Nucleate Boiling Ratio (DNBR).

The predicted parameters produced from this code for steady state operation include: channel flow rate, axial fuel centerline temperature distribution, axial clad temperature distribution, axial bulk coolant temperature distribution and axial DNBR. To simplify the RELAP5-3D model, it was assumed that there is no cross flow between adjacent channels. This assumption is conservative since higher values of temperature and lower margins to DNB are predicted when cross flow between adjacent channels is ignored.

One, two, and eight channel RELAP5-3D models were individually analyzed against the HEU BOL core. Cross flow was incorporated in the two and eight channel models through junctions connected at each individual axial nodal location between adjacent subchannels. The axial and radial fuel temperature distributions were assumed to be identical in each model.

Figure 4.34 provides a quantitative comparison of the bulk coolant temperature distribution found in the one, two and eight channel models. This comparison provides evidence that with an increase in the number of subchannels there is an expected corresponding decrease in exit bulk coolant temperature.

The coolant equilibrium quality and subchannel mass flux as a function of axial position are presented in Figure 4.35. These properties, along with system pressure, are the primary parameters for CHF. With an increase in the number of subchannels the mass flux is perturbed greater due to cross flow in the lower axial portion of the core. The equilibrium quality for the single, two, and eight channel models remain similar through the majority of the axial length of the core. As a result of the increased mass flux in the eight channel model near the exit of the subchannel, less energy is deposited into the fluid producing lower equilibrium quality values for the eight channel model relative to the two and one channel models.

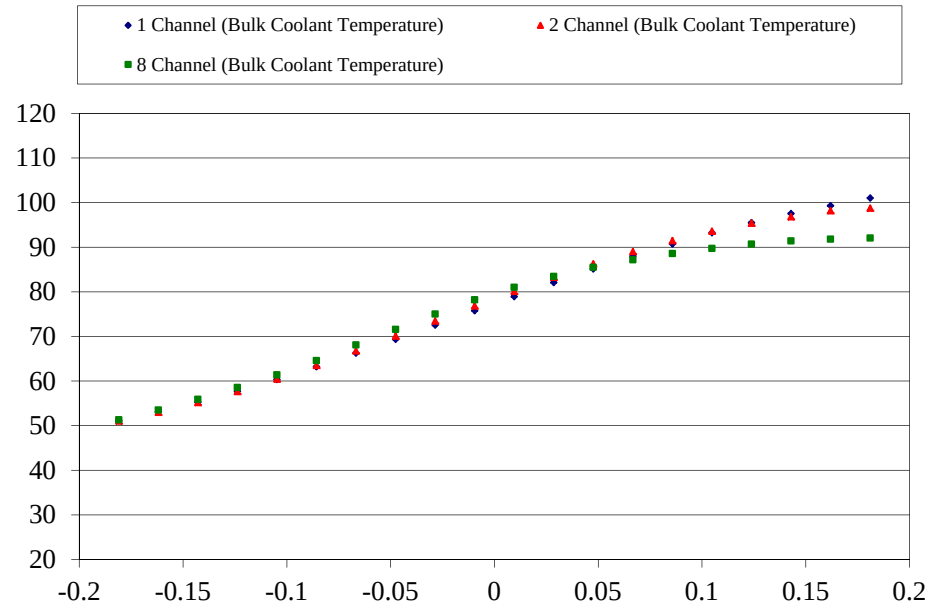

Figure 4.34 Axial Bulk Coolant Temperature Distribution for 1, 2, & 8 Channel Model (HEU Beginning of Life Normal Core)

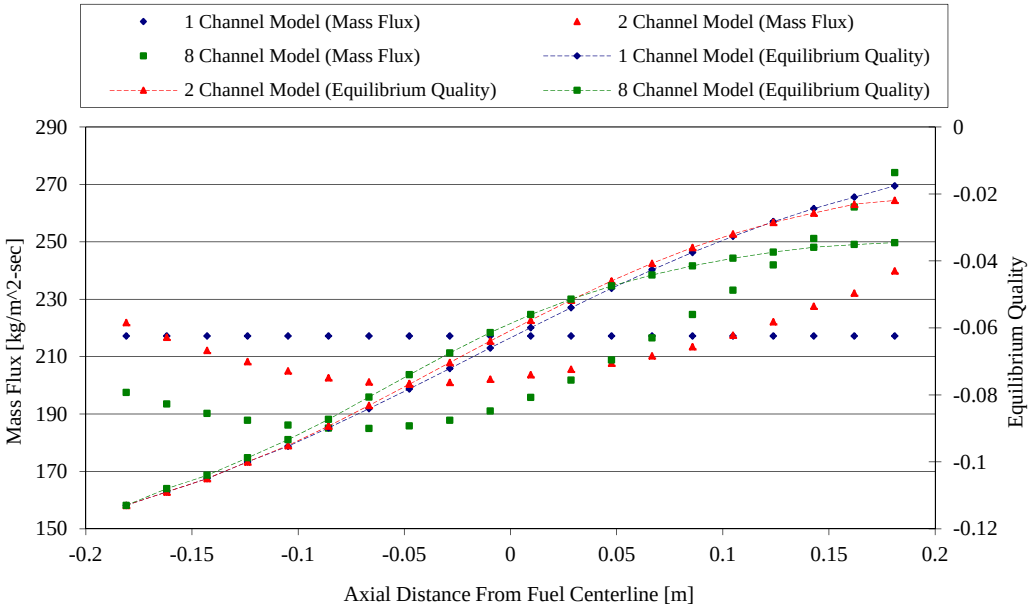

Figure 4-35 Mass Flux and Equilibrium Quality Distribution for 1, 2, & 8 Channel Model (HEU Beginning of Life Normal Core)

Figure 4.36 presents the CHFR determined using the 2006 Groeneveld AECL look-up tables and Bernath correlation for the one, two, and eight channel models. Small differences in the CHFR values for the different models compared can be accounted for by the observations made above.

The exit CHFR value for the eight channel model is larger than for the two channel model, which is larger than the one channel model. This is due to a decrease in equilibrium quality near the exit of the subchannel. Although there are small deviations in the CHFR axial distributions it is important to note that the minimum critical heat flux ratio (MCHFR) differs by only 0.3% on average for the look-up tables and 0.6% for the Bernath correlation. This is well within the error margin associated with each CHF method of calculation.

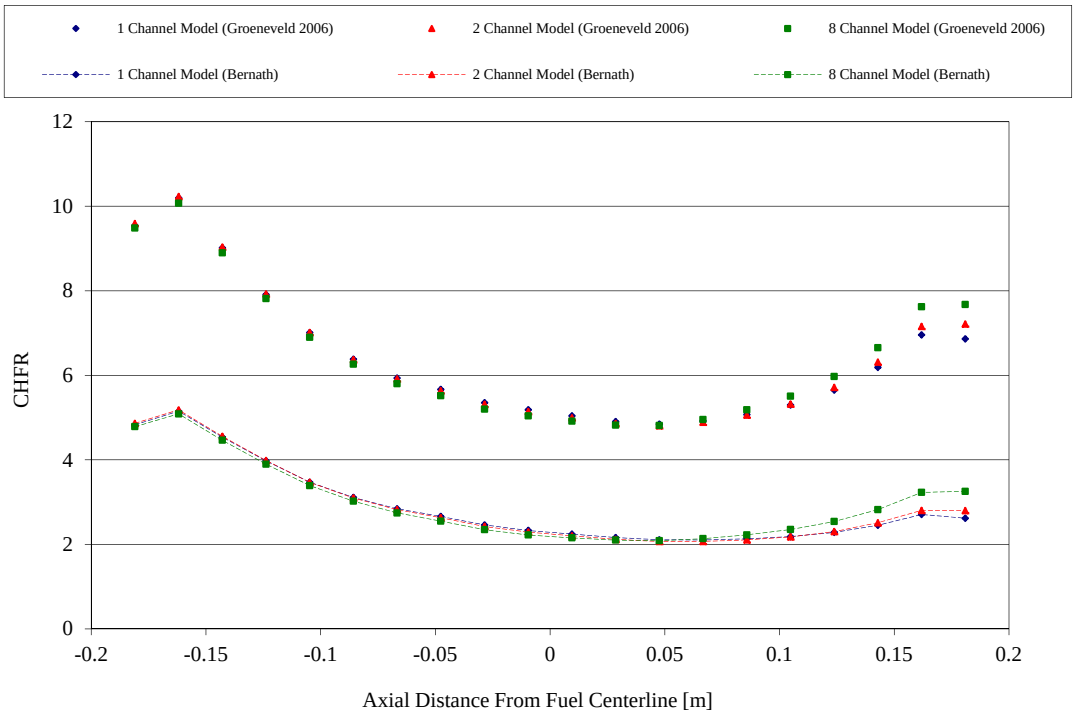

Figure 4.36 Axial CHFR Distribution for 1, 2, & 8 Channel Model (HEU Beginning of Life Normal Core)

Based on a conservative method for safety analysis, the single channel model provides critical heat flux results using the 2006 Groeneveld look-up tables within ~1.0 % of those produced from the eight channel model. The single channel model produced the most conservative results relative to the two and eight channel models.

The parametric inputs into RELAP5-3D include:

1) Inlet coolant temperature
2) System pressure at the top of the core
3) Radial and axial heat source distribution
4) Discretized spacing of heat source nodes
5) Inlet and exit pressure loss coefficients

4.6.1 Thermal Hydraulic Analysis

The analysis was performed using a single flow channel divided into axial segments (nodal distribution is described below). The reactor geometry and hydraulic data for the RELAP5-3D input are given in Table 4-16. The coefficients presented in Table 4-15 come from a study conducted by General Atomics for the OSTR developed a methodology for calculating each effective subchannel form loss rather than local form losses within the core [Ref. 4.15]. Flow channels in the OSTR are triangular, square or irregular, depending on core location. The analysis assumes a triangular rod lattice configuration because the hottest flow channel is shown to occur adjacent to the A and B rings, and in this location, the lattice is triangular.

Table 4-16 RELAP5-3D Input for Reactor and Core Geometry and Heat Transfer

Hydraulic Data	
Inlet pressure loss coefficient	2.26
Exit pressure loss coefficient	0.63
Absolute pressure at the top of the core [Pa]	1.43E5

A constant pressure of 1.01E5 Pa (14.7 psia) is assumed to exist at the top of the reactor pool. The OSTR technical specification requires a minimum water column height above the top of the core to be 4.2672 m (168 inches or 14 feet), so this equivalent water column pressure boundary condition is used in the RELAP5-3D model. RELAP5-3D requires that input pressure conditions be entered as absolute pressure, therefore the input RELAP5-3D pressure used in the model at the top of the core is 1.43E5 Pa (20.7717 psia).

The RELAP5-3D thermal hydraulic analysis was performed on the maximum powered channel. The analysis was conducted assuming (conservatively) that the maximum powered channel was also the most restrictive flow channel location found in the OSTR. The flow parameters for the most restrictive flow channel are given in Table 4.17. The geometry of the maximum powered channel is shown in Figure 4.37.

It is conservatively assumed that all rods bordering the maximum powered subchannel are operating at the same power as the maximum powered rod as determined for each core configuration.

Table 4-17 Hydraulic Flow Parameters for the Hot Channel

Parameter	Value
Flow area [m^2]	3.80E-04
Fuel Element Pitch [m]	0.04064
Wetted perimeter [m]	0.117
Hydraulic diameter [m]	1.301E-02
Heated diameter [m]	3.724E-02
Fuel element heated length [m]	0.381
Fuel element surface area [m^2]	4.469E-02
Fuel element surface roughness [m]	2.134E-06

The B Ring in the OSTR contains the smallest pitch from fuel rod centerline to centerline, and also contains the smallest subchannel flow area. It is for this reason that the subchannel flow area for the RELAP5-3D model is calculated with reference to the B Ring subchannel flow area, depicted in Figure 4.37.

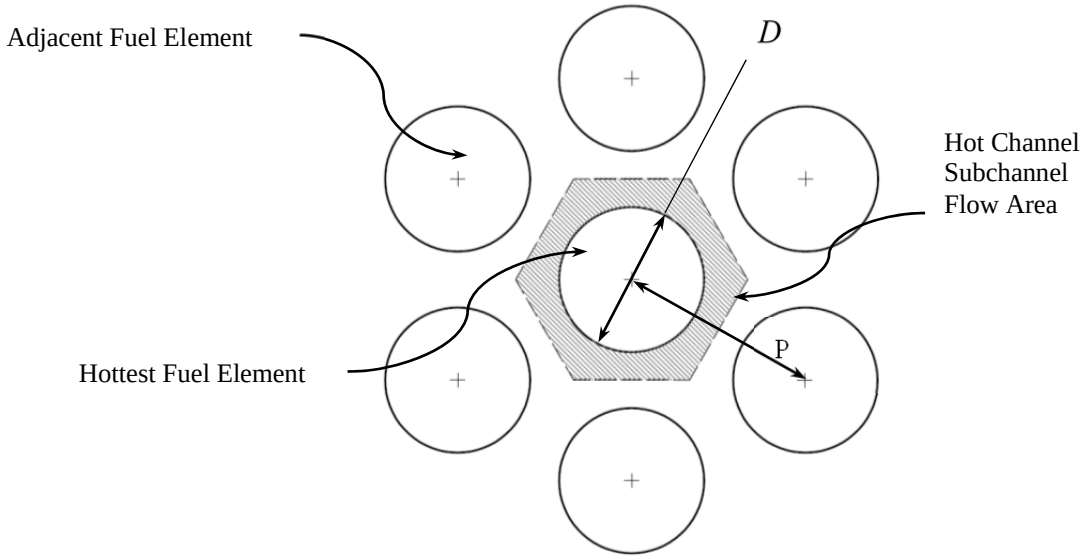

Figure 4.37 Hexagonal Array Axial Average unit subchannel dimensions

The pitch for the B Ring subchannel is 0.04064 m (1.60 in) [Ref. 4.16]. The fuel rod outer diameter for all OSTR core fuel rods is defined as 0.037 m (1.47 in). Equation (27) defines the subchannel flow area for a hexagonal array [Ref. 4.17].

$$A_{fi} = \frac{\sqrt{3}}{4} P^2 - \frac{\pi D^2_{\text{outer clad}}}{8} \qquad (4\text{-}27)$$

where P represents fuel rod pitch and D represents the fuel rod outer diameter. From Equation (27) the subchannel flow area is calculated to be 1.90E-4 m^2 (0.295 in^2).

The wetted perimeter for the subchannel only encompasses one half of an entire fuel rod in the Figure 4.37 above. Therefore the total flow area for the subchannel input into the RELAP5-3D model is 3.80E-4 m^2 (0.589 in^2).

The fuel element heated surface area in the RELAP5-3D model was calculated by referring to Figure 4.1. The axial length of the fueled portion of the fuel rod is 0.381 m. (15.0 in) while the diameter of the outer cladding is 0.037 m (1.47 in). The total surface area of the fueled portion of the fuel rod is therefore 4.469E-2 m^2 (69.27 in^2).

The wetted perimeter is defined as $P_{\text{wetted}} = \pi D_{\text{outer clad}}$. This equation produces a value of 0.117 m (4.618 in) for the wetted perimeter of a fuel rod.

The hydraulic diameter is calculated per Equation (28). With reference to the previously calculated wetted perimeter and subchannel flow area, the hydraulic diameter is calculated to be 1.301E-2 m (0.512 in).

$$D_h = \frac{4A_{fi}}{P_{wetted}} \tag{4-28}$$

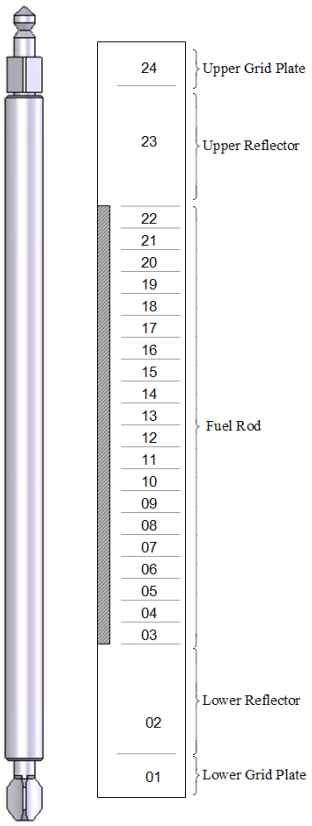

Figure 4.38 Comparison of OSTR Fuel Rod Axial Characteristics and RELAP5-3D Hot Channel

Figure 4.38 shows a comparison between a physical OSTR fuel element and the RELAP5-3D discretized subchannel volume. Node dimensions are given. in Table 4-17. Nodes 01 and 24 represent the lower and upper grid plates. The lower grid plate is 0.0191 m (0.75 in) thick. The upper gridplate is 0.0159 m (0.625 in) thick. The bottom surface of the upper grid plate is 0.6731 m (26.5 in) above the top surface of the lower grid plate [Ref. 4.18]. The fuel element axial nodal dimensions are given in Table 4-18.

Node 02 extends from the bottom of the fuelled portion of the fuel rod to the top of the lower gridplate. The equation used to calculate the length of Node 02 (lower unheated node) is:

$$L_{02} = \frac{\left(0.6731 - L_{fuel} - L_{Upper,graphite} - L_{Lower,graphite}\right)}{2} + L_{Lower,graphite} \quad (4\text{-}29)$$

where:

L_{02} is the length of Node 02 and $L_{Upper,graphite}$ and $L_{Lower,graphite}$ are the upper and lower graphite lengths of the fuel element.

From Table 4-18 the fuel nodal lengths must be discretized accordingly and this can be done by use of Equation (30) for Nodes 03 through 22:

$$L_{03\rightarrow 22} = \frac{L_{fuel}}{n_{fuel}} \quad (4\text{-}30)$$

$L_{03\rightarrow 22}$ refers to the nodal length for Nodes 03 through 22, n_{fuel} is the number of nodes defined in the fuel region (i.e. 20 nodes).

Equation (31) is used to calculate the nodal length for Node 23 (upper unheated node).

$$L_{23} = \frac{\left(0.6731 - L_{fuel} - L_{Upper,graphite} - L_{Lower,graphite}\right)}{2} + L_{Upper,graphite} \quad (4\text{-}31)$$

Table 4-18 Hot Channel Axial Nodal Lengths

Core Volume Axial Nodal Lengths		
Nodal Description	Node Number	Nodal Length [m] (in)
Upper Grid Plate	24	0.01905 (0.75000)
Upper Graphite	23	0.14567 (5.73504)
Fuel	22	0.01905 (0.75000)
	21	0.01905 (0.75000)
	20	0.01905 (0.75000)
	19	0.01905 (0.75000)
	18	0.01905 (0.75000)
	17	0.01905 (0.75000)
	16	0.01905 (0.75000)
	15	0.01905 (0.75000)
	14	0.01905 (0.75000)
	13	0.01905 (0.75000)
	12	0.01905 (0.75000)
	11	0.01905 (0.75000)
	10	0.01905 (0.75000)
	09	0.01905 (0.75000)
	08	0.01905 (0.75000)
	07	0.01905 (0.75000)
	06	0.01905 (0.75000)
	05	0.01905 (0.75000)
	04	0.01905 (0.75000)
	03	0.01905 (0.75000)
Lower Graphite	02	0.14643 (5.76504)
Lower Grid Plate	01	0.01905 (0.75000)

A cross sectional view of a fuel element is shown in Figure 4.39. The radial nodal distribution is shown in Figure 4.40. The fuel portion of the fuel pin consists of an annular U/ZrH/Er casting. The fuel slugs are hydrided and then forced into stainless steel tubes. The central void which aids the hydriding process is backfilled with a zirconium plug. A nominal gap exists between the fuel slug and the stainless steel clad. This gap is initially filled with air, but as burnup of the fuel progresses, hydrogen and fission gasses migrate into the gap.

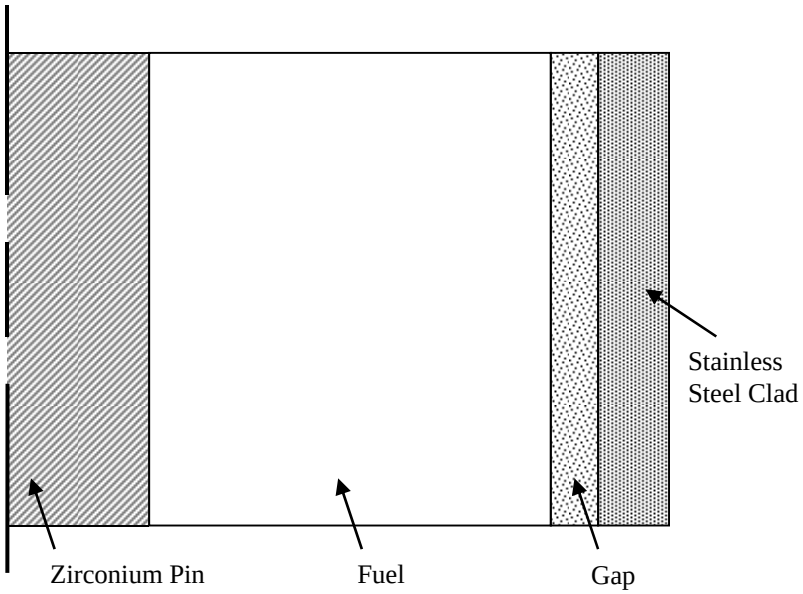

Figure 4.39 Cross Sectional View of Fuel Element

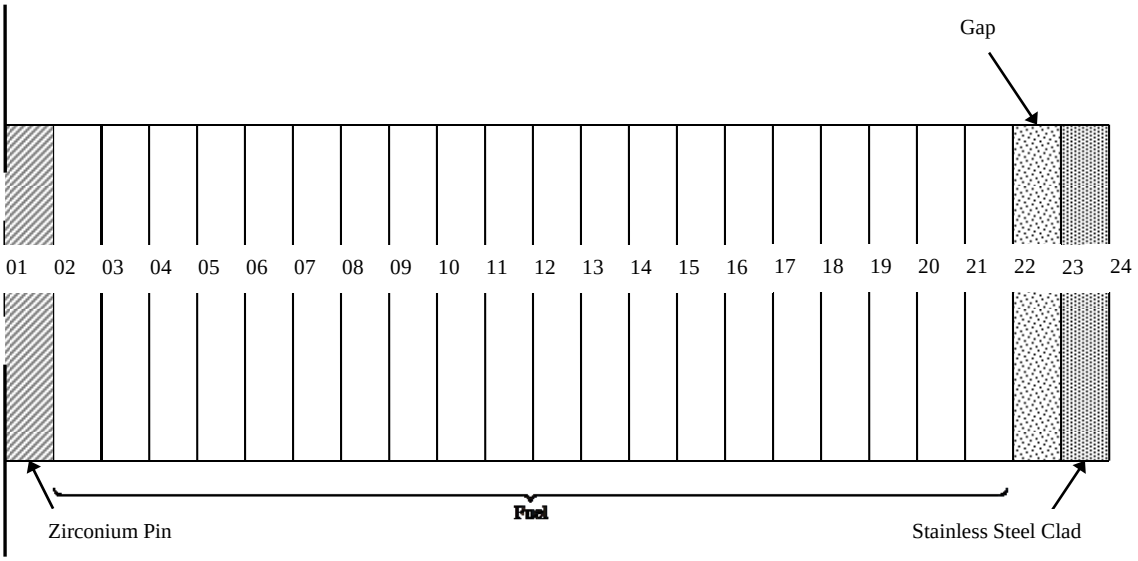

Figure 4.40 Radial Nodal Distribution in a Fuel Element

The mesh points within the fuel region used in the RELAP5-3D model correspond to one node for the central zirconium pin, twenty nodes of equal radial thickness for the fuel meat, one node for the fuel to clad gap and one node for the clad. The radial location of each node is identified in Table 4-19. The outer gap coordinate (Node 22) is varied during this study to simulate different gap widths. Several references for TRIGA® fuel identify that the gap between the stainless steel and the fuel can vary from 1.27E-4 to 1.016E-3 m (0.05 to 0.4 mils). RELAP5-3D input requires that radial mesh points be defined in order to specify all material properties and to calculate temperature gradients within the heat structure. All CHF correlations considered during the analysis use the heat flux of the outer cladding at a given nodal location. Because of this the outer cladding serves as both the wetted diameter and the heated diameter for the bernath correlation ($D_H = D_{outer\ clad}$ = 3.724E-02 meters).

Table 4-19 Radial Fuel Element Nodal Locations (from fuel center)

Heat Structure Radial Node Lengths		
Nodal Description	Node Number	Node Coordinate [m] (in)
Inner Zirconium Pin	01	0.00000 (0.00000)
	02	0.00318 (0.12500)
Fuel	03	0.00355 (0.13976)
	04	0.00430 (0.16929)
	05	0.00506 (0.19921)
	06	0.00581 (0.22874)
	07	0.00656 (0.25827)
	08	0.00731 (0.28779)
	09	0.00807 (0.31772)
	10	0.00882 (0.34724)
	11	0.00957 (0.37677)
	12	0.01032 (0.40630)
	13	0.01108 (0.43622)
	14	0.01183 (0.46575)
	15	0.01258 (0.49527)
	16	0.01333 (0.52480)
	17	0.01409 (0.55472)
	18	0.01484 (0.58425)
	19	0.01559 (0.61378)
	20	0.01634 (0.64331)
	21	0.01710 (0.67323)
	22	0.01785 (0.70275)
Outer Gap	23	0.01785-0.01786 (0.70285-0.70305)
Outer Stainless Steel Clad	24	0.01873 (0.73750)

Power peaking factors for each core configuration were analyzed using MCNP5. The highest power rod for each configuration was determined by calculating the total power produced in each fuel element present in the configuration. After the highest power rod had been determined, further analyses were performed to find the detailed axial and radial power shapes associated with that rod. The axial and radial power shapes were determined for twenty equally spaced nodes in both the axial and radial directions. The MCNP5 results were used to calculate three peaking factors:

Hot Channel Peak Factor = (maximum fuel rod power)/(core average fuel rod power)

Hot channel Fuel Axial Peak Factor = (maximum axial power in the hot rod)/(average axial power in the hot rod)

Hot Channel Fuel Radial Peak Factor = (maximum radial power in the hot rod)/(average radial power in the hot rod)

It is crucial that average fuel rod power in the core, average axial power in the hot rod and average radial power in the hot rod be properly calculated in order to obtain correct peak factors. The average fuel rod power in the core is calculated by taking the numerical average with each rod weighted equally. The fission rate in the hot rod is then calculated as discussed above and expressed in cylindrical (r,z) coordinates. The average axial power in the hot rod is calculated by taking the numerical average of the power density within each of the twenty axial segments.

The effective peak factor for each configuration is the product of these three individual peaking factors. The results of the MCNP5 analyses for the various core configurations, listing the location of the highest power rod along with its associated peaking factors, are summarized in Table 4-11 for the LEU core. Note that these peaking factors are calculated for cores with control rods removed. This is conservative since the presence of control rods in the central regions of a core will result in flatter power distributions and lower hot channel peak factors.

It was assumed that all rods in the core have approximately the same axial heat distribution shape, and thus the maximum powered rod would produce the maximum local heat flux. Although minor variations in axial power shape occur throughout the core, we made the conservative assumption that the hot channel is bordered on all sides by a fuel rod having the same characteristics as the hot rod. In reality, the hot channel will likely be bordered by the hot rod, and two other rods of lower power. Thus even in the unlikely event that the maximum heat flux does not occur in the hot rod, the conditions in the hot channel are still expected to bound conditions at all other points in the core.

Two Critical Heat Flux correlations were used in conjunction with this study; the 2006 AECL Groeneveld Look-up Tables [Ref. 4.19], and the Bernath [Ref. 4.20] correlation. These correlations were implemented as discussed below.

4.6.2 AECL Groeneveld Look-up Tables

$$CHF = f\left(G, X_e, P_{abs}, \text{geometry}\right) \tag{4-32}$$

By interpolating in the Groeneveld look-up tables given the mass flux (G), equilibrium quality (X_e) and absolute pressure (P_{abs}) produced in the RELAP5-3D model, a critical heat flux value for the system is produced (CHF_{int}). The appropriate correction factors, K_1 to K_6, must then be multiplied by the interpolated CHF value.

$$CHF = K_1 \cdot K_2 \cdot K_3 \cdot K_4 \cdot K_5 \cdot K_6 \cdot CHF_{\text{int}} \tag{4-33}$$

Three correction factors affect the CA SAR: K_1, K_2, and K_4. The other correction factors are assumed to have a value of one.

$$K_1 = \left(\frac{0.008}{D_h} \right)^{\frac{1}{2}}, \tag{4-34}$$

where:

the hydraulic diameter is measured in meters.

$$K_2 = \min\left[0.8, 0.8 \cdot \exp\left(-0.5 X_e^{(1/3)} \right) \right], \tag{4-35}$$

where:

X_e is the equilibrium quality. If X_e is less than zero, it is set to zero.

$$K_4 = \exp\left(\frac{D_H}{L} e^{2\alpha} \right), \tag{4-36}$$

where:

$$\alpha = \frac{X_e}{\left[X_e + \frac{\rho_g}{\rho_l (1 - X_e)} \right]} \tag{4-37}$$

and L [meters] is the distance from the start of the heated length to the middle of the node. If D_H/L is greater than 0.2, it is set to 0.2. The quantities ρ_l and ρ_g [kg/m^3] are the liquid density and gas density respectively, while D_H is the heated diameter [meters].

In 1986 Groeneveld et al. developed a critical heat flux (CHF) prediction method by compiling the world's CHF data for water and relating it to a corresponding mass flux, equilibrium quality, and pressure. By interpolating in the Groeneveld look-up tables using these parameters one can acquire a predicted CHF value. This value corresponds to a tube of diameter 0.008 meters uniformly heated on the inner surface. In order to adapt this CHF prediction for systems other than the geometry described above, six correction factors have been added to the interpolated CHF value. These correction factors allow for the adaption of a single 8 millimeter cylinder to be broadened to incorporate phenomena such as a change in hydraulic diameter (K_1), rod bundle effects (K_2) such as cross flux and additional surface friction, grid plate spacer dependency (K_3), Axial heated position to include phase change dependence (K_4), Axial flux distribution factor (K_5) to account for non-uniform axial heat distributions, vertical/horizontal orientation factor (K_6) to account for gravitational effects associated with flow regimes.

Three of the six correction factors were used (K_1, K_2, and K_4). All other correction factors were assumed to be equal to or very close to 1.0 such that there impact on the final CHFR is insignificant. K_3 was neglected because the OSTR has an upper and lower grid plate only, no grid spacers are found in the axially heated region of interest, therefore K_3 is equal to 1.0. K_5 was

neglected because it is only applied under conditions in which the equilibrium quality is greater than zero. All departure from nucleate boiling circumstances for the OSTR occur in negative equilibrium quality values. Therefore the K_5 factor is not applicable under OSTR operating conditions and is assumed to be equal to 1.0. K_6 corrects for flow direction only if the flow direction opposes the gravitational buoyancy directions (i.e. forced downward convection). Because the OSTR operates under natural circulation where the primary coolant velocity is in the positive vertical direction (upward vertical direction) K_6 is not a valid correction factor to apply under the OSTR's operational conditions and is therefore assumed to be equal to 1.0.

Three correction factors apply to the OSTR under operational conditions; K_1 corrects for the change in hydraulic diameter from 0.008 meters and an inner heater surface to a 0.001301 meter hydraulic diameter with an outer heated surface (i.e. external flow). K_2 predicts the correct trend of equilibrium quality, and must be taken into consideration because the OSTR operates under low flow, upward vertical conditions in which the equilibrium quality has a significant impact on the final CHF prediction value. K_4 significantly affects the final CHF prediction value because it predicts the phase change effects from liquid to vapor in the subchannel as a function of axial position. By incorporating K_4, the CHF prediction value incorporates the additional buoyancy and velocity effects due to subchannel vapor, which has potential to increase the predicted CHF value.

All of the descriptions provided for the Groeneveld correction factors are presented in the original 1986 AECL-UO paper [Ref. 4.26]. An investigation by Argonne National Laboratory further supported the correction factors used during the steady state analysis for the OSTR under operational conditions [Ref. 4.27].

4.6.3 The Bernath Correlation

CHF is defined in units of pound- centigrade per hr-ft^2 per the following equations.

$$CHF = h_{BO}\left(T_{w_{BO}} - T_b\right) \tag{4-38}$$

$$h_{BO} = 10890\left(\frac{D_h}{D_h + D_H}\right) + \Delta v \tag{4-39}$$

$$\Delta = \begin{cases} \dfrac{48}{D_h^{0.6}} & \text{if } D_h \leq 0.1 \text{ ft} \\ \dfrac{10}{D_h} + 90 & \text{if } D_h \geq 0.1 \text{ ft} \end{cases} \tag{4-40}$$

$$T_{w_{BO}} = 57\ln\left(P_{abs}\right) - 54\left(\frac{P_{abs}}{P_{abs} + 15}\right) - \frac{v}{4} \tag{4-41}$$

where:

h_{BO}	Limiting film coefficient [p.c.u./hr-ft^2-°C]
T_b	Fluid bulk temperature [°C]
$T_{w_{BO}}$	Wall temperature at CHF [°C]
v	Fluid velocity [ft/sec]
Δ	"slope"
P_{abs}	Absolute pressure [psi]
D_H	Heated diameter [ft]
D_h	Hydraulic diameter [ft]

Six different methods for calculating critical heat flux with reference to the core conversion study were considered. In order to quantitatively compare the relationship of these correlations, the HEU Beginning of Life NORMAL core was chosen for analysis.

RELAP5-3D internally calculates the critical heat flux with reference to the 1986 AECL Groeneveld look-up tables. All other correlations were calculated externally using the thermal hydraulic properties resulting from the RELAP5-3D model. In order to verify that these external calculations were being completed in the correct manner, the critical heat flux was calculated externally with reference to the 1986 AECL Groeneveld look-up tables. The result of this comparison is shown in Figure 4.41. The external calculations produced values that deviated from those conducted in RELAP5-3D by ~1.0% on the conservative side. The deviation was potentially caused by round off error. Qualitatively, this deviation was estimated to be within an acceptable margin. The axial CHFR distribution for the RELAP5-3D internally calculated values as well as all external calculated values are presented in Figure 4.41.

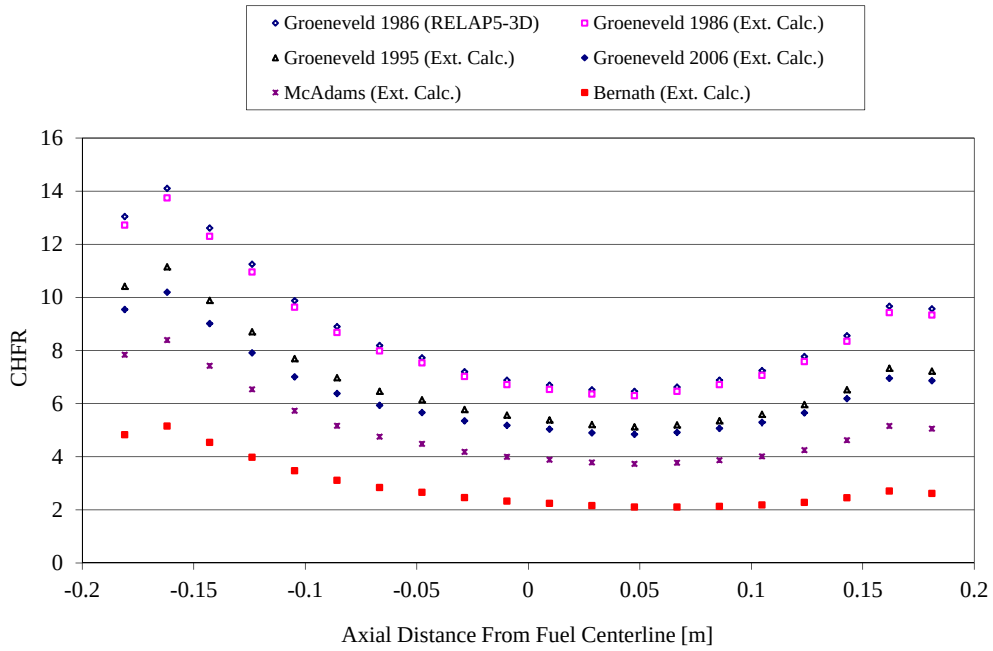

Figure 4.41 Axial CHFR Distribution, Correlation Comparison

As presented in Figure 4.41, the 1986 AECL Groeneveld look-up tables produce the least conservative CHFR distribution values, followed by the 1995 and 2006 Tables. The McAdams correlation and Bernath correlation, produce the most conservative CHFR distribution values. Based on the results presented in Figure 4.41, the 2006 Groeneveld look-up tables and the Bernath correlation were used in this analysis and for the following reasons:

Bernath -

- It is traditionally used as a supplement in research reactor SARs with respect to the RERTR program including the recent submission of the Washington State University Research Reactor [Ref. 4.23].
- The correlation produces the most limiting CHFR values over all other correlations considered during this study.

2006 AECL Groeneveld look-up Tables –

- The correlation is the most current method for calculating CHF values over all others considered during this study.

4.6.4 Fuel Meat to Cladding Gap Size

At 1.1 MW_{th}, the HEU BOL NORMAL core has a corresponding 18.02 kW hot rod in the B3 position. For the HEU Beginning of Life core at a power of 1.0 MW_{th}, the temperature measured at the IFE (B4 position) ranged from 356°C to 373°C. Predicted IFE power at 1.0 MW_{th} is $17.39(1.0/1.1) = 15.81$ kW. A RELAP5-3D model was run, simulating the IFE (located in grid position B-1) at 15.81kW while using a gap thickness of 0.1 mills and produced Figure 4.42. Predicted steady state IFE temperature is larger than measured steady state IFE temperature by approximately 17°C or 34°C, depending on which IFE temperature is used from Table 4-19. Use of a 0.1 mil gap is thus conservative, and therefore all other core calculations use a gap thickness of 0.1 mills.

The content of the gap gases was chosen to be the default setting for RELAP which assumes a mixture of He, Kr, and Xe at molar fractions of 0.1066, 0.134 and 0.7594, respectively. Although the backfill gas at the BOL for TRIGA® fuel is air, the content at MOL and EOL is unknown. However, because of the difference in thermal conductivity between the gas mixtures is different, the default RELAP mixture will produce higher fuel temperatures and is therefore conservative.

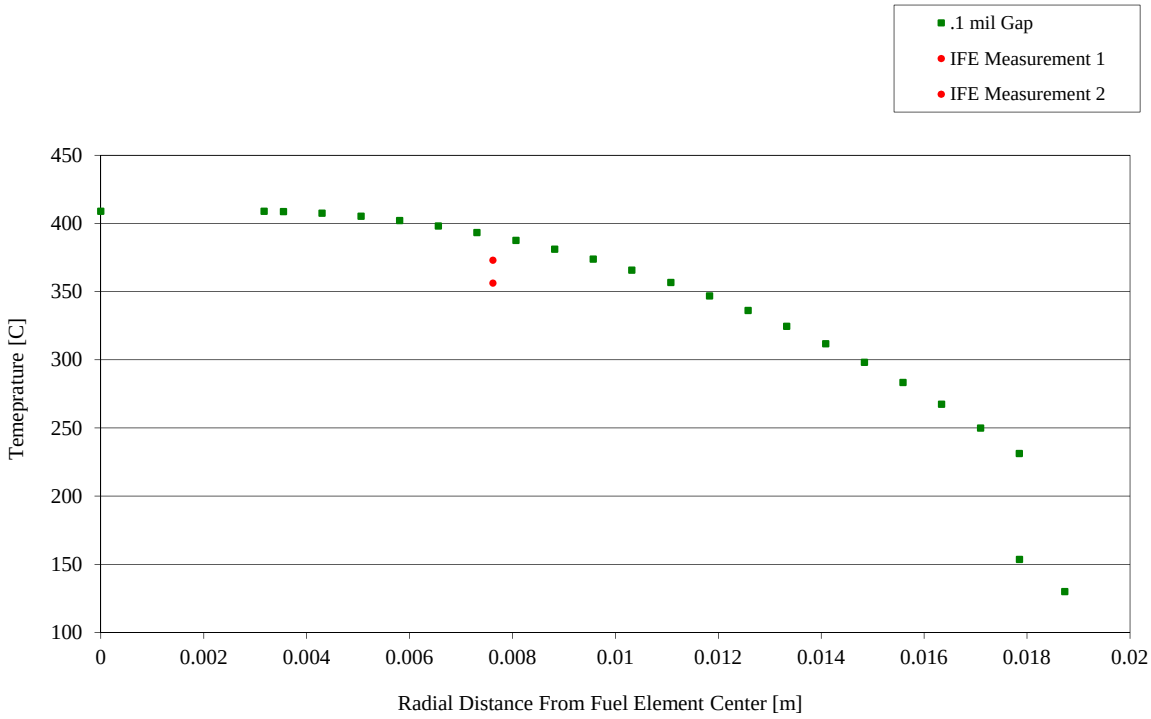

Figure 4.42 IFE Radial Temperature Distribution at 15.81 kW (HEU-BOL NORMAL Core)

The radial temperature distribution in the hot rod at the hottest axial elevation is shown in Figure 4.43. Figure 4.44 shows the radial temperature distribution in the hot rod with a core power of 1.1 MW_{th}. The different curves correspond to different values of the fuel to clad gap ranging from 1.27E-4 to 1.016E-3 m (0.05 to 0.4 mils). The hot rod in the BOL HEU core is located in position B3. The Instrumented Fuel Element (IFE) in the BOL HEU core was located in position B4. A summary of the HEU Beginning of life core temperature results is shown in Table 4-20. These results are based on a 0.1 mil fuel to clad gap. The gap properties were held constant over time for this analysis.

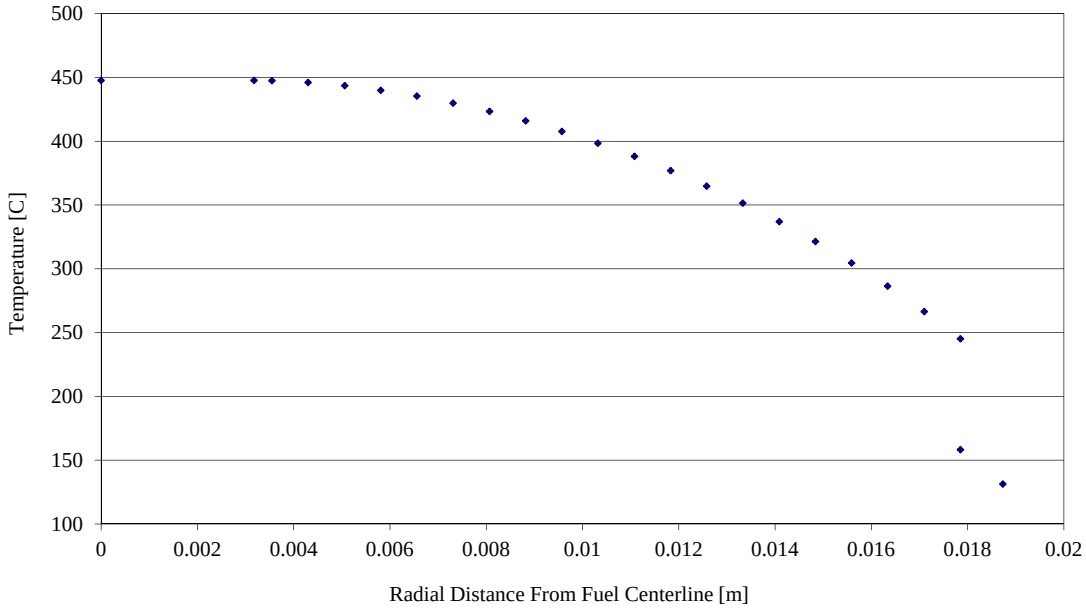

Figure 4.43 Radial Fuel Temperature Distribution at 18.02 kW (HEU-BOL NORMAL Core)

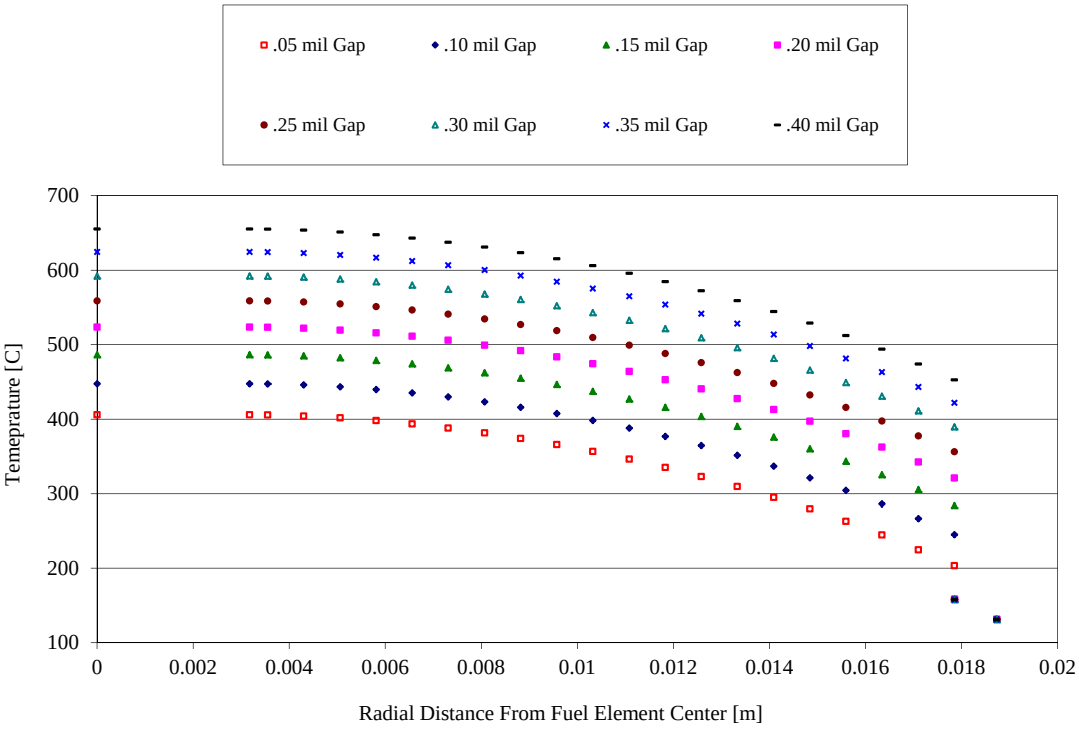

Figure 4.44 Fuel Element Radial Temperature Distribution at 1.1 MW_{th}

For pulse calculations a 0.1 mil gap is also justified. Pulse characteristics are typically adiabatic and thus insensitive to gap size. Furthermore, at the high fuel temperatures expected during the limiting pulse, differential radial expansion will significantly reduce gap size.

Table 4-20 Calculated and Measured Fuel Temperatures

$P_{hot\text{-}channel}$ (kW)	Measured [°C]	Calculated [°C]			
	T_{IFE}	T_{max}	$T_{0.3}$	T_{clad}	$T_{coolant}$
14.00	356, 373*	377	360	129	95
16.00		412	394	130	99
18.02		448	427	131	101
20.00		482	459	132	102
22.00		517	491	133	103

* Initial measured values, HEU BOL NORMAL core at 1.0 MW_{th}.

4.6.5 LEU Beginning of Life ICIT Core Thermal Hydraulic Analysis

All LEU core configurations (NORMAL, ICIT and CLICIT) contain fuel elements that are geometrically similar and therefore the hot channel geometric parameters (i.e. hydraulic diameter, length, etc.) do not change. The hot channel power summary in terms of parameters and results are given in Table 4-21 and Table 4-22, respectively.

Figures 4.45 through 4.49 graphically illustrate the results of the analysis on the LEU ICIT BOL core.

Each parameter in Figure 4.45 is taken at a different elevation in the hot subchannel. The fuel centerline temperature is shown at the axial nodal location which produces the maximum fuel centerline temperature (fuel axial center). The outer cladding temperature is shown at the axial location which produces the maximum outer cladding temperature (slightly above the axial fuel centerline). The bulk coolant temperature is shown at the location which produces the maximum bulk coolant temperature (highest vertical subchannel node). Coolant mass flux is shown as the mass flux which corresponds to the maximum bulk coolant temperature (highest vertical subchannel node). Each location was selected to show the most limiting value of the associated parameter.

Table 4-21 Steady State Results for LEU BOL ICIT core at 1.1 MW_{th}

Parameter	Value
Flow rate for hottest rod [kg/s]	0.0843
Maximum flow velocity [m/s]	0.2339
Maximum wall heat flux [kW/m^2]	504.49
Maximum fuel centerline temperature [°C]	448.13
Maximum clad temperature [°C]	131.93
Exit clad temperature [°C]	126.36
Exit bulk coolant temperature [°C]	101.32
MDNBR [Groeneveld 2006, Bernath]	4.796, 2.083

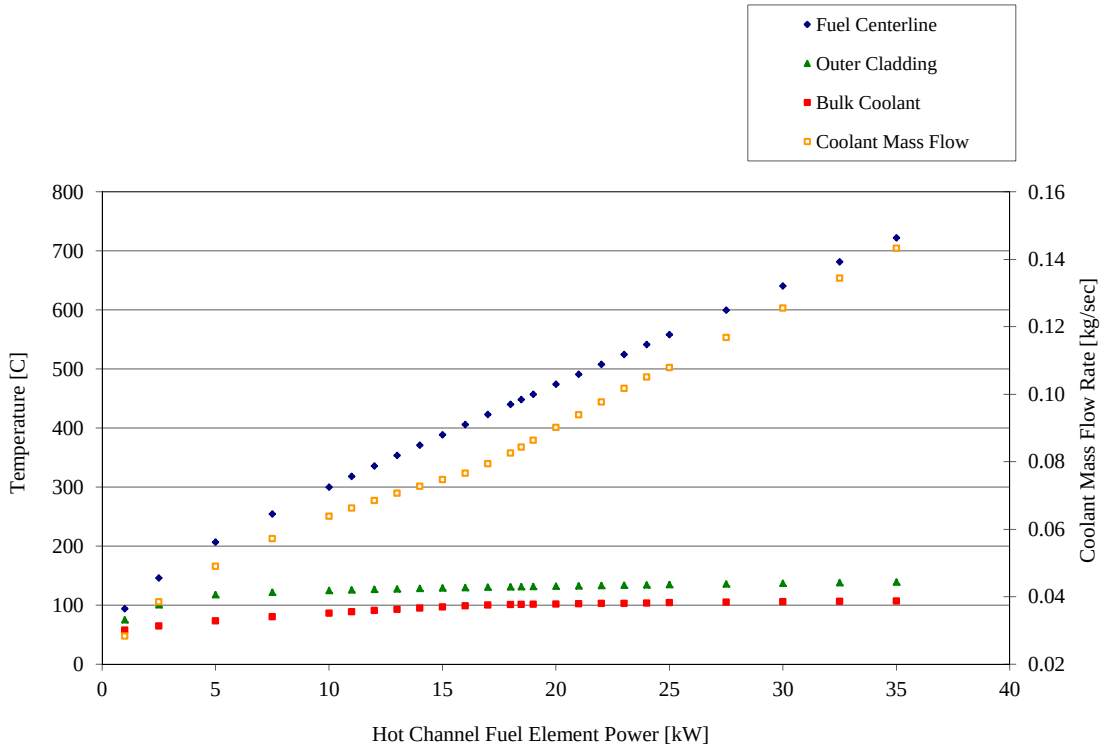

Figure 4.45 Hot Channel Properties (LEU BOL ICIT Core)

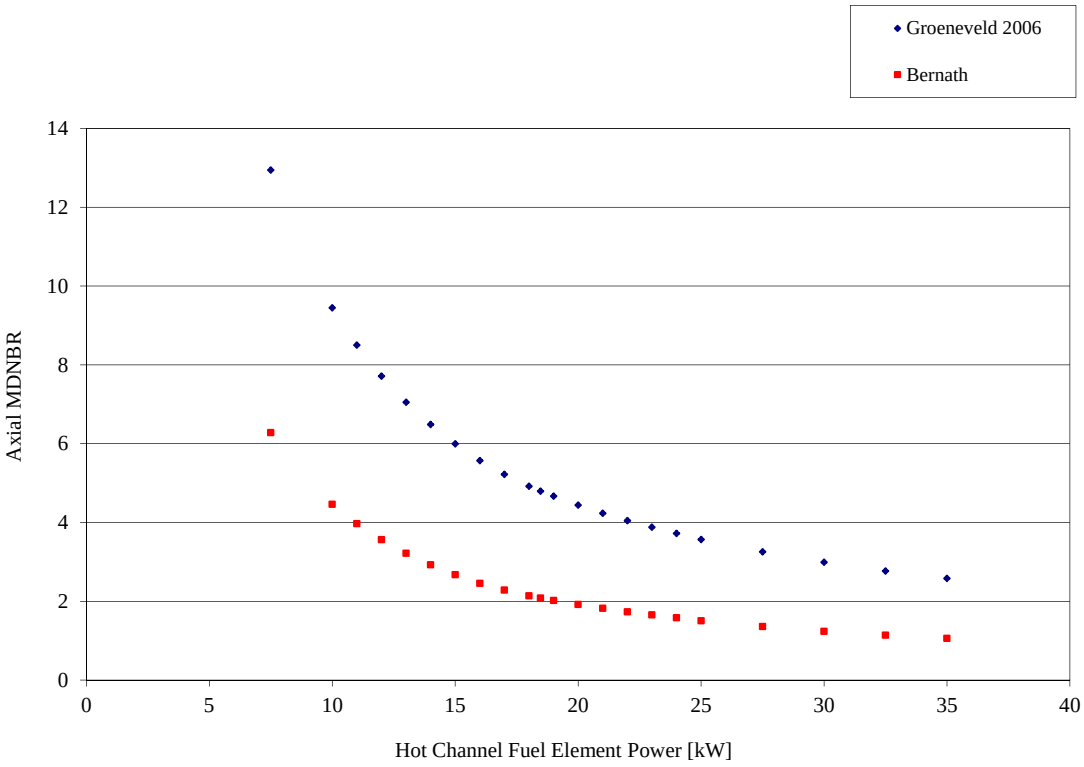

Figure 4.46 Hot Channel MDNBR (LEU BOL ICIT Core)

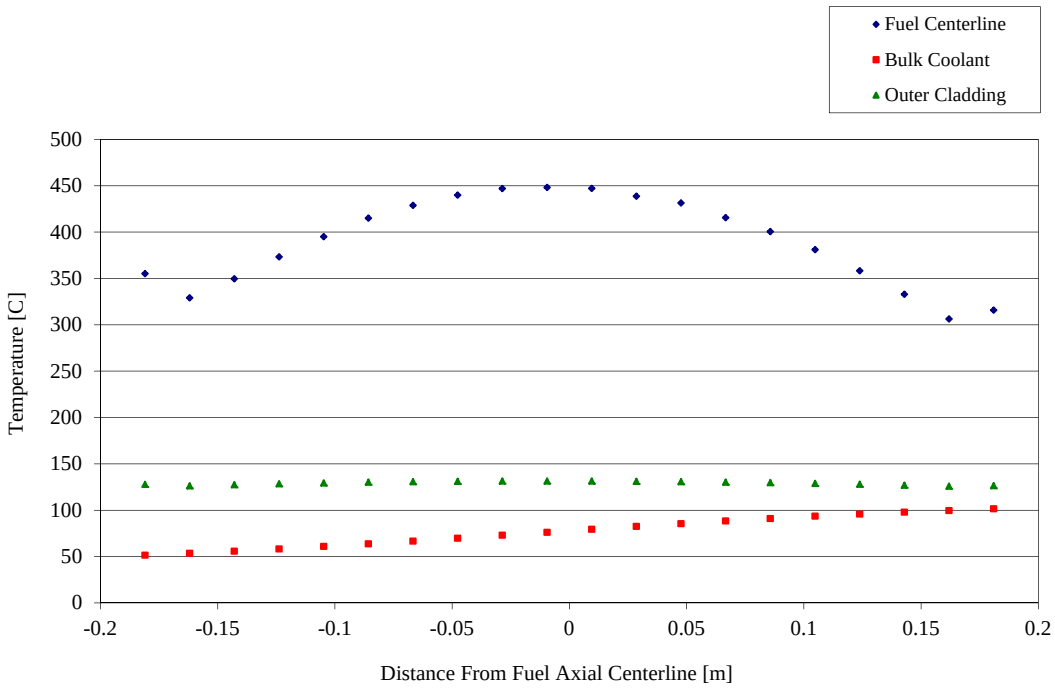

Figure 4.47 Axial Temperature Distribution at 18.47 kW (LEU BOL ICIT Core)

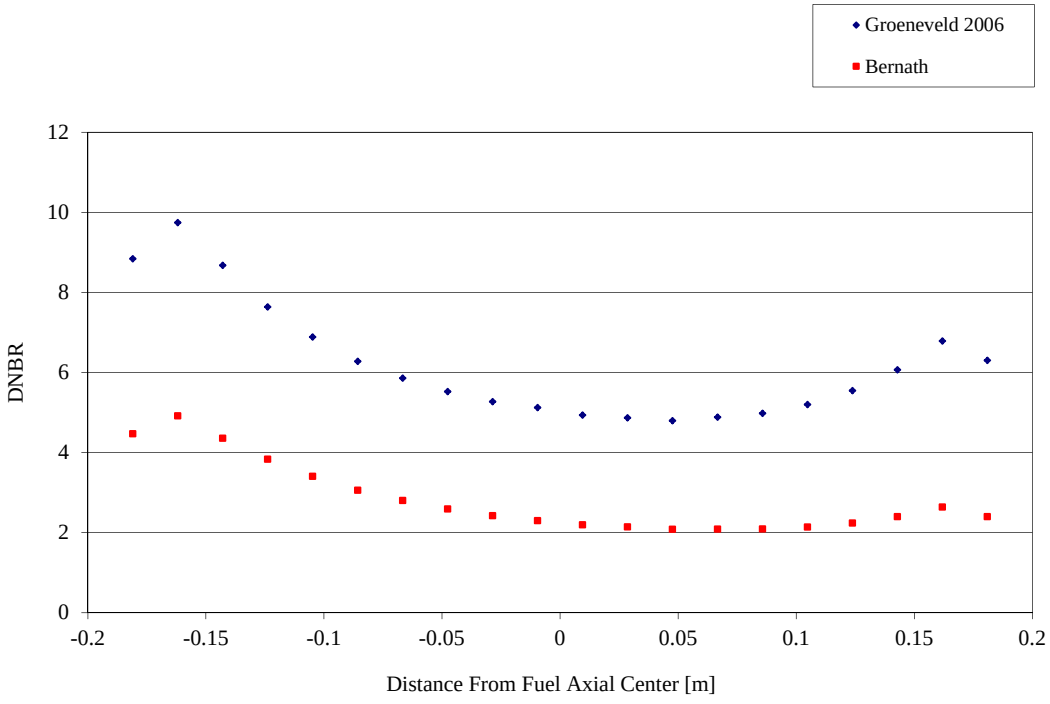

Figure 4.48 Hot Channel Axial DNBR at 18.47 kW (LEU BOL ICIT Core)

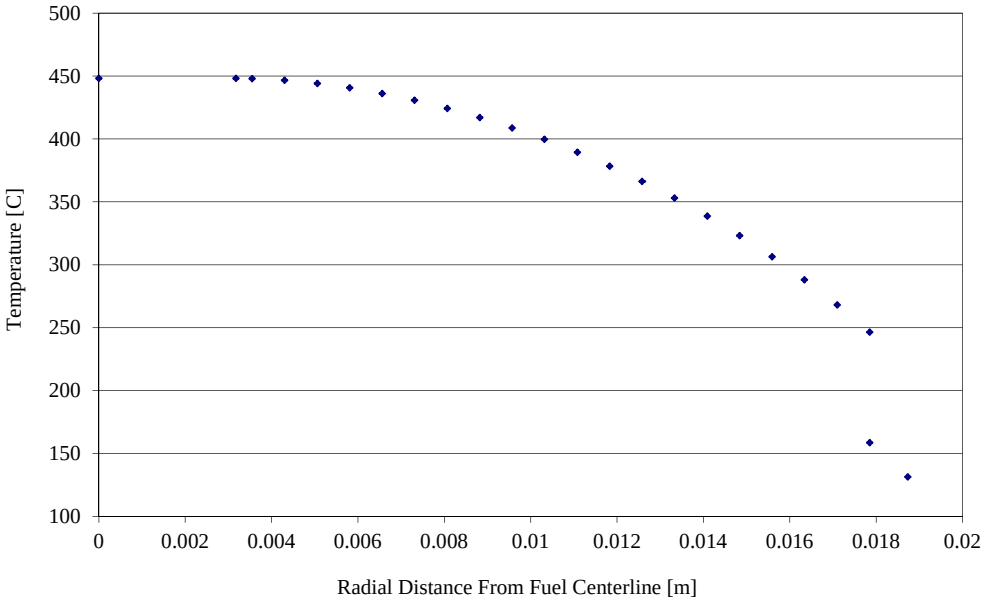

Figure 4.49 Radial Temperature Distribution at 18.47 kW (LEU BOL ICIT Core)

Table 4-22 Calculated Fuel Temperatures for Various Channel Powers in the LEU BOL ICIT Core

$P_{hot\text{-}channel}$ (kW)	Calculated [°C]			
	T_{max}	$T_{0.3}$	T_{clad}	$T_{coolant}$
14.00	371	358	129	95
16.00	406	391	130	99
18.47	448	431	131	101
20.00	474	455	132	102
22.00	508	487	133	103

The LEU steady state results shown above are for the ICIT core configuration. The LEU BOL ICIT core has a higher effective peaking factor than the LEU BOL CLICIT core or the LEU BOL NORMAL core, and thus is the bounding core for steady state operation. Figure 4.46 shows that the MDNBR in the hot channel will reach a value of 2.00 at approximately 20 kW hot channel steady state power. This is 108.3% of the 18.47 kW produced in the hot channel of the LEU BOL ICIT core operating at 1.1 MW_{th}. Using either the Bernath or the Groeneveld 2006 correlations, the LEU BOL ICIT core is operating at power well below that required for departure from nucleate boiling.

4.6.6 LEU Middle of Life ICIT Core Thermal Hydraulic Analysis

The results for the LEU Middle of Life ICIT Core Analysis are presented in this section. Hot channel temperature profiles are shown in Figures 4.50 through 4.54. The hot channel power summary of parameters and results are given in Tables 4-23 and 4-24, respectively.

Table 4-23 Steady State Results for LEU MOL ICIT core at 1.1 MW_{th}

Parameter	Value
Flow rate for hottest rod [kg/s]	0.0844
Maximum flow velocity [m/s]	0.2352
Maximum wall heat flux [kW/m^2]	507.74
Maximum fuel centerline temperature [°C]	457.66
Maximum clad temperature [°C]	131.46
Exit clad temperature [°C]	125.98
Exit bulk coolant temperature [°C]	101.40
MDNBR [Groeneveld 2006, Bernath]	4.754, 2.06

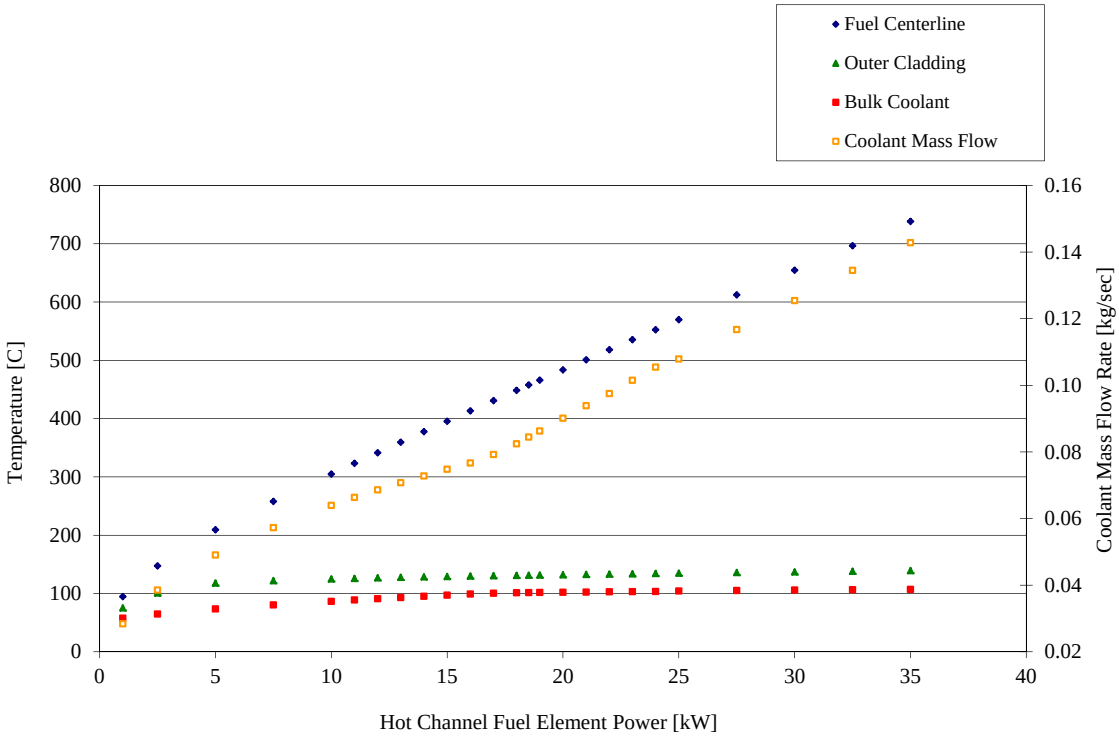

Figure 4.50 Hot Channel Properties (LEU MOL ICIT Core)

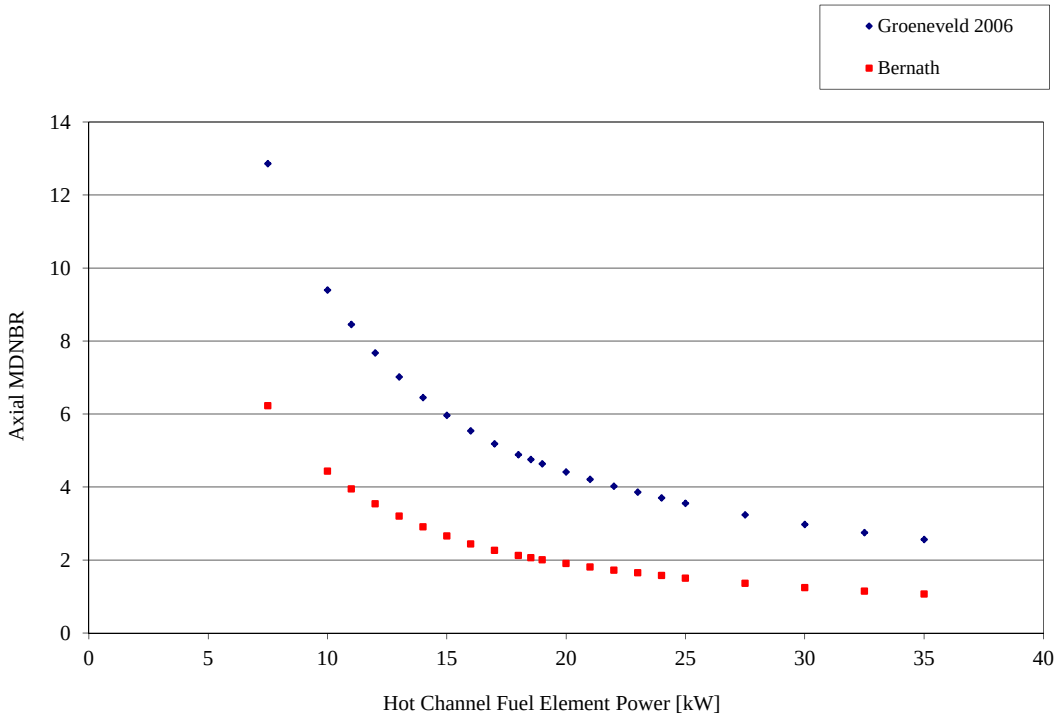

Figure 4.51 Hot Channel MDNBR (LEU MOL ICIT Core)

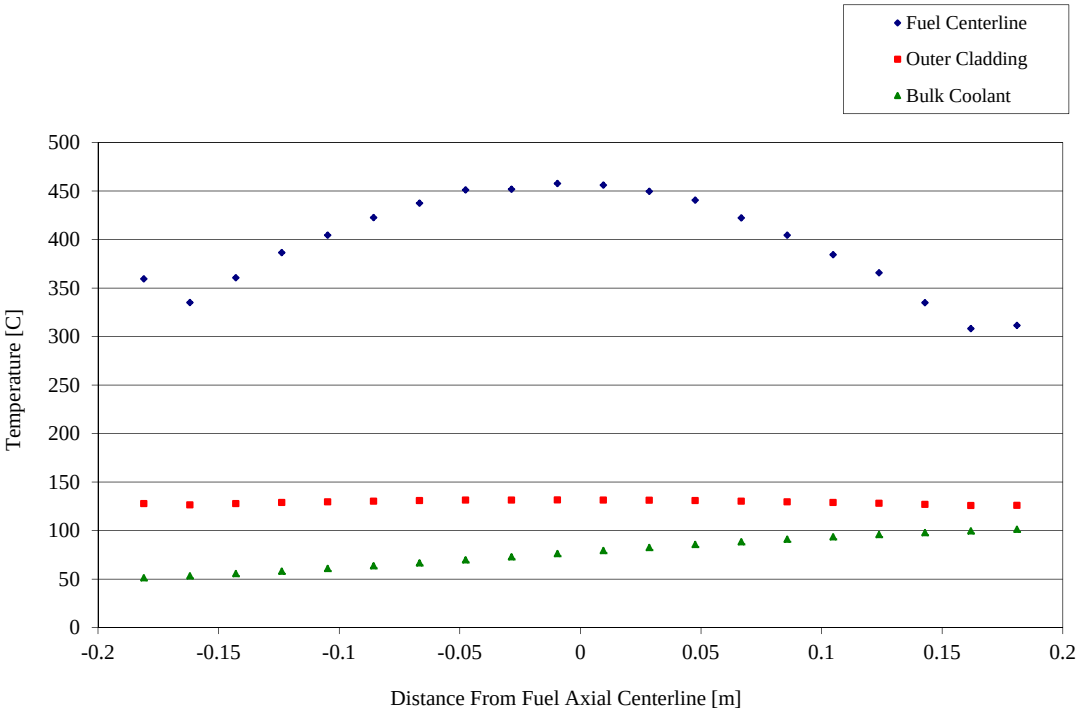

Figure 4.52 Axial Temperature Distribution at 18.52 kW (LEU MOL ICIT Core)

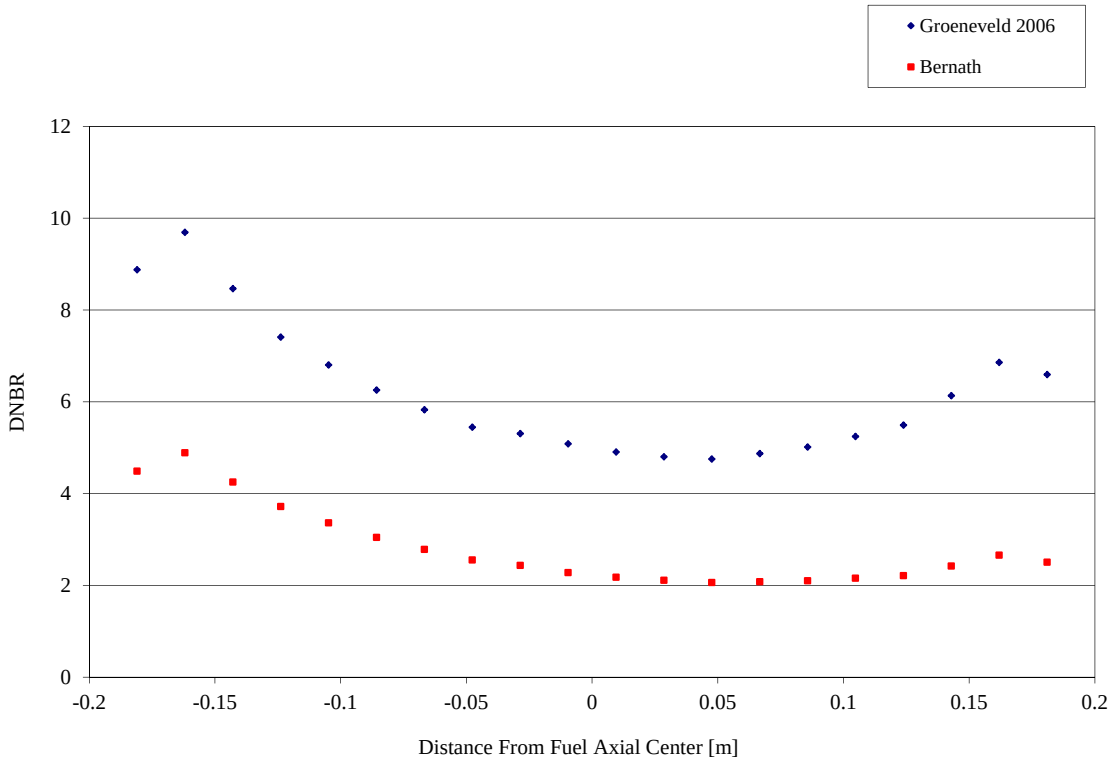

Figure 4.53 Hot Channel Axial DNBR at 18.52 kW (LEU MOL ICIT Core)

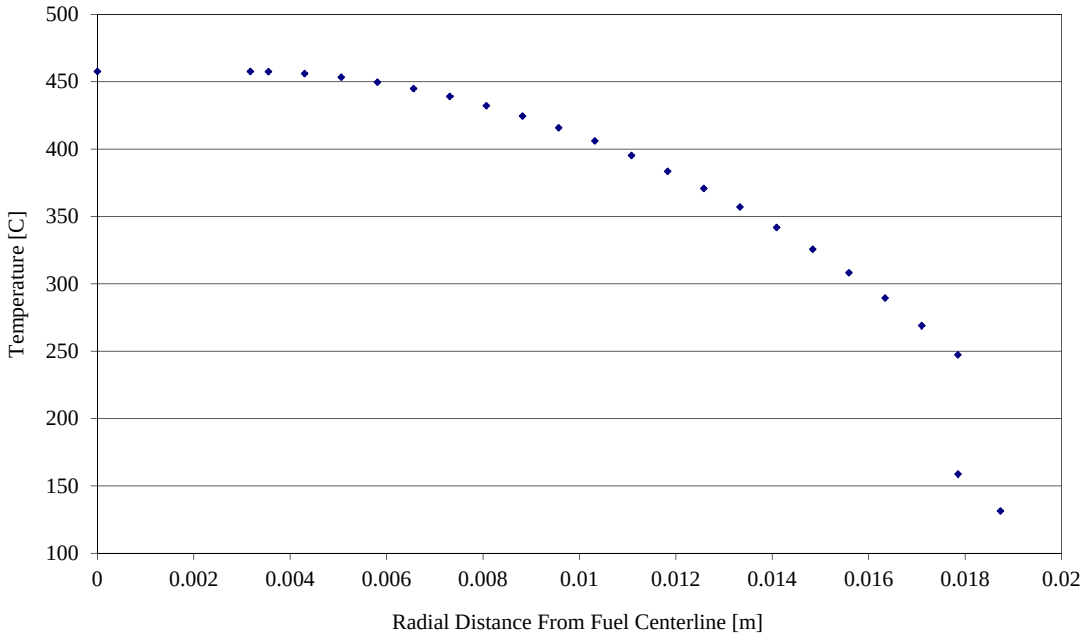

Figure 4.54 Radial Fuel Temperature Distribution at 18.52 kW (LEU MOL ICIT Core)

Table 4-24 Calculated Fuel Temperatures for Various Channel Powers in the LEU MOL ICIT Core

$P_{hot\text{-}channel}$ (kW)	Calculated Temperature[°C]			
	T_{max}	$T_{0.3}$	T_{clad}	$T_{coolant}$
14.00	378	361	129	95
16.00	413	394	130	99
18.52	458	436	131	101
20.00	483	460	132	102
22.00	518	492	133	103

The ICIT core was analyzed because it has the highest predicted hot rod thermal power and effective peaking factor for each of the core configurations and burn up time periods. Figure 4.51 shows that the MDNBR in the hot channel will reach a value of 2.00 at approximately 19.85 kW hot channel steady state power using the Bernath correlation and significantly higher yet using the Groeneveld 2006 correlation. Additionally, the value of 19.85 kW is larger than the predicted hot channel steady state power of 18.52 kW. Taken together, the LEU MOL ICIT core is predicted to operate at a power well below that required for departure from nucleate boiling.

4.6.7 LEU End of Life ICIT Core Thermal Hydraulic Analysis

The results for the LEU End of Life ICIT core analysis are presented in this section. Hot rod temperature profiles are shown in Figures 4.55 through 4.59. The hot channel power summary of parameters and results are given in Tables 4-25 and 4-26, respectively.

Table 4-25 Steady State Results for LEU EOL ICIT core at 1.1 MW_{th}

Parameter	Value
Flow rate for hottest rod [kg/s]	0.0812
Maximum flow velocity [m/s]	0.2245
Maximum wall heat flux [kW/m^2]	465.55
Maximum fuel centerline temperature [°C]	438.39
Maximum clad temperature [°C]	130.57
Exit clad temperature [°C]	125.87
Exit bulk coolant temperature [°C]	100.78
MDNBR [Groeneveld 2006, Bernath]	5.048, 2.202

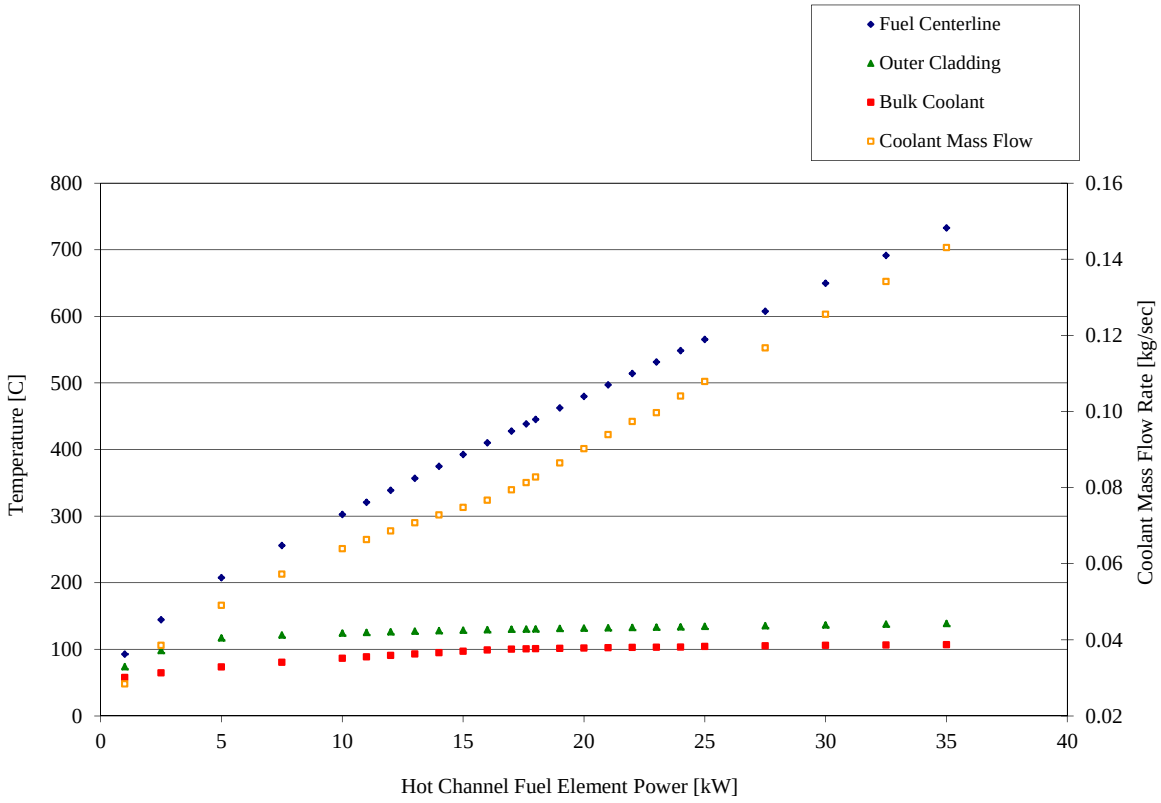

Figure 4.55 Hot Channel Properties (LEU EOL ICIT Core)

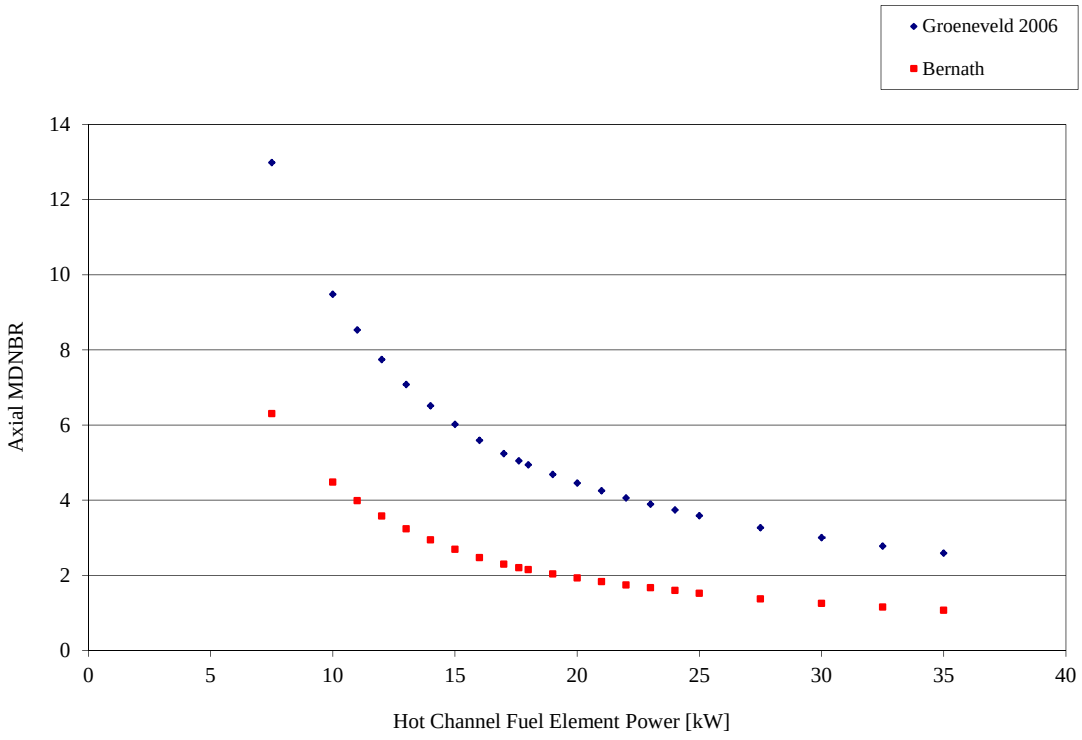

Figure 4.56 Hot Channel MDNBR (LEU EOL ICIT Core)

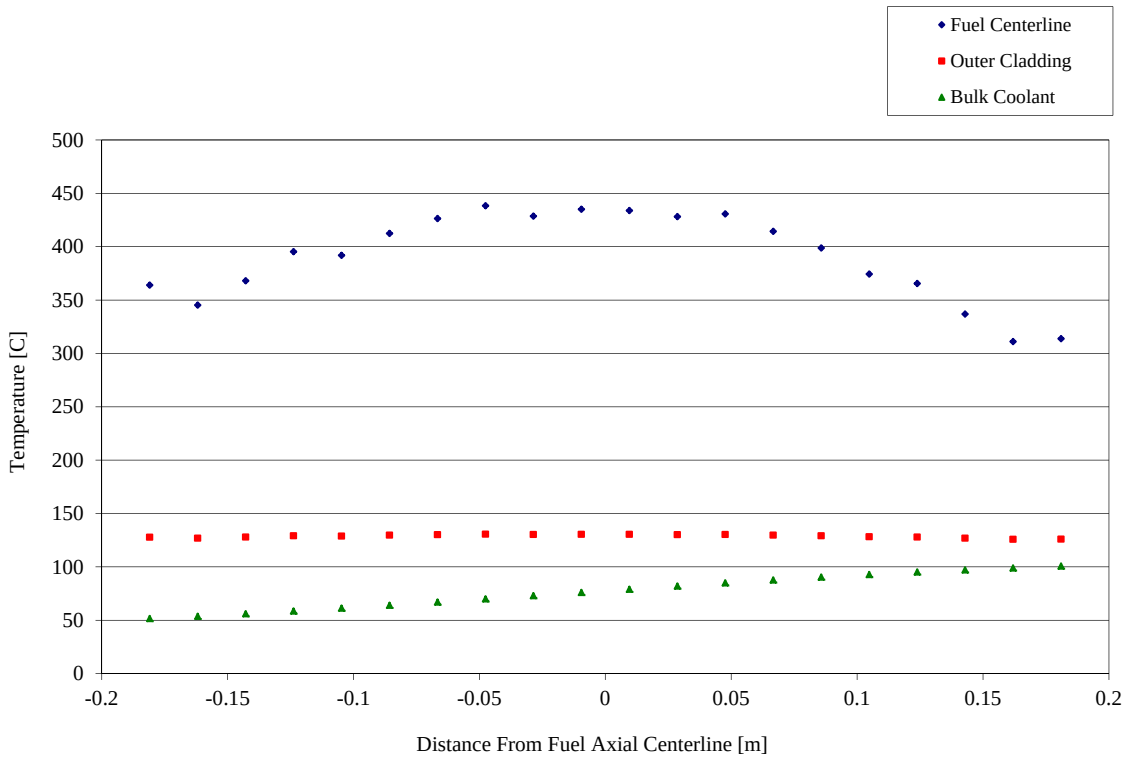

Figure 4.57 Axial Temperature Distribution at 17.61 kW (LEU EOL ICIT Core)

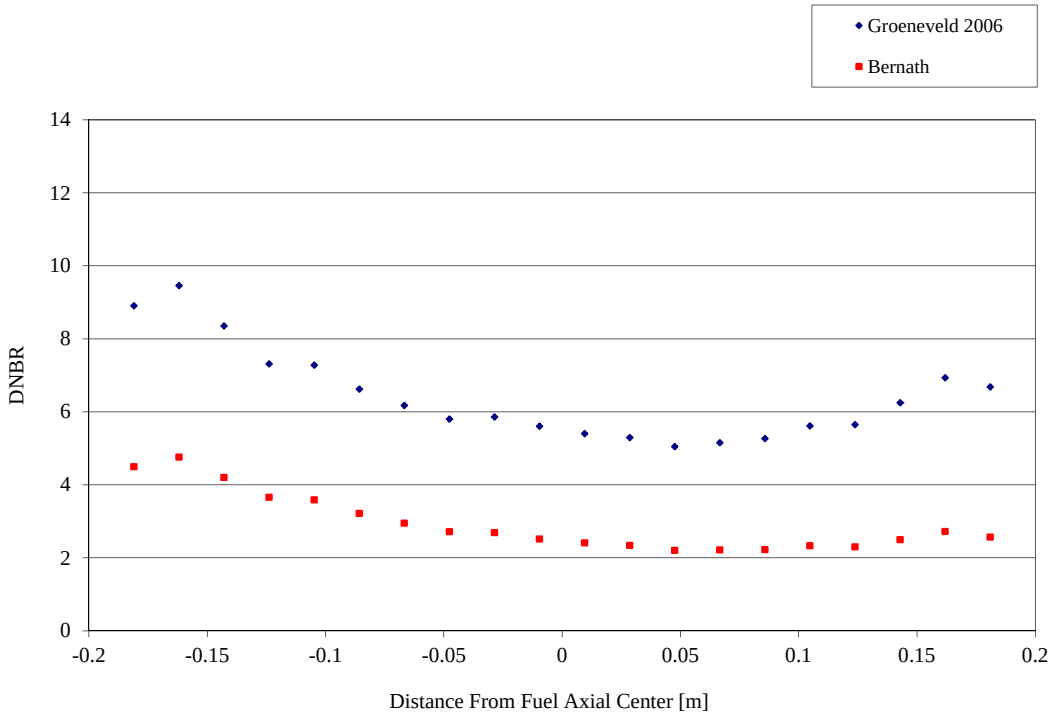

Figure 4.58 Hot Channel Axial DNBR at 17.61 kW (LEU EOL ICIT Core)

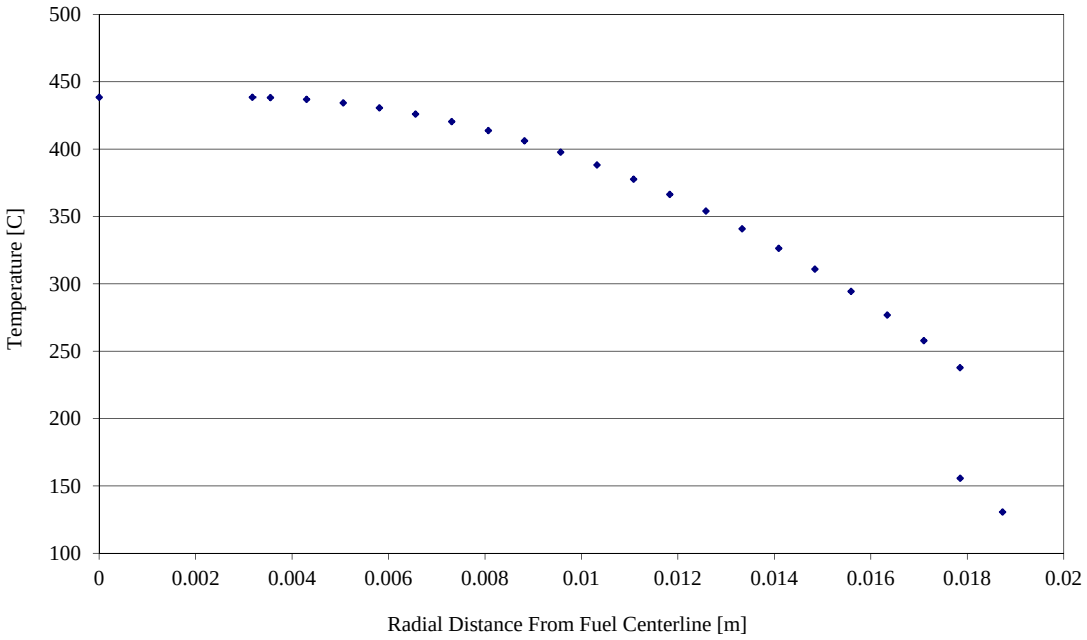

Figure 4.59 Radial Fuel Temperature Distribution at 17.61 kW (LEU EOL ICIT Core)

Table 4-26 Calculated Fuel Temperatures for Various Channel Powers in the LEU EOL ICIT Core

$P_{hot\text{-}channel}$ (kW)	Calculated [°C]			
	T_{max}	$T_{0.3}$	T_{clad}	$T_{coolant}$
14.00	375	358	128	95
16.00	410	391	130	99
17.61	438	417	131	101
20.00	480	456	132	102
22.00	514	488	133	103

The steady state results shown above are for the LEU ICIT EOL core configuration. The ICIT core was analyzed because it has the highest predicted hot rod thermal power and effective peaking factor for each of the core configurations and burn up time periods. Figure 4.56 shows that the MDNBR in the hot channel will reach a value of 2.00 at approximately 20 kW hot channel steady state power using the Bernath correlation and are significantly higher yet using the Groeneveld 2006 correlation. Additionally, the value of 20 kW is larger than the predicted hot channel steady state power of 17.61 kW. Taken together, the LEU EOL ICIT core is predicted to operate at a power well below that required for departure from nucleate boiling.

4.7 Pulsing Analysis Methodology

The behavior of the reactor during a pulse was simulated using the point reactor kinetics function built into RELAP. RELAP calculates the reactivity during the pulse transient using the following equation where $r_{fueltemp}$ represents the fuel temperature reactivity feedback, r_{pulse} represents the reactivity inserted during the pulse and r_b is a bias used by RELAP to ensure that the reactivity is zero prior to the insertion of the pulse. Reactivities in this equation are in dollars.

$$r_t = r_b + r_{pulse} + r_{fueltemp} \tag{4-42}$$

Both $r_{fueltemp}$ and r_{pulse} are input using user defined tables in RELAP where reactivity is a function of fuel temperature and time respectively. Since the fuel temp at the beginning of the transient is often not at a temperature corresponding to 0.0 reactivity in the $r_{fueltemp}$ table, r_b is used by RELAP to ensure that the transient starts at \$0.0 reactivity. The values used in for the analysis were: bulk coolant temperature (49ºC), initial fuel temperature (25ºC), number of elements (88 for LEU core), initial power (1kW), β/Λ (described later), volumetric specific heat (described in section 4.2.1.7), and a the temperature coefficient of reactivity (described later). The mean generation time (Λ) is frequently used in point reactor kinetics equations and is defined as:

$$\Lambda(t) = \frac{l_p}{k(t)} \tag{4-43}$$

A two channel model was developed in order to study pulse transients in the OSTR for different core configurations and reactivity insertions. Figure 4.60 presents the schematic of the two channel model constructed for this quantitative comparison. The models were based on 85 fuel elements for the HEU core and 88 fuel elements for the LEU core which includes all fuel followed control rods and the instrumented fuel element. A relation for the two channel model is presented below assuming the number of fuel elements found in the HEU core.

The two channel model was implemented for the pulse analysis of core conversion project only. In the case of the HEU and LEU cores, all fuel elements have the same geometry, therefore the heated perimeter is equal to the product of the number of fuel elements incorporated in a given subchannel times the heated perimeter of a single fuel element. A similar statement can be made with reference to the heated surface area of the average core relative to the hot channel. The average core hydraulic diameter was scaled as the product of the number of fuel elements in the subchannel times the hydraulic diameter of the hot channel. However, because time scales of less than 0.5 seconds are considered during the pulse analysis, the channel flow area associated with the average core has no impact on the maximum fuel temperature solution.

The pulse transient simulated by RELAP5-3D implements the point reactor kinetics model that has been built into the code. The following parameters defined in the model are the dominant factors in the outcome of the point reactor kinetics solution:

- Volumetric Heat Capacity $\rho C_p(T)$
- Effective Delayed Neutron Fraction / Mean Neutron Generation β/Λ
- Prompt Fuel Temperature Coefficient $\alpha(T)$

Because the parameters listed above were obtained for this study as core average parameters it is paramount that they be represented in the model as such. In order to correctly insert a given reactivity $(\$)$, into the RELAP5-3D model it must be done such that it is distributed through all fuel elements in the core.

Referring to Figure 4.60 volume 102, as the core average solution is produced from the point reactor kinetics model, the heat generation information is then passed to the hot rod (volume 101). The hot rod is a single separate channel which includes radial, axial, and hot channel peak factors. The solution in the hot channel (i.e. heat generation and removal) is then produced for a given time step as a result of the thermal power solution that was produced from the point reactor kinetics solution in the average core.

As a result of this, since a total of 88 fuel elements are found in the OSTR LEU core, 88 heat structure elements must be included in the RELAP5-3D model. Eighty-seven heat structure elements are included in the core average volume (volume 102) which produce a core average solution for a given reactivity insertion, and a single separated heat structure (volume 101) is used to determine hot rod temporal conditions.

The pulse analysis conducted as a part of the core conversion project was done using an explicit numerical scheme to solve the point reactor kinetics model incorporated into RELAP5-3D. Because the prompt fuel temperature coefficient is a temperature dependant property of the fuel, it must be explicitly solved along with the point reactor kinetics equations, this is done in RELAP5-3D by volume weighting the average temperature in fuel portion of the heat structure. After volume weighting the average temperature, RELAP5-3D then linearly interpolates on the prompt fuel temperature coefficient and moves into the next time step solving the point reactor kinetics equations. It is important to acknowledge that the volume weighted average temperature is only considered within the fuel portion of the fuel element, this is the only region affected by the prompt fuel temperature coefficient.

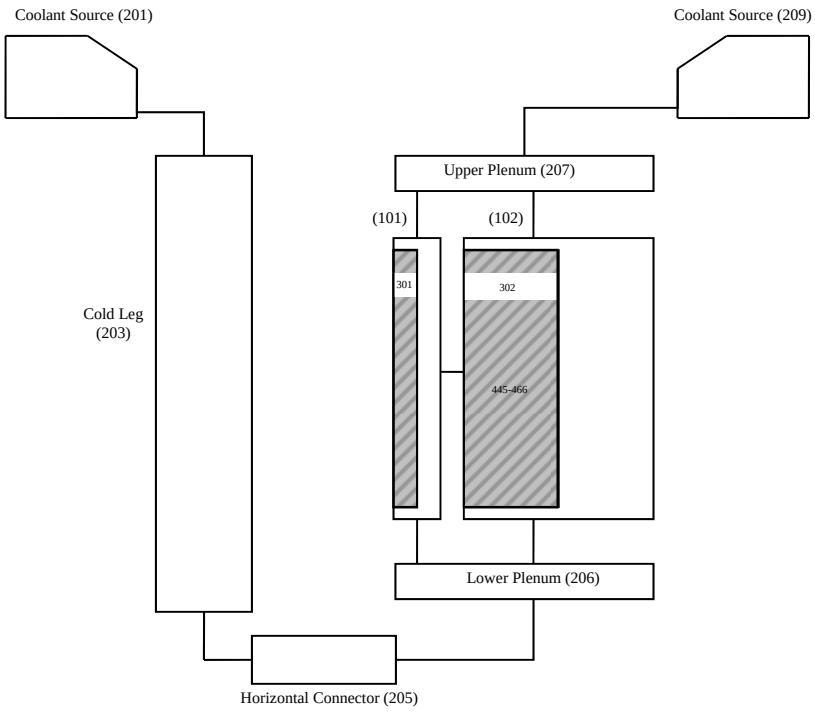

Figure 4.60 Two Channel RELAP5-3D Model Schematic

RELAP Version 2.4.2 was used for all calculations. This version included the point kinetics error. Investigation showed that this error had little impact on the predicted maximum temperature during a reactor pulse. The maximum temperatures predicted by version RELAP5 version 2.4.2 are higher than those predicted by other methods and thus are conservative.

To verify that this error did not significantly effect calculation results, a point reactor kinetics model was developed from basic principles. This model incorporated six delayed neutron precursor groups, a prompt negative fuel temperature coefficient and adiabatic conditions in the fuel. The basic equations used to model the core are:

$$\frac{d}{dt}P(t)=\left(\frac{\rho(t)-\beta}{\Lambda}\right)P(t)+\sum_{i=1}^{6}\lambda_i C_i(t) \tag{4-44}$$

$$\frac{d}{dt}C_i(t)=-\lambda_i C_i(t)+\frac{\beta_i}{\Lambda}P(t),\quad i=1...6 \tag{4-45}$$

$$\text{and}\ \int_{\rho_o}^{\rho} d\rho=\int_{T_o}^{T}\alpha(T')dT' \tag{4-46}$$

where all symbols are defined as usual. A benchmark problem originally published by General Atomics [Ref. 4.24] was run using RELAP and the point reactor kinetics model. A comparison of results is shown below in Table 4-27 and Figure 4-61. Predicted values were in reasonably good agreement with the most conservative (i.e. highest) peak temperature being predicted by the RELAP model.

Table 4-27 Comparison of three different methods for predicting pulse behavior

Pulse Results Summary			
	GA Paper	RELAP5-3D	OSU PRKM
Maximum Power [MW]	20000	20606	21058
Time of Maximum Power [sec]	~0.0207	0.02108	0.02032
Pulse FWHM	~0.00351	0.00464	0.00454
Peak Adiabatic Fuel Temp. [°C]	1000	1083.1	880.665
Average Adiabatic Core Temp [°C]	500	492.032	473.249
Core Energy Release After 0.1 sec [MJ]	106	109.47	108.24

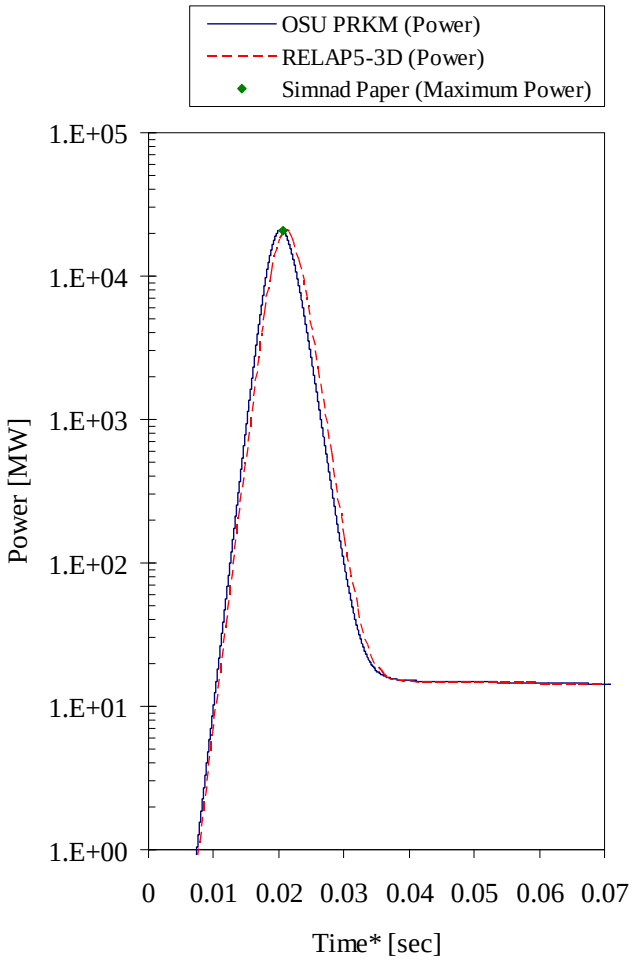

Figure 4.61 Pulse power trace for three different analytical methods

During the pulse analysis the only feedback mechanism incorporated into the RELAP5-3D model is the prompt negative fuel temperature coefficient associated with fission heating. Because the pulse transients occur on such short timescales and the thermal resistance in the fuel, gap, and clad are very large, the heat flux at the outer clad surface does not change until several seconds after the pulse initiates. To verify these assertions, two RELAP5-3D cases were considered. The first case involved only fuel feedback. The second case involved both fuel and moderator feedback. The results are shown in Figure 4.62.

The reactivity is identical for the case with and without moderator feedback. This is because there is not enough heat that is transferred into the moderator to affect its temperature or density within the extremely short time frame. Note that this calculation did not account for moderator heating due to gamma heating. This is believed to be conservative since higher moderator temperatures would result in stronger negative reactivity feedback and hence smaller pulses.

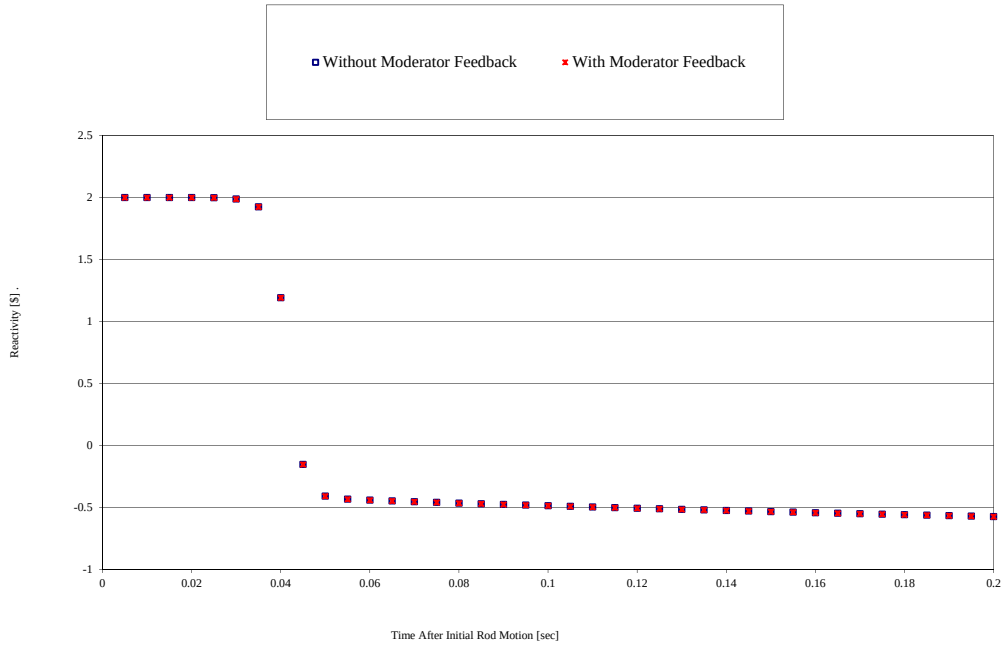

Figure 4.62 Transient Reactivity Comparison ($2.00 Insertion)

One other point needs to be clarified. For average temperature of the fuel, the pulse analysis calculations did not include the included the temperature of the gap and the clad. When using fuel temperature to determine the magnitude of temperature coefficient feedback, it is more accurate to consider the temperature of fuel only. An average including only the volume of the fuel tends to result in a higher spatially averaged fuel temperature which causes stronger prompt temperature feedback, thus resulting in smaller pulses for a given reactivity.

4.7.1 LEU Core Pulse Analysis

For all stages of life and all core configurations, the LEU MOL ICIT core has the highest effective peak factor and therefore the limiting core configuration for a pulse analysis. Figures 4.63 through 4.65 summarize pulsing performance for the LEU MOL ICIT core. These include the fuel temperature as a function of time, the temperature distribution as the moment the peak temperature is observed and a summary of the temperatures as a function of reactivity. Values of important parameters are summarized in Table 4.28.

The pulse summary figures graphically display the following information for a series of pulses of different magnitudes:

1. the peak power of the core during the pulse
2. the prompt maximum value of the fuel in the hot channel
3. the maximum thermocouple temperature during the pulse, assuming that the IFE is located in the hot rod position

Table 4-28 Summary of LEU MOL ICIT Pulse Behavior

LEU-MOL ICIT Core Configuration Pulse Results Summary					
Reactivity Insertion [$]	1.50	1.75	2.00	2.25	2.50
Peak Total Core Power [MW]	875	1910	3316	5087	7270
Prompt Peak Fuel Temperature [°C]	448	582	697	800	894
Max. Thermocouple Temperature [°C]	375	480	574	657	724

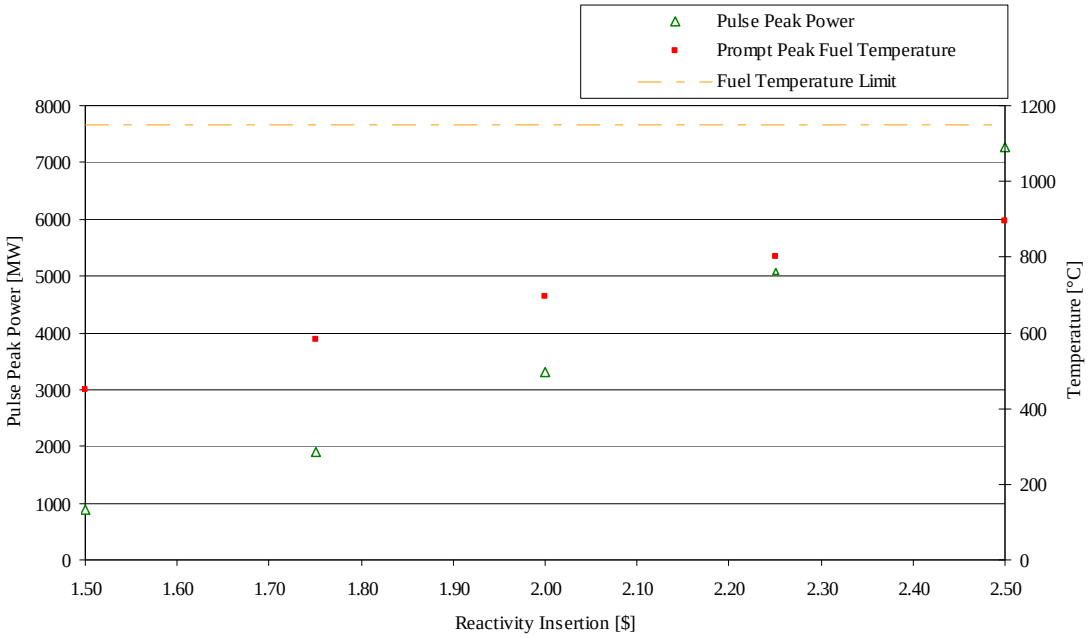

Figure 4.63 Pulse Summary (LEU MOL ICIT Core)

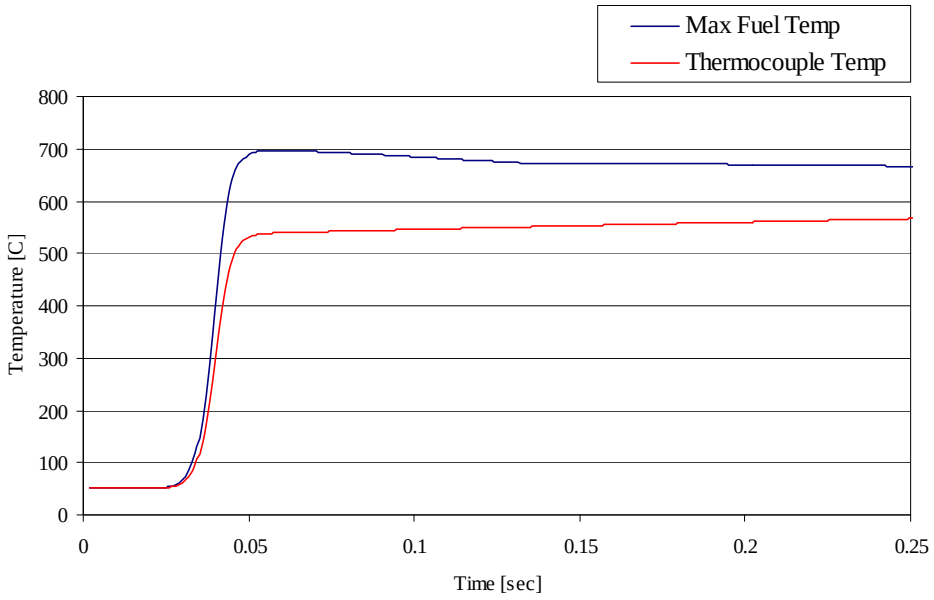

Figure 4.64 LEU MOL ICIT, Hot Channel Fuel Temperature ($2.00 Pulse)

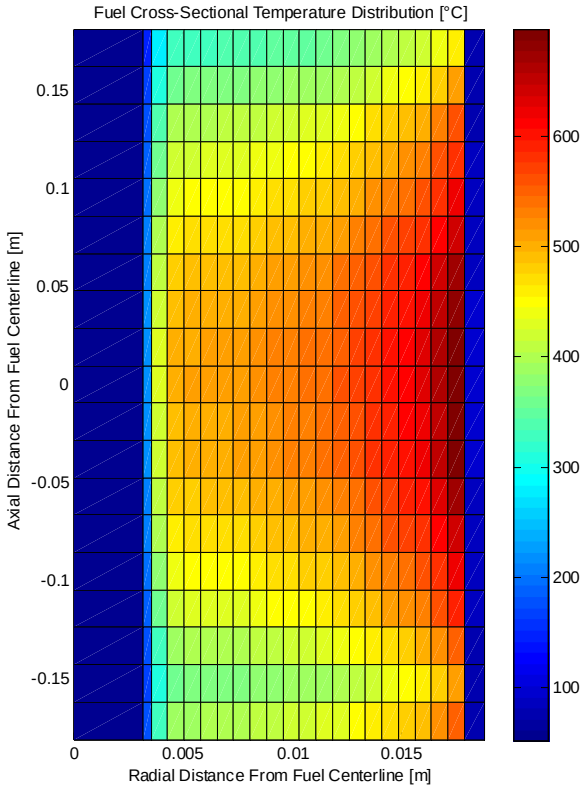

Figure 4.65 LEU MOL ICIT, Fuel Temperature Distribution at Time of Prompt Maximum Fuel Temperature ($2.00 Pulse)

Peak temperature observed during a pulse is linearly proportional to the prompt reactivity insertion. Linear extrapolation of the peak temperatures associated with the $2.25 and $2.50 pulses in the LEU MOL ICIT core indicate that a reactivity insertion of $2.30 will produce a maximum temperature of 819ºC. A pulse reactivity insertion limit of $2.30 will ensure that at all times in core life, and in all core configurations, the maximum fuel temperature in the core will not exceed 950°C, providing a margin of more than 200ºC from the Safety Limit.

4.7.2 Effect of Fresh Fuel on Pulsing

Increased power peaking caused by the insertion of a fresh fuel element into a MOL or EOL core will affect the pulse characteristics. In the MOL ICIT core, the highest power element increases from 18.52 to 19.55 kW, or an increase of 6 percent with a commensurate 6 percent increase in the hot channel peak factor. In the EOL ICIT core, the highest power element increases from 17.61 to 19.88 kW, or an increase of 13 percent. The hot channel peak factor is used for the pulse analysis. All pulse analyses were performed on un-perturbed cores. Due to a combination of prompt temperature coefficient and peaking factors, the LEU MOL ICIT core is the most

limiting core in terms of pulse behavior. However, the assumption that the pulsing reactor maintains the same power profile as the steady state reactor is conservative. Thus even though the hot channel peak factor in the perturbed LEU MOL ICIT core is 6 percent greater than in the un-perturbed core (13 percent greater than in the un-perturbed LEU EOL ICIT core), the conservative analyses performed on the LEU ICIT cores would still produce fuel temperatures below the safety limit.

4.7.3 Effects of Pulsing at Full Power

The consequences of pulsing the reactor from full power have been considered. The core configuration containing the largest effective peak factor value is the LEU Middle of Life ICIT Core. As a result of this the LEU Middle of Life ICIT Core was chosen to compare pulse characteristics for a scenario in which the OSTR is at steady state at its interlock power of 1.0kW$_{th}$ and then pulsed to the maximum reactivity insertion for the LEU core of \$2.15. A second case is considered where the OSTR operates at maximum licensed steady state power of 1.1 MW$_{th}$ and is then pulsed with \$2.15 reactivity insertion.

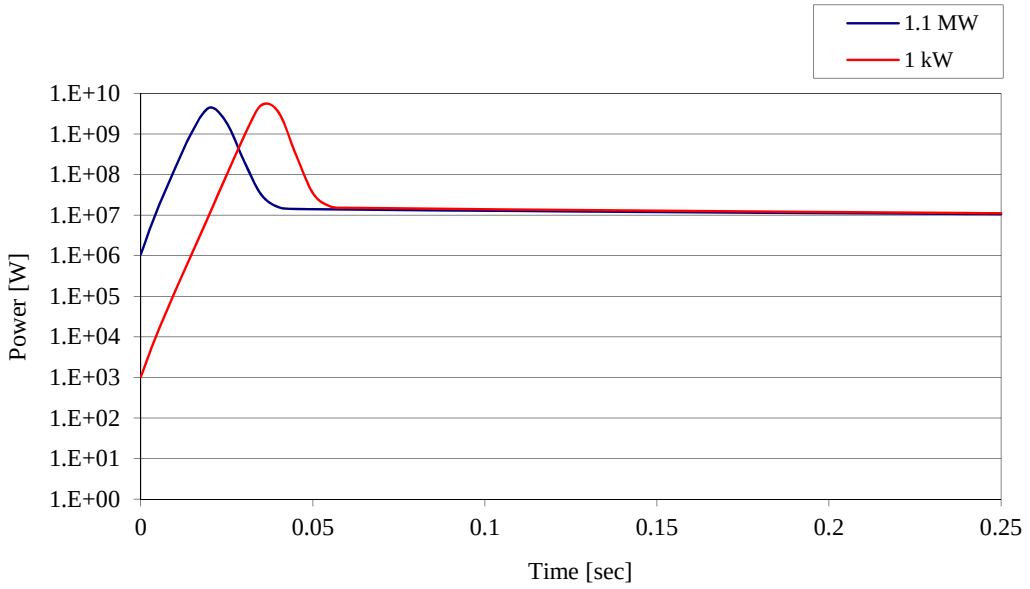

Figure 4.66 Pulse Power Trace Comparison for given initial Conditions (\$2.15 Insertion) (LEU-Middle of Life ICIT Core Configuration)

As shown in Figure 4.66, the pulse power trace for an initial steady state core at 1.1 MW$_{th}$ has a total core peak power value of 4504 MW$_{th}$ which produces a maximum prompt fuel temperature of 900.1 °C, while for the case where the core is initially at 1.0 kW$_{th}$ steady state the total core peak power reaches a value of 5198 MW$_{th}$ and produces a maximum prompt fuel temperature of 939.2 °C. A summary of the pulse comparison results are presented in Table 4-29.

Table 4-29 Pulse Initial Conditions Sensitivity Study
(LEU-Middle of Life ICIT Core Configuration)

LEU-EOL ICIT Core Configuration Initial Conditions Sensitivity Study		
Initial Steady State Power [kW]	1.0	1.1E3
Reactivity Insertion [$]	2.15	2.15
Peak Total Core Power [MW_{th}]	5198	4504
Time of Peak Total Core Power [sec]	0.045	0.03
Prompt Peak Fuel Temperature [°C]	939.2	900.1
Time of Prompt Peak Fuel Temperature [sec]	0.05	0.035

As a result of this comparison it is demonstrated that although the initial steady state power is much greater for the case where the reactor is pulsed from 1.1 MW_{th} it results in a lower maximum prompt fuel temperature than that of the lower initial steady state power. This is due to the temperature dependant prompt fuel temperature coefficient that is inherent to the TRIGA® Fuel.

4.8 References

4.1 "The U-ZrH_x Alloy: Its Properties and Use in TRIGA® Fuel," GA Report 414, February 1980, Mt. Simnad.

4.2 "Fission Product Releases from TRIGA®-LEU Reactor Fuels," GA-A16287, November 1980, Baldwin, Foushee, and Greenwood.

4.3 "Summary of TRIGA® Fuel Fission Product Release Experiments," Gulf-EES-A10801, September 1971.

4.4 Merten, U., et. al., "Thermal Migration of Hydrogen in Uranium-Zirconium Alloys," General Dynamics, General Atomic Division Report GA-3618, 1962.

4.5 G. A. Report, "Low Enriched TRIGA Fuel-Water Quench Safety Test," GA-15413, June 1979.

4.6 Dee, J. B., et. al., "Annular Core Pulse Reactor," General Dynamics, General Atomics Division Report GACD-6977, Supplement 2, 1966.

4.7 Johnson, H. E., "Hydrogen Disassociation Pressures of Modified SNAP Fuel," Report NAA-SR-9295, Atomics International, 1964.

4.8 M. T. Simnad, "The U-ZrHx Alloy: Its Properties and Use in TRIGA® Fuel," Nuclear Engineering and Design **64** (November 1980), 403-422.

4.9 NUREG -1282, op. cit.

4.10 Ibid.

4.11 Ibid.

4.12 Ibid.

4.13 "MCNP—A General Monte Carlo N-Particle Transport Code, Version 5," LA-CP-03-0245, F. B. Brown, Ed., Los Alamos National Laboratory (2003).

4.14 RELAP5-3D Code Development Team, "Volume 1: code structure, system models, and solution methods, in RELAP5-3D code manual'" 2005, Idaho National Laboratory: Idaho Falls, Idaho. p. 600.

4.15 Bene, J. V. D., "TRIGA® Reactor Thermal-Hydraulics Study, STAT-RELAP Comparison," General Atomics Report, to be published.

4.16 Top Gridplate, TRIGA® Mark III, General Atomics Drawing T13S210J106 rev. C.

4.17 Todreas, N. E., Kazimi, M. S., "Nuclear Systems II: Elements of Thermal Hydraulic Design," Vol. 2, 2001. Taylor and Francis Group LLC 506, New York.

4.18 Reflector Assembly, Oregon, General Atomics Drawing T2D210J110 rev. A.

4.19 Groeneveld, D. C., et. al., "The 2006 CHF Lookup Table," Nuclear Engineering and Design, 2007, p. 1-24.

4.20 Bernath, L., "A Theory of Local Boiling Burnout and its Application to Existing Data," Chemical Engineering Progress Symposium. Series No. 30, Volume 56, pp. 95-116 (1960).

4.21 Bretscher, M., "β_{eff}/l_p for Water-Reflected Fresh Critical Cores of the Oak Ridge Research Reactor Reflected by Water," RERTR Program, Argonne National Laboratory, July 31, 1986.

4.22 M. T. Simnad, F. C. Foushee, and G. B. West, "Fuel Elements for Pulsed TRIGA® Research Reactors," *Nuclear Technology* **28** (1976) 31-56.

4.23 General Atomics, Safety Analysis for the HEU to LEU Core Conversion of the Washing State Univesity Reactor, (2007) p. 1-112.
4.24 Simnad, M., Foushee, F., and West, G., Fuel Elements for Pulsed TRIGA Research Reactors. San Diego, CA, 1975.
4.25 The BEBUS-MCNP Linkage, J. G. Stevens, ANL (Draft).
4.26 Greenveld, D. C., Cheny S. C., and Doan, T. Heat Transfer Eng., 7, 1-2, 46 (1986).
4.27 Feldman, E. E. "Fundamental Approach ot TRIGA Steady State Thermal-Hydraulic CHF Analysis," presented at the 24th Int. Mtg. Reduced Enrichment for Research and Test Reactors (RERTR), Prague, Czech Republic, September 23-27, 2007.

CHAPTER 5

REACTOR COOLANT SYSTEMS

Chapter 5 - Valid Pages
Rev. 1 5/1/2012

i	Rev. 0 7/1/2004
ii	Rev. 0 7/1/2004
1	Rev. 0 7/1/2004
2	Rev. 0 7/1/2004
3	Rev. 0 7/1/2004
4	Rev. 0 7/1/2004
5	Rev. 0 7/1/2004
6	Rev. 0 7/1/2004

TABLE OF CONTENTS

LIST OF FIGURES

THIS PAGE INTENTIONALLY LEFT BLANK

5 REACTOR COOLANT SYSTEMS

5.1 Summary Description

Water is used in the OSTR to cool the reactor, to provide a shield for the reactor while still maintaining visibility, and to moderate (thermalize) the fast neutrons to enable the fission reactions to take place. The reactor core is located at the bottom of a shielded 6.5-foot diameter, 20.5-foot deep aluminum open-top tank. Water level over the core is normally maintained at 16 feet to provide radiation shielding over the core. The reactor core is cooled by natural circulation water flow through the core area combined with a forced-flow of water into and out of the reactor tank. A remote secondary heat exchanger transfers core heat from the reactor tank primary flow to a fan-assisted, roof-mounted, water-to-air heat exchanger to assist in maintaining low coolant temperatures during extended 1-MW full-power operations.

5.2 Primary Coolant System

The primary coolant system, shown in Figure 5.1, consists principally of a pump and heat exchanger connected by suitable four-inch diameter aluminum piping to the reactor tank. The stainless steel case and impeller primary pump deliver approximately 490 gpm of water through the secondary heat exchanger. The pump is directly-coupled to a 20-hp motor.

Approximately 50 gpm of the primary coolant return-flows through a diffuser nozzle pointing down onto the top of the core. This has the effect of delaying ^{16}N as it rises to the surface of the reactor tank.

Temperature probes in the primary water system assist the operator in monitoring water temperatures at various locations to assess system operation and ensure that the maximum tank water temperature is not exceeded. In the event of coolant system leakage, an underground holding tank collects and stores the fluid for eventual discharge. In-tank level alarms provide operator notification of decreasing tank level. Minimum water level in the tank is maintained by siphon break holes in the in-tank system piping at 22 inches below normal tank level.

5.3 Secondary Coolant System

The secondary coolant system, shown in Figure 5.2, consists principally of a pump, heat exchanger, cooling tower, connecting piping and associated instrumentation. The flow rate in this water system is set at approximately 700 gpm.

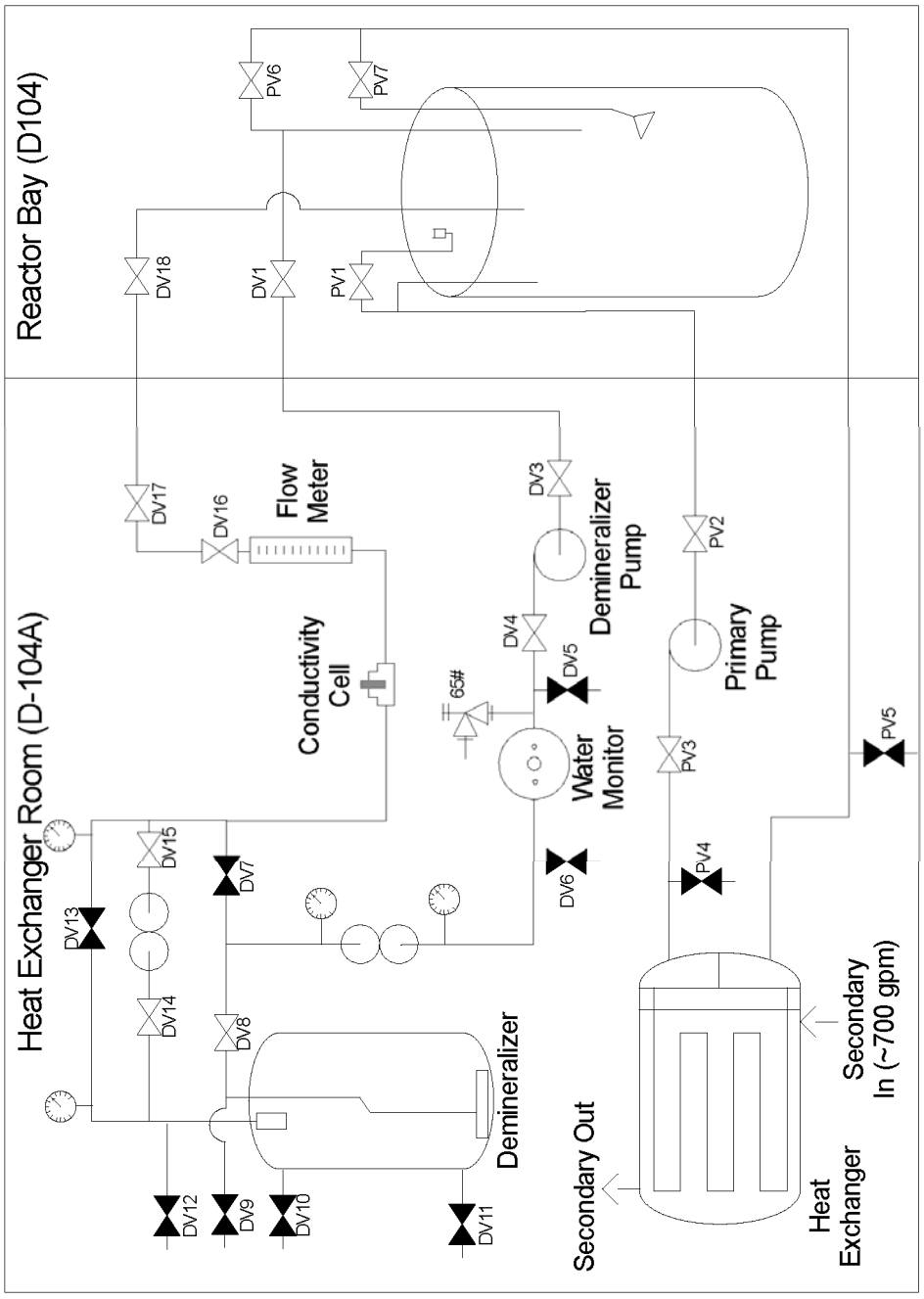

Figure 5.1 Primary Coolant System Schematic

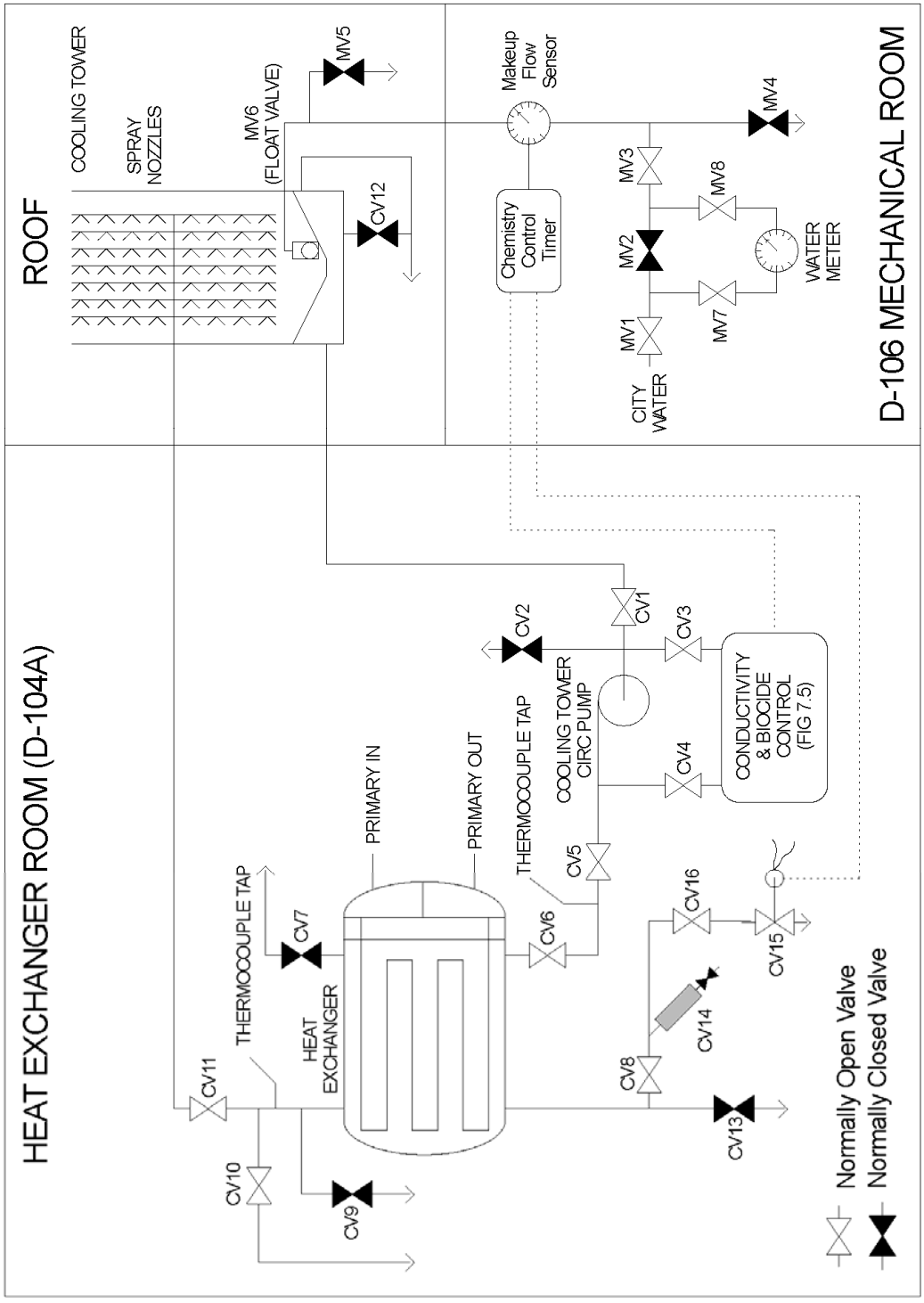

Figure 5.2 Secondary Coolant System Schematic

A tube-and-shell type heat exchanger is used for the removal of heat from the reactor primary coolant loop. The carbon steel shell contains 72 U-shaped stainless steel tubes that are welded into a removable stainless steel tube bundle. All parts of the heat exchanger that are in contact with the demineralized primary water are made of Type 304 stainless steel. The water in the secondary coolant system flows into the carbon steel shell side of the heat exchanger. The heat exchanger has an operating capacity of approximately 1 MW of thermal energy.

The secondary system cooling tower is located on the reactor building roof and holds approximately 400 gallons of water. The tower basin has a "V"-shaped trough that is designed for self-cleaning. A set of coarse screens is mounted in the basin to catch coarse debris. Forced air for cooling the inlet water spray is provided by two, 3-phase motors, each turning a set of three squirrel cage fans. Secondary system pressure exceeds primary system pressure to ensure that a heat exchanger leakage results in the containment of potentially contaminated primary fluid.

Make-up water to the cooling tower comes from the city water system and is automatically added as needed by a float valve. An overflow is provided to prevent accidental overfilling of the cooling tower basin which would flood into the squirrel cage fans.

To prevent damage from freezing, the cooling tower is fitted with two automatic heaters that will turn on at a preset water temperature. Secondary chemistry is maintained by an automatic water conditioning system. One portion of the system helps control corrosion, which is important from the standpoint of equipment longevity and maintaining good heat transfer capabilities in the heat exchanger, while another chemical addition loop helps control water-born biological growth and maintain the water conductivity.

As shown in Figure 5.3, the chemical addition and blow-down regime is based on cooling tower makeup flow. A flow pulse meter valve located on the cooling tower makeup line sends a signal to a dual pulse timer. After a given amount of flow, the timer will start a chemical addition pump for a preset time period. Later, the timer will blow down the secondary coolant for a given period of time. The timer only operates when the secondary pump is in operation.

The secondary pressure is higher than the primary pressure when both pumps are shut down. The pressure on the primary side is estimated at 8.6 psi, conservatively assuming a maximum of 20 feet of head. The pressure on the secondary side is estimated at 13.0, again conservatively assuming a minimum of 30 feet of head. The differential pressure is then 4.4 psid. The actually differential pressure is likely higher using more realistic elevations.

5.4 Primary Coolant Cleanup System

The primary water purification system, also shown in Figure 5.1, consists principally of a pump; a monitoring chamber that contains probes for measuring temperatures, radioactivity, and conductivity; two fiber cartridge filters; a mixed-bed demineralizer; and a flow meter. A small

portion of the inlet primary flow is diverted to the purification system components and is returned directly to the reactor tank. The purification system is constructed of 1-inch aluminum and 1-inch PVC plastic piping. A siphon break hole provides protection against water loss due to pipe leakage. The purification system pump is a 0.75-hp pump driven by a directly-coupled induction motor. The demineralizer vessel contains 3 cubic feet of resin with an equal and homogenous mixture of anion and cation resin. It is mounted behind a concrete shield wall. Local area radiation monitoring is provided to evaluate collected debris. Maximum water flow through the demineralizer is maintained at 10 gpm. Replaceable fiber cartridges of 25-micron ratings are used in the purification system to remove insoluble particulate matter from the reactor water system. Four pressure gauges are positioned in the demineralizer lines to measure the pressure drop (ΔP) across the filters as an aid in determining the extent of filter clogging. An aluminum cylinder in the purification system acts as a water monitoring vessel and contains: (1) a temperature probe for measuring demineralizer inlet water temperature, (2) a conductivity probe for measuring demineralizer inlet water purity, and (3) a Geiger tube for detecting any radioactivity in the water. An additional conductivity probe is located in the demineralizer outlet line to monitor resin bed efficiency.

A surface skimmer is provided to assist in maintaining the cleanliness of the reactor tank water surface. The surface skimmer collects foreign particles on the surface of the reactor tank water. The floating foreign particles are collected in a floating basket as the skimmer draws in water from the surface. The skimmer is connected to the primary coolant system suction line by a small diameter aluminum pipe and throttle valve.

5.5 Primary Coolant Makeup Water System

The makeup water system provides distilled water from a common facility reverse osmosis (RO) distilling unit for the reactor and bulk shield makeup tanks. This very pure water source is used to prolong resin life and further reduce primary water activity. Makeup water to compensate for reactor tank evaporation and sampling is added by pumping water from the makeup tank through the demineralizer and its discharge system directly to the reactor tank.

There is no direct physical connection between the city water system and the reactor primary water system. Water is added to the primary only after it has passed through the RO unit. Water is passed from one side of the RO unit to the other by dripping into a flask, thereby precluding the possibility of siphoning. Additionally, all water entering the building is protected against siphoning with a reverse pressure backflow prevention device which is inspected annually.

5.6 ^{16}N Control System

A portion of the reactor tank inlet water is diverted through a diffuser located above the core to create a lateral dispersion of ^{16}N rising from the core. This dispersion significantly increases ^{16}N hold-up time.

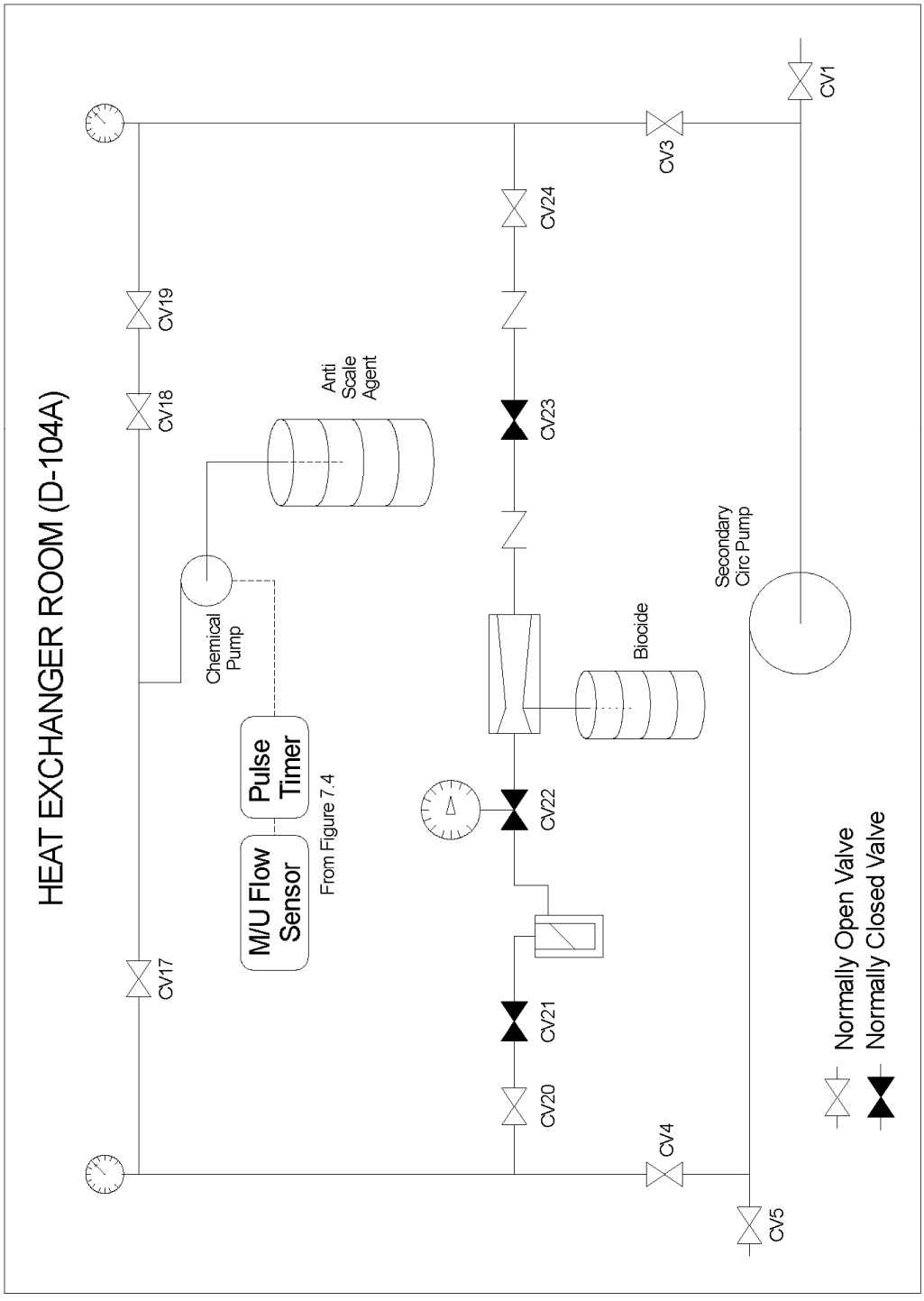

Figure 5.3 Secondary Coolant Chemical Treatment System

CHAPTER 6

ENGINEERED SAFETY FEATURES

(The OSTR does not have any credited Engineered Safety Features)

THIS PAGE INTENTIONALLY LEFT BLANK

CHAPTER 7

INSTRUMENTATION AND CONTROL SYSTEMS

Chapter 7 - Valid Pages
Rev. 1 5/1/2012

i	Rev. 0 7/01/2004
ii	Rev. 0 7/01/2004
1	Rev. 0 7/01/2004
2	Rev. 0 7/01/2004
3	Rev. 0 7/01/2004
4	Rev. 0 7/01/2004
5	Rev. 0 7/01/2004
6	Rev. 0 7/01/2004
7	Rev. 0 7/01/2004
8	Rev. 0 7/01/2004
9	Rev. 0 7/01/2004
10	Rev. 0 7/01/2004
11	Rev. 0 7/01/2004
12	Rev. 0 7/01/2004
13	Rev. 0 7/01/2004

TABLE OF CONTENTS

7 INSTRUMENTATION AND CONTROL SYSTEMS

LIST OF FIGURES

THIS PAGE INTENTIONALLY LEFT BLANK

7 INSTRUMENTATION AND CONTROL SYSTEMS

7.1 Summary Description

The reactor is operated from a console located in the control room. Additional instrumentation is housed in cabinets on either side of the console. An annunciator panel is mounted above the console.

The operating mode of the reactor is determined by a five-position mode switch on the console. In Automatic and Steady-State modes, the reactor can operate at power levels up to 1 MW. In Square Wave mode, a step insertion of reactivity rapidly raises reactor power to a steady-state level up to 1 MW. In Pulse High and Pulse Low modes, a large-step insertion of reactivity results in a short duration reactor power pulse.

The reactor instrumentation is all solid-state analog circuitry with the exception of the console digital data recorders which have no control functions.

7.2 Design of Instrumentation and Control Systems

Three independent power measuring channels provide for a continuous indication of power from the source level to peak power resulting from the maximum allowed pulse reactivity insertion. Trips are provided for over power, high rate, and loss of operability of the channels. Fuel temperature is measured for display as well as use by the reactor protection system. Parameters not used by the reactor protection system are also monitored and displayed.

7.2.1 Design Criteria

The instrumentation and control system is designed to provide the following:

- complete information on the status of the reactor and reactor-related systems;
- a means for manually withdrawing or inserting control rods;
- automatic control of reactor power level;
- automatic scrams in response to over power, excessive rate of change of power, and high fuel temperature;
- automatic scrams in response to a loss of operability of the power measuring channels; and
- monitoring of radiation and airborne radioactivity levels.

7.2.2 Design-Basis Requirements

The primary design basis for the OSTR is the safety limit on fuel temperature. To prevent exceeding the safety limit, automatic scrams are provided for high fuel temperature and high power conditions. Interlocks limit the magnitude of transient reactivity insertions.

7.2.3 System Description

7.2.3.1 Reactor Power Measurements

Reactor power is measured by three separate detectors; a fission chamber and two uncompensated ion chambers. The signal from the fission chamber is used by the wide range log channel, the period channel, and the wide range linear channel. One uncompensated ion chamber is connected to the safety channel. A second uncompensated ion chamber is used by the percent power and pulsing channels. Figure 7.1 shows the relative ranges of the channels and the detectors.

The detector current selector switch allows routing the current signals from the ion chambers to an external pico-ammeter. When either ion chamber is switched to the external meter, the rod withdrawal prohibit interlock is activated.

The fission chamber is connected to a pre-amplifier at the reactor top. The pre-amplifier monitors the high voltage to the fission chamber, provides an input point for test signals, and pre-amplifies the fission chamber signal for use in the wide range log and linear channels. If a loss of high voltage to the fission chamber is sensed, a bistable circuit will be tripped, resulting in a scram.

The wide range log channel provides a continuous indication from 10^{-8} to 110% of full power for the local meter and the console data recorder. The log power level signal is also used by the low source count bistable circuit, the 1 kW permissive bistable, the pulsing channel, and the period channel.

The period signal is obtained by differentiating the wide range log signal. Reactor period is displayed on a local meter. A bistable circuit provides a scram and an alarm when rate exceeds a predetermined limit. The period signal is also used by the servo system. The period circuit is disabled initially in Square-Wave mode and at all times in Pulse mode.

The wide range linear channel provides a signal based on 0 to 110% of the range selected by a 19-position range switch. The wide range linear signal is used by the console data recorder and the servo system.

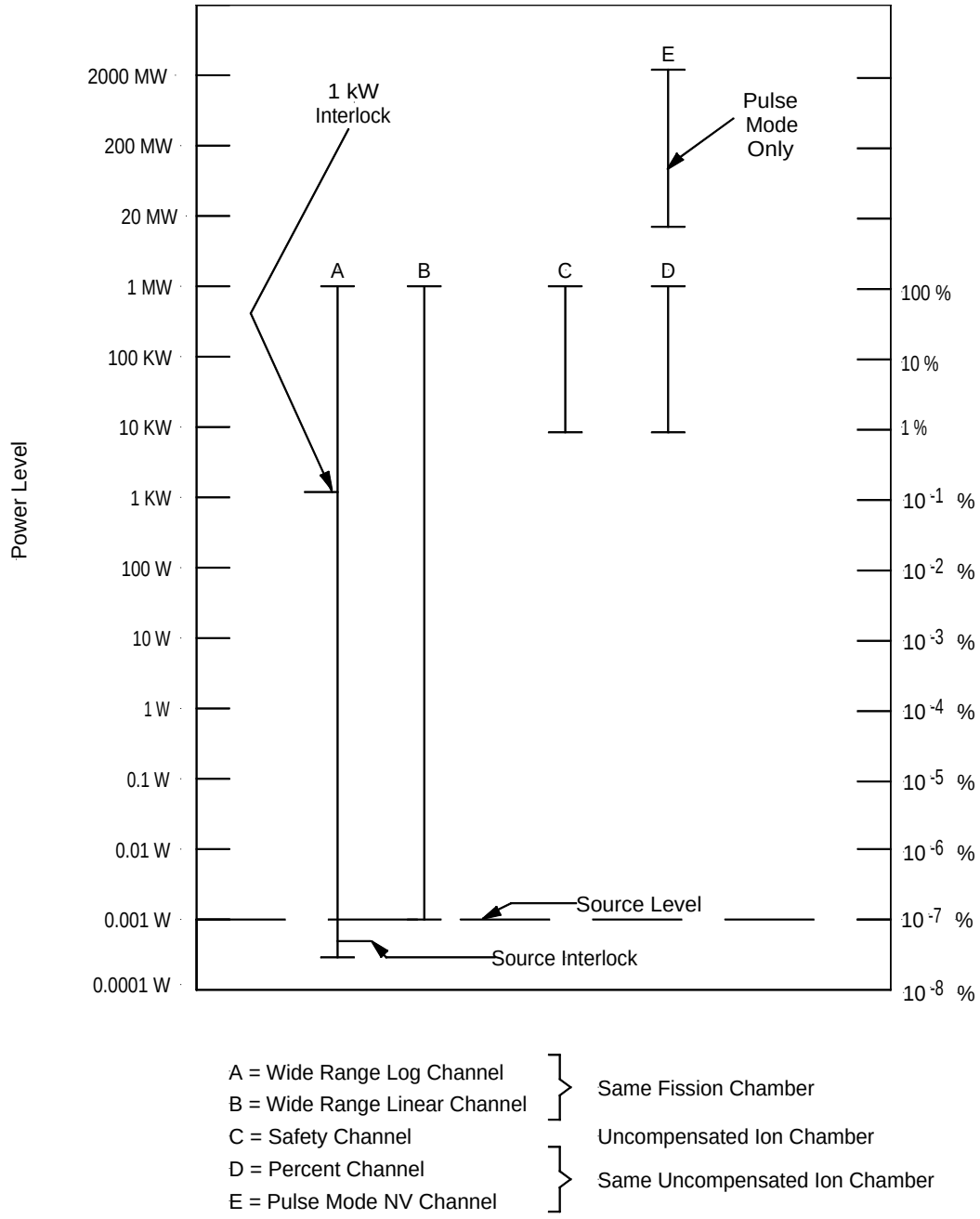

Figure 7.1 Relative Ranges of the OSTR Power Instrumentation

The safety channel provides a signal to a local meter scaled at 0 to 110% of full power. A bistable circuit provides scram and alarm functions if the high power setpoint is exceeded. The detector input to the safety channel is grounded in the Pulse mode of operation. A separate bistable circuit provides output to the reactor protection system upon a loss of detector high voltage.

The percent power channel is redundant in function to the safety channel. The percent power signal is also displayed on the scale of 0 to 110% of full power with high power scram and alarm outputs.

The pulsing channel displays peak power from a pulse on the scale of 0 to 100% of 1,000 MW in Pulse Low and 4,000 MW in Pulse High. A display of integrated energy is also provided on the scale of 0 to 100% of 20 MW-s for Pulse Low and 80 MW-s for Pulse High. A switch selects the energy to be displayed from either a two- or ten-second integration time. The pulsing Channel is enabled when the mode switch is placed in either Pulse position. The energy integration period starts when the wide range log signal exceeds a reference level. This also enables the peak hold circuit and starts a one-minute timer. The peak power and energy displays are reset at the end of the one-minute period. The peak power is also recorded on the console data recorder.

The percent power channel and the pulsing channel are both part of the power range monitor. The power range monitor will produce a scram and alarm output in response to a non-operable condition. A non-operable condition results from one or more of the following: test switches activated, loss of operating voltage, or loss of detector high voltage.

7.2.3.2 Temperature Measurements

As illustrated in Figure 7.2, fuel temperature is measured by three thermocouples embedded in the instrumented fuel element. A multipoint selector on the console allows selection of one of the thermocouples or a test signal for display and comparison against the high and low setpoints. The displayed temperature is also recorded on the console data recorder. The high and low setpoint comparators both send alarms to the annunciator panel. In addition, the high comparator sends a scram signal to the reactor protection system. The multipoint selector also allows test inputs to be selected. When the multipoint selector is not in a position corresponding to an active thermocouple, the rod withdrawal prohibit interlock is activated.

Temperature of the bulk pool water is measured by two thermocouples located on either side of the primary tank. One thermocouple is connected to a dedicated thermometer on the console for display. A setpoint comparator sends a high temperature alarm to the annunciator panel when the measured temperature exceeds the setpoint. A selector switch allows the second bulk water thermocouple as well as various points throughout the primary, secondary, and demineralized water systems to be selected for display on the console.

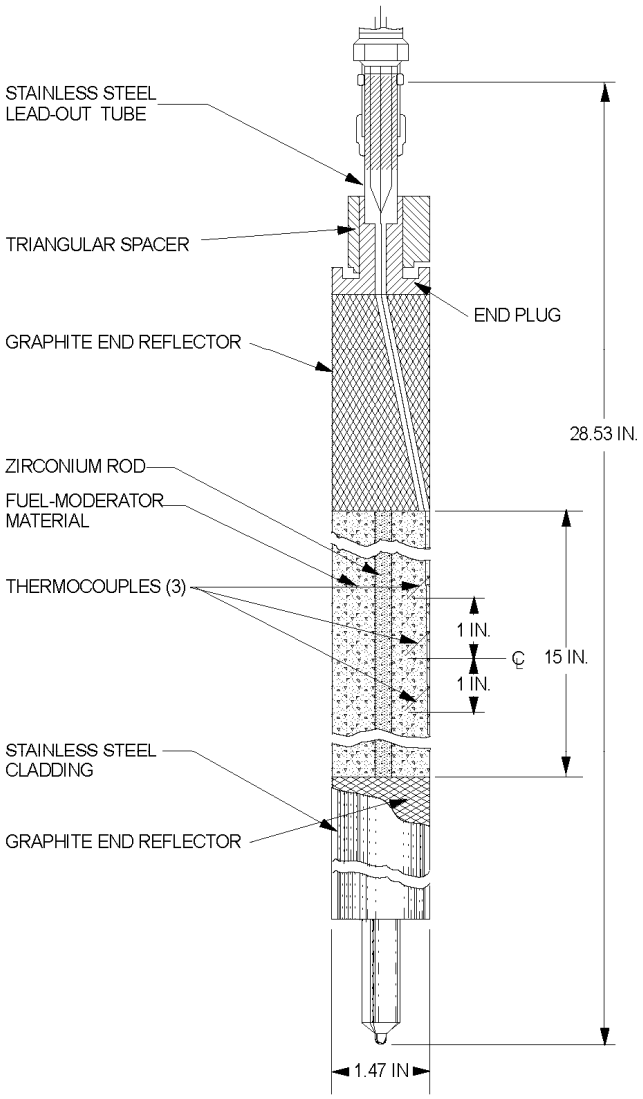

Figure 7.2 Instrumented Fuel Element

7.3 Reactor Control System

7.3.1 Control Rod Drives

The four control rods are positioned by control rod drives mounted on the reactor top center channel.

As illustrated in Figure 7.3, the safety, shim, and regulating control rod drives are rack-and-pinion linear actuators. An electromagnet is secured to the bottom of the draw tube to which the rack is mounted. The magnet is moved up or down in response to rotation of the pinion shaft. The control rod is attached to the armature by a long connecting rod. When the magnet is energized, the armature is magnetically coupled to the draw tube. De-energizing the magnet causes the rod to drop. A dash pot is incorporated into the armature section to decelerate the rod near the bottom following a scram. Limit switches sense when the magnet is fully withdrawn, the magnet is fully down, and the armature (and thereby the rod) is fully down. A ten-turn potentiometer is coupled to the pinion shaft to provide for rod position indication. The pinion shafts of the safety and shim control rod drives are shaft-coupled to AC gear reduction motors. The pinion shaft of the regulating control rod drive is chain-and-sprocket coupled to a DC stepper motor.

A connecting rod couples the transient rod to a piston rod assembly. As illustrated in Figure 7.4, the piston resides within an externally threaded cylinder. A ball screw nut acts on these external threads to raise or lower the cylinder. Rotation of the ball screw nut is accomplished by a worm gear coupled to an AC motor. A potentiometer is gear-driven by the worm gear shaft to provide rod position indication. A hydraulic shock absorber is incorporated into the top of the cylinder. Air from a compressor is connected to a normally-closed port of a three-way air solenoid valve. The common port is connected to the transient control rod drive cylinder below the piston. The normally-open port is vented. When the air solenoid valve is energized, air pressure is placed on the bottom of the piston causing the piston to be brought in contact with the shock absorber. The resulting reactivity insertion is dependant on the position of the cylinder prior to applying air. With air applied, energizing the motor in the up or down direction will cause the cylinder, piston, and control rod to move up or down as a unit. Scram of the transient rod is accomplished by de-energizing the air solenoid valve. This vents the air pressure under the piston and results in the control rod dropping. As illustrated in Figure 7.5, limit switches provide for sensing cylinder up, cylinder down, and rod down. A bracket extends over the top of the cylinder. A switch on the bracket opens a contact in the up circuitry when the shock absorber assembly contacts it. The bracket itself is substantial enough to stall the motor should the switch contact fail to open.

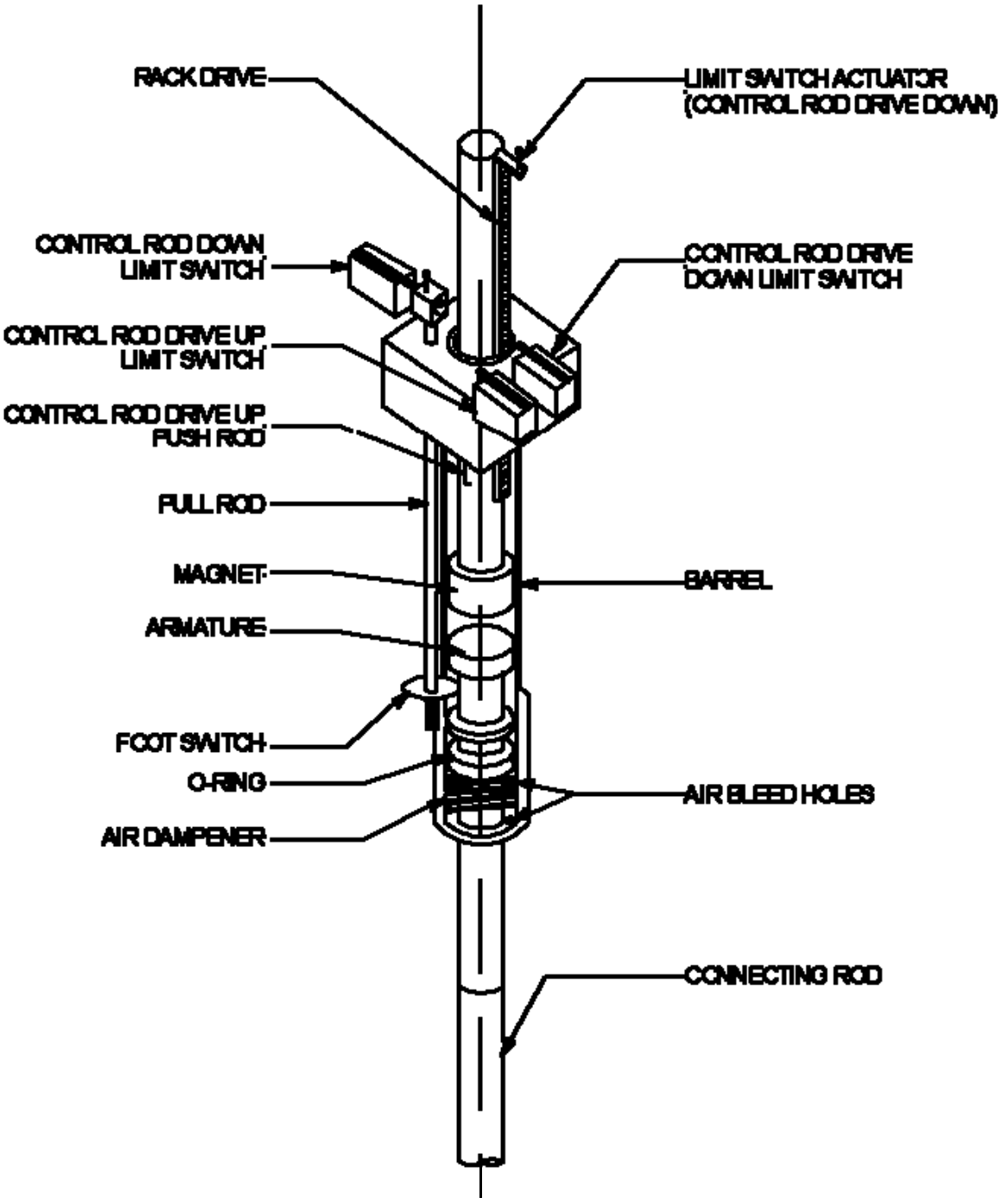

Figure 7.3 Standard Control Rod Drive and Limit Switches

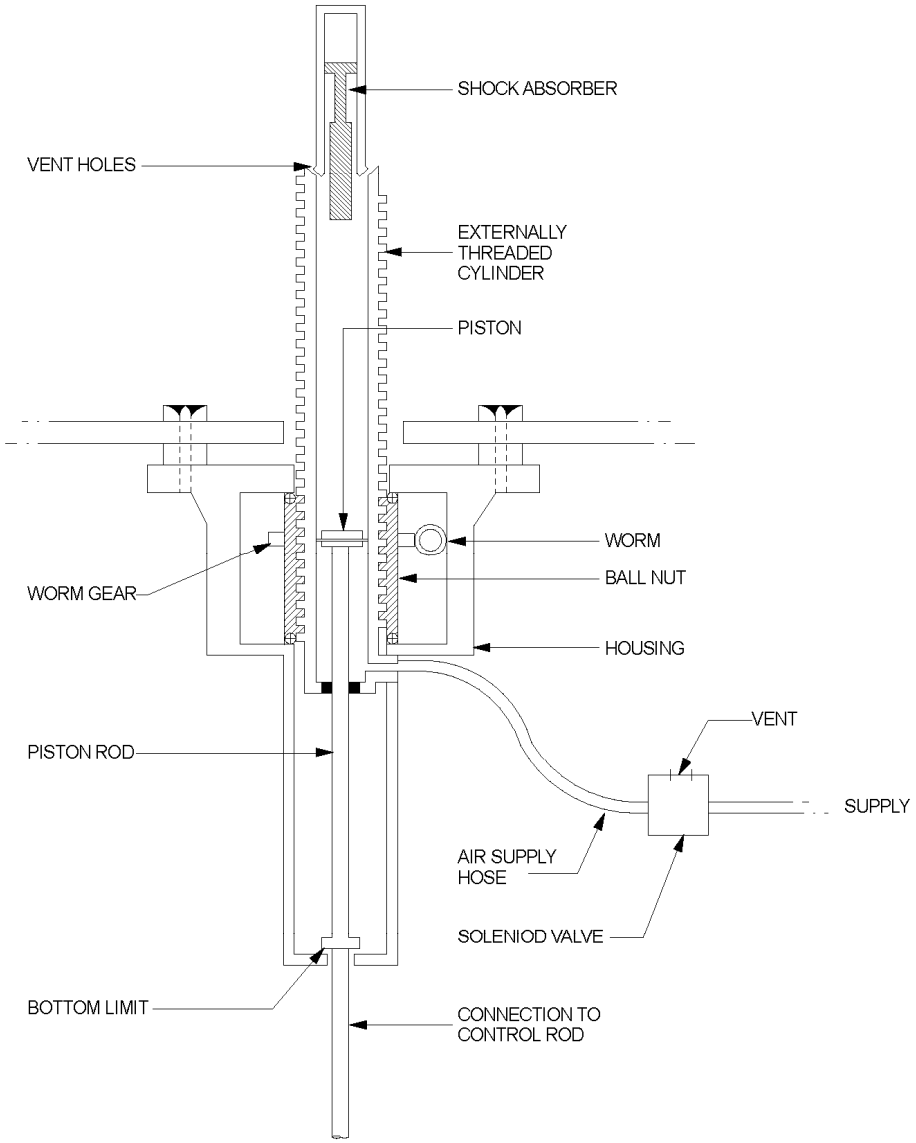

Figure 7.4 Transient Rod Drive

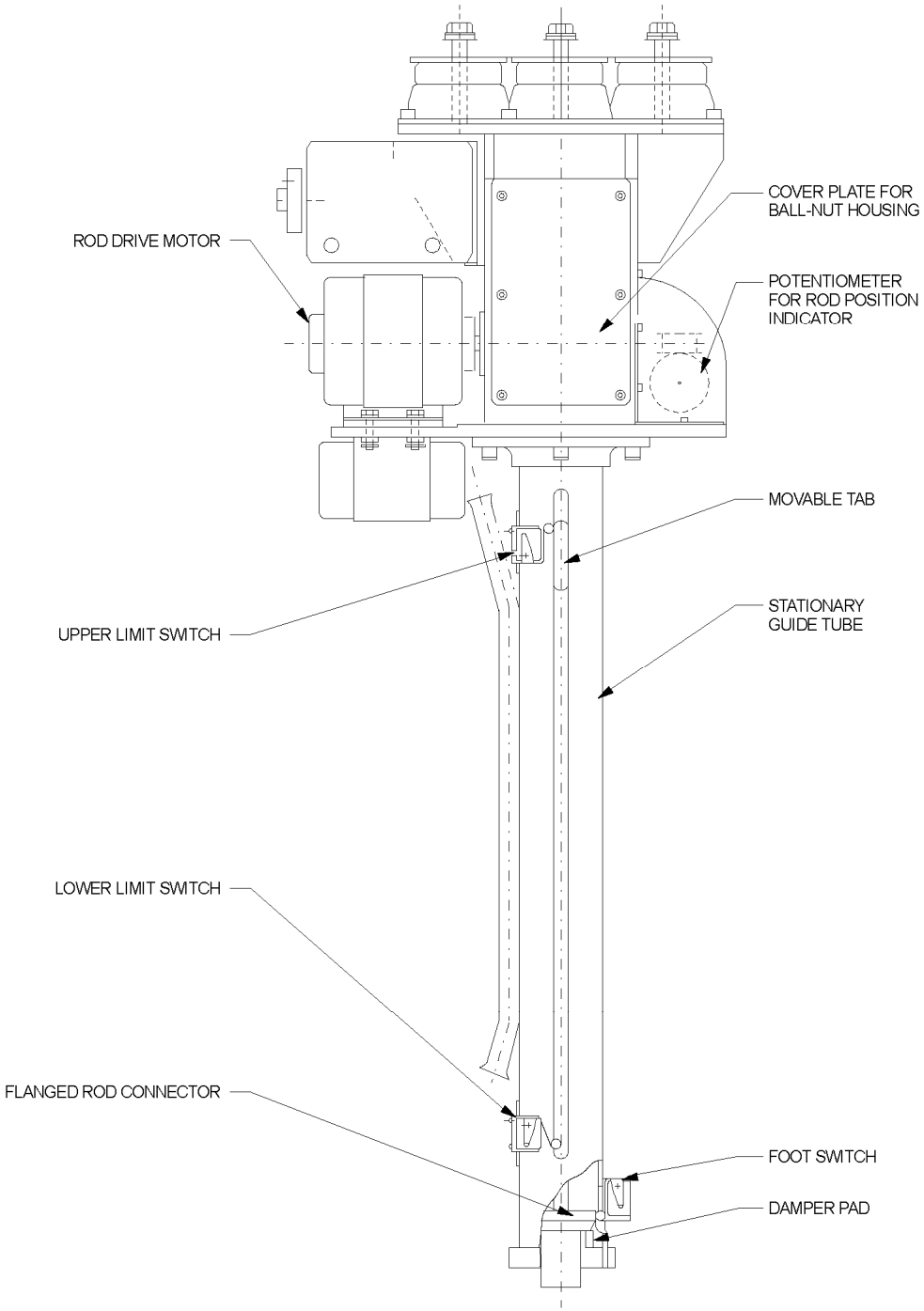

Figure 7.5 Transient Rod Drive Limit Switches

7.3.2 Servo System

In the Automatic and Square-Wave modes of operation, the regulating rod is controlled by the servo system to control reactor power based on input signals from the wide range linear channel, the reactor period channel, and the percent demand control.

In Automatic, wide range linear power is compared against the percent demand setting to obtain power error. The power error is limited at about 30 percent of full scale. The limited power error is compared against the inverted period signal to obtain total error. To reduce hunting, deadband comparators limit rod motion to total errors in excess of +/- 1%. The absolute of the total error is used for error proportional pulse width control. In response to a large error signal, the rod is driven almost continuously. As the magnitude of the total error gets smaller, the rod is driven for a smaller percentage of each 0.5-second interval. This reduces system overshoot during transients.

To perform a Square-Wave, the reactor must be configured in Steady-State mode. First, the reactor power is raised to some nominal low power (usually 15 W) with the air to the transient rod off. Second, the transient rod cylinder is raised to the position corresponding to the desired reactivity insertion. Third, the desired range is selected with the linear range switch. This causes wide-range linear power to indicate at the low end of scale. Finally, the mode switch is moved from Steady-State to Square Wave and the fire button pressed. Reactor power will increase to the desired power level and behave as if in Automatic mode.

7.3.3 Interlocks

The following are the interlocks utilized by the OSTR console:

- the transient rod, interlocked, both electrically and mechanically, to limit pulse reactivity insertions to less than the technical specification requirement;
- the 1-kW permissive interlock to prevent pulsing when wide range log power is above 1 kW;
- interlocks to prevent the safety, shim, and regulating rod drives from moving in pulse mode;
- interlock to ensure that only one control rod can be manually withdrawn at a time;
- the rod withdrawal prohibit interlock, activated by the low source count bistable circuit when wide-range log power is not greater than 2 cps and also activated by the period/log test switch, the detector current selector switch, and the fuel temperature multipoint selector. An alarm on the annunciator panel is activated by the rod withdrawal prohibit interlock.

7.4 Reactor Protection System

7.4.1 Scram Circuits

The scram circuits function to shut down the reactor by dropping all four control rods to their fully inserted positions. Scram is accomplished by de-energizing the magnets for the safety, shim, regulating rods and by de-energizing the air solenoid valve for the transient rod.

A reactor scram will result under any of the following conditions:

- operator-initiated manual scram;
- fuel element temperature in excess of LSSS;
- safety or percent power channels measuring power in excess of the setpoint;
- period channel measuring rate of power increase in excess of the setpoint;
- loss of high voltage to the power measuring channels; or
- external scram.

7.5 Engineered Safety Features Actuation System

There are no engineered safety feature actuation systems.

7.6 Control Console and Display Instruments

7.6.1 Console Data Recorder

The console data recorder digitally records and displays wide-range log and linear power and fuel temperature. In Pulse mode, the log input is disconnected and the linear input is replaced with peak power.

7.6.2 Rod Position Indication

Four rod position indicators are mounted in the console, each above the respective rod control switches. Rod position is displayed as 0 to 100 % of withdrawal with 0.1% resolution.

7.6.3 Annunciator Panel

The annunciator panel displays the alarm status of various instrumentation found in the facility. It is located above the console. The display for the annunciator panel is in the same direction as the display for the instrumentation on the console itself such that the reactor operator need only look up from the console.

7.6.4 Irradiation Facility Indication and Control

Irradiation facility status is available on the console for the pneumatic system and the beam ports. For the pneumatic system, a switch on the console turns the fan blower on and off. In the event that the operator suspects a malfunction or loss of control of the system or samples, the reactor operator can turn the fan blower off. This will prevent a sample from being inserted into the reactor or prevent the return of a sample to the receiving station if the sample has already at the terminus assembly. A detailed description of the pneumatic system can be found in section 10.2.4. A diagram of this control capability can be found in Figure 10.1.

Each of the four beam ports may internally contain a wooden plug equipped with an electrical circuit consisting of a position switch mounted on the inner face of the plug and an electrical connector on the outer face of the plug. The switch can be actuated only by the inner concrete plug when it is installed in the beam port. This switch is connected to the control room annunciator such that the reactor operator will have indication when the plugs have not been properly installed. Annunciation of status for other irradiation facilities or reactor experiments are done on an case-by-case basis.

7.7 Radiation Monitoring Systems

7.7.1 Area Radiation Monitors

Radiation levels are monitored at strategic locations throughout the reactor building. Each channel consists of a detector, a local meter with alert and alarm functions in the control room, and a remote indicator.

7.7.2 Airborne Radioactivity Monitors

Two dual channel airborne radioactivity monitors are in use at the OSTR. One unit samples the effluent from the reactor bay exhaust stack. The other unit is used as a continuous air monitor (CAM) on the reactor top.

In the stack monitor, air from the reactor bay exhaust stack is pulled through a paper particulate filter in close proximity to a detector connected to the particulate count rate meter. The sampled air then passes through a volume containing a detector connected to the gaseous count rate meter. The sampled air passes through the pump before being returned to the ducting on the suction side of the reactor bay exhaust fan. The pump is bypassed by a throttle valve to provide for flow adjustment.

The reactor top CAM samples and discharges air on the reactor top. In all other respects the operation of the CAM is similar to the stack monitor.

Alarms are provided on the annunciator panel for high and low counts on all four channels as well as low air flow. A stack monitor high particulate or gaseous activity alarm will result in a ventilation shutdown signal to the reactor bay ventilation controller.

7.7.3 Primary Water Activity Monitor

A probe with a GM detector is located in a cavity in the monitor vessel in the demineralized water system. The detector is connected to a count rate meter in the right-hand-side cabinet. An alarm with adjustable setpoint is connected to the annunciator panel to alert the operator to a significant increase in primary water activity.

CHAPTER 8

ELECTRICAL POWER SYSTEMS

Chapter 8 - Valid Pages
Rev. 1 5/1/2012

i	Rev. 0 7/01/2004
ii	Rev. 0 7/01/2004
1	Rev. 0 7/01/2004
2	Rev. 0 7/01/2004
3	Rev. 0 7/01/2004
4	Rev. 0 7/01/2004

TABLE OF CONTENTS

LIST OF FIGURES

THIS PAGE INTENTIONALLY LEFT BLANK

8 ELECTRICAL POWER SYSTEMS

8.1 Normal Electrical Power Systems

The design of the OSTR is such that the reactor can be shut down and safely maintained in a shutdown condition under a complete loss of electrical power.

A schematic representation of the electrical power system is provided in Figure 8.1.

Normal electrical power for the reactor and its associated equipment is supplied by a 4160-VAC, three-phase services from a substation located to the west of the Radiation Center. The service entrance conductors are contained in underground conduits from the substation.

The reactor loads, as well as the majority of the Radiation Center complex, are supplied by a 500-KVA transformer located in the penthouse of the Radiation Center. A 400-amp breaker in the main switchgear supplies sub-distribution panel A located in machinery room D106. From there, power is distributed to panels and loads throughout the reactor building.

Power for reactor control and instrumentation equipment is conditioned by the 3.1-KVA uninterruptible power supply (UPS).

8.2 Emergency Electrical Power Systems

The emergency power systems consist of a 25-kW diesel-fueled generator, a 3.1-KVA UPS, and associated panels and switchgear.

The emergency power systems are designated as Systems A and B. As shown in Figure 8.2, System A loads are supplied by the 3.1-KVA UPS. These loads include the reactor console and side cabinets, the reactor building public address amplifier, and the ventilation system controller. These loads normally receive conditioned power from the UPS and are unaffected by a loss of power to the building. The UPS is capable of carrying these loads on battery power for at least 15 minutes. A make-before-break bypass switch allows the UPS to be bypassed for maintenance without losing power to the System A loads.

System B loads include partial lighting for the control room and the adjacent hallway, CCTV monitors, the stack monitor pump, and the building fire alarm panel. These loads normally receive power from the building power distribution system. Upon a loss of power, these loads are interrupted. If the power loss lasts longer than about 20 seconds, the generator will automatically start and supply power to these loads and the UPS. Upon restoration of building power, the generator will continue to run for about one minute before automatically stopping. There is sufficient propane onsite to run the generator for several days, if necessary.

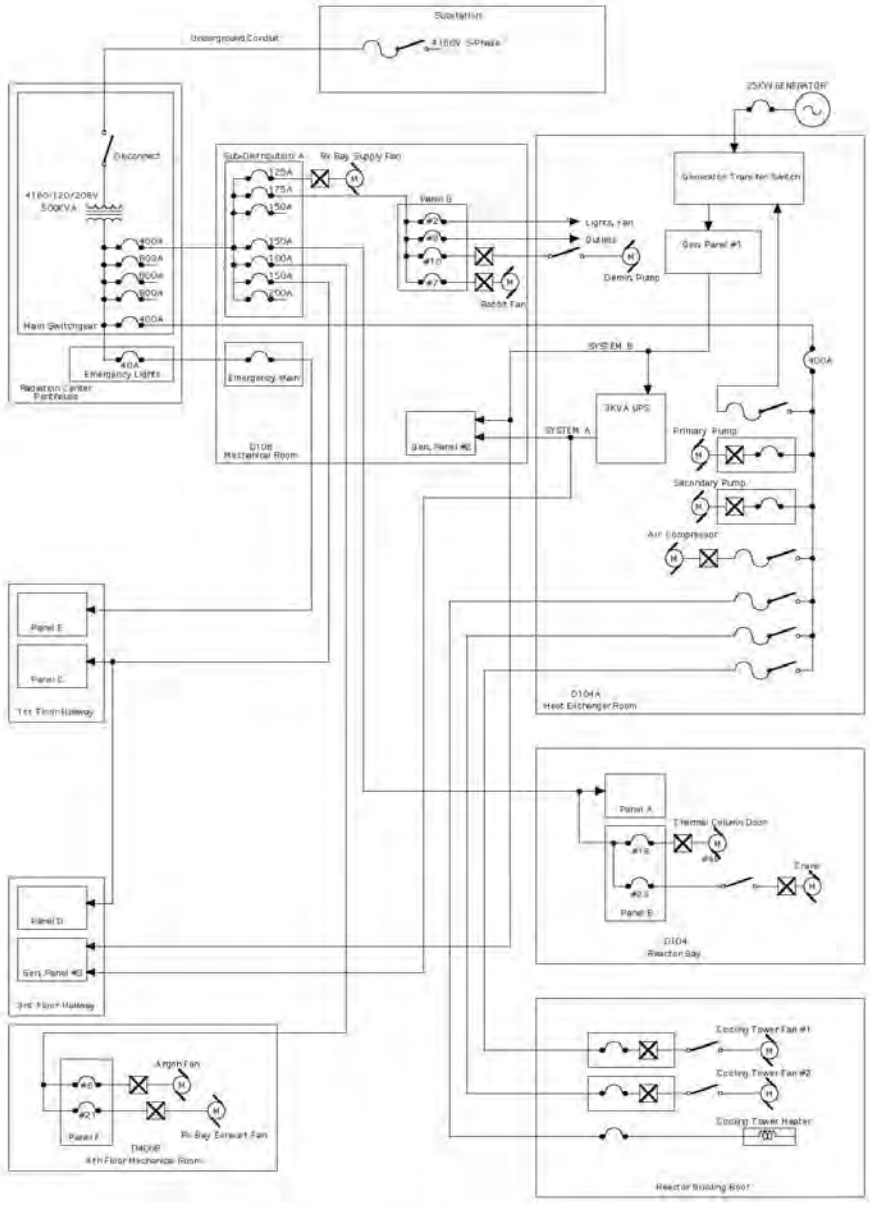

Normal Electrical Power System

Figure 8.1 Electrical Power System

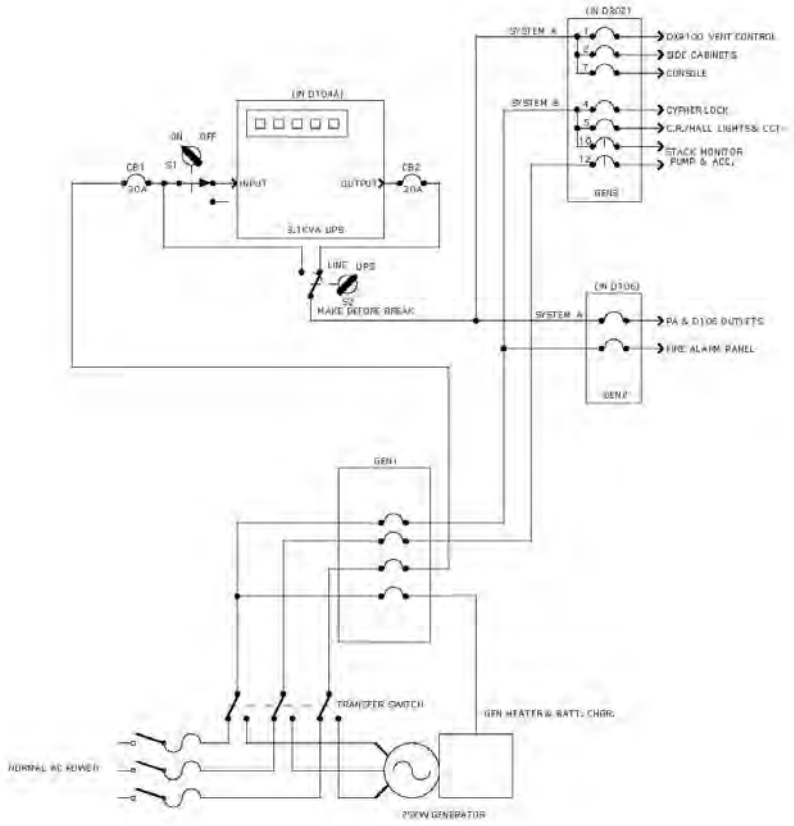

Emergency Electrical Power System

Figure 8.2 Emergency Electrical Power System

CHAPTER 9

AUXILIARY SYSTEMS

Chapter 9 - Valid Pages
Rev. 1 5/1/2012

i	Rev. 0 7/01/2004
ii	Rev. 0 7/01/2004
1	Rev. 0 7/01/2004
2	Rev. 0 7/01/2004
3	Rev. 0 7/01/2004
4	Rev. 0 7/01/2004
5	Rev. 0 7/01/2004
6	Rev. 0 7/01/2004
7	Rev. 0 7/01/2004

TABLE OF CONTENTS

LIST OF FIGURES

THIS PAGE INTENTIONALLY LEFT BLANK

9 AUXILIARY SYSTEMS

9.1 Heating, Ventilation, and Air Conditioning Systems

The controlled ventilation system acts to reduce the consequences of fission products released from the fuel or other experimental facilities. The objective of the structure surrounding the OSTR is to ensure that provisions are made to reduce the amount of radioactivity released into the environment by maintaining a negative pressure within the reactor building during operation. Automatic shutdown of the ventilation system confines the free air volume of the reactor building during emergency conditions. Remote monitoring of the conditions within the reactor building can be conducted.

9.1.1 Reactor Building Confinement

The reactor bay floor is a 6-inch concrete slab placed on a 6-inch compacted granular base. The building superstructure consists of precast-prestressed exterior wall panels and poured-in-place pilasters. The building has a structural steel roof frame with a metal deck and insulating concrete fill, as well as a structural steel interior floor frame with metal formed concrete slabs. A bridge crane with a 5-ton capacity serves the reactor bay area.

The first floor contains: (1) the main floor area of the reactor bay, which accommodates the reactor and the fuel storage pits; (2) the heat exchanger room, which houses the reactor cooling system components; (3) the rabbit lab, which houses the pneumatic transfer system receiver-sender stations; (4) the reactor support lab; (5) the mechanical equipment room, which contains the reactor bay ventilation fan, pneumatic transfer system blower, and the reactor building pressure regulating systems; and (6) the hot cell, which is used as a radiation source storage area.

The second floor contains: (1) two offices, (2) a rest room, which incorporates a decontamination shower and dressing room; and (3) the health physics office and lab.
A walkway is provided from the second floor hallway to the second level of the reactor structure. However, the door to the walkway is kept permanently locked for security reasons.

The third floor contains: (1) a conference room, which has windows that overlook the reactor bay; (2) the control room, which houses all the reactor controls and instrumentation; and (3) the reactor supervisor's office, which is adjacent to the control room. A walkway is provided from the third hallway to the third level (top) of the reactor structure.

The fourth floor contains: (1) an office; and (2) a mechanical equipment room, which houses the fume hood fans, main reactor bay exhaust fan, argon system fan, hot drain exhaust fan, and the stack monitor equipment.

The reactor building has a dry gravel roof. The reactor secondary system cooling tower is located on the south end of the roof adjacent to the reactor bay exhaust stack.

9.1.2 Heating and Ventilation

The reactor bay ventilation system, a schematic of which is shown in Figure 9.1, provides fresh air to the reactor bay area at the rate of 4.4E6 cm^3 s^{-1} and is independent of the Radiation Center or even the laboratories located in the reactor building. The incoming air travels through a pneumatic-operated damper, filter, heater coil, and the supply fan. The conditioned air then discharges into the reactor bay through four outlet ducts near the ceiling. The exhaust air exits the reactor bay through four outlet ducts; three near the ceiling and one near the floor. The floor duct exhausts half of the total volume of effluent to help facilitate mixing within the bay. Air exits the exhaust system through the main exhaust stack. The stack extends approximately 7.2 meters above the roof of the building, which places the exhaust approximately 20 meters above the ground. The air is discharged at approximately 1.97E3 cm s^{-1}, which ensures that the exhaust air carries to higher elevations and mixes rapidly with the surrounding air.

The reactor bay is maintained at a negative pressure in relationship to outside static air pressure by controlling the amount of air pumped into the bay. As illustrated in Figure 9.2, a stand-alone controller with a variety of system monitoring analog/digital inputs and analog-to-pneumatic outputs controls the reactor bay pressure by modulating the supply duct pneumatic operating cylinders and their attached dampers. The controlling analog-to-pneumatic signal will change depending on the difference in pressure between the reactor bay and the outside atmosphere. Changes in atmospheric pressure and filter loading are automatically compensated for to maintain a preset bay pressure. Other analog output signals from the controller act to control inlet duct air temperature based on reactor bay temperature and a supply duct temperature detector located downstream of the heating coils. Two different sized steam valves are used to control the inlet duct air temperature. Sensed bay temperature causes the controller to modulate the steam valves to vary inlet duct air temperature between 70EF and 80EF when inlet air temperature is below 70°F. This supply temperature band helps to limit temperature stratification within the bay. Steam supply coil freeze protection is provided by an automatic shutdown of the system fans, damper closure, and steam valve full-open signals should inlet duct temperatures drop below 37°F.

Exhaust from the laboratories located in the reactor building is discharged above the roof of the building through individual exhaust fans. The laboratories are under slight negative pressure with respect to the outside and slightly positive with respect to the reactor bay. Drains for radioactively-contaminated liquids from the reactor building laboratories do not incorporate water traps. These drains are vented by an exhaust fan. The drain exhaust fan discharges into the reactor bay main exhaust plenum. This discharge arrangement ensures the detection of radioactive gases from the drain line by the stack monitor.

All reactor building ventilation fans can be started and stopped manually from the control room. The reactor bay exhaust and supply fans are interlocked to start and stop with a single switch. In addition, the argon exhaust and the pneumatic transfer room hood fans are interlocked to turn off at the same time as the reactor bay fans.

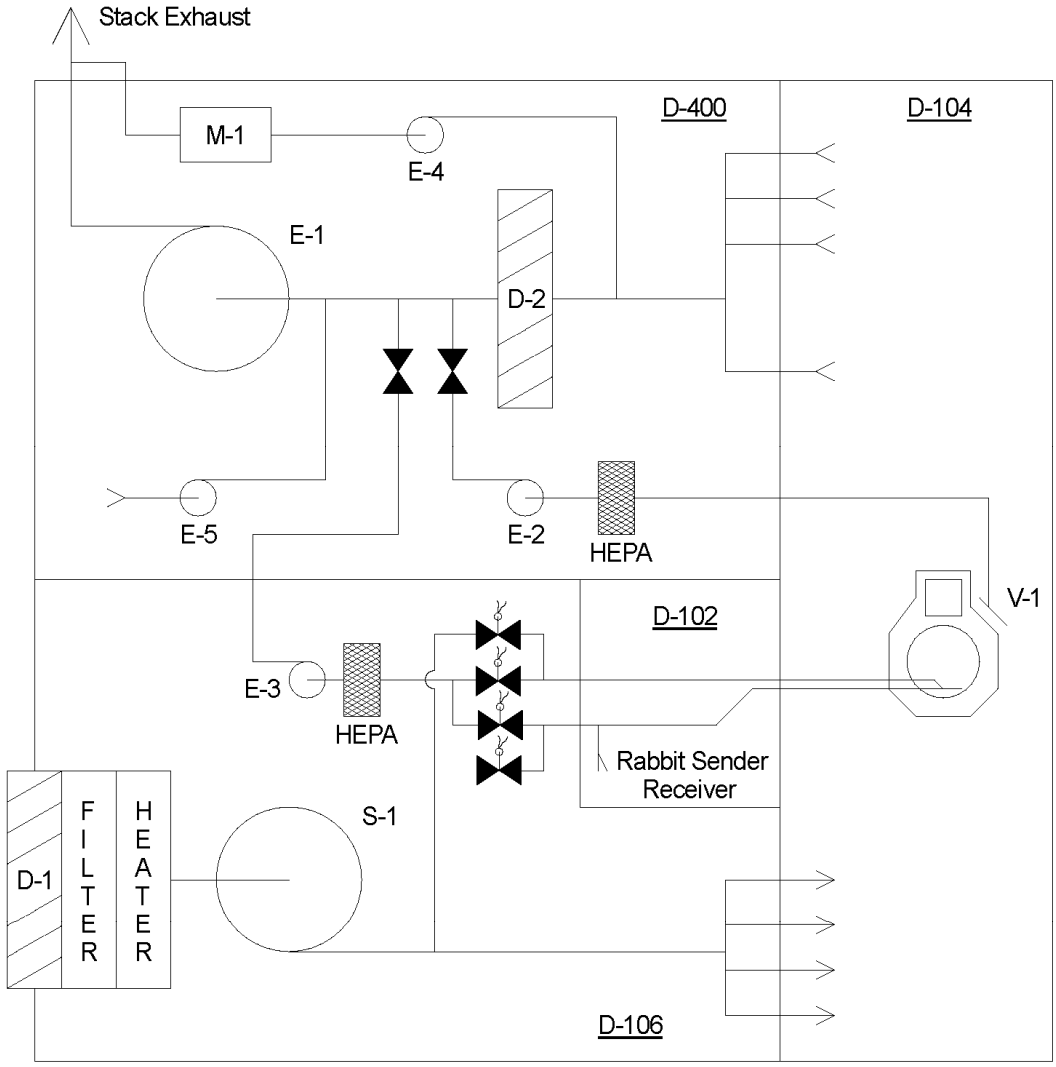

SYMBOL	Function
S-1	Rx Room Supply (12,000 CFM)
E-1	Rx Room Exhaust (12,000 CFM)
E-2	Argon Exhaust Fan (~5 CFM)
E-3	Rabbit Suction / Exhaust (135 CFM)
E-4	Stack Gas / Particulate Monitor Blower (~8 CFM)
E-5	Contaminated Water Drain Vent Fan
D-1	Supply Damper
D-2	Pressure Control Damper
M-1	Stack Gas Particulate Radiation Monitor
V-1	Argon Manifold

Figure 9.1 Reactor Bay Ventilation Schematic

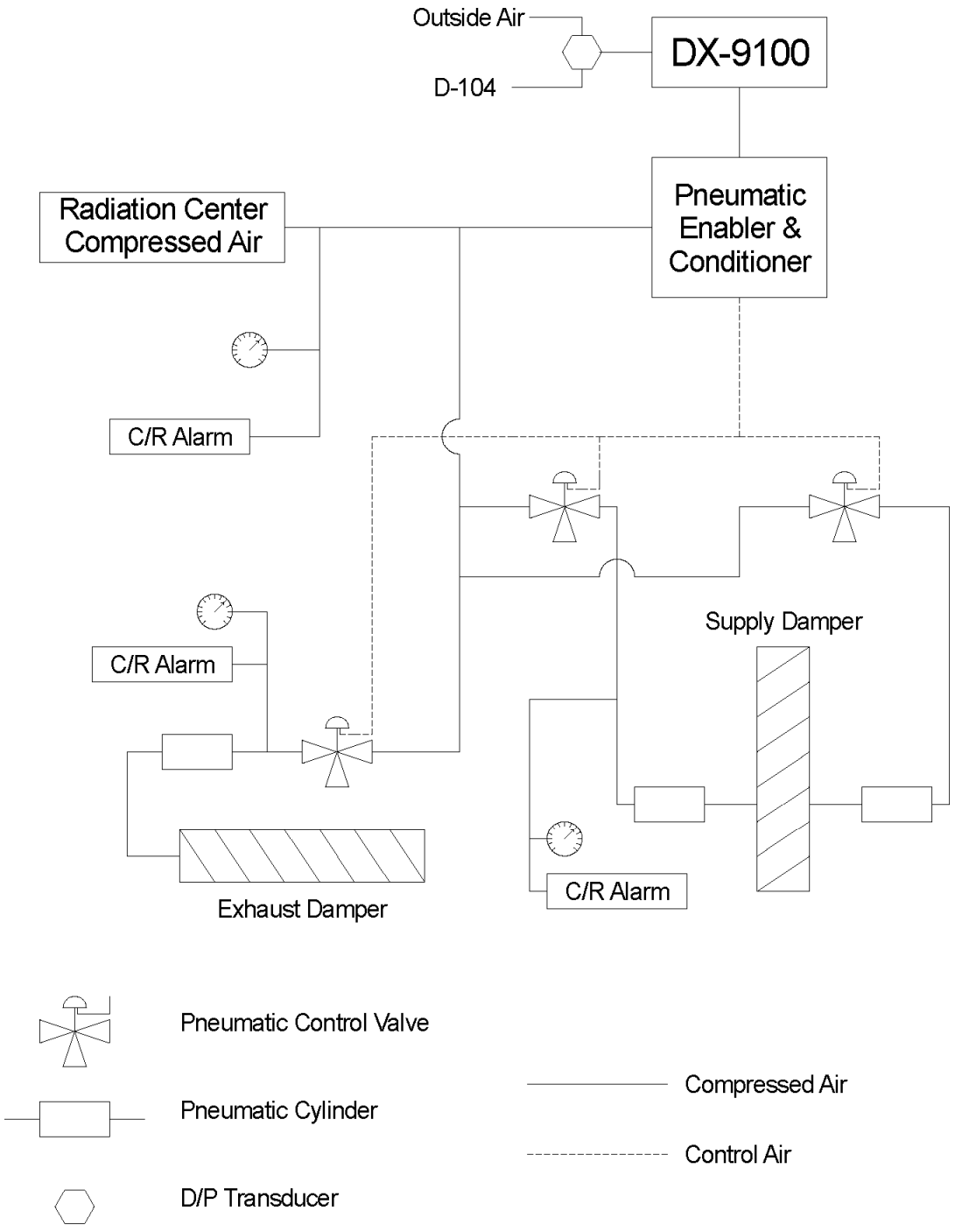

Figure 9.2 Reactor Bay Ventilation Control Schematic

9.1.3 Ventilation System Emergency Shutdown

The ventilation system is designed to provide for the automatic containment of airborne radioactive material. Stack gas and particulate detectors constantly monitor the outgoing reactor bay airflow using an isokinetic probe in the vertical exhaust stack to ensure accurate activity monitoring. Only two radioactive gases are normally produced: ^{16}N and ^{41}Ar. However, due to transport delays, the amount of ^{16}N (formed from $^{16}0$ in the pool water) reaching the detector is insignificant. Most of the ^{41}Ar produced during routine operation comes from the experimental facilities which have their own argon ventilation system exhausting directly to the stack. When the exhaust activity indicates that a substantial release of radioactivity is occurring, the ventilation system controller will open contacts for both the supply and exhaust fan motors. At the same time, the signal to the 3-way solenoid valves on the supply and exhaust dampers will be lost, causing them to vent and, thereby, closing the system supply and exhaust dampers. In addition, the argon and pneumatic transfer system hood fans will be shut down by opening contactors in-line with their power supply. The reason for ensuring that the hood fan in the pneumatic transfer station switches off when the reactor bay exhaust fan goes off is to maintain a negative pressure differential between the reactor bay and the adjoining rooms. The argon exhaust fan will not restart until the reactor supply and exhaust fans have been in operation for approximately one minute. A manual reset input by the operator is required to restart the system if the ventilation system is shut down for any reason.

9.2 Handling and Storage of Reactor Fuel

The fuel loading for the OSTR consists of approximately 100 elements, including three control rods, a transient rod, and instrumented element and graphite elements. The fuel elements can be stored within the reactor tank grid plate, in-tank hanging storage racks, and storage pits in the reactor bay floor.

Fuel handling consists of :

- receiving unirradiated fuel elements;
- transferring fresh unirradiated fuel into the reactor tank; and
- moving irradiated fuel elements within the core or to/from in-tank storage racks.

9.2.1 In-Tank Storage Racks

The OSTR has four in-tank storage racks. They are identified as the “X”, “Y”, “Z”, and “S” racks. The X, Y, and Z are capable of holding up to 20 fuel elements in a 2X10 array. The S rack holds up to 6 fuel elements in a 2X6 array. The storage racks do not contain any poison materials. Each rack has a upper “grid plate” and a lower “grid plate” that the fuel slides through. Once in the grid plates, the fuel rests on a plate that contains no penetrations. This arrangement provides for adequate convective cooling to maintain any stored fuel elements below the design criteria for the fuel. Two 15-foot aluminum rods are used to support each rack. These rods are fastened at their lower ends to the rack and at the upper ends to brackets on the top edge of the reactor tank. This mounting arrangement prevents the racks from tipping or being

laterally displaced. All of these racks were designed and fabricated by General Atomics® when the reactor was originally built. All racks have a multiplication constant (K_{eff}) that is less than 0.8. (Ref. 9.1).

9.2.2 Fuel Handling Tool

Tools are provided for handling individual fuel elements and for manipulating other core components. Individual fuel elements are handled with a flexible tool provided by General Atomics®. The tool utilizes a locking ball-detent grapple that attaches to the top end fitting of a fuel element. All fuel handling tools are provided with the capability of being locked and secured when not in use.

9.2.3 Fuel Element Inspection Tool

The fuel element inspection tool is used to accurately inspect fuel elements for longitudinal growth and for bowing. The upper support plate of the inspection tool is secured to the top of the reactor tank. The inspection tool extends downward into the tank permitting the inspection of an irradiated fuel element while maintaining water shielding over the element. All parts of the tool that come in contact with the reactor water are either aluminum or stainless steel. The aluminum support tube is open at the bottom and top to allow water to fill the interior of the pipe.

Bowing of a fuel element is detected by a carefully machined cylinder (called a go/no-go gauge) attached to the bottom of the tool. If a fuel element will slide completely into the machined cylinder, its bow, if any, is less than the specified limit. When the element passes through the cylinder, it will come to rest on the plunger of a spring-loaded bellows assembly. The length of the fuel element is measured by pushing downward on the indexing rod until the indexing rod plug moves an incremental amount and touches the indexing plate. This action places the upper surface of the fuel element's triangular spacer at an indexed position common to all fuel elements measured. At the same time, the lower surface will displace a plunger. This displacement is measured with a dial indicator.

9.3 Fire Protection System

The purpose of the fire protection system is to provide detection and notification capability which will mitigate loss of property and life in the event of a fire. The reactor bay has thermal fixed/rate-of-rise fire detection as well as manual pull stations. The system is zoned, reports to an annunciator in room A100 of the Radiation Center, reports automatically to the dispatch room for OSU Department of Public Safety which is occupied 24/7/365 , and activates an audible alarm system throughout the Radiation Center. OSU Department of Public Safety notifies Corvallis Fire Department if necessary. A number of fire extinguishers are positioned in the reactor bay, adjacent rooms and laboratories. The fire extinguishers and detection system are regularly inspected by a contractor employed by OSU.

9.4 Communications

The reactor control room is equipped with a single line commercial telephone. An intercom system is installed in various locations within the reactor bay, control room, entrances into the reactor bay, and surrounding supporting offices and laboratories. This system provides two-way communications with every other station and all-call capability for paging. Additionally, a public address system provides one-way paging ability throughout the reactor building and Radiation Center.

9.5 Possession and Use of Byproduct, Source and Special Nuclear Material

All activities using byproduct, source, and special nuclear material covered under the reactor license take place within the reactor building (any room designated with "D"). Material covered under the reactor license may be located in various rooms within the Radiation Center for the purpose of analyzing samples with instrumentation otherwise unavailable in the reactor building (e. g., gamma spectroscopy, liquid scintillation counting, gross alpha/beta counting). Byproduct, source and special nuclear material use other than identified above is covered under State of Oregon Broad Scope License ORE-90005.

9.6 Cover Gas Control in Closed Primary Coolant Systems

This section is not applicable because no such system exists.

9.7 Compressed Air System

Filtered and regulated compressed air is provided to the reactor building for general use and to operate the transient rod air cylinder. The primary system utilizes a 7.5 Hp 480 VAC 3 phase skid mounted two-cylinder two-stage reciprocating compressor, water separator/cooler and a pressure tank located in room D104A. An outlet pressure regulator maintains the supply air pressure at 80 psig. Low pressure alarms annunciate on the reactor control room annunciator panel to provide indication of inadequate air supply. Backup service can be provided, if needed, by cross connecting the distribution system to the two compressor systems used for the Radiation Center.

9.8 References

9.1 Memorandum, Fabian C. Foushee to Distribution, "Storage of TRIGA® Fuel Elements," General Dynamics, General Atomic Division, March 1, 1966.

CHAPTER 10

EXPERIMENTAL FACILITIES AND UTILIZATION

Chapter 10 - Valid Pages
Rev. 1 5/1/2012

i	Rev. 0 7/01/2004
ii	Rev. 0 7/01/2004
1	Rev. 0 7/01/2004
2	Rev. 0 7/01/2004
3	Rev. 0 7/01/2004
4	Rev. 0 7/01/2004
5	Rev. 0 7/01/2004
6	Rev. 0 7/01/2004
7	Rev. 0 7/01/2004
8	Rev. 0 7/01/2004
9	Rev. 0 7/01/2004
10	Rev. 0 7/01/2004
11	Rev. 0 7/01/2004

TABLE OF CONTENTS

10 EXPERIMENTAL FACILITIES AND UTILIZATION

LIST OF FIGURES

THIS PAGE INTENTIONALLY LEFT BLANK

10 EXPERIMENTAL FACILITIES AND UTILIZATION

10.1 Summary Description

The Oregon State TRIGA® Reactor (OSTR) provides neutron and gamma irradiation facilities for use by Oregon State University instructors and researchers, and other public and institutional users. All systems are designed and operated to control the amount of radiation exposure received by the general public, as well as facility personnel. Incidental production of ^{41}Ar is also mitigated in order to minimize both the environmental release amounts and the exposure of personnel within the reactor facility. The following experimental facilities are provided at the OSTR:

- Three Radial Beamports and one Tangential Beamport;
- The Thermal Column;
- The Thermalizing Column;
- The Pneumatic Transfer system;
- The Central Thimble;
- Vertical Irradiation Tubes;
- The Rotating Rack.

A list of currently approved experiments is maintained at the facility, and includes evolutions such as normal reactor operation and routine use of experimental facilities. Any evolution not included on the current list of approved experiments must be reviewed and approved in accordance with Section 10.3 prior to performance.

10.2 Experimental Facilities

10.2.1 Beamport Facilities

Four beamports penetrate the concrete shield and pass through the reactor tank water to the reflector region of the core. These ports provide beams of neutron and gamma radiation for a variety of experiments. They also provide irradiation facilities for large specimens (up to 6-inch diameter) in a region close to the core. Three of the beamports are oriented radially with respect to the center of the core, and the other port (B.P. #3) is tangential to the outer edge of the core. Two of the radial ports (B.P. #1 and B.P. #2) terminate at the outer edge of the reflector assembly; however, B.P. #1 is aligned with a cylindrical void in the reflector graphite. The last radial port (B.P. #4), which is called the piercing beamport, penetrates into the graphite reflector and terminates at the inner surface of the reflector assembly, just at the outer edge of the core. The tangential beamport (B.P. #3) terminates at the outer surface of the reflector, but it is also aligned with a cylindrical void, which intersects the piercing port in the reflector graphite. This tangential port provides a neutron beam while reducing the amount of core gamma radiation. The purpose of the graphite void is to maximize the total radiation streaming down the port.

To shield the radiation streaming through the clearance between the beamports and the inner shielding plugs, the outer embedded portions of the beamports are stepped to allow larger diameter (8-inch) shielding plugs. These outer sections of the beamports are made of steel and are cadmium-plated on the inside for protection against corrosion. A small pipe to the argon vent system leads from each of these outer beamport sections and makes it possible to purge any accumulated radioactive gases.

The beamport inner sections are made of aluminum and are divided into two parts; one part with a nominal 6-inch inside diameter tube embedded in the concrete shield, and the other part a nominal 6-inch inside diameter tube welded to the aluminum tank. A gap, between the aluminum section embedded in the concrete and the aluminum section welded to the tank, has been provided to prevent stresses resulting from thermal expansion in the aluminum tank.

A steel shadow shield is placed around each beamport (in the concrete bioshield) to provide additional shielding for the area adjacent to the beamport. The shadow shield surrounds the 6-inch diameter aluminum portion of the beamport immediately adjacent to the 8-inch diameter steel section.

The piercing beamport that penetrates the reflector (B.P. #4) consists of a tube section embedded in the concrete shielding and a tube section flange-welded to the aluminum tank (these sections are discussed in the preceding paragraph). The innermost region is comprised of a tube section welded into the reflector assembly and a flexible bellows assembly that connects the inner two tube sections and compensates for construction tolerances.

Shielding is provided along the axis of the beamports to minimize the radiation levels outside the concrete structure when the beamports are not in use. The shielding consists of an inner concrete plug, an outer wooden plug, a lead-filled shutter and a lead-lined door.

The inner part of the beam-port shielding is a concrete-filled aluminum plug which is joined to an outer steel head. The shielding material in the inner plug consists of a thin liner of boral on the inner end followed by about 4 inches of lead, which is then followed by borated normal-density concrete and the outer steel head. The inner end of the shielding plug is cone-shaped to help guide the plug (during insertion) over the step in the beamport where the change in diameter occurs. The inner plug provides the major shielding in the beamport.

The outer section of the beamport shield is a wooden plug equipped with button-like protrusions to ensure centering and to reduce friction during insertion and removal. The outer plug is equipped with an electrical circuit consisting of a position switch mounted on the inner face of the plug and an electrical connector on the outer face of the plug. The switch can be actuated only by the inner plug when it is installed in the beamport. A beam plug annunciator circuit is provided in the control room which will indicate (by a light on the annunciator panel) when the inner and outer beam plugs are not both properly installed.

The outer end of the beamport is equipped with a lead-filled safety shutter and door to provide limited gamma shielding when the plugs are removed. It is mounted in a rectangular recessed

box in the concrete shield. It is about 4 inches thick and is welded from steel plate and filled with lead. The shutter can be moved either by hand (if the beamport door is open) or by a push rod.

The recessed shutter box is covered with a steel door, which is lined with lead for additional shielding. The door is equipped with a rubber gasket and several screw-type clamps which permit the door to be closed tightly to prevent rapid loss of reactor tank water if a beamport should develop a serious leak. Whenever the beamport is not in use, the door is closed and locked to prevent accidental or unauthorized use.

10.2.2 The Thermal Column

The thermal column is a large, boral-lined, graphite-filled aluminum container situated on the south side of the reflector. Its outside dimensions are 4 feet by 4 feet in cross section by approximately 5 feet in length.

The thermal column liner is a seal-welded container fabricated in two sections from aluminum plate. The outer section is embedded in the concrete shield and the inner section is welded to, and is an integral part of, the aluminum tank. The surfaces of the outer section which are in contact with the concrete are wrapped with plastic tape for corrosion protection. The inner section (welded to the aluminum tank) extends to the graphite reflector and matches the contour of the reflector. The horizontal centerline coincides with that of the core centerline. In a vertical plane, the column extends approximately 12 inches above and below the reflector, with the centerlines of the column and the reflector coinciding.

The aluminum container is open toward the reactor room. Blocks of AGOT nuclear-grade graphite occupy the entire volume. The individual blocks are approximately 4 inches by 4 inches in cross section, the longest being 50 inches in length. All pieces are stamped with identification letters and numbers.

Five graphite blocks serve as removable stringers. These five stringers were machined slightly undersize for easy removal and insertion. The central stringer is aligned with an access plug in the thermal column door and it could, therefore, be removed and inserted without having to move the entire door. To gain access to the other four stringers, the thermal column door must be rolled back on its tracks.

Surrounding the graphite on the inside of the aluminum casing (on all four sides) are sheets of boral, which are incorporated in the design to reduce the production of capture gamma by reducing the neutron flux in the surrounding concrete shield.

The outer face of the thermal column is shielded by a track-mounted door. The door is recessed into the biological concrete shielding and is flush with the shield structure when closed. To reduce the radiation streaming, the door configuration is of a stepped design. The door is filled with heavy-aggregate concrete. Its total weight is about 19 tons. A four-wheeled carriage

supports the door and rolls on two steel rails which are flushwith the door. A boral sheet is attached to the movable door on the door surface facing the thermal column (inner side).

10.2.3 The Thermalizing Column

The thermalizing column is situated on the west side of the reflector, and is constructed into sections similar to the thermal column, but smaller. Its outer section extends from the bulk-shielding tank through the concrete shielding up to the aluminum reactor tank. The inner section of the column is welded to, and is an integral part of, the tank and extends inward to the reflector assembly and matches its contour. The construction of the thermalizing column in to two sections allows for thermal expansion of the aluminum reactor tank during reactor operation. The bulk-shielding experimental tank is 12 feet deep, 8 feet wide, and 9 feet long. The tank is lined with welded stainless steel.

The thermalizing column is fabricated from seal-welded aluminum. The horizontal centerline coincides with the centerline of the reactor core. The surface of the outer section, which is in contact with the concrete, is wrapped with plastic tape for corrosion protection. An aluminum (neutron window) cover plate separates and seals the bulk-shielding tank water from the thermalizing column. In the region adjacent to the concrete shield, the aluminum container is lined with boral sheets in the same manner as the thermal column.

At the inner end (the end nearest the reactor core), the column is filled with graphite blocks to an axial thickness of 8 inches. All the blocks are made from standard machined blocks of AGOT nuclear-grade graphite. This 8-inch wall of graphite is backed by a 2-inch thick lead slab.

10.2.4 The Pneumatic Transfer System

Very short-lived radioisotopes can be produced for analysis with the aid of the pneumatic transfer system which rapidly conveys specimens to and from the reactor core. The pneumatic transfer system, also known as the rabbit system, consists of a blower-and-filter assembly, a valve assembly, a terminus assembly, a receiver assembly, a control assembly, tubing and fittings.

The system is controlled from the sample preparation and receiving area (Room D-102) and may be operated either manually or automatically, i.e., with an electric timing device so the specimen capsule can be retrieved automatically from the core after a predetermined length of time. Four solenoid-operated valves control the air flow. The system operates on a pressure differential, drawing the specimen capsule into and out of the core by vacuum. Thus, the system is always under a negative pressure so that any leakage is always into the tubing system. All the air from the pneumatic system is passed through an absolute filter before it is discharged to the building exhaust system. A cutout switch in the reactor control room (D-302) provides electric power to the blower motor, thus precluding unauthorized use of the rabbit system.

The specimen capsule, or rabbit is made of polyethylene. The capsule is designed to pass freely in a tube with a curved section no smaller than 2 feet. There are two styles of rabbit capsules

used at the OSTR, a long version and a shorter version. A capsule is discarded when it shows a significant discoloration, as this indicates that is becoming embrittled by irradiation. A brittle capsule could shatter upon impact in the terminus, which would necessitate removal of the terminus from the core to retrieve the pieces of the capsule.

The blower-and-filter assembly is installed in room D-106 on a wall-mounted steel angle support. The assembly consists of a blower, a manifold, plenum chambers, and a filter. The blower exhausts the system air into a vent pipe that discharges to the building exhaust stack. The blower is driven by a 220-VAC motor and is equipped with sealed ball bearings that have permanent lubrication and thus require no regular maintenance. The filter, which is sandwiched between the plenum chambers, has a medium of superfine glass and separators composed of Kraft paper. The minimum filter efficiency is 99.97 percent. This filter cannot be cleaned for reuse, but must be replaced when periodic visual inspection indicates a reduction in efficiency due to accumulation of impurities on the filter.

Adjacent to the blower assembly, four solenoid-operated valves are mounted on a common bracket. In the de-energized condition (for sample withdrawal from the core), valves 2 and 4 are open and valves 1 and 3 are closed. In the energized condition (for sample insertion), the valve lineup is opposite. Valves 1 and 4 open to the filtered air incoming from the building fresh air supply, and valves 2 and 3 are connected by flexible hoses through the plenum chambers and filter to the blower suction (See Fig. 10.1). Energized and de-energized configurations ensure that pressure inside the rabbit system is always lower than ambient pressure whenever the blower is running.

The terminus assembly is located in the reactor tank. The bottom part which is a double tube, extends into the reactor core. The terminus support is shaped like the tip of a fuel-moderator element and will, therefore, fit into any fuel location in the core lattice. The prescribed location for the terminus assembly is in the “G” ring of the lattice and is presently located in G-2. The bottom part extends into the reactor core. The terminus support is shaped like the tip of a fuel-moderator and can, therefore, fit into any fuel location in the core lattice. The prescribed location for the terminus assembly is in the “G” ring of the lattice and is presently located in G-2. Approximately 6 inches above the top grid plate, the terminus end of the tube branches into two separate tubes, both of which extend to the top of the reactor tank. The tubes are made of aluminum. These tubes continue in to the pipe trench; one tube connecting the terminus assembly to the receiver, and the other connecting it to the blower assembly. To counteract buoyancy, the terminus assembly is weighted to keep it firmly in place in the core. The bottom of the internal tube is equipped with an aluminum spring shock absorber to absorb the impact of the specimen container when it is inserted into the terminus.

The specimen capsule is inserted in, and removed from, the pneumatic system through an aluminum cover in the receiver-sender assembly located in room D-102. The cover is hinged on the upper side and has a latch on the lower side, and it is designed to stop the ejected capsule in the receiver assembly. When inserted into the assembly, the capped end of the rabbit will rest on a removable shelf (with foam rubber on top) permitting proper closure of the cover. The foam rubber cushions the impact of the returning rabbit.

The control assembly consists of a mounted box that contains an electrical timer and control switches. The system can be run manually or is automatic. The electrical timer will retrieve the "rabbit" after a pre-set time provided the selector is in "automatic."

10.2.5 The Central Thimble

The central thimble, located in the center of the core, provides space for the irradiation of small samples at the top of the upper grid plate. It also makes possible the extraction of a highly collimated beam of neutron and gamma radiation.

The thimble is an aluminum tube and extends from the bridge straight down through the central hole of the removable hexagonal section in the top grid plate then through the lower grid plate, terminating at the safety plate. The central thimble is supported by the safety plate which is situated beneath the lower grid plate. An aluminum filler plug is used in the central thimble to preclude flux peaking in the core center.

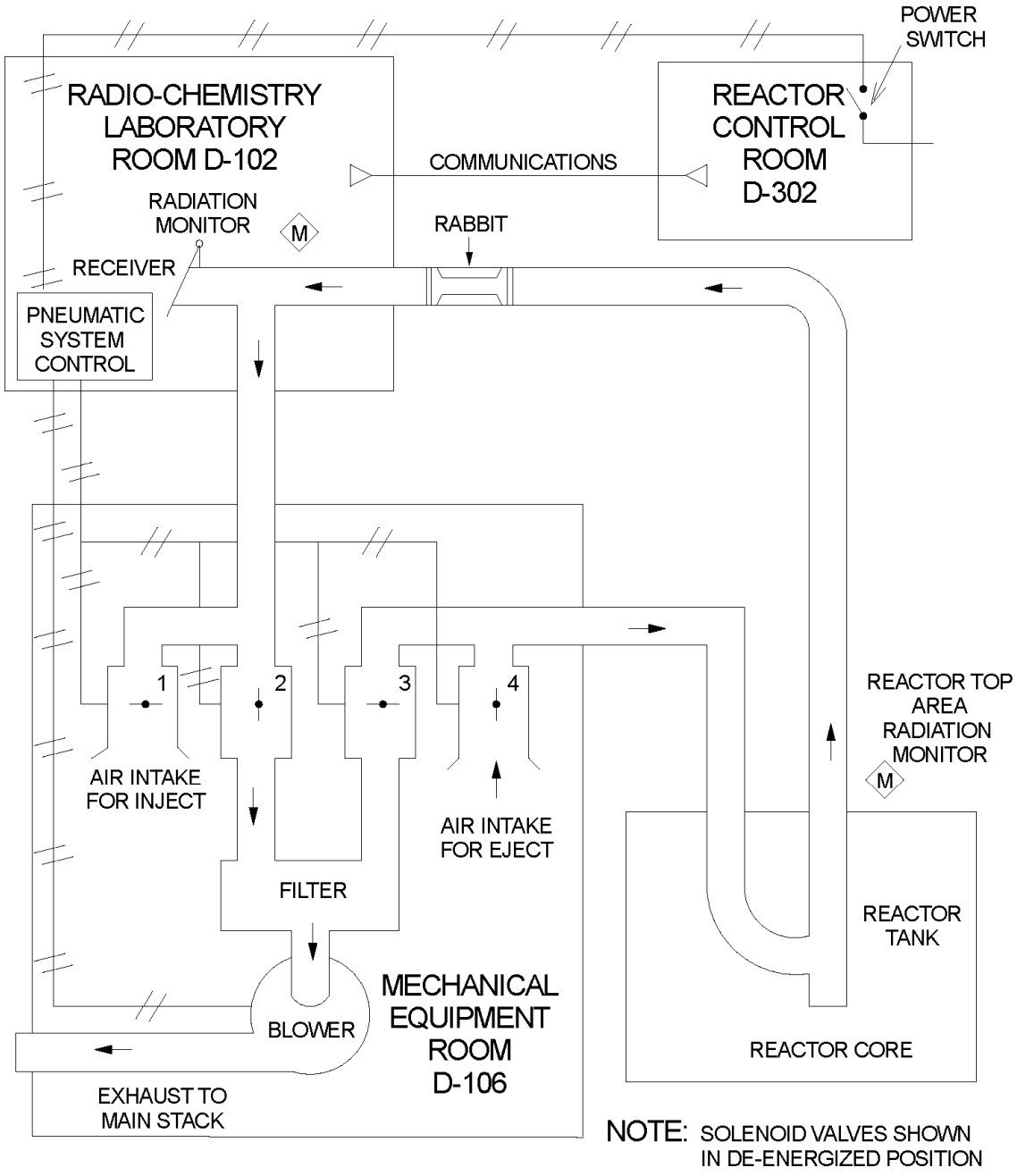

Figure 10.1 Pneumatic (Rabbit) System Schematic

Removable aluminum rings are located on the lower section of the central thimble tubing just above and below the removable hexagonal upper grid section. The rings, which are each fastened to the central thimble with set screws, support the hexagonal section and ensure its proper vertical placement in the top grid plate.

The top end of the central thimble is fastened by a holding fixture screwed into the center channel mounting plate. The holding fixture (a modified Weatherhead union) permits the tube to slide freely through it when loosened, but can be tightened to hold the tube securely in the fixture.

The water in the thimble can be removed (to make a neutron beam available for experimentation) by attaching a special cap to the top of the tube and applying air pressure to force the water down and through four small holes located near the bottom of the thimble.

10.2.6 Vertical Irradiation Tubes

The in-core irradiation tube (ICIT) and the cadmium-lined in-core irradiation tube (CLICIT) facilities are vertical tubes designed to irradiate samples in the reactor core. These facilities, when being used, are placed in a selected fuel element position in the core grid. This is usually the B-1 position. The CLICIT and ICIT consist of thin-walled aluminum tubing, a terminus assembly, cadmium lining (CLICIT only), a cap with a vent adapter and a vent hose.

Each tube is made up of two sizes of aluminum tubing. The longer inner tube is made of a 1¼-inch O.D. tube, 19 feet long, with a wall thickness of 0.058 inches. The shorter outer tube consists of a 1½-inch O.D. tube with a wall thickness of .065 inches turned down to 1.475-inch O.D. This outer tube is about 3 feet long and acts as the facility outer liner and terminus. It is shaped similar to a standard fuel element. Each has a 16-inch offset produced by bends of 10< positioned such that there is sufficient water above or below to reduce radiation streaming from the core through each vertical section.

10.2.7 The Rotating Rack

The rotating rack facility, also known as the Lazy Susan, consists primarily of four components:

- the rotary specimen rack, located in a circular well in the reflector assembly;
- the specimen-removal chute assembly;
- the tube-and-drive-shaft assembly; and
- the drive-and-indicator assembly.

The rotary specimen rack is an annular aluminum holder which surrounds the core and holds specimens during irradiation. This rack is located inside a ring-shaped, seal-welded aluminum housing, and is positioned by centering screws attached to the reflector assembly. The rack rotates on a stainless steel ball bearing assembly and consists of forty evenly-spaced tubular aluminum containers, open at the top and closed at the bottom, which serve as receptacles for

specimen containers. Provisions have been made to remove condensation from the rack which could result from high humidity in the reactor area and low operating temperature.

The specimen-removal chute is an aluminum thin-walled pipe that begins in a funnel just below the top plate of the center-channel assembly. This funnel aids in insertion of the specimen container. Loading and unloading of the forty specimen containers in the rack takes place through the specimen-removal chute. The chute is offset by approximately 18 inches by means of large-radii tube bends to ensure adequate radiation shielding.

The rack is rotated from a drive system on top of the reactor; rotation is transmitted through a drive shaft inside a thin-walled pipe housing to a sprocket-and-chain drive in the rotary specimen rack housing. Motive force is provided by an electric motor or a hand crank. Since the thin-walled pipe enclosing the drive shaft is in a straight line from the reflector, radiation shielding is provided by several feet of polystyrene enclosed within the pipe.

The drive-and-indicator assembly is located on the center-channel cover at the top of the reactor tank. The assembly includes an indicator dial with 40 divisions (one for each rack position), a crank for rotating the specimen rack gear train, and a locking rod handle. The motorized drive permits continuous rotation at about one revolution per minute. The motorized drive consists of an electric motor, a worm gear and a slip clutch located inside the drive-and-indicator assembly box. Use of the motor assures a uniform average flux to all samples in the rack.

10.3 Experiment Review

Administrative requirements are in place at the OSTR to assure that all experiments are performed in a manner which will ensure the protection of the public. Experiment review meets the requirements of Regulatory Guide 2.2, and Standard ANSI N401-1974 (ANS-15.6) as modified by Regulatory Guide 2.4.

Experiments are classified according to potential impact on the facility, and potential radioisotope production as follows:

- Class A: these are experiments which involve small changes in reactivity, no external shielding changes, and/or limited amounts of radioisotope production;

- Class B: these experiments may involve larger changes in reactivity, external shielding changes, and/or larger amounts of radioisotope production; and

- Class C: these are special experiments involving unusual experiment setups, irradiation of special materials, such as explosives, unusual fuel element arrangements, large in-core experimental facilities, etc.

Prior to performance, any new experiment must be reviewed and approved by the Reactor Operations Committee (ROC), a group of individuals generally knowledgeable in the fields of

reactor engineering and nuclear safety. The composition and responsibilities of the ROC are specified in Chapter 12. Experiments are reviewed to ensure their performance in accordance with facility requirements. The ROC review and approval process also follows the provisions of 10 CFR 50.59 and the guidance found in Regulatory Guide 1.186.

As part of the approval process, the experiment will be assigned a classification. Once an experiment has been approved, each performance of the experiment will be controlled and documented by an Irradiation Request (IR). The IR is also used to document that any isotopes produced are transferred only to appropriately-licensed users of radioactive material. For Class A experiments, the IR can be approved by the Reactor Supervisor. For Class B experiments, approval from the Reactor Supervisor and the Senior Health Physicist is required. Class C experiments are treated as new experiments each time they are performed, and must be resubmitted through the ROC for each performance.

In order to ensure the protection of the public, limitations are placed on experiments to minimize potential release of radioactive material due to 1) experimental failure [breach], 2) damage to reactor components, and 3) damage to reactor fuel. These limits are explicitly stated in Chapter 14. These limitations specify:

- maximum worth of any non-secured experiment, maximum worth of any single experiment and maximum total experiment worth. These limits determine maximum fuel element temperature;

- maximum amount of explosive material that may be placed in an experimental facility. This limit prevents damage to reactor components and fuel;

- maximum amount of ^{131}I - ^{135}I isotopes which may be present in a fueled experiment. This limit determines the maximum amount of these isotopes that could be released due to an experiment failure; and

- actions required in the event that hazardous material is introduced into the reactor tank. This limit ensures that the reactor shall not be operated with damaged fuel or components.

The radioisotopes produced at the OSTR may only be transferred to properly-licensed users. Individuals associated with Oregon State University may be approved to receive radioactive material under the authority of the OSU license by the Radiation Safety Committee. Other users must have a current Radioactive Material License. This information is verified during the approval of the IR, prior to performance of every experiment.

CHAPTER 11

RADIATION PROTECTION PROGRAM AND WASTE MANAGEMENT

Chapter 11 - Valid Pages
Rev. 1 5/1/2012

i	Rev. 0 7/01/2004
ii	Rev. 0 7/01/2004
1	Rev. 0 7/01/2004
2	Rev. 0 7/01/2004
3	Rev. 0 7/01/2004
4	Rev. 0 7/01/2004
5	Rev. 0 7/01/2004
6	Rev. 0 7/01/2004
7	Rev. 0 7/01/2004
8	Rev. 0 7/01/2004
9	Rev. 0 7/01/2004
10	Rev. 1 5/1/2012
11	Rev. 1 5/1/2012
12	Rev. 0 7/01/2004
13	Rev. 0 7/01/2004
14	Rev. 0 7/01/2004
15	Rev. 0 7/01/2004
16	Rev. 0 7/01/2004
17	Rev. 0 7/01/2004
18	Rev. 0 7/01/2004
19	Rev. 0 7/01/2004
20	Rev. 0 7/01/2004
21	Rev. 0 7/01/2004
22	Rev. 0 7/01/2004
23	Rev. 0 7/01/2004
24	Rev. 0 7/01/2004

TABLE OF CONTENTS

LIST OF TABLES

11 RADIATION PROTECTION PROGRAM AND WASTE MANAGEMENT

This chapter deals with the radiation protection and waste management programs of the Oregon State TRIGA® Reactor (OSTR). The OSTR is housed within the OSU Radiation Center (RC) which is the University's institutional facility for the accommodation of teaching, research and service programs involving the use of ionizing radiation and radioactive material.

11.1 Radiation Protection

In order to ensure safety and productivity, the use of radiation-producing machines and radioactive materials must be conducted in strict accordance with established federal and state safety standards in order to minimize unnecessary radiation exposure to the users and to members of the general public. The objective of the OSTR Radiation Protection Program is to keep radiation exposures at the RC and to the general public "as low as reasonably achievable" (ALARA).

11.1.1 Radiation Sources

11.1.1.1 Airborne Radiation Sources

The radioisotopes ^{41}Ar and ^{16}N are the only airborne radioisotopes produced during normal reactor operations. In the reactor bay, ^{41}Ar is produced primarily from irradiation of dissolved air in the primary water which eventually evolves into the air of the reactor bay. This evolution results from the reduced solubility of argon gas in water as the water temperature increases. Additionally, ^{41}Ar can be generated from activated argon in air-filled irradiation facilities (e. g., rotating rack, thermal columns, beamports, and the pneumatic transfer system), but little or none of this ^{41}Ar gets into the reactor bay air.

Nitrogen-16 is predominately created by the reaction of fast neutrons with ^{16}O in water passing through the core. The amount of oxygen present in air, either in a beam path or entrained in the water near the reactor core, is insignificant compared to the amount of oxygen in water. Calculations and measurements have been performed to determine production and release rates of ^{41}Ar and ^{16}N due to normal reactor operations.

11.1.1.1.1 Estimated Annual Dose in the Unrestricted Area from ^{41}Ar Released During Routine Reactor Operations

The OSTR discharges ^{41}Ar through an exhaust stack that is 19.812 meters above ground level. Atmospheric dilution will reduce the ^{41}Ar concentration considerably before the exhaust plume returns to ground level.

When all irradiation facilities are configured such that the production of ^{41}Ar is maximized, the emission rate of ^{41}Ar in the stack effluent has been measured to be approximately $11 \mu Ci\ s^{-1}$. Gamma spectroscopy of samples taken from the stack effluent on a quarterly basis have consistently found only ^{41}Ar present.

Based on this emission rate, the maximum ground level concentration of ^{41}Ar ($\prod_{max}$) can be calculated from the Gaussian plume model as follows (Ref. 11.1):

$$\chi_{max} = \left[\frac{Q}{\pi \sigma_y \sigma_z \mu} \right] e^{\left[-\frac{1}{2} \left(\frac{y^2}{\sigma_y^2} + \frac{h_e^2}{\sigma_z^2} \right) \right]} \quad (11\text{-}1)$$

where:

Q = emission rate (11 :Ci s^{-1});
σ_y = horizontal standard deviation of plume contaminant (m);
σ_z = vertical standard deviation of plume contaminant (m);
y = crosswind distance (0 m - centerline);
h_e = effective stack height (m); and
μ = mean wind speed (m s^{-1}).

The effective stack height (h_e) can be calculated from the following equation (Ref. 11.1):

$$h_e = h + d\left(\frac{v_s}{\mu} \right)^{1.4} \quad (11\text{-}2)$$

where:

h = physical stack height (19.812 m);
d = stack diameter (0.533 m);
v_s = stack effluent velocity (19.7 m s^{-1}); and
μ = mean wind speed (m s^{-1}).

The maximum ground level concentration occurs on the plume center line, for any atmospheric condition, at the downwind distance as follows (Ref 11.1):

$$\sigma_z = \frac{h_e}{\sqrt{2}} \quad (11\text{-}3)$$

The distance at which the maximum concentration occurs (d_{max}) can then be determined from charts illustrating σ_z vs. distance using the value of σ_z that corresponds to the maximum ground level concentration. Values for σ_y can likewise be determined from charts illustrating σ_y vs. distance at d_{max} (Ref. 11.1). Using the values given in Reference 11.2, the maximum TEDE, signified as D_{max}, received by a member of the general public may be estimated.

The results of calculating the annual TEDE to the general public from routine releases of ^{41}Ar into the unrestricted area are given in Table 11-1. It should be noted that in order to receive the doses shown in Table 11-1, an individual would be required to continuously occupy the specified location for a full year while the reactor operated continuously for a year in a configuration

maximizing ^{41}Ar release and the atmospheric stability class remained constant. That being said, all calculated doses are well within all applicable limits in 10 CFR 20 for all scenarios.

Table 11-1 ^{41}Ar Concentrations and Annual Doses in the Unrestricted Area from ^{41}Ar Released During Routine Reactor Operations at Various Atmospheric Stability Classes

Atmospheric Stability Condition	μ(m s^{-1})	h_e (m)	σ_y (m)	σ_z (m)	χ_{max} (μCi m^{-3})	d_{max} (m)	D_{max} (mrem)
A	1	54.5	54	39	6.25E-4	240	4
B	2	32.9	40	23	6.98E-4	240	5
C	4	24.8	30	18	6.18E-4	240	4
D	6	22.6	32	16	4.23E-4	400	3
E	2	32.9	55	23	5.07E-4	1000	3
F	2	32.9	75	23	3.72E-4	2200	3

As mentioned above, it is important to recognize that χ_{max} is based upon the release rate when all irradiation facilities are configured such that the production of ^{41}Ar is maximized. Normal operation involves running the reactor at full power with all beamport rod valves closed and all argon manifold inputs from the beamports and thermal column valved-shut. This has the effect of trapping the air in the irradiation facilities. Additionally, a liquid nitrogen tank is allowed to evaporate into the rotating rack. This is called a nitrogen purge. As the nitrogen gas moves into the rotating rack, it displaces the air in the cavity. This, along with closing the argon manifold valves for the beamports and thermal column, significantly reduces the amount of ^{41}Ar produced and released.

The calculations performed in Table 11-1 assume that the nitrogen purge for the rotating rack is off and all the irradiation facility ventilation valves are open. This has the effect of introducing a maximum amount of air into various irradiation facilities, thereby maximizing the amount of ^{41}Ar generated. However, extensive experience and measurements show that when the nitrogen purge is used and the ventilation valves associated with the various irradiation facilities are closed (i.e., the configuration in which the OSTR is routinely operated), the effluent emission rate of ^{41}Ar, which almost entirely originates from the primary tank, is reduced by a factor of 10 down to approximately 1 μCi s^{-1}. The values of χ_{max} and D_{max} are therefore also reduced by a factor of 10.

Determination of radiation dose to the general public from airborne effluents may also be carried out using several computer codes recognized by regulatory authorities. One such method involves the use of COMPLY (Ref. 11.3). Application of this code (V1.5D) to the projected ^{41}Ar releases from the OSTR using the data from Table 11-1 for atmospheric stability condition B predicts a maximum annual TEDE to the general public of 4.5 mrem.

The contribution of dose from the shine of the released plume is negligible. Using the highest release rate of 11 µCi s^{-1} and a volumetric flow rate of 4.4 x 10^{-6} cm^3 s^{-1}, the concentration would be 2.5 x 10^{-6} µCi cm^{-3}. The fence line is 17 m from the reactor building and the highest diffusion parameter would be 1.36 m. The effective stack height is 32 m. Using Microshield 5.05, a cylinder with a diameter of 1.36 m, length of 34 m and concentration of 2.5 x 10^{-6} µCi cm^{-3} is used as the source and the dose point is located 17 m along the length of the cylinder and 32 m from the cylinder. The dose rate at this location is 6.88 x 10^{-5} mR hr^{-1}. The length of the cylinder is twice the distance from the wall to the fence line to take into account shine from the passing plume. A sensitivity analysis showed no significant increase past this point. The highest diffusion parameter at 34 m is 2.72 m. Changing only the diameter of the source cylinder, results in a dose rate of 2.75 x 10^{-4} mR hr^{-1}.

11.1.1.1.2 Occupational Exposure to ^{41}Ar from Routine Reactor Operations

The only significant source of ^{41}Ar that contributes to occupational radiation exposure is that which is generated in, and released from, the reactor tank, regardless of the ventilation or irradiation facility valve configuration. As noted in the previous section, the stack effluent discharge rate for ^{41}Ar when the nitrogen purge is used and the ventilation valves associated with the various irradiation facilities are closed (i.e., the configuration in which the OSTR is routinely operated) is approximately 1 µCi s^{-1}. With a stack effluent discharge rate of 1 :Ci s^{-1}, a volume flow rate of 4.4E6 cm^3 s^{-1}, and assuming uniform mixing in the reactor bay, the concentration of ^{41}Ar in the reactor bay would be approximately 2.7E-7 µCi cm^{-3}. This is well below the 10 CFR 20 listed Derived Air Concentration (DAC) for ^{41}Ar of 3.0E-6 µCi ml^{-1}.

If one assumes that all the ^{41}Ar activity detected in the stack effluent while the OSTR is operating in a configuration which maximizes the ^{41}Ar production (a stack effluent discharge rate of 11 µCi s^{-1}), to be present in the reactor bay air (a volume flow rate of 4.4E6 cm^3 s^{-1}), and uniform mixing in the reactor bay air, the concentration of ^{41}Ar in the reactor bay would be approximately 2.5E-6 µCi cm^{-3}. This is also below the DAC for ^{41}Ar. However, this is not a credible assumption based on the design of the ventilation system and the irradiation facilities. While it is common practice to assume that uniform mixing occurs in the reactor bay air, measurements of ^{41}Ar in the reactor bay air suggest that it does not occur (Ref. 11.4). Air concentrations of ^{41}Ar varied measurably at different locations within the reactor bay. At the ground level of the reactor bay, concentrations reached an equilibrium of 5.0E-7 µCi ml^{-1} only after approximately four hours of continuous reactor operation at 1 MW. Air concentrations found on the surface of the reactor top averaged 2.4E-6 µCi ml^{-1}. However, concentrations fell off dramatically as a function of height above the reactor top indicating that immersion dose calculations due to ^{41}Ar will greatly overestimate the dose. In fact, at a height of 1.0 meter above the reactor top, only one out of the five measurement locations yielded a result above the ^{41}Ar lower limit of detection (95%) of 1.8E-7 µCi ml^{-1}.

All operational scenarios show that the concentration of ^{41}Ar will be significantly less than the DAC. Given the above considerations, any estimated occupational doses must be considered

highly conservative upper limits for the TEDE due to ^{41}Ar evolving from the primary tank or irradiation facilities and certainly, in all cases, less than the limits specified in 10 CFR 20.

11.1.1.1.3 Occupational Exposure to ^{41}Ar Originating from the Beamports

Another source of ^{41}Ar from routine operations will be from beams exiting the bioshield into shielded beam halls. The largest possible beam would produce a 14 x 17-inch beam area at approximately 6 feet from the bioshield surface. If it is conservatively assumed that this cross-sectional area remains constant from the inner end of the beamport to 6 feet outside of the bioshield (17 feet), the entire volume of the beam would be 7.9E5 cm^3.

The total number of neutrons per second (I) passing at the end of the beam (exterior of the bioshield) can be calculated from:

$$I = JR , \tag{11-4}$$

where:

J = neutron beam intensity (4E6 n cm^{-2} s^{-1}); and
R = beam area (1,535 cm^2).

From this, the neutron intensity at the end of the beam (exterior to the bioshield) will be 6.1E9 n s^{-1}. The neutron intensity at the start of the beam (I_o) can be calculated using the equation:

$$I = I_o e^{-\Sigma t f} \tag{11-5}$$

where:

Σ = ^{40}Ar macroscopic thermal neutron absorption cross section (1.7E-5 cm^{-1});
t = beam length (518.16 cm); and
f = fraction of argon in air (9.4E-3).

The total interaction rate along the length of the beam (I- I_o) was calculated to be 5.1E5 s^{-1}. The production rate (P) of ^{41}Ar from the beam is calculated by:

$$p = \frac{(I_o - I)\lambda}{c} \tag{11-6}$$

where:

c = 3.7E4 Bq per μCi.

The production of ^{41}Ar is calculated to be 1.5E-3 μCi s^{-1}. Assuming that the ^{41}Ar activity is evenly distributed over the entire room volume, the ^{41}Ar concentration can be calculated from:

$$\left[{}^{41}Ar\right] = \frac{S}{\lambda V_r + q} \qquad (11\text{-}7)$$

where:

$[^{41}Ar]$ = ^{41}Ar concentration in the reactor bay (μCi ml $^{-1}$);
S = source production rate of ^{41}Ar (1.5E-3 μCi s^{-1});
λ = decay constant for ^{41}Ar (1.06E-4 s^{-1});
V_r= room volume (3.877E9 cm^3); and
q = exhaust rate (4.4E6 cm^3 s^{-1}).

The concentration of ^{41}Ar in the reactor bay from the utilization of a beamport while the OSTR is operating at 1 MW was calculated to be 3.0E-10 μCi ml $^{-1}$. This is insignificant since this concentration is three orders of magnitude smaller than that produced by the primary tank.

11.1.1.1.4 Estimated Annual Dose in the Unrestricted Area from ^{16}N Released During Routine Reactor Operations

^{16}N is generated by the reaction of fast neutrons with oxygen. The oxygen present in air, either in a beam path or entrained in the water near the rector core, is insignificant compared to the oxygen in the water molecule in the liquid state. Production of ^{16}N resulting from the oxygen in air or air entrained in the cooling water can therefore be neglected.

The use of gamma spectroscopy to determine the concentration of ^{16}N in the air is difficult due to its very short half-life (7.2 s). Use of stack continuous air monitor data is not appropriate because the ^{16}N has decayed significantly by the time it reaches the stack. Exposure to the general public is negligible for this reason.

11.1.1.1.5 Occupational Exposure to ^{16}N from Routine Reactor Operations

The average exposure rate observed at the surface of the reactor tank is approximately 100 mR h^{-1} while the reactor is at 1 MW and with the diffuser in operation. In order to estimate the amount of ^{16}N being produced, it will be assumed that the only source term for the 100 mR h^{-1} exposure rate is ^{16}N. This is a conservative assumption because it neglects any contribution from ^{41}Ar or the core itself.

The exposure rate at the tank surface arising from ^{16}N near the surface is calculated by (Ref. 11.5):

$$\dot{X} = \frac{\lambda\left[{}^{16}N\right]_w}{2\mu K}\left(1 - E_2\left(\mu h\right)\right) \qquad (11\text{-}8)$$

where:

$[^{16}N]_w$ = concentration of ^{16}N in the water (atoms cm^{-3});
λ = ^{16}N decay constant (9.71E-2 s^{-1});
μ = attenuation coefficient for 6 MeV-photons in water (0.0277 cm^{-1});
K = flux-to-exposure rate conversion (1.6E5 photons R^{-1} h cm^{-2} s^{-1});
h = thickness of ^{16}N bearing water; and
$E_2(\mu h)$ = exponential integral function (0).

For this calculation, the second order exponential integral function was conservatively assumed to be zero.

Aside from the dose rate at the reactor tank water surface, the contribution to exposure rate from ^{16}N in the air is also important. In the reactor bay, the ^{16}N activity is affected by dilution, ventilation, and decay. The accumulation of ^{16}N in the reactor bay under equilibrium conditions ($[^{16}N]_a$) is determined by:

$$\left[^{16}N\right]_a = \frac{\left[^{16}N\right]_w v_e A}{\lambda V_r + q} \qquad (11\text{-}9)$$

where:

$[^{16}N]_w$ = concentration of ^{16}N in the water (atoms cm^{-3});
v_e = escape velocity of ^{16}N from the water surface (0.009 cm s^{-1})[Ref. 11.6];
A = area of water surface (3.08E4 cm^2);
λ = decay constant for ^{16}N (9.71E-2 s^{-1});
V_r= room volume (3.877E9 cm^3); and
q = exhaust rate (4.4E6 cm^3 s^{-1}).

The gamma exposure rate due to immersion from an equilibrium concentration of ^{16}N in the air is calculated by:

$$\dot{x} = \frac{\left[^{16}N\right]_a B\lambda\left(1 - e^{-\mu_s R_0}\right)}{2\mu_s g} \qquad (11\text{-}10)$$

where:

B = dose buildup factor (assumed 1);
$[^{16}N]_a$ = ^{16}N concentration in the reactor bay air (atoms cm^{-3});
8 = decay constant for ^{16}N (9.71E-2 s^{-1});
μ_s = linear absorption coefficient (3.03E-5 cm^{-1} for air at 6 MeV);
R_o = radius of "reactor bay sphere" (975 cm); and
g = dose conversion factor (160 Bq cm^{-2} mR^{-1} h).

When the above three equations are solved simultaneously, the iteratively determined value for the concentration of ^{16}N in the primary water ($[^{16}N]_w$) was 9E6 atoms cm^{-3}.

However, the values in Table 11-2 are nominally equal to or lower than the limits for water effluent concentration found in Column 2, Table 2, Appendix B of 10 CFR20 and therefore could not negatively impact the health and safety of the public.

The resulting value for the concentration of ^{16}N in the reactor bay air ($[^{16}N]_a$) was 6.5 atoms cm^{-3}. These values will produce exposure rates at the water surface and immersion in air of 98.6 and 3.8 mR h^{-1}, respectively.

Shutting off the ventilation system (q=0) has very little effect upon the results. Similarly, experience has shown that shutting off the diffuser increases the exposure rate on the primary water surface by less than a factor of 2.

11.1.1.1.6 ^{41}Ar and ^{16}N from the Pneumatic Transfer System

Both ^{41}Ar and ^{16}N are produced in the section of the pneumatic transfer system that is located in the reactor core. During operation of the transfer system, air containing very small amounts of these two radioisotopes is exhausted from the system through a HEPA filter to the facility stack. However, even after numerous operations of this system, there have been no detectable increases in the release of these two radioisotopes. Therefore, the ^{41}Ar and ^{16}N from the pneumatic transfer system is not considered to be a measurable contributor to the radioisotopes released or exposure rates associated with OSTR operations.

11.1.1.2 Liquid Radioactive Sources

No liquid radioactive material is routinely produced or used in normal operations of the OSTR except for the neutron activation product impurities in the primary coolant. The majority of these impurities are removed by a mechanical filter and demineralizer resins. Non-routine liquid radioactive waste could be generated from decontamination or maintenance activities; however, based on past experience, the quantity and radioactivity concentrations would be small.

Radionuclides and their concentrations in the primary coolant vary depending on reactor power, reactor operating time and time since reactor shutdown, assuming that other variables remain constant. Routine liquid scintillation counting and gamma spectroscopy analysis of primary coolant water samples taken after several hours at 1 MW (equilibrium) reveal the presence of several radioisotopes. Typical concentration values for these radioisotopes are shown in Table 11-2. It is OSTR policy not to release liquid radioactivity as an effluent; therefore, the primary coolant does not represent a source of exposure to the general public during normal operations. However, the values in Table 11-2 are nominally equal to or lower than the limits for water effluent concentration found in Column 2, Table 2, Appendix B of 10 CFR 20 and therefore could not negatively impact the health and safety of the public. Occupational exposure from liquid sources is also limited because there are few operations which require contact with the primary coolant and because of the short half-lives of most radionuclides present. In cases where contact is a potential, the primary water could be allowed to decay in order to significantly reduce radioactivity concentrations. Additionally, experience at the OSTR and other TRIGA® reactors has shown that ^{3}H is not a significant source of occupational exposure.

11.1.1.2.1 ^{16}N Radiation Dose Rates from the Primary Coolant System Components

The source term of ^{16}N has been addressed previously in Section 11.1.1.2, however, the potential for ^{16}N radiation dose rates from primary water piping and from the heat exchanger were not included in that discussion. Measurements of gamma dose rates at contact with these coolant system components after extended operation at 1 MW indicate that contact dose rates in the range of a 1-10 mrem h^{-1} are common. These radiation levels are not considered to represent a radiation protection problem as the entire system resides in the reactor bay which is designated a radiation area. There is no routine occupancy of locations close to these components. Consequently, occupational dose from this source is minimal.

Table 11-2 Predominant Radionuclides in the OSTR Primary Coolant

Radionuclide	Half-life	Typical Equilibrium Concentration (μCi ml^{-1})
^{24}Na	14.96 h	8.34E-5*
^{27}Mg	9.46 min	8.85E-5*
^{41}Ar	1.8 h	9.90E-4*
^{56}Mg	2.58 h	6.09E-5*
^{3}H	12 y	3.34E-4*
^{16}N	7.14 sec	2.36E+1‡

*Measured value
‡Calculated value

11.1.1.3 Solid Radioactive Sources

The major source of radiation and radioactivity from solid sources is the fission product generation in the reactor fuel. A typical OSTR fuel element will generate a radiation field of greater than 100 R h^{-1} in air at three feet if removed from the reactor tank. As long as the fuel is contained within the water-filled tank, this source of radiation dose presents no personnel hazard. The tank is designed to preclude loss of its water and reactor operation would not take place if there were any difficulty in maintaining water level. The radiation field created by the complete loss of all water from the tank is addressed in Chapter 13.

Other possibilities for radiation exposure from solid radioactive material are from samples irradiated for research studies and reactor components which have spent a long time near the core. Dose rates from reactor fuel in cooling are several orders of magnitude lower than those in the operating core. This fuel is stored in fuel storage racks within the reactor tank. Sample handling equipment, procedures, and the use of aluminum for almost all structures near the core reduce exposure rates from samples and activated materials to levels which create no significant personnel hazard during operation or maintenance of the reactor. Radioactivity produced in research samples during irradiations is estimated before the irradiations are performed and equipment and procedures are in place to deal with the activity after the irradiation is completed.

Another source of solid wastes are the resins used to remove both anion and cations from the primary water. The annual solid waste volume transferred to OSU Radiation Safety for land burial disposal typically runs 15-20 cubic feet and contains various radioisotopes such as ^{60}Co, ^{54}Mn, ^{46}Sc, and ^{47}Sc with a total activity in the high μCi range. A summary of the major sources of radioactive material at the OSTR is shown in Table 11-3. Because the actual inventory of reactor fuel and other sources is subject to continuous change as part of the normal OSTR operation, the information in Table 11-3 is to be considered only representative.

Table 11-3 Representative Solid Radioactive Sources for the OSTR

Source	Radionuclides	Nominal Activity (Ci)	Physical Characteristic	Uranium Content (wt%)	Approximate Original Mass	
					^{235}U (g)	Total U (g)
90 TRIGA® 30/20 Fuel Elements	Enriched Uranium		In Core	30	14,760	75,150
6 TRIGA® 30/20 Fuel Elements	Enriched Uranium		New	30	984	5,010
7 Exxon Fuel Pins	Enriched Uranium		New		26	834
AGN Reactor Core	Enriched Uranium		Cooling		622	3,142
6 Fission Chambers	Enriched Uranium		1 In Core 5 Storage	95	4	4
Reactor Startup Source	^{241}Am-Be	3	Sealed Source, In Core			
Subcritical Assembly (License ORE90005)	Natural Uranium		Sealed Source			2,050,000
Irradiated Samples	Mixed Activation Products	~1E-6 to 10	Unsealed Irradiated Samples			
Solid Waste	Mixed Activation Products	~1E-6 to 1	~20 ft^3 annually of resin, paper, gloves, etc.			

11.1.2 Radiation Protection Program

The organization of the OSTR radiation safety program is discussed in Chapter 12. The Radiation Center's Radiation Protection Program is the responsibility of the RC Director and is under the supervision of the Senior Health Physicist. The Senior Health Physicist reports to the Radiation Center Director on all operational matters, but may report directly to the OSTR Reactor Operations Committee and/or OSU Radiation Safety Committee should such action be deemed necessary.

11.1.2.1 Organization of the Health Physics Staff

In addition to the Senior Health Physicist, the Health Physics Staff (radiation protection staff) includes a Health Physicist and Health Physics Monitors. The organizational structure, reporting pathways, and working relationships relating to the OSTR radiation protection program may be found in Chapter 12. Position qualifications will follow those outlined in ANSI/ANS 15.4, *Selection and Training of Personnel for Research Reactors*. The positions of authority and responsibility within the Health Physics Staff are as follows:

- Senior Health Physicist - the Senior Health Physicist reports directly to the Radiation Center Director. The Senior Health Physicist is responsible for directing the activities of the Health Physics Staff including the development and implementation of the OSTR Radiation Protection Program. The Senior Health Physicist has the authority and responsibility to halt perceived unsafe practices;

- Health Physicist - the Health Physicist reports to the Senior Health Physicist. The Health Physicist is responsible for implementing the OSTR Radiation Protection Program policies and procedures, and for providing day-to-day technical support and guidance to the Health Physics Monitors. The Health Physicist has the authority and responsibility to halt perceived unsafe practices; and

- Health Physics Monitors - Health Physics Monitors report to either the Senior Health Physicist or the Health Physicist. Health Physics Monitors are responsible for the required radiation surveys (daily, weekly, monthly, etc.) and other duties as assigned. The Health Physics Monitors have the authority and responsibility to halt perceived unsafe practices.

11.1.2.2 Working Interface Between Health Physics and Reactor Operations

The working relationship of the health physics program relative to reactor operations is described in Chapter 12. As shown in Figure 12.1, there is a clear separation of responsibilities for the two groups, each with a clear reporting line to the Radiation Center Director.

11.1.2.3 Health Physics Procedures and Document Control

Operation of the health physics program is carried out under the direction of the Senior Health Physicist using formal Radiation Center Health Physics Procedures. These procedures are reviewed and approved by the Senior Health Physicist. Procedures and other operational aspects of the Health Physics Staff are also audited an annual basis by the OSTR Reactor Operations Committee. Changes to the procedures, responsibilities, or other operational aspects of the Health Physics Staff are made at the discretion of the Senior Health Physicist. The original copy of the procedures is maintained by the Senior Health Physicist, who is also responsible for the distribution of the reproduced copies.

While not intended to be all inclusive, the following list provides an indication of typical radiation protection procedures used in the OSTR program:

- testing and calibration of area radiation monitors, facility air monitors, laboratory radiation detection systems, and portable radiation monitoring instrumentation;
- working in laboratories and other areas where radioactive materials are used;
- facility radiation monitoring program including routine and special surveys, personnel monitoring, monitoring and handling of radioactive waste, and sampling and analysis of gaseous effluents released from the facility;
- monitoring radioactivity in the environment surrounding the facility;
- administrative guidelines for the facility radiation protection program, including personnel orientation and training;
- receiving of radioactive materials at the facility and unrestricted releasing of materials and items from the facility;
- leak testing sealed sources containing radioactive materials;
- safe transporting of radioactive materials;
- general and personnel decontamination procedures;
- personnel exposure investigation procedures;
- personnel access procedures for the reactor bay;
- spill procedures;
- radiation work permit procedures; and
- ALARA procedures.

11.1.2.4 Radiation Protection Training

The radiation protection training is conducted by the Health Physics Staff. It is structured at different levels in order to meet the needs of different categories of facility staff and researchers using the reactor. All personnel and visitors entering the OSTR Reactor Building shall receive training in radiation protection sufficient for the work/visit, or shall be escorted by an individual who has received such training. Training shall cover the following areas in sufficient depth for the work being done. The general levels of training are as follows:

- Radiation/Radioactive Material User Orientation - All personnel permitted unescorted access to the OSTR Reactor Building shall receive training in radiation protection as required by 10 CFR 19.12. Initial training shall cover the following areas in sufficient depth for the work being done:

- storage, transfer, and use of radiation and/or radioactive material in portions of the restricted area, including radioactive waste management and disposal;

- health protection problems and health risks (including prenatal risks) associated with exposure to radiation and/or radioactive materials;

- precautions and procedures to minimize radiation exposure (ALARA);

- purposes and functions of protective devices;

- applicable regulations and license requirements for the protection of personnel from exposure to radiation and/or radioactive materials;

- responsibility of reporting potential regulatory and license violations or unnecessary exposure to radiation or radioactive materials;

- appropriate response to warnings in the event of an unusual occurrence or malfunction that involves radiation or radioactive materials; and

- radiation exposure reports which workers will receive or may request.

An examination to demonstrate understanding of the material is required for each section of training. Refresher training is required on a three-year cycle thereafter, including an examination to demonstrate understanding of the material.

- Reactor Bay (Vital Area) Unescorted Access Orientation - All personnel permitted unescorted access to the OSTR vital area shall receive additional training to include the following:

- reactor bay access control rules;

- emergency evacuation procedures for the reactor bay;

- dosimetry requirements for the reactor bay;

- reactor control room entry procedures and control requirements;

- key checkout and return;

- reactor top security;

- location and use of communication systems;
- security door requirements;
- general checkout procedures when exiting the reactor bay; and
- emergency equipment location and use.

11.1.2.5 Audits

Specific auditing responsibilities and requirements are defined in Chapter 12. Briefly, auditing of the radiation protection program is performed by the Reactor Operations Committee (ROC). The ROC provides objective and independent reviews, evaluations, advice and recommendations on matters affecting nuclear safety at the OSTR. With respect to health physics activities, the ROC is responsible for auditing all procedures, personnel radiation doses, radioactive material shipments, radiation surveys, and radioactive effluents released to unrestricted areas.

11.1.2.6 Health Physics Records and Record Keeping

Radiation protection program records such as radiological survey data, personnel exposure reports, training records, inventories of radioactive materials, environmental monitoring results, waste disposal records, and many more, are maintained by the Health Physics Staff. The records will be retained for the life of the facility either in hard copy, or on photographic or electronic storage media. Records for the current and previous years are normally retained in the Health Physicist's office in binders or file cabinets. Other records are retained in long-term storage. Radiation protection records are required to be reviewed and signed by the Senior Health Physicist prior to filing.

11.1.3 ALARA Program

An ALARA program for the OSTR has been established in accordance with 10 CFR 20.1101. The bases for this program are the guidelines found in ANSI/ANS 15.11. The Radiation Center Director has the ultimate responsibility for the ALARA program, but has delegated this responsibility to the Senior Health Physicist.

The OSTR ALARA program is embedded in every aspect of health physics procedures and reactor operation to include, but not limited to:

- the Senior Health Physicist being required to review all proposed new uses of radiation or radioactive materials, including each time a sample is irradiated in the OSTR;

- exposure investigations being initiated when an individual receives a dose in any reporting period greater than 1% of the applicable regulatory limit for those individuals who received dosimetry;

- personnel doses, shipping papers, radiation surveys, and radiation releases to the unrestricted area being audited quarterly while the procedures are reviewed annually; and

- the Senior Health Physicist being required to be involved during planning, design approval , and construction of new facilities; during planning implementation of new OSTR use; during maintenance activities; and during the management and disposal of radioactive waste.

11.1.4 Radiation Monitoring and Surveying

The main purpose of the radiation survey program is to assure radiological surveillance over selected OSTR work areas in order to provide current as well as characteristic data on the status of radiation conditions in such areas. Information of this type is used to confirm that safe radiation working conditions exist within the various operational areas under surveillance. The first objective is to assure that the monitoring program is organized such that routine radiation level and contamination level surveys of specific areas and activities within the facility are performed, and special radiation surveys necessary to support non-routine facility operations are also performed. A second objective of the program is to make frequent on-the-spot personal observations (along with recorded data) of radiation work areas. These observations may provide advance warning of needed corrections in order to ensure safe use and handling of radiation sources and other radioactive materials. A third objective is to use the information which has been gathered through completion of the first two objectives in order to ensure (and document) that all phases of the OSTR operational and radiation protection programs are in line with the goal of keeping radiation doses to personnel and releases of radioactivity to the environment ALARA.

11.1.4.1 Radiation Monitoring Equipment

Radiation monitoring equipment used in the OSTR is summarized in Table 11-4. Because equipment is updated and replaced as technology and performance changes, the equipment listed in Table 11-4 should be considered representative only.

11.1.4.2 Instrument Calibration

All radiation monitoring instrumentation is calibrated annually according to ANSI N323A-1997. If the instruments are not calibrated at the OSTR, they are sent to an appropriate calibration facility. Instrument calibrations are tracked by a computer-based system. Instrument calibration records are maintained by the Health Physics Staff. Calibration stickers showing pertinent calibration information (i. e., counting efficiency, the most recent calibration date, and the date the next calibration is due) are attached to all instruments.

Table 11-4 Radiation Monitoring Equipment Used in the OSTR Radiation Protection Program

Item	Location	Function
Continuous Air Monitor	Reactor Top	Airborne Particulate
Continuous Air Monitor	Effluent Stack	Airborne Particulate and Gas
Area Radiation Monitors	Various locations in reactor bay	Measure ambient gamma radiation fields
Portable Ion Chamber Survey Meters	Reactor Bay, D204, D102	Measure beta/gamma exposure rates
Portable Pancake-Probe GM Survey Meters	Reactor Bay, D204, D102	Measure beta/gamma surface contamination
μR Survey Meters	D204	Measure gamma exposure rates
Neutron Survey Meter	D104	Measure neutron dose rates
Alpha Survey Meters	D204	Measure alpha surface contamination
HPGe Gamma Spectroscopy System	B125	Gamma spectroscopy
Gas-Flow Proportional Counter	A138	Measure alpha/beta contamination on swipes
Hand-and-Foot Monitors	Reactor Building D-corridor 1st and 3rd Floors	Measure potential contamination on hands and feet prior to leaving radiation restricted areas
Direct Reading Pocket Dosimeters	Radiation Center Receptionist and reactor control room	Measure personnel gamma dose
TLDs	Various on-site and off-site locations	Measure environmental gamma radiation doses

11.1.4.3 Radiation Surveys

The radiation survey program is structured to make sure that adequate radiation measurements of both radiation fields and contamination are made commensurate with the amount and type of work being performed with radioactive material. The intent of such surveys is to prevent uncontrolled release of radioactive material and to minimize exposure. This program includes, but is not limited to:

- Daily Surveys - Daily Surveys are performed in areas where radioactive materials are frequently used. Such surveys involve direct radiation level measurements in areas known to contain constant or changing radiation fields and contamination surveys of the floors and other surfaces in the affected area are also done. Areas requiring daily surveys are determined at the discretion of the Senior Health Physicist;

- Weekly Surveys - Weekly Surveys are performed in areas where radioactive materials are less frequently used. These surveys involve direct radiation level measurements in areas known to possess constant or changing radiation fields and contamination surveys of the floors and other surfaces in the affected area are also

done. Areas requiring weekly surveys are determined at the discretion of the Senior Health Physicist;

- Monthly Surveys - Monthly Surveys are performed in areas where radioactive materials are infrequently used. The monthly surveys involve direct radiation level measurements in areas known to possess constant or changing radiation fields and contamination surveys of the floors and other surfaces in the affected area are also done. Areas requiring monthly surveys are determined at the discretion of the Senior Health Physicist;

- Receipt Radiation Surveys - Receipt Radiation Surveys are required of all incoming packages of radioactive material;

- Special Surveys - Special Surveys are any non-routine radiation survey requested by any member of the OSTR staff when needed; and

- Release Surveys - A Release Survey is required of any object that is removed from a designated radiation/contamination area prior to it being released from that area.

11.1.5 Radiation Exposure Control and Dosimetry

11.1.5.1 Shielding

With regard to the basic shielding design of the OSTR:

- General Atomics has developed source terms to serve as a basis for reactor shielding design analysis;

- reactor shields for 1-MW TRIGA® reactors have been built and proven based on the preceding design analysis. Actual radiation measurements at the surface of the OSTR shield at 1 MW have shown that most radiation levels are about 1 to 2 mrem h^{-1} or less; and

- the OSTR shield is very similar in material type and thickness to other proven TRIGA® shields. Where basic shielding configurations have been changed (e. g., beamports), supplemental shielding was added, as needed, to maintain doses ALARA.

11.1.5.2 Ventilation

The OSTR ventilation system is specifically covered in Chapter 3. This section discusses only those ventilation design features that apply to radiation protection. The reactor bay ventilation system:

- maintains ^{41}Ar and ^{16}N levels at concentrations in the reactor bay consistent with keeping occupational doses below the limits in 10 CFR 20;

- is balanced such that the reactor bay is negative to both the laboratories and offices found in D-Corridor and to the outside atmosphere; and

- has HEPA filters on all ducts originating from irradiation or sample handling facilities.

11.1.5.3 Entry Control

In accordance with the regulations found in 10 CFR 20, the OSTR has many locations posted and controlled as radiation areas. Most other areas within the OSTR are restricted areas. The OSTR does not have any high or very high radiation areas. Should any be created, the entry controls and postings will follow that required in 10 CFR 20, Subpart G.

11.1.5.4 Protective Clothing and Equipment

Personnel protective clothing and equipment used in the OSTR include lab coats, gloves, safety glasses, face shields, coveralls, hoods and shoe covers. The OSTR has one decontamination shower and numerous pre-positioned decontamination kits and emergency equipment cabinets. The requirements for use of the various clothing and equipment are found in the health physics procedures.

Levels of airborne radioactive material do not warrant implementation of a respiratory protection program. Should the situation change in order to meet ALARA objectives, a program will be implemented in accordance with 10 CFR 20, Subpart H.

11.1.5.5 OSTR Occupational Radiation Levels

The OSTR typically operates for only one shift per day (40 hours per week). Additionally, an occupationally-exposed individual only spends a fraction of the time in areas where there is a potential for measurable radiation levels. Radiation surveys of the OSTR within the restricted area have been made numerous times during full-power operations. Typical values of radiation levels at various locations around the OSTR are given in Table 11-5. Taking into consideration the limited occupancy times, the relatively low dose rates observed, and typical personnel doses received by the OSTR staff (See Section 11.1.5.6), it is evident that all occupational doses can be maintained below the regulatory limits given in 10 CFR 20.

Table 11-5 Typical Radiation Levels at Various OSTR Locations at 1 MW

Facility/Location	Typical Dose Equivalent Rate at Contact (mrem h^{-1})	Typical Dose Equivalent Rate at 30 cm (mrem h^{-1})
Reactor Top	100	65
Reactor Bay Floor	1	1
Demineralizer Tank	25	1
Primary Water Pipes	10	2
Primary Water Filter	3	<1
Argon Manifold	3	1

11.1.5.6 Personnel Dosimetry

The Radiation Center provides personnel dosimeters to occupational workers to ensure compliance with the dose limits specified in 10 CFR 20. Personnel dosimetry devices used at the OSTR have been selected to provide monitoring of all radiation categories likely to be encountered. Table 11-6 summarizes the devices typically used.

Table 11-6 Typical Personnel Monitoring Devices Used at the OSTR

Type	Dose	Radiation Measured	Reading Frequency
Pocket Ion Chamber	Deep Dose Equivalent	Gamma	As Needed
TLD	Deep Dose Equivalent Eye Dose Equivalent Shallow Dose Equivalent	Beta, Gamma	Quarterly
Albedo TLD	Deep Dose Equivalent	Thermal Neutron	Quarterly
TLD Finger Ring	Extremity Dose Equivalent	Beta, Gamma	Monthly
CR-39 Track Etch	Deep Dose Equivalent	Fast Neutron	Quarterly

Before work with radioactive materials begins, the health physics staff will evaluate the likely or possible doses that an individual may receive. Personnel dosimeters are issued for any of the following conditions:

- before entry into high or very high radiations areas;
- when the deep dose equivalent could exceed 50 mrem in any one month;

- when the shallow dose equivalent could exceed 500 mrem in any one month; or

- when the total effective dose equivalent to minors or a declared-pregnant worker could exceed 50 mrem in a year.

Internal dosimetry evaluation is limited to two bioassay methods. The Radiation Center may analyze urine for the presence of ^{3}H using a liquid scintillation counter. Iodine uptake in the thyroid may be analyzed *in vivo* through a thyroid counting program established by OSU Radiation Safety. In emergency situations, arrangements would have to be made with Pacific Northwest National Laboratory in Richland, Washington for whole body *in vivo* counting using gamma spectroscopy. Bioassay is required under the following conditions:

- 2-24 hours after handling unsealed ^{3}H in any chemical form in quantities of 50 mCi or more in any week;

- 6-72 hours after handling unsealed radioactive iodine in any chemical form in quantities of 0.1 mCi or more; or

- as required by the Senior Health Physicist.

An abnormal dose reading investigation (ADRI) is performed by the health physics staff if a personnel dosimeter shows a reading that exceeds the stated ALARA investigation level or is unacceptable from an ALARA point of view. An ADRI involves documenting the abnormal reading, investigating the cause, and evaluating how it might be mitigated in the future. The ADRI is then filed with OSU Radiation Safety, the affected individual, and the OSTR. The ADRI is automatically performed when the dose in any reporting period exceeds 1% of the applicable regulatory limit for occupational workers in 10 CFR 20. Additionally, an ADRI is initiated for individuals designated as visitors when a measured dose exceeds 10 mrem.

Table 11-7 Average Annual Dose Equivalent Incurred by OSTR Staff in 2002

Type of Dose Incurred	Average Annual Dose Equivalent (mrem)	Highest Individual Annual Dose Equivalent (mrem)	Lowest Individual Annual Dose Equivalent (mrem)
Deep	44	77	10
Eye	54	84	20
Shallow	70	115	27
Extremity	102	441	0

11.1.5.7 Dosimetry Records

Records of personnel dosimetry, radiation surveys, effluent monitoring, environmental sample analysis, environmental dose rate measurements, area dosimetry, and environmental area dosimetry are kept for the life of the facility. The dosimetry results shown in Table 11-7 are only to be regarded as typical. As expected, annual doses vary due to changes in facilities, work, and procedures.

11.1.6 Contamination Control

Radioactive contamination is controlled at the OSTR by using written procedures for radioactive material handling, by using trained personnel, and by operating a monitoring program designed to detect contamination in a timely manner. The program for routine monitoring to detect and identify fixed and loose contamination is described in Section 11.1.4. In addition to this monitoring program, the following items are also part of the program for contamination control at the OSTR:

- the reactor bay (Room D104) and the entire first floor of D-corridor are considered to be potentially contaminated with loose radioactive contamination. All personnel are required to survey before exiting these areas. All objects that leave these areas are also required to be surveyed before they are removed from these areas;

- at a minimum, all personnel are required to wear proper dosimetry, a lab coat, and gloves when working with unsealed radioactive material in the above areas;

- removal of samples from the reactor requires the presence of a Health Physics Monitor;

- procedures have been established for monitoring and handling contaminated equipment and components;

- staff and visitors are trained on the risks of contamination and on the techniques for avoiding, limiting, and controlling contamination;

- contamination events are documented in a Special Survey; and

- events which result in fixed contamination are normally documented as a report in the OSTR Decommissioning File.

11.1.7 Environmental Monitoring

Procedures have been developed to ensure the operation of a comprehensive monitoring program which incorporates an adequate number of sample types, collected at the appropriate frequencies, analyzed with sufficient sensitivity, and reported in a timely manner to provide an early indication of any environmental impacts.

On a quarterly basis, the Reactor Operations Committee audits the OSTR environmental monitoring program and the environmental data generated by the program. As a result of these audits, modifications have been made to improve the quality of the program.

With the exception of ^{41}Ar, there are virtually no pathways for radioactive materials from the OSTR to enter the unrestricted environment during normal facility operations.

The current environmental monitoring program consists of taking environmental samples at approximately 25 different locations and generally within 1,000 feet of the OSTR. Measurements taken include the following:

- direct gamma radiation measurements performed monthly (sensitivity ~5 $\mu R\ h^{-1}$);
- TLD measurements exchanged quarterly (sensitivity ~10 mR $quarter^{-1}$);
- soil samples obtained quarterly and analyzed for gross beta/gamma (sensitivity ~10 pCi g^{-1}), and gross alpha (sensitivity ~0.1 pCi g^{-1});
- vegetation samples obtained quarterly and analyzed for gross beta/gamma (sensitivity ~50 pCi g^{-1}), and gross alpha (sensitivity ~2 pCi g^{-1}); and
- water samples obtained quarterly and analyzed for gross alpha (sensitivity ~0.02 pCi ml^{-1}), gross beta (sensitivity ~0.06 pCi ml^{-1}), ^{3}H (sensitivity ~3 pCi ml^{-1}), and by gamma spectroscopy.

11.2 Radioactive Waste Management

The objective of the radioactive waste management program is to ensure that radioactive waste is minimized, and that it is properly handled, stored and disposed of. The Health Physics Staff is responsible for administering the radioactive waste management program which also includes any records associated with the program. All records are retained for the life of the facility.

11.2.1 Radioactive Waste Control

At the OSTR, radioactive waste is generally considered to be any item or substance which is no longer of use to the facility and which contains, or is suspected of containing, radioactivity above the natural background radioactivity. Equipment and components are categorized as waste by the OSTR staff. When possible, radioactive waste is initially segregated at the point of origin from items that will not be considered waste.

11.2.2 Solid Waste

As with most non-power reactors, solid waste is generated from reactor maintenance operations and irradiations of various experiments. The amount of solid waste is generally on the order of 20 cubic feet per year. No solid radioactive waste is intended to be retained or permanently

stored on site. Appropriate radiation monitoring instrumentation will be used for identifying solid radioactive waste. Radioactive waste is packaged in metal drums within the reactor bay of the OSTR. The waste is then transferred to OSU Radiation Safety for disposal.

11.2.3 Liquid Waste

It is the OSTR's policy not to routinely release radioactive liquid waste. Normal operations of the OSTR do not produce liquid radioactive waste, and if so, the liquid waste is contained locally and transferred to OSU Radiation Safety for disposal. The OSTR does have a 2,500-gallon hold-up tank, which is occasionally discharged to the local sewer system. Sampling, analysis, and release of the holdup tank contents are governed by a written procedure that assures that the release of any radioactivity that happens to be present is within the limits stated in 10 CFR 20, Appendix B, Table 3.

11.2.4 Gaseous Waste

Although ^{41}Ar is released from the OSTR stack as part of the facility ventilation exhaust, this release is not considered to be waste in the same sense as the solid and liquid waste which are collected and disposed of by the facility. The ^{41}Ar is usually classified as an effluent which is a routine part of the normal operation of the OSTR. In the OSTR facility, as in many non-power reactors, there are no special off-gas collection systems for the ^{41}Ar. Typically, this gas simply mixes with reactor room and other facility air and is discharged along with the normal ventilation exhaust.

11.3 References

11.1 Slade, D.H., Meteorology and Atomic Energy - 1968, TID-24190.

11.2 "External Dose-Rate Conversion Factors for Calculation of Dose to the Public," DOE/EH-0070, U.S. Department of Energy, Washington, D.C., 1988.

11.3 EPA 520/1-89-003, U.S. Environmental Protection Agency, Washington, D.C., (1.5D), 1989.

11.4 Anellis, L.G., Johnson, A.G., and Higginbotham, J.F., Argon-41 Production and Evolution at the Oregon State TRIGA® Reactor (OSTR). Eleventh Biennial U.S. TRIGA® User's Conference, Washington, D.C., 1988.

11.5 Schiager, K.J., Analysis of Radiation Exposures on or Near Uranium Tailings Piles, Radiation Data and Reports, pp. 411-425, July 1974.

11.6 Dorsey, N.E., "Properties of Ordinary Water-Substances," pp. 537-544, Reinhold Publ. Co., New York, New York.

CHAPTER 12

CONDUCT OF OPERATIONS

```
```

Chapter 12 - Valid Pages
Rev. 1 5/1/2012

i	Rev. 0 7/01/2004
ii	Rev. 0 7/01/2004
1	Rev. 0 7/01/2004
2	Rev. 0 7/01/2004
3	Rev. 0 7/01/2004
4	Rev. 0 7/01/2004
5	Rev. 0 7/01/2004
6	Rev. 0 7/01/2004
7	Rev. 0 7/01/2004
8	Rev. 0 7/01/2004
9	Rev. 0 7/01/2004
10	Rev. 0 7/01/2004
11	Rev. 0 7/01/2004
12	Rev. 0 7/01/2004
13	Rev. 0 7/01/2004
14	Rev. 0 7/01/2004

TABLE OF CONTENTS

12 CONDUCT OF OPERATIONS

LIST OF FIGURES

12 CONDUCT OF OPERATIONS

This chapter describes and discusses the Conduct of Operations at the Oregon State TRIGA® Reactor (OSTR). The Conduct of Operations involves the administrative aspects of facility operations, the facility emergency plan, the security plan, the reactor operator selection and requalification plan, and environmental reports.

12.1 Organization

The formal licensee of the OSTR is the President, Oregon State University. However, the Radiation Center Director is responsible for licensing and reporting information to the NRC. The President is informed of license issues via the normal university reporting channel, originating from the Radiation Center Director through the Vice Provost for Research (level 1) to the President.

12.1.1 Structure

The management organization of the OSTR is structured to provide comprehensive and redundant internal oversight of reactor operations and radiation protection programs. It also meets the intent of ANSI/ANS 15.11, *Radiation Protection at Research Reactor Facilities*. As shown in Figure 12.1, the level 2 (Director) and level 3 (Reactor Administrator and Senior Health Physicist) have formal reporting lines as well as documented secondary lines-of-communication if nuclear or radiation safety concerns cannot be resolved with the normal administrative reporting lines. Interaction between the health physicists, health physics monitors, Reactor Supervisor, and reactor operators is constant, although the reporting lines may be separate.

12.1.2 Responsibility

The following is a list of various offices/committees/personnel and their associated duties:

- President, Oregon State University - chief executive officer of the university;
- Executive Vice President and Provost - research and educational programs are administered through the Office of the Executive Vice President and Provost. Separate officers assist with the administration of research activities and academic affairs with functions delegated to the Vice Provost for Research and the Vice President for Finance and Administration.

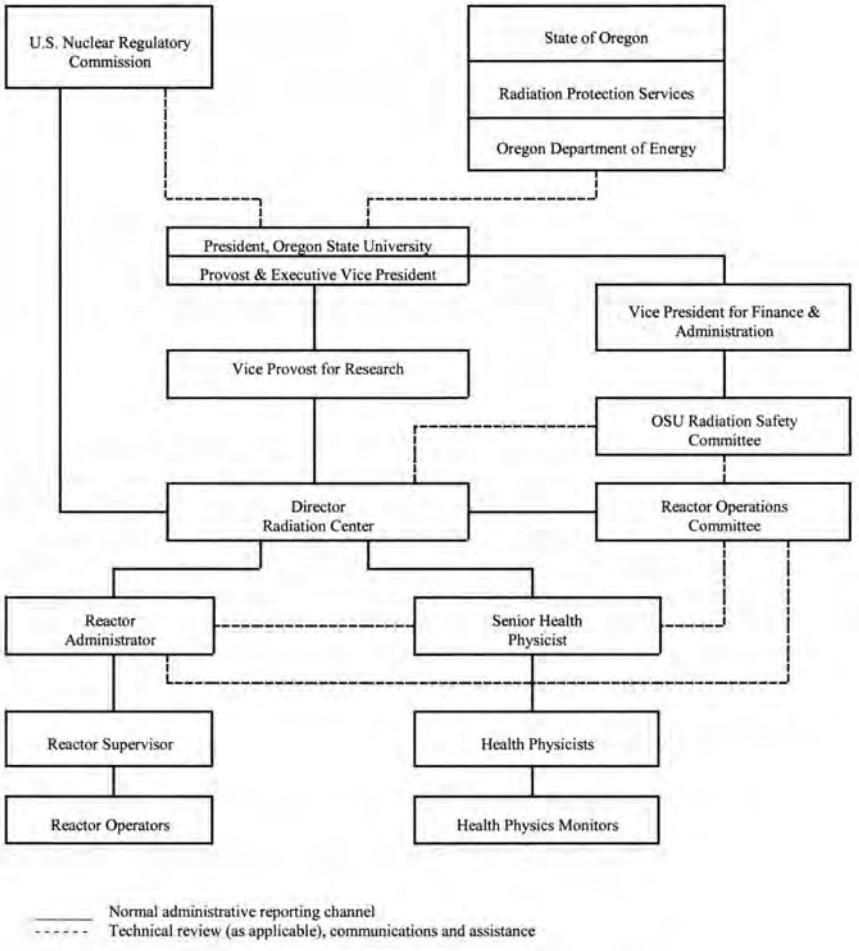

Figure 12.1 OSTR Administrative Organizational and Reporting Line Chart

- Vice Provost for Research - research programs associated with the university are administered through the Research Office. The Radiation Center is administered through the Research Office. This is a level 1 position;

- Vice President for Finance and Administration - university business activities are administered through the Office of Finance and Administration. One responsibility of the office is the administration and operation of safety programs for the university;

- Radiation Safety Committee - this standing university committee has jurisdiction over matters dealing with radiation uses and radiological safety necessary to protect the health and welfare of the staff and students of Oregon State University;

- Reactor Operations Committee - this standing university committee independently reviews, evaluates, and approves safety standards associated with the operation and use of the Oregon State TRIGA® Reactor and its experimental facilities;

- Radiation Center Director - the Director is accountable for ensuring all licensing requirements, including implementation and enforcement, in accordance with the NRC codes and guides. This is a level 2 position;

- Reactor Administrator - the Reactor Administrator is responsible to the Radiation Center Director for guidance, oversight, and technical support of reactor operations. The Reactor Administrator shall be certified as a Senior Reactor Operator. This is a level 3 position;

- Senior Health Physicist - the Senior Health Physicist is responsible to the Radiation Center Director for directing the activities of Health Physics personnel including the development and implementation of the Radiation Safety Program. This is a level 3 position;

- Reactor Supervisor - the Reactor Supervisor is responsible to the Reactor Administrator for directing the activities of Reactor Operators and for the day-to-day operation and maintenance of the reactor. The Reactor Supervisor shall be certified as a Senior Reactor Operator. This is a level 3 position;

- Reactor Operator - the Reactor Operator reports to the Reactor Supervisor and is primarily involved in the manipulation of reactor controls, monitoring of instrumentation, and operations and maintenance of reactor related equipment. A Reactor Operator shall be certified as either a Senior Reactor Operator or a Reactor Operator. This is a level 4 position;

- Health Physicist - the Health Physicist is responsible to the Senior Health Physicist for the implementation of the Radiation Safety Program; and

- Health Physics Monitor - the Health Physics Monitor is responsible to the Health Physicist for radiological monitoring of all aspects of reactor operations.

12.1.3 Staffing

All reactivity changes shall be made by, or in the presence and under the direction of, the licensed operator of record at the time the reactivity changes are made.

At least two of the following people, the licensed operator of record included, shall be present in the Radiation Center Complex while the reactor is operating:

- Radiation Center Director;

- Reactor Administrator;

- Reactor Supervisor;

- Senior Reactor Operator or Reactor Operator;

- Senior Health Physicist; or

- Health Physicist.

The Reactor Supervisor shall be required to be present at the facility only during the initial startup each day or at the initial startup of a new experiment. At all other times while the reactor is, or may be, operating, the Reactor Supervisor may be away from the facility provided:

- he/she carries a portable radio receiver or cell phone which is operable;

- he/she verifies with the operator on duty at least daily that the receiver is operable;

- he/she remains at all times within the range of the radio receiver and at no time further than 10 miles from the facility;

- he/she contacts the facility (via telephone or radio receiver) within 10 minutes after receiving any message from the operator on duty; and

- he/she is able to go to the facility expeditiously, if necessary.

For any maintenance affecting the components inside the reactor tank or affecting other installed experimental facilities such as the beamports, at least two persons shall be present at the maintenance site, one of whom must be, at a minimum, a licensed reactor operator.

12.1.4 Selection and Training of Personnel

The OSTR shall select individuals with the requisite experience and qualifications recommended in ANSI/ANS 15.4, *Selection and Training of Personnel for Research Reactors*. All personnel shall have a combination of academic training, experience, health, and skills commensurate with their level of responsibility. General orientation and training for all personnel who work in the Radiation Center meets the requirements of 10 CFR 19 and ANSI/ANS 15.4. Topics covered as part of this training include:

- Organization;
- Security and Access Control;
- Radiation and Occupational Safety; and
- Emergency Procedures.

12.1.4.1 General Training for Radiation Center Personnel

Training for all personnel within the Radiation Center who work with radioactive materials is specifically discussed in Chapter 11.

12.1.4.2 Initial Reactor Operator Training

For initial training for either a reactor operator or a senior reactor operator, the following documents shall be studied and knowledge demonstrated:

- Training Volume 1: General Description of Reactor and Facilities;
- Training Volume 2: Reactor Instrumentation and Control;
- Training Volume 3: Reactor Physics, Kinetics, and TRIGA® Characteristics;
- Training Volume 4: Reactor Operating Procedures;
- Training Volume 5: Radiation Protection;
- Emergency Response Plan;
- Emergency Response Implementation Plan;

- License, Technical Specifications, and Experiments; and
- Physical Security Plan.

12.1.5 Radiation Safety

This is covered in Chapter 11.

12.2 Review and Audit Activities

The general scope of responsibility of the Reactor Operations Committee (ROC) shall be to independently review, evaluate, and approve safety standards associated with the operation and use of the OSTR and its experimental facilities.

12.2.1 Composition and Qualifications

Appointed by the Radiation Center Director, the ROC membership shall be composed of at least five members, including the chairman. The ROC membership should include, but is not limited to, the following individuals:

- Radiation Center Director;
- Reactor Administrator;
- Reactor Supervisor;
- Senior Health Physicist;
- individual with expertise in nuclear engineering;
- individual with expertise in another branch of engineering; and
- individual with expertise in radiation chemistry, nuclear chemistry, health physics, or radiation biology.

12.2.2 Charter and Rules

The ROC shall conduct its review and audit functions in accordance with a written charter. This charter shall include provisions for:

- meeting frequency;
- voting rules;
- quorums;

- method of submission and content of presentations to the committee;
- use of subcommittees; and
- review, approval and dissemination of meeting minutes.

12.2.3 Review Function

The responsibilities of the ROC, or a designated subcommittee thereof, shall include, but are not limited to, the following:

- review and approval of experiments utilizing the reactor facilities;
- review and approval of all changes to the safety analysis report or technical specifications;
- review and approval of all new procedures and substantive changes to existing procedures;
- review all changes to the facility or safety evaluations under 10 CFR 50.59;
- review of the operation and operational records of the facility;
- review of abnormal performance of plant equipment and operating anomalies; and
- review of all events which are required by regulations or Technical Specifications to be reported to the NRC within 24 hours.

12.2.4 Audit Function

The ROC, or a designated subcommittee thereof, shall audit the reactor operations and health physics programs annually. The audit shall include, but not be limited to, the following:

- inspection of reactor operating records;
- inspection of the reactor operating area; and
- reportable occurrences.

12.3 Procedures

Written procedures shall be prepared and approved prior to initiating any of the activities listed in this section. Unsubstantive changes to existing procedures may be made with the approval of the Reactor Administrator. New procedures or substantive changes to existing procedures shall

be approved by the ROC. The procedures are reviewed by the ROC annually to ensure that they are appropriate. The procedures shall be adequate to assure the safe operation of the reactor, but will not preclude the use of independent judgement and action should the situation require. The following two sections list areas that will typically require written procedures.

12.3.1 Reactor Operations

The following activities will typically require written procedures:

- startup, operation, and shutdown of the reactor;
- Technical Specifications surveillance requirements;
- fuel loading, unloading, and movement;
- routine maintenance of the control rod drives and reactor safety and interlock systems or other routine maintenance that could have an effect on reactor safety;
- testing and calibration of reactor instrumentation and controls, control rods and control rod drives;
- administrative controls for operations, maintenance, and conduct of irradiations and experiments that could affect reactor safety or core reactivity;
- implementation of the Emergency Response Plan; and
- actions to be taken to correct specific and foreseen potential malfunctions of any systems, including responses to alarms and abnormal reactivity changes.

12.3.2 Health Physics

The following activities will typically require written procedures:

- testing and calibration of area radiation monitors, facility air monitors, laboratory radiation detection systems, and portable radiation monitoring instrumentation;
- working with radioactive materials;
- facility radiation monitoring program including routine and special surveys, personnel monitoring, monitoring and handling of radioactive waste, and sampling and analysis of solid and liquid waste and gaseous effluents released from the facility;
- monitoring radioactivity in the environment surrounding the facility;
- personnel orientation and training;

- receipt of radioactive materials at the facility, and unrestricted release of materials and items from the facility; and

- transportation of radioactive materials.

12.4 Required Actions

This is covered in the OSTR Technical Specifications.

12.5 Reports

This is covered in the OSTR Technical Specifications.

12.6 Records

This is covered in the OSTR Technical Specifications.

12.7 Emergency Planning

The OSTR Emergency Response Plan contains detailed information concerning the OSTR response to emergency situations. The OSTR Emergency Response Plan is written to be in accordance with ANSI/ANS 15.16, *Emergency Planning for Research Reactors*.

The Emergency Response Plan is designed to provide response capabilities to emergency situations involving the OSTR. Detailed implementing procedures are referenced in this plan. This approach provides the OSTR emergency staff the flexibility to cope with a wide range of emergency situations without requiring frequent revisions to the plan.

Primary responsibility for the plan and response to and recovery from emergencies rests with the Emergency Director who is normally the Radiation Center Director. Implementation of the plan on a day-to-day basis is the responsibility of the Reactor Administrator who serves as the Emergency Coordinator in an emergency. Provisions for reviewing, modifying, and approving the emergency implementation procedures are defined in the plan to assure that adequate measures to protect the staff and general public are in effect at all times.

12.8 Security Planning

The OSTR Physical Security Plan contains detailed information concerning the OSTR security measures. The plan provides the OSTR with criteria and actions for protecting the facility from such acts as intrusion, theft, civil disorder and bomb threats.

Primary responsibility for the plan and facility security rests with the Principal Security Officer who is normally the Radiation Center Director. Implementation of the plan on a day-to-day basis during hours of operations is also the responsibility of the Principal Security Officer.

12.9 Quality Assurance

Quality assurance can be found throughout the operating and health physics procedures. It is not called out as a separate document.

12.10 Operator Training and Requalification

This reactor operator training and requalification program is designed to satisfy the requirements of the NRC's rules contained in 10 CFR 55. It also generally complies with the requalification program in ANSI/ANS 15.4, *Selection and Training of Personnel for Research Reactors*.

12.10.1 Responsibility

The responsibility for this program rests with the Reactor Supervisor. This responsibility shall cover the following items:

- selecting knowledgeable individuals to give classroom lectures and to supervise retraining operations;
- certifying to the Reactor Administrator that each individual has successfully completed the requalification program; and
- granting of exemptions to the requalification program as provided for in this plan.

12.10.2 Schedule

The requalification program shall be conducted on a cycle not to exceed two years. Upon conclusion, it will be promptly repeated.

12.10.3 Content

The requalification program shall consist of preplanned lectures, written examinations, an annual operating examination, and routine reactor operations.

12.10.4 Annual Lectures

Lectures shall be given annually (not to exceed 15 months) which cover the following:

- Emergency Response Plan; and
- Physical Security Plan.

12.10.5 Biennial Lectures

Lectures shall be given biennially (not to exceed 30 months) which cover the following:

- facility design, characteristics, instrument control and safety systems;
- reactor principles;
- operating procedures, Technical Specifications, and administrative procedures; and
- radiation protection.

12.10.6 Written Examinations

Written examinations shall be given covering the lecture material. The individual giving the lecture on a particular subject shall formulate, administer, and grade the written examination on that subject. Any licensed individual preparing and grading an examination is exempt from taking that examination. All written examinations will be proctored by the individual administering the exam, or by their appointed representative, but shall not be an individual taking the exam.

A grade equal to or greater than 75% will constitute a passing grade. Failure to achieve a passing grade will result in an accelerated retraining program in the subject area failed. This accelerated retraining program will be left to the discretion of the Reactor Supervisor.

The Reactor Supervisor may require an operator to participate in an accelerated requalification program when it is deemed needed by virtue of examinations or operating test results.

12.10.7 Quarterly Operating Requirements

To maintain a current license, each calendar quarter, a reactor operator shall operate the reactor for a minimum of four (4) hours and perform a supervised reactor startup, including a core excess measurement and increase to power.

To maintain a current license, each calendar quarter, a senior reactor operator shall operate the reactor for a minimum of four (4) hours and perform a supervised reactor startup, including a core excess measurement and increase to power. For senior reactor operators, direct supervision of these operations may be considered equivalent to actual performance.

If a licensed reactor operator or senior reactor operator has not met the quarterly operating requirements, then before resumption of licensed duties, the operator or senior operator shall:

- satisfactorily perform the annual operating exam; and
- operate the reactor for a minimum of six (6) hours under the direction of a Senior Reactor Operator.

12.10.8 Annual Operating Exam

To maintain a current license, each calender year, each reactor operator or senior reactor operator shall successfully complete an annual operating exam to be administered by the Reactor Supervisor. Successful completion is left to the discretion of the Reactor Supervisor. The annual operating exam for the Reactor Supervisor shall be administered by a senior reactor operator.

The annual operating exam shall include the following:

- reactor startup;
- core excess measurement;
- increase power to 1 MW;
- change in power level >10% in manual;
- record a set of console logs;
- respond to any annunciators;
- shut down the reactor;
- state responses, or respond to, all of the following situations:
    a) loss of coolant;
    b) loss of electrical power;
    c) loss or malfunction of a nuclear instrumentation;
    d) rod drop;
    e) inability to drive rods;
    f) fuel cladding failure; and
    g) reactor top or stack CAM alarm.

.

12.10.9 Medical Certification

All reactor operators and senior reactor operators shall undergo a medical examination by a physician biennially. The physician should be conversant with the medical requirements of this program. Following completion of the medical examination, an NRC Form 396 shall be signed by the Radiation Center Director.

12.10.10 Records

Required documents and records pertaining to the requalification program for a reactor operator or senior reactor operator shall be maintained until the respective operator's license is renewed or surrendered.

12.11 Startup Plan

This is not applicable.

12.12 Environmental Reports

This shall be submitted as a separate document.

CHAPTER 13

ACCIDENT ANALYSES

Chapter 13 - Valid Pages
Rev. 1 5/1/2012

i	Rev. 1 5/1/2012	20	Rev. 1 5/1/2012
ii	Rev. 1 5/1/2012	21	Rev. 1 5/1/2012
iii	Rev. 1 5/1/2012	22	Rev. 1 5/1/2012
iv	Rev. 1 5/1/2012	23	Rev. 1 5/1/2012
1	Rev. 1 5/1/2012	24	Rev. 1 5/1/2012
2	Rev. 1 5/1/2012	25	Rev. 1 5/1/2012
3	Rev. 1 5/1/2012	26	Rev. 1 5/1/2012
4	Rev. 1 5/1/2012	27	Rev. 1 5/1/2012
5	Rev. 1 5/1/2012	28	Rev. 1 5/1/2012
6	Rev. 1 5/1/2012	29	Rev. 1 5/1/2012
7	Rev. 1 5/1/2012	30	Rev. 1 5/1/2012
8	Rev. 1 5/1/2012	31	Rev. 1 5/1/2012
9	Rev. 1 5/1/2012	32	Rev. 1 5/1/2012
10	Rev. 1 5/1/2012	33	Rev. 1 5/1/2012
11	Rev. 1 5/1/2012	34	Rev. 1 5/1/2012
12	Rev. 1 5/1/2012	35	Rev. 1 5/1/2012
13	Rev. 1 5/1/2012	36	Rev. 1 5/1/2012
14	Rev. 1 5/1/2012	37	Rev. 1 5/1/2012
15	Rev. 1 5/1/2012	38	Rev. 1 5/1/2012
16	Rev. 1 5/1/2012	39	Rev. 1 5/1/2012
17	Rev. 1 5/1/2012	40	Rev. 1 5/1/2012
18	Rev. 1 5/1/2012	41	Rev. 1 5/1/2012
19	Rev. 1 5/1/2012	42	Rev. 1 5/1/2012

TABLE OF CONTENTS

13.0 ACCIDENT ANALYSIS

LIST OF TABLES

13.0 ACCIDENT ANALYSIS

13.1 Introduction

In about 1980, the U.S. Nuclear Regulatory Commission requested an independent and fresh overview analysis of credible accidents for TRIGA® and TRIGA®-fueled reactors. Such an analysis was considered desirable since safety and licensing concepts had changed over the years. The study resulted in NUREG/CR-2387, Credible Accident Analysis for TRIGA® and TRIGA®-fueled Reactors (Ref. 13.1). The information developed by the TRIGA® experience base, plus appropriate information from NUREG/CR-2387, serve as a basis for some of the information presented in this chapter.

The reactor physics and thermal-hydraulic conditions in the OSTR at a power level of 1 MW are established in Chapter 4. In this chapter, it was assumed that 30/20 LEU TRIGA® fuel tis used in the OSTR.

The fuel temperature is a limit on operation in both steady-state and pulse modes. This limit stems from the out-gassing of hydrogen from U-ZrH fuel and the subsequent stress produced in the fuel element cladding material. The strength of the stainless steel cladding as a function of temperature sets the upper limit on the fuel temperature. Fuel temperature limits of 1,100 ^{o}C (with clad < 500 ^{o}C) and 930 ^{o}C (with clad > 500 ^{o}C) for U-ZrH with a H/Zr ratio less than 1.70 have been set to preclude the loss of clad integrity.

Nine credible accidents for research reactors were identified in NUREG-1537 (Ref. 13.2) as follows:

- the maximum hypothetical accident (MHA);
- insertion of excess reactivity;
- loss of coolant accident (LOCA);
- loss of coolant flow;
- mishandling or malfunction of fuel;
- experiment malfunction;
- loss of normal electrical power;
- external events; and
- mishandling or malfunction of equipment.

This chapter contains analyses of postulated accidents that have been categorized into one of the above nine groups. Some categories contain accidents that do not appear applicable or credible for the OSTR, but this is acknowledged in a brief discussion of the category. Some categories contain an analysis of more than one accident even though one is usually limiting in terms of impact. Any accident having significant radiological consequences was included.

For those events that do not result in the release of radioactive materials from the fuel, only a qualitative evaluation of the event is presented. Events leading to the release of radioactive material from a fuel element were analyzed to the point where it was possible to reach the

conclusion that a particular event was, or was not, the limiting event in that accident category. The MHA for TRIGA® reactors is the cladding failure of a single irradiated fuel element in air with no radioactive decay of the contained fission products taking place prior to the release.

13.2 Accident Initiating Events and Scenarios, Accident Analysis, and Determination of Consequences

13.2.1 Maximum Hypothetical Accident (MHA)

13.2.1.1 Accident Initiating Events and Scenarios

A single fuel element could fail at any time during normal reactor operation or while the reactor is in a shutdown condition, due to a manufacturing defect, corrosion, or handling damage. This type of accident is very infrequent, based on many years of operating experience with TRIGA® fuel, and such a failure would not normally incorporate all of the necessary operating assumptions required to obtain a worst-case fuel-failure scenario.

For the OSTR, the MHA has been defined as the cladding rupture of one highly irradiated fuel element with no radioactive decay followed by the instantaneous release of the noble gas and halogen fission products into the air. The failed fuel element was assumed to have been operated at the highest core power density for a continuous period of one year at 1 MW. This results in all of the halogens and noble gases (except Kr-85) reaching their saturated activities.

This is the most severe accident for a TRIGA® reactor and is analyzed to determine the limiting or bounding potential radiation doses to the reactor staff and to the general public in the unrestricted area. A less severe, but more credible accident, involving this same single element having a cladding failure in water will also be analyzed. This latter accident more correctly falls into the Mishandling or Malfunction of Fuel accident category and will be addressed there.

During the lifetime of the OSTR, used fuel within the core may be moved to new positions or removed from the reactor. Fuel elements are moved only during periods when the reactor is in a shutdown condition. Also, the OSTR is never operated continuously at 1 MW for a period longer than 8-10 hours, let alone a period of one year.

Nevertheless, this MHA has been analyzed for the OSTR.

Three different scenarios have been chosen for analysis:

- Scenario A:

  In this scenario, the entire north wall of the reactor room instantly vanishes. No credible cause for this occurrence can be imagined. The noble gas and halogen fission products that have been released to the reactor room air are assumed to mix instantly and uniformly with the room air. This reactor room air then moves out through the missing wall at the mean wind speed

(1 m sec^{-1}). This is assumed to be a ground level release. It takes 8.52 seconds for the entire volume of the reactor room air to be evacuated. Thus, individuals outside the reactor room will be exposed to a radioactive cloud for a period of 8.52 seconds;

- Scenario B:

  This scenario again assumes that the noble gas and halogen fission products instantly and uniformly mix with the reactor room air. The fission products that have been released to the reactor room air are then exhausted at the stack ventilation rate (4.39E6 cm^3sec^{-1}). The path for this release is not specified. It could possibly be through the small door on the NE corner of the building, or it could be through the stack if the vent fans didn't shut down and the dampers did not close. The air is assumed to be discharged at ground level, and no credit is taken for an elevated release. The time to evacuate the entire volume of the reactor room is 14.7 minutes, and this is, therefore, the exposure time for individuals outside the reactor room; and

- Scenario C:

  This scenario also assumes that the noble gas and halogen fission products instantly and uniformly mix with the reactor room air. The reactor room air then leaks from the room at the leak rate of 1.69E4 cm^3sec^{-1} as specified in the original OSTR SAR (Ref. 13.3). The leakage from the room is through the walls brought about by a pressure differential between the room and outside. This pressure differential was assumed to arise through the unlikely combination of a drop in atmospheric pressure of 1.5" Hg and an increase in room temperature of 40^oC in 12 hours. Using the ideal gas law, $P_1V_1/T_1= P_2V_2/T_2$, where temperature is in K, pressure is in inches of Hg, and volume is in cubic centimeters. The initial conditions of T_1=295.2 K (22.2 ^oC) and P_1=29.4" Hg in the RX bay of volume 3.74E4 cm^3, the increase in temperature of 40^oC would result in the pressure increasing to 33.4" Hg. The atmospheric drop 0f 1.5" Hg would mean an increase in room pressure to 34.9" Hg and assuming an outside temperature of 8.7 ^oC, the resulting bay volume would be 3.01E9 cm^3. The leak rate is determined by the difference in the initial and final bay volumes which is 7.3E8 cm^3 divided by 12 hrs. or 43200 sec to equal 1.69E4 cm^3 sec^{-1}.

  In this case, it would take 63.7 hours for the entire volume of the reactor room air to be evacuated, and this is the exposure time for individuals outside the reactor room. This is also assumed to be a ground level release.

13.2.1.2 Accident Analysis and Determination of Consequences

As stated earlier, it is assumed that the OSTR is fueled with 30/20 LEU fuel elements and that the reactor has operated continuously at 1 MW for a period of one year. Thus, all halogens and

all noble gases (except Kr-85) are at their saturation activity. The highest-power-density element fails and releases the noble gases and halogens to the cladding gap. This highest-power-density element has a power density of 15.9 kW per element, and a maximum-to-average power factor of 1.42 (Ref. 13.4). The fission product inventory of halogen and noble gases are given in Table 13-1 for this element. The inventory assumes a saturated activity is present and is based upon the fission yield for each isotope.

Considerable effort has been expended to measure and define the fission product release fractions for TRIGA® fuels. Data on this aspect of fuel performance are reported in Refs. 13.5 - 13.13. Using this data, GA developed a conservative correlation for fission product release to be

$$e = 1.5x10^{-5} + 3.6x10^{3} \exp\left\{\frac{-1.34E4}{T+273}\right\}. \qquad (13\text{-}1)$$

At an average fuel temperature of 500 ^{o}C, this release fraction is 1.22E-4. This fuel temperature (500 ^{o}C) is much higher than the actual expected average fuel temperature of 322 ^{o}C, and results in a release fraction about 7.8 times higher.

Once the fission products are released to the gap, this activity is released when the cladding fails. If the release is in air (MHA), then this activity is released directly into the reactor room air. If the release occurs in the pool water, then the fission products must migrate through the water before being released to the reactor room air. Once released into the reactor room air, a further reduction of the halogen activity is expected to occur due to plateout in the building.

Thus, the fraction (w) of the fission product inventory released from a single fuel element which reaches the reactor room air and, subsequently, the atmosphere in the unrestricted environment is:

$$w = e\ f\ g\ h; \qquad (13\text{-}2)$$

where:

e = the fraction released from the fuel to the fuel-cladding gap;
f = the fraction released from the fuel-cladding gap to the reactor room air (if no water is present), or to the pool water (if water is present);
g = the fraction released from the pool water to the reactor room air; and
h = the fraction released from the reactor room air to the outside unrestricted environment, due to plateout in the reactor room.

Table 13-1 Saturated Activities for Highest Power Density Fuel Element

Isotope	Half Life	Saturated Activity (mCi)	Released Activity to Reactor Room Air NO POOL WATER (mCi)	Released Activity to Reactor Room Air WITH POOL WATER (mCi)
Br-82	35.3 h	3.90E+01	0.00	0.00
Br-83	2.40 h	8.04E+04	2.45	0.12
Br-84m	6.0 min	5.50E+03	0.17	0.01
Br-84	31.8 min	1.47E+05	4.48	0.22
Br-85	2.87 min	1.86E+05	5.66	0.28
Br-86	55.5 sec	2.59E+05	7.90	0.40
Br-87	55.9 sec	2.91E+05	8.89	0.45
Total Bromine		9.69E+05	29.55	1.48
I-131	8.02 days	4.62E+05	14.10	0.71
I-132	2.28 h	7.15E+05	21.81	1.09
I-133	20.8 h	1.08E+06	32.94	1.65
I-134	52.6 min	1.23E+06	37.56	1.88
I-135	6.57 h	1.01E+06	30.92	1.55
I-136	83.4 sec	3.79E+05	11.55	0.58
Total Iodine		4.88E+06	148.88	7.47
Kr-83m	1.86 h	8.04E+04	9.81	9.81
Kr-85m	4.48 h	1.85E+05	22.63	22.63
Kr-85	10.76 years	4.03E+04	4.92	4.92
Kr-87	76.2 min	3.66E+05	44.68	44.68
Kr-88	2.84 h	5.16E+05	63.01	63.01
Kr-89	3.15 min	6.63E+05	80.88	80.88
Total Krypton		1.85E+06	225.92	225.92
Xe-131m	11.9 days	5.62E+03	0.69	0.69
Xe-133m	2.19 days	3.22E+04	3.93	3.93
Xe-133	5.24 days	1.08E+06	131.93	131.93
Xe-135m	15.3 min	2.06E+05	25.18	25.18
Xe-135	9.10 h	1.07E+06	130.83	130.83
Xe-137	3.82 min	9.77E+05	119.16	119.16
Xe-138	14.1 min	9.92E+05	121.05	121.05
Total Xenon		4.37E+06	532.76	532.76
Total Halogens		5.85E+06	178.43	8.95
Total Noble Gases		6.22E+06	758.69	758.69

For the accident where the cladding failure occurs in air, it is very conservatively assumed that 25% of the halogens released to the cladding gap are eventually available for release from the reactor room to the outside environment. This value is based on historical usage and recommendations (Refs. 13.5 - 13.13), where Reference 13.5 recommends a 50% release of the halogens from the gap to the air. References 13.6 and 13.7 apply a natural reduction factor of

50% due to plateout in the reactor building. Combining the 50% release from the gap with the 50% plateout results in the 25% total release. However, this value appears to be quite conservative, since References 13.10 and 13.11 quote a 1.7% release from the gap rather than 50%.

For the accident in air, 100% of the noble gases are assumed to be available for release to the unrestricted environment.

For the accident in water, it is conservatively assumed that most of the halogens released from the cladding gap remain in the water and are removed by the demineralizer. A small fraction, 5%, of the halogens is assumed to escape from the water to the reactor room air. Combining this with the 50% release from the gap to the water, the result is that 2.5% of the halogens in the gap are released to the reactor room. Again, 50% of these plateout in the reactor room before release to the outside environment. For the noble gases in water, 100% are assumed to be available for release to the unrestricted environment.

The experience at TMI-2, along with recent experiments, indicate that the 50% halogen release fraction is much too large. Possibly as little at 0.06% of the iodine reaching the cladding gap may be released into the reactor room due in part to a large amount of the elemental iodine reacting with cesium to form CsI, a compound much less volatile and more water soluble that elemental iodine (Ref. 13.11).

The values for these various release fractions are given in Tables 13-2 and 13-3. For the OSTR, the prevailing wind is from the south, blowing to the north. The minimum distance to the unrestricted environment (10 m), the minimum distance to the nearest occupied office building (100 m), and the minimum distance to the nearest permanent residence (267 m) are also to the north. For this accident, therefore, it was assumed that the wind is blowing from south to north.

For any atmospheric stability (Pasquill) class, a ground-level release always gives a higher concentration at any given distance than an elevated release. Thus, it was assumed that there were only ground level releases, which do not take credit for any release heights nor building wake effects. Furthermore, the more stable the atmospheric class, the higher the concentration. Therefore, it was assumed that the most stable atmospheric class (Pasquill F) prevailed for all scenarios. Also, the lower the wind speed, the higher the concentration. Thus, it was assumed that a low wind speed of 1 m sec^{-1} existed for all scenarios.

Table 13-2 Release Fraction Components

Fission product	f No pool water	f With pool water	g No pool water	g With pool water	h
Noble gas	1.0	1.0	N/A	1.0	1.0
Halogens	0.5	0.5	N/A	0.05	0.5

Table 13-3 Total Release Fraction

Fission product	w No pool water	w With pool water
Noble gas	1.22E-4	1.22E-4
Halogens	3.05E-5	1.53E-6

The methodology of NRC Regulatory Guide 1.145 (Ref. 13.14) was used. For distances greater than 100 m, the values for horizontal and vertical dispersion coefficients were also taken from this guide. For distances from 10 m to 100 m, which are not treated in Regulatory Guide 1.145, data were obtained locally from the OSTR (Ref. 13.15). The values for the dispersion coefficients and χ/Q are given in Table 13-4.

Furthermore, it was assumed that all of the fission products were released to the unrestricted area by a single reactor room air change, which would maximize the dose rate to persons exposed to the plume during the accident.

Table 13-4 Atmospheric Dispersion Coefficients and χ/Q Values for Pasquill F and Mean Wind Speed of 1 m sec^{-1}

Distance (m)	σ_y (m)	σ_z (m)	χ/Q (sec m^{-3})
10	1.29	1.04	5.93E-2
50	2.45	1.20	2.71E-2
100	3.90	2.20	9.27E-3
150	6.18	3.22	4.00E-3
200	8.21	4.13	2.35E-3
250	10.21	4.98	1.57E-3
267	10.88	5.25	1.39E-3

Additional parameters used in this accident were:

- reactor room ventilation exhaust rate: 4.39E+6 cm^{3}sec^{-1};
- reactor room leak rate: 1.69E+4 cm^{3}sec^{-1};
- reactor room volume: 3.88E+9 cm^3;
- area of north face of reactor building: 2.31E+2 m^2;
- receptor breathing rate: 3.3E-4 m^{3}sec^{-1}: (NRC "light work" rate); and
- dose conversion factors:
  - internal: based on DOE/EH-0071 (Ref. 13.16);
  - external: based on DOE/EH-0070 (Ref. 13.17).

The committed dose equivalent (CDE) to the thyroid and the committed effective dose equivalent (CEDE) for members of the general public at a given distance downwind from the facility for all isotopes of concern may each be calculated by:

$$\left(\text{CDE or CEDE}\right)_D = \sum_i \left[\frac{\left(\frac{\chi}{q}\right)_D \text{BR DCF}_{\text{int},i} A_i \lambda_v \left[e^{-\lambda_i t_i} - e^{-\lambda_i t_2} \right]}{\lambda_i} \right], \qquad (13\text{-}3)$$

where:

$(\chi/Q)_D$ = atmospheric dispersion factor at a given distance D (s m^{-3});
BR = breathing rate (m^3 s^{-1});
$DCF_{int,i}$ = internal dose conversion factor for isotope i (mrem μCi^{-1}) [Ref. 13.16];
A_i = initial activity of isotope i released into the reactor room (μCi);
R_v = ventilation or leakrate of air from the reactor bay (m^3 s^{-1});
V = reactor room volume (m^3);
λ_v = ventilation constant = R_v/V (s^{-1});
λ_i = decay constant for isotope i (s^{-1});
t_1 = time when plume first arrives at the receptor point (s); and
t_2 = time when plume has passed the receptor point (s).

The deep dose equivalent (DDE) to members of the general public at a given distance downwind from the facility for both the thyroid and the whole body may each be calculated by:

$$\left(DDE_{Thyroid}\ or DDE_{WB}\right)_D = \sum_i \left[\frac{\left(\frac{\chi}{Q}\right)_D DCF_{ext,i} A_i \lambda_v \left[e^{-\lambda_i t_1} - e^{-\lambda_i t_2} \right]}{\lambda_i} \right], \qquad (13\text{-}4)$$

where:

$DCF_{ext,i}$ = external dose rate conversion factor for isotope i (mrem m^3 μCi^{-1} s^{-1}) [Ref. 13.17].

For calculating dose to occupational workers in the reactor room, stay times of 2 and 5 minutes were used. Experience indicates that the reactor room can easily be evacuated in 2 minutes. The value of 5 minutes is thought to be a reasonable longer period of time assuming an worker is performing some task (i.e., determining if a false alarm has occurred). The CDE and CEDE for personnel in the reactor room for a given stay-time may each be calculated by:

$$\left(CDEorCEDE\right)_{ST} = \sum_{i}\left[\frac{DCF_{\text{int},i}A_i BR\left[1-e^{\lambda_{eff}t_{ST}}\right]}{\lambda_{eff}V}\right] \tag{13-5}$$

where:

$\lambda_{eff} = \lambda_i + \lambda_v$; and
t_{ST} = stay-time of personnel (s).

The DDE to personnel in the reactor room for a given stay-time for both the thyroid and the whole body may be calculated by:

$$\left(DDE_{Thyroid}orDDE_{WB}\right)_{ST} = \sum_{i}\left[\frac{DCF_{ext,i}A\left[1-e^{-\lambda_{eff}t_{ST}}\right]}{\lambda_{eff}V}\right]. \tag{13-6}$$

The results of these calculations for all three scenarios are shown in Tables 13-5 through 13-10. As seen from the tables, Scenario A gives the highest doses to the general public at any distance, as might be expected since the activity was released in a very short time leaving little time for radioactive decay. Scenario C gives the lowest doses at any given distance since the release occurs over a long time and radioactive decay becomes significant. Also, as expected, the doses were highest at the shortest distance (i.e., the site boundary). In all cases, doses for the general public and occupational workers were all well below the annual dose limits specified by 10 CFR 20.

Table 13-5 Occupational Radiation Doses in the Reactor Room Following a Single Element Failure in Air Scenario A

Reactor Room Occupancy (minutes)	$CDE_{Thyroid} + DDE_{Thyroid}$ (mrem)	TEDE (mrem)
2	33	2
5	33	2

Table 13-6 Radiation Doses to Members of the General Public Following a Single Element Failure in Air Scenario A

Distance (m)	$CDE_{Thyroid}$ + $DDE_{Thyroid}$ (mrem)	TEDE (mrem)
10	450	21
50	206	9
100	70	3
150	30	1
200	18	1
250	12	1
267	10	<1

Table 13-7 Occupational Radiation Doses in the Reactor RoomFollowing a Single Element Failure in Air Scenario B

Reactor Room Occupancy (minutes)	$CDE_{Thyroid}$ + $DDE_{Thyroid}$ (mrem)	TEDE (mrem)
2	219	10
5	496	22

Table 13-8 Radiation Doses to Members of the General PublicFollowing a Single Element Failure in Air Scenario B

Distance (m)	$CDE_{Thyroid}$ + $DDE_{Thyroid}$ (mrem)	TEDE (mrem)
10	447	19
50	204	9
100	70	3
150	30	1
200	18	1
250	12	<1
267	10	<1

Table 13-9 Occupational Radiation Doses in the Reactor RoomFollowing a Single Element Failure in Air Scenario C

Reactor Room Occupancy (minutes)	$CDE_{Thyroid}$ + $DDE_{Thyroid}$ (mrem)	TEDE (mrem)
2	234	11
5	585	26

Table 13-10 Radiation Doses to Members of the General Public Following a Single Element Failure in Air Scenario C

Distance (m)	$CDE_{Thyroid}$ + $DDE_{Thyroid}$ (mrem)	TEDE (mrem)
10	323	10
50	147	5
100	50	2
150	22	1
200	13	<1
250	9	<1
267	8	<1

The direct exposure of individuals outside of the reactor bay from airborne material inside the reactor bay was calculated using Microshield V5.05. The source term was assumed to be the entire reactor bay volume. The exposure rates from each isotope in Table 13.1 with and without pool water at a distance from the outside wall was calculated used in the following equation to determine the total exposure:

$$X = \sum_i \frac{\dot{X}_i \times \left(1-e^{-\lambda_{eff} t_{st}}\right)}{\lambda_{eff}} \qquad (13\text{-}7)$$

t_{st} = stay time of personnel and $\lambda_{eff} = \lambda_i + \lambda_v$ where λ_i is the decay constant for the ith isotope and λ_v is the ventilation constant for the appropriate scenario. The initial exposure is at t = 0 and the other is for the exposure time for each scenario. For this calculation, the integrated times for Scenarios A, B, and C were 8.52 s, 14.7 min, and 63.7 h, respectively. The thyroid dose was calculated by multiplying the total by 0.03. The results presented in Table 11 and 12 show that the contribution of exposure from the source term inside the reactor bay to anyone outside is negligible.

Table 13-11 Exposure as a Function of Distance for a Reactor Bay Volume Source With Pool Water

Distance from Wall (m)	Scenario A Thyroid DDE (mR)	Scenario A Whole Body (mR)	Scenario B Thyroid DDE (mR)	Scenario B Whole Body (mR)	Scenario C Thyroid DDE (mR)	Scenario C Whole Body (mR)
10	1.16E-07	3.87E-06	1.78E-04	5.93E-03	6.07E-03	2.02E-01
50	1.37E-08	4.58E-07	2.10E-05	7.02E-04	7.21E-04	2.40E-02
100	3.30E-09	1.10E-07	5.05E-06	1.68E-04	1.68E-04	5.59E-03
150	1.25E-09	4.16E-08	1.91E-06	6.36E-05	6.15E-05	2.05E-03
200	5.79E-10	1.93E-08	8.83E-07	2.94E-05	2.78E-05	9.28E-04
250	3.02E-10	1.01E-08	4.60E-07	1.53E-05	1.42E-05	4.74E-04

Table 13-12 Exposure as a Function of Distance for a Reactor Bay Volume Source Without Pool Water

Distance from Wall (m)	Scenario A Thyroid DDE (mR)	Scenario A Whole Body (mR)	Scenario B Thyroid DDE (mR)	Scenario B Whole Body (mR)	Scenario C Thyroid DDE (mR)	Scenario C Whole Body (mR)
10	2.10E-07	7.00E-06	2.25E-04	7.51E-03	1.26E-02	4.19E-01
50	2.48E-08	8.27E-07	2.67E-05	8.89E-04	1.49E-03	4.98E-02
100	6.01E-09	2.00E-07	6.38E-06	2.13E-04	3.44E-04	1.15E-02
150	2.29E-09	7.64E-08	2.40E-06	7.99E-05	1.25E-04	4.18E-03
200	1.07E-09	3.57E-08	1.11E-06	3.68E-05	5.53E-05	1.84E-03
250	5.62E-10	1.87E-08	5.73E-07	1.91E-05	2.77E-05	9.22E-04

13.2.2 Insertion of Excess Reactivity

13.2.2.1 Accident Initiating Events and Scenarios

The most credible generic accident is the inadvertent rapid insertion of positive reactivity that could, if large enough, produce a transient resulting in fuel overheating and a possible breach of cladding integrity. Operator error or failure of the automatic power level control system could cause such an event due to the uncontrolled withdrawal of a single control rod, or possibly even the withdrawal of more than one control rod. Flooding or removal of beamport inserts could also have a positive effect on reactivity, but not as severe as the removal of a control rod. In a separate scenario, a large reactivity insertion was postulated to create fuel cladding temperatures that might cause a metal-water reaction, but for many reasons this accident is not considered to be a safety risk in TRIGA® reactors.

13.2.2.2 Accident Analysis and Determination of Consequences

13.2.2.2.1 Maximum Reactivity Insertion

The maximum reactivity insertion was covered in section 4.7.

13.2.2.2.2 Uncontrolled Withdrawal of a Control Rod

Pulse reactivity limits are determined in section 4 of this SAR.

Uncontrolled withdrawal of a control rod may be caused by operator error or equipment malfunction. Interlocks prohibit the simultaneous manual or automatic withdrawal of more than one control rod. For a single delayed neutron group model with the prompt jump approximation, a linear (ramp) reactivity increase results in the following equation for power as a function of time:

$$\frac{P(t)}{P_0} = \left(e^{-\lambda t}\right)\left[\frac{\beta}{\beta - \gamma t}\right]^{(1+\lambda\beta/\gamma)} \qquad (13\text{-}8)$$

where: $P(t)$ = power at time t

P_0 = initial power level

β = total delayed neutron fraction = 0.0076

λ = one group decay constant = 0.405 (sec^{-1})

t = time (sec)

γ = linear insertion rate of reactivity ($\Delta k/k\text{-}sec^{-1}$)

Control rod data for the NORMAL core is shown in **Table** . The same values for total rod withdrawal times for the HEU core are used. Calculations, measurements and operating experience indicate that the NORMAL core gives the highest control rod worths.

Table 13-13 Control Rod Data for NORMAL configuration LEU core.

Rod	Total Worth	Total Withdrawal time (sec)	Average insertion rate ($/sec)	Total reactivity at SCRAM ($)
Transient	2.86	33.81	0.0846	$0.95
Safety	2.60	48.09	0.0541	$0.87
Shim	2.55	48.20	0.0529	$0.86
Regulating	3.36	36.18	0.0929	$0.96

For the LEU core, the regulating control rod has the highest total worth, and also the highest reactivity insertion rate. For the reactivity insertion accident, starting power levels of 100W and 1.0 MW were considered. The SCRAM setpoint was assumed to be 1.06 MW, and 0.5 seconds delay time was assumed between reaching the SCRAM setpoint and actual release of the control rods.

For the case with initial power of 100W, the reactor power was calculated to reach the trip setpoint in 9.86 seconds, and the peak reactivity insertion was $0.96. For the case with initial power of 1.0 MW, the reactor power was calculated to reach the trip setpoint in 0.55 seconds, and the peak reactivity insertion was $0.10. In both cases, the peak reactivity insertion is well below the pulse reactivity insertion limit, and thus would produce no adverse safety effects.

13.2.2.2.3 Uncontrolled Withdrawal of All Control Rods

The very unlikely accident involving the simultaneous withdrawal of all four control rods was also considered. An initial power of 100W is assumed, with a scram setpoint of 1.06 MW and a 0.5 second delay time. The reactivity insertion rate for four control rods is 0.2844 $/sec. The trip setpoint is reached in 3.47 seconds and the total amount of reactivity inserted is $1.13. This is still well below the pulse reactivity insertion limit. Note that the HEU SAR analysis was also conducted with the same assumption that the SCRAM setpoint is 1.06 MW, even though licensed power is 1.1 MW. If the SCRAM is assumed to occur at 1.1 MW, the values calculated for total reactivity at SCRAM will be slightly higher. In the bounding case of simultaneous withdrawal of four rods, the reactivity inserted for a SCRAM at 1.06 MW is $1.129987 and the reactivity inserted for a SCRAM at 1.1 MW is $1.130174.

13.2.2.2.4 Beamport Flooding

The only credible accident in the class is the possible flooding of one or more of the beamports. In this case air or inert gas would be replaced with water, and this would constitute a positive reactivity insertion. It has been estimated that the worth of one flooded beamport tube would be about $0.25 (Ref. 13.26). If all four beamports were flooded, the total effect would be $1.00 of positive reactivity added. Even if this estimate of beamport reactivity worth doubled, the net effect would still be less than the limiting reactivity insertion as described in section 4.7. This, therefore, does not represent a significant safety event.

13.2.2.2.5 Metal-Water Reactions

Although metal-water reactions have occurred in some reactor accidents or destructive tests, the evidence from these events and laboratory experiments shows that a dispersed liquid metal is required for a violent chemical reaction to occur (Refs. 13.1 and 13.18). The conditions for a solid metal-water reaction are not readily achievable in a reactor system such as the OSTR.

Water quench tests on TRIGA® fuel have been conducted to fuel temperatures as high as 1,200 ^{o}C without significant effect. Since the operating temperatures at 1 MW do not approach this temperature, this effect does not represent a safety risk. The only credible way in which temperatures high enough to allow metal-water reactions can be created in a TRIGA® reactor is through a large reactivity insertion. The limits set on excess reactivity preclude this.

13.2.3 Loss of Coolant Accident (LOCA)

13.2.3.1 Accident Initiating Events and Scenarios

Loss of coolant from the OSTR could occur primarily through one of two scenarios: pumping water from the reactor tank, or reactor tank failure. These scenarios are analyzed as part of this section.

13.2.3.2 Accident Analysis and Determination of Consequences

13.2.3.2.1 Pumping Water from the Reactor Tank

The outlet for the primary water is located about 4 feet below the normal tank water level. This line and the primary water inlet line each have a syphon break about 22 inches below the normal tank water level. The intake for the water purification system is at the normal water level surface, and if the water level drops about 3 inches or more, this begins to suck air. Thus the normal water systems could only pump water down about 22 inches below the normal tank water level, and could not accidentally pump the tank dry.

13.2.3.2.2 Reactor Tank Failure

There are only two mechanisms that could cause tank failure: corrosion, leading to small leaks in the tank or one of the tank penetrations (beamports, thermal column, etc.), or a mechanical failure of the tank or one of the penetrations.

Leaks caused by corrosion would be small leaks, which would be detected in the routine daily inspection, and makeup water could be supplied before the tank water level had lowered significantly. If the leak persisted or was larger, the reactor fuel could be unloaded and the leak repaired.

Mechanical failure of the tank or one of the penetrations could cause a large and immediate loss of tank water. The only credible mechanism for causing such a failure would be an earthquake greater than the design basis earthquake for the OSTR. Even if such an event occurred while the reactor was operating at peak power, the reactor would shut down because of the voiding of the water from the core, even if there were no scram.

In this unlikely event, almost all of the water pouring on the reactor floor would run into the pipe trench that goes from the base of the reactor into the heat exchanger room. This trench drains into the waste holdup tank. The volume of the waste holdup tank is about 2,950 gallons. The water in this tank is checked for release concentrations, then the water is dumped when the tank level reaches about 1,800 gallons. Thus there is always at least about 1,100 spare gallons in the tank, and often more. The trench can hold about 3,000 gallons. Therefore, about 4,100 gallons or more of the total 4,600 gallons of reactor tank water could be held in the pipe trench and holdup tank.

There are two immediate considerations of such a catastrophic loss of water: cooling of the reactor core, and dose rates around the uncovered core. The consequences of each of these will be discussed in the following sections.

13.2.3.2.2.1 Cooling of Reactor Core

If all coolant is suddenly lost when the reactor has been operating at full power for a considerable period, the primary concern is the maximum fuel temperature that might be reached and whether or not the fuel cladding will remain intact. This accident has been analyzed in numerous reports previously (Refs. 13.3, 13.4, 13.21 - 13.23) , and addressed in Chapter 4 of this report. All of these reports reach the same conclusion: natural convective air cooling of the fuel will keep the maximum fuel temperature well below the temperature for cladding failure if the reactor operates at a maximum power level of 1.5 MW or below. In NUREG/CR-2387, this accident was also examined and the conclusion was that, for a reactor such as the OSTR, a loss of coolant accident was not credible (Ref. 13.1).

13.2.3.2.2.2 Radiation Levels from the Uncovered Core

If the reactor core suddenly becomes uncovered after sustained operation at full power, high radiation doses might be expected from the uncovered core. Radiation doses at three locations are calculated here: at the grating over the top of the reactor, at a point in the reactor room, and at the nearest fence boundary to the unrestricted area. These latter two doses would be scattered doses from the reactor room roof.

The basic assumption is that the reactor has been operating at a maximum power level of 1 MW for one continuous year, and then the water is instantly lost. This is a very conservative assumption, since there is no conceivable way the OSTR could be operated continuously, 24 hours per day, at 1 MW for one year. The OSTR only operates on an 8-hour-per-day shift for 5 days per week.

The total fission product activity as a function of time after shutdown was determined using the standard equation (Ref. 13.24):

$$A(t) = 1.4\text{E}6P\left[t^{-0.2} - (t+T)^{-0.2}\right](Ci) \qquad (13\text{-}9)$$

where:

P = reactor thermal power (MW);
t = time after shutdown (days); and
T = operating time (days).

For this calculation: P = 1 MW and T = 365 days.

The total fission product activity will be calculated at 5 different times after shutdown: 10 seconds, 1 hour, 1 day, 1 week, and 1 month.

The reactor core was modeled as a cylinder of radius 22.2 cm and a height of 38.1 cm. This assumes that the fuel is filling all grid positions out through the F ring of the core, which is essentially the case for a normal core configuration. Therefore, the source term for this analysis (S_v) was determined by dividing the total activity by the volume of this cylinder where:

$$S_v = \frac{(3.7\text{E}10)A}{\pi R^2 h}(\gamma\ cm^{-3}\sec^{-1}), \qquad (13\text{-}10)$$

R = core radius (cm) = 22.2 cm;
h = core height (cm) = 38.1 cm; and
3.7E10 converts curies to gamma rays, assuming one gamma ray of energy 1 MeV per disintegration.

The total activity and the source strength are shown in Table 13-15.

13.2.3.2.2.3 Dose Rate Directly Above Core

The reactor core, shutdown and drained of water, was treated as a uniform bare cylindrical source of 1-MeV photons. Its dimensions were taken to be equal to those of the active core lattice. No accounting was made of sources other than fission product decay gammas, and no credit was taken for attenuation through the fuel element end pieces and the upper grid plate. The first of these assumptions is optimistic, the second conservative, and the net effect is conservative. The conservative assumption of a uniformly distributed source of 1-MeV gammas was balanced by not assuming any buildup in the core.

Table 13-14 Total Fission Product Activity and Source Strength After Shutdown

Time After Shutdown	Fission Product Activity (Ci)	Source Strength S_v (cm^{-3} sec^{-1})
10 seconds	8.15E6	5.11E12
1 hour	1.24E6	7.78E11
1 day	9.70E5	6.08E11
1 week	5.20E5	3.26E11
1 month	2.86E5	1.79E11

The dose rate was calculated at a point on the axis of the core cylinder at a distance of 610 cm (20 feet) from the top of the core. This is the distance from the top of the core to a point about 3 feet above the tank cover grating.

The dose rate was determined from the equation:

$$\phi = \left[\frac{S_v R^2}{4\mu_c A^2}\right]\left[1 - \exp(\mu_c h)\right] \left(\gamma cm^{-2}\,\mathrm{sec}^{-1}\right), \qquad (13\text{-}11)$$

where:

R = core radius (22.2 cm);
H = core height (38.1 cm);
μ_c = core attenuation coefficient (0.28 cm^{-1});
a = distance from top of core to dose point (610 cm); and
S_v = source strength.

The dose conversion factor, K, for effective dose equivalent per unit photon fluence was obtained from ICRP 51, Table 2 (Ref. 13.25). This has been calculated for photons incident on an anthropomorphic phantom from various geometries. The worst case (highest dose factor) was for the anterior to posterior geometry, and this was used for this case. For 1-MeV photons, this value of K was 4.60E-12 Sv cm^2 γ^{-1}.

The results are given in Table 13-16 and are in agreement with the MNRC and Torrey Pines TRIGA® reactors (Refs. 13.22 and 13.26), when corrections are made for the operating power levels.

Table 13-15 Dose Rates on OSTR Reactor Top After a Loss of Pool Water Accident Following 1-MW Operation

Time After Shutdown	Effective Dose Equivalent Rate (rem h^{-1})
10 seconds	1.00E4
1 hour	1.52E3
1 day	1.19E3
1 week	6.39E2
1 month	3.51E2

13.2.3.2.2.4 Dose Rate From Scattered Radiation in Reactor Room

The purpose of this section is to calculate the dose rate to a person in the reactor room not in the direct beam from the exposed core, but subject to scattered radiation from the reactor room ceiling. The dose point was chosen to be 3 feet above the reactor room floor at a point in the SE corner of the room. This is the area where radioactive material is packaged for shipping and is frequently occupied. It is also the farthest distance one can get from the edge of the reactor and remain in the reactor room. The ceiling is about 20.6 feet above the reactor top. The ceiling is assumed to be a concrete slab. The concrete slab assumption gives the worst case scattering, but it should be noted that the roof over the reactor is only corrugated metal and not a thick concrete slab. Therefore, in reality the scattering will not be as great as calculated because the radiation from the unshielded core will undergo minimal interaction with the roof.

The following equation was used to find the flux at the dose point from scattered radiation (Ref. 13.27):

$$\phi = \frac{(6.03\text{E}23)\,\rho Z I_0 C \dfrac{\delta\sigma}{\delta\Omega}}{Ax^2\left\{\mu_o + \mu_1\left[\dfrac{\cos\theta_0}{\cos\theta_1}\right]\right\}}\left(\gamma cm^{-1}\sec^{-1}\right), \qquad (13\text{-}12)$$

where:

ρ = density of the scattering material (concrete) = 2.3 g cm^{-3};
Z/A = ratio of the average atomic number to the atomic mass;
I_oC = incident beam times the cross section of the beam ((sec^{-1});
x = distance from scattering point to dose point = 1.78E3 cm;
μ_0 = attenuation coefficient in scattering material for incident photons
= 0.146 cm^{-1};
μ_1 = attenuation coefficient in scattering material for scattered photons
= 0.292;
θ_0 = incident angle, measured from normal to the scatterer = 0^o;
θ_1 = scattered angle, measured from normal to the scatterer = 49^o; and
$\delta\sigma/\delta\Omega$ = differential Klein-Nishina scattering cross section (cm^2).

It was assumed that the source photons which reached the top of the reactor tank were incident normally to the concrete roof ($2_o = 0$) at a point directly over the core. Thus:

$$I_0 C = S_0 \omega = \frac{\pi R^2 S_v \omega}{\mu_c}, \tag{13-13}$$

where S_o is the strength of a point source equal to the total radioactivity and placed at a point which is one mean free path from the top of the reactor (μ_c^{-1}).

The expression T is the fractional solid angle subtended by the equivalent point source to the top of the reactor tank. Thus:

$$\omega = \frac{1}{2}\left\{1 - \frac{z}{\left[z^2 + r^2\right]^{\frac{1}{2}}}\right\}, \tag{13-14}$$

where:

r = radius of reactor tank = 99.1 cm; and
z = distance from equivalent point source to top of tank = 521.7 cm.

The energy of the scattered photons is given by:

$$E = \frac{E_0}{1 + \frac{E_0\left[1 - \cos\beta\right]}{0.51}}, \tag{13-15}$$

where E_o is the incident photon energy (1 MeV) and β is the scattering angle = π- (θ_0+ θ_1). In this case, $\theta_o = 0^o$. For this case, $\beta = 131^o$ and E = 0.234 MeV.

The differential scattering cross section is given by:

$$\frac{\delta\sigma}{\delta\Omega} = \frac{r_e^2}{2\left\{\frac{E}{E_0} - \frac{\left[E\sin\beta\right]^2}{E_0^2}\left[\frac{E}{E_0}\right]^3\right\}}\left(cm^2\right), \tag{13-16}$$

where r_e is the classical electron radius = 2.818E-13 cm.

$$\frac{\delta\sigma}{\delta\Omega} = 8.56E\text{-}27cm^2. \tag{13-17}$$

For this case,

As before, the ICRP 51, Table 2 dose factors were used. Again, the anterior to posterior geometry was used as it gave the largest dose factor for 0.234-MeV scattered photons. This dose factor was 1.15E-12 Sv cm^{-2} γ^{-1}.

The results of the calculations for the scattered radiation into the reactor room are given in Table 13-17.

Table 13-16 Scattered Radiation Dose Rates in the OSTR Reactor Room After a Loss of Pool Water Accident Following 1-MW Operation

Time after shutdown	Effective Dose Equivalent Rate (mrem h^{-1})
10 seconds	327
1 hour	49.7
1 day	38.9
1 week	20.8
1 month	11.4

13.2.3.2.2.5 Dose Rate from Scattered Radiation at Facility Fence

The purpose of this section is to calculate the dose rate to a person at the north facility fence not in the direct beam from the exposed core, but subject to scattered radiation from the reactor room ceiling. The dose point was chosen to be 3 feet above the ground at the north facility fence. This is the closest point a member of the public would be able to occupy. The slant distance to this point from the center of the reactor room ceiling above the reactor tank (the scattering point) is about 125.9 feet, or 3.836E3 cm.

The calculational methodology is exactly the same as that used in Section 13.2.3.2.2.2. Values used were the same except as indicated below:

μ_1 = 0.292 cm^{-1};
2_1 = 72.3°;
E = 0.281 MeV;
β = 107.7°;
x = 3.836E3 cm;
$\delta\sigma/\delta\Omega$= 9.19E-27; and
K = 1.45E-12 Sv cm^2 sec^{-1}.

If credit is taken for attenuation in the scattered beam as it passes through the reactor room north wall, then the scattered flux is multiplied by an additional factor of exp [$-\mu_w$ b], where μ = attenuation coefficient for concrete for 0.28-MeV photons (0.254 cm^{-1}) and b is the slant distance through the wall (16.6 cm).

The results of this calculation are given in Table 13-18.

Table 13-17 Scattered Radiation Dose Rates at the OSTR Facility Fence After a Loss of Pool Water Accident Following 1-MW Operation

Time After Shutdown	Effective Dose Equivalent Rate (mrem h^{-1}) No attenuation in reactor wall	Effective Dose Equivalent Rate (mrem h^{-1}) Including attenuation in reactor wall
10 seconds	50.6	1.49E-2
1 hour	7.7	2.27E-3
1 day	6.0	1.78E-3
1 week	3.2	9.5E-4
1 month	1.8	5.22E-4

13.2.3.2.2.6 Fuel Temperatures

The temperature of the fuel and cladding was analyzed by TRIGA® International (Ref. 13.28). The strength of the fuel element clad is a function of its temperature. The stress imposed on the clad is a function of the fuel temperature as well as the hydrogen-to-zirconium ratio, the fuel burnup, and the free gas volume within the element. The analysis of the stress imposed on the clad and strength of the clad uses the following assumptions:

1) The fuel and clad are the same temperature.
2) The hydrogen-to-zirconium ratio is 1.7 for standard fuel (8.5 wt%) and 1.6 for 30/20 fuel.
3) A space one-eighth inch high within the clad represents the free volume within the element.
4) The reactor contains fuel that has undergone burnup equivalent to 54 MW-days for LEU 30/20 fuel.
5) Maximum operating temperature of the fuel is 600°C.

The fuel element internal pressure P is given by:

$$P = P_{h+} P_{fp+} P_{air} \qquad (13\text{-}18)$$

where:

P_h is the hydrogen pressure;
P_{fp} is the pressure exerted by volatile fission products; and
P_{air} is the pressure exerted by trapped air.

For the hydrogen-to-zirconium ratios greater than about 1.58, the equilibrium hydrogen pressure can be approximated by:

$$P_h = \exp\left(1.76 + 10\ .3014\ x\ \frac{19740.37}{T_k}\right) \quad (13\text{-}19)$$

where:

x is the ratio of hydrogen atoms to zirconium atoms, and
T_k is the fuel temperature (K).

The pressure exerted by the fission product gasses is given by:

$$P_{fp} = f\ \frac{n}{E}\frac{RT_k}{V}E \quad (13\text{-}20)$$

where:

f is the fission product release fraction;
$\frac{n}{E}$ is the number of moles of gas evolved per unit of energy produced(mol/MW-day);
R is the gas constant (8.206E-2 L-atm/mol-K);
V is the free volume occupied by the gasses (L); and
E is the total energy produced in the element (MW-days)

The fission product release fraction is given by:

$$f = 1.5\text{E-}5 + 3.6\text{E}3\exp\left(\frac{-1.34\text{E}4}{T_\circ}\right) \quad (13\text{-}21)$$

where:

$T_\circ$ is the maximum fuel temperature in the element during normal operation (K).

The fission product gas production rate $\frac{n}{E}$, varies slightly with power density. The value 1.19E-3 mol/MW-day is accurate to within a few percent over the range from a few kilowatts per element to well over 40kW per element. The free volume occupied by the gases is assumed to be a space of one-eighth inch (0.3175cm) high at the top of the fuel so that

$$V = 0.3175\ \ \pi \cdot r_i^2 \quad (13\text{-}22)$$

where:

r_i is the inside radius of the clad (1.745cm).

The LEU 30/20 fuel has been tested to 50% burnup. As the fission product gas pressure is propotional to the energy released, assume that fuel in the reactor has undergone maximum burn-up.

Finally, the air trapped within the fuel element clad will exert pressure

$$P_{air} = \frac{RT_k}{24} \tag{13-23}$$

where it is assumed that the initial specific volume of the air is 22.4 L/mol. Actually, the air forms oxides and nitrides with the zirconium, so that after relatively short operation the air is no longer present in the free volume inside the fuel element clad. The results of the stress imposed on the clad for Zr-H fuel can be found in Figure 4.5. These results confirm the conclusion of NUREG-1282 that the LEU 30/20 fuel has a safety limit of 950°C when the clad temperature equals the fuel temperature.

The maximum fuel cladding temperature after a loss of pool water depends on the fuel rod power and the time delay between reactor shutdown and uncovering of the core. For the case of no delay, a value of 21 KW/element is reported to prevent fuel temperatures from exceeding 900°C [Ref. 13.29]. The analysis developed a two dimensional transient-heat transport computer code model TAC2D for calculating the maximum fuel temperatures after the loss of pool water for various delay times. During the loss of pool water, the low water level alarm occurs when the water is 18ft above the top of the core. The time between the actuation of the pool level alarm and the uncovering of the fuel for a catastrophic failure of an eight-inch beam tube is assumed to be 15 minutes (900 sec.) Figure 13-1 presents a curve of maximum fuel cladding temperature versus fuel rod power density using a 15 minute delay. The results show that a TRIGA fuel element can remain below 950°C at a power density 23.5kW/element. This power density is above the maximum power density of 18.52 kW/element for the OSU LEU MOL ICIT core operating at 1.1 MW. Additional delay time is likely since the most likely initiator of a beam tube rupture is the dropping of a large heavy object from above the reactor pool. Such activity is not anticipated for several hours after reactor shutdown.

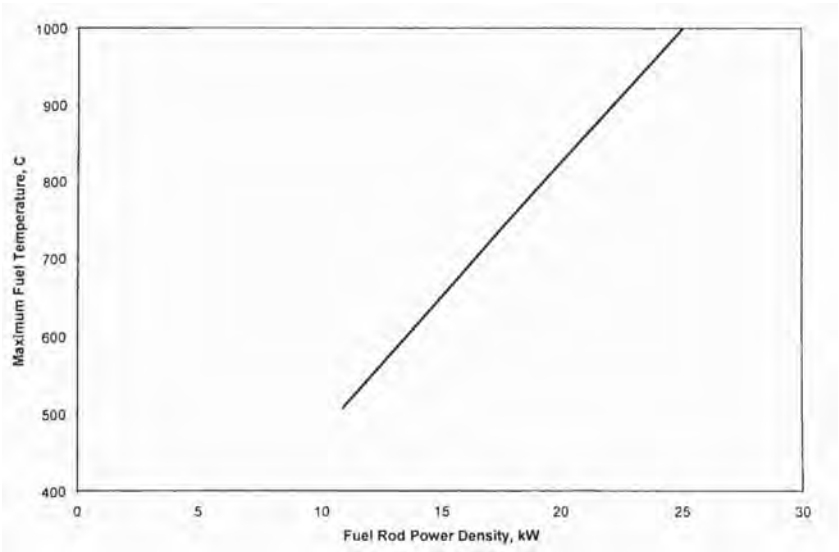

Figure 13-1 Maximum Fuel Rod Temperature for Loss of Coolant 15 Minutes After Shutdown

If the reactor operates for seventy MW-hours or less per week, power generation per element values approximately 20% higher are sufficient to meet the safety limits. Thus, 26.7 kW/elements for standard and 28.2 kW/element for FLIP and LEU 30/20 fuel are adequate power densities. A comparison of decay heat generation versus time following loss of coolant for infinite reactor operations and 70MW-hours per week cycle operations are in Figure 13-2 [34].

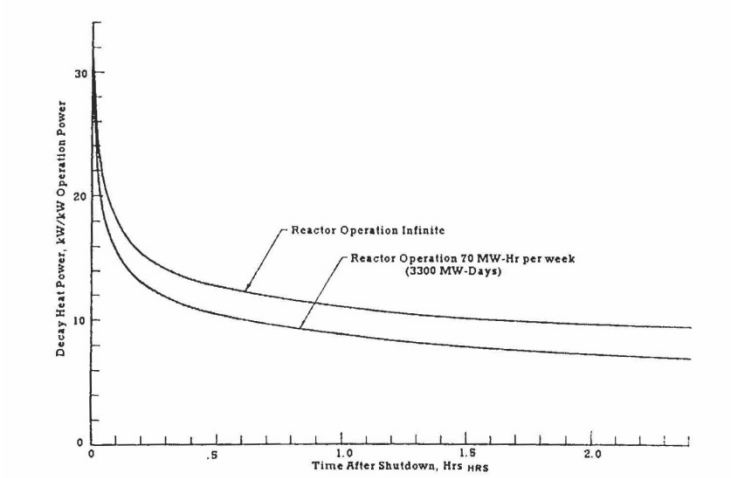

Figure 13-2 Decay Heat Power Generation Following Loss of Coolant for Infinite Reactor Operations and Periodic Reactor Operations

13.2.4 Loss of Coolant Flow

13.2.4.1 Accident Initiating Events and Scenarios

Loss of coolant flow could occur due to failure of a key component in the reactor primary or secondary cooling system (e.g., a pump), loss of electrical power, or blockage of a coolant flow channel. Operator error could also cause loss of coolant flow.

The OSTR tank holds 4,600 gallons of water, or about 1.74E4 kg of water. At a steady-state power level of 1 MW, the bulk water temperature would increase adiabatically at a rate of about 0.82 ^{o}C min^{-1}. Under these conditions, the operator has ample time to reduce the power and place the heat-removal system back into operation before any abnormal temperature is reached in the reactor bulk water. The OSTR has annunciators indicating that the primary water pump is off, the secondary water pump is off, and cooling tower fans are off. These will alert the operator to an abnormal condition and should allow time for corrective action prior to reaching the bulk water temperature alarm setpoint of 42 ^{o}C.

13.2.4.2 Accident Analysis and Determination of Consequences

13.2.4.2.1 Loss of Coolant Flow Without Immediate Operator Action

If the OSTR were operated without coolant flow for an extended period of time, and there was no heat removal by the reactor coolant systems, voiding of the water in the core could occur and the water level in the reactor tank would decrease because of evaporation. The sequence of events postulated for this very unlikely scenario is as follows:

- the reactor would continue to operate at a power level of 1 MW (provided the rods were adjusted to maintain power) and would heat the tank water at a rate of about 0.82 ^{o}C min^{-1} until the tank water reached the bulk water high temperature alarm setpoint. This setpoint is at 42 ^{o}C. The normal bulk water temperature, when operating at 1 MW, ranges from 35 to 40 ^{o}C, depending on the outside air temperature. Thus, it would take from 2.4 minutes to 8.5 minutes to reach the alarm setpoint. Assuming the operator did not notice this alarm and did not take any corrective action, the bulk water would continue to rise above 42 ^{o}C. It would then take an additional 70.7 minutes for the water in the tank to reach the saturation temperature. At this time, voids in the core would cause power oscillations and the negative void coefficient would cause a reduction in power if control rods were not adjusted to maintain power; and

- if it is assumed that the operator or automatic control system maintained power at 1 MW, and still assuming that the system is adiabatic except for the evaporation process, about 1,596 kg h^{-1} would be vaporized. The reactor tank water level would decrease, and it would take about 9.4 hours for the water level to reach the top of the core, and an additional 1.5 hours to vaporize all of the water remaining

in the tank. The reactor, however, would shut down as the water level dropped past the top of the fuel.

It is considered inconceivable that such an operating condition would go undetected. Water level, water flow, and water temperature alarms would certainly alert the operator. Also, as the water level decreases, the reactor room radiation monitors would alarm. Because of all of these factors, water would be added to the tank and/or the reactor would be shut down to mitigate the problem.

13.2.5 Mishandling or Malfunction of Fuel

13.2.5.1 Accident Initiating Events and Scenarios

Events which could cause accidents at the OSTR in this category include (1) fuel handling accidents where an element is dropped underwater and damaged severely enough to breach the cladding, (2) simple failure of the fuel cladding due to a manufacturing defect or corrosion, and (3) overheating of the fuel with subsequent cladding failure during steady- state or pulsing operations.

13.2.5.2 Accident Analysis and Determination of Consequences

All three scenarios mentioned in Section 13.2.5.1 result in a single fuel element failure in water. In the unlikely event that this failure occurred in air, this is the MHA analyzed in Section 13.2.1.2.

At various points in the lifetime of the OSTR, fuel elements are moved to new positions or removed from the core. Fuel elements are moved only during periods when the reactor is shutdown.

Assumptions for this accident are almost exactly the same as those used for the MHA, except for one thing: the presence of the pool water contains most of the halogens and, thereby, reduces the halogen dose contribution.

The assumptions for this accident and the method of analysis of this accident were described in Section 13.2.1.2. The same three scenarios (A, B, and C) used in the MHA are used to analyze this accident, although Scenario C is the most credible for this accident. The results for this accident for the three scenarios are given in Tables 13-19 to 13-24.

The results of this accident show that for all three scenarios the radiation doses to the general public are well below the annual limits in 10 CFR 20, with the maximum dose being 6 mrem TEDE at 10 meters (the site boundary) for any of the scenarios. The occupational radiation doses to workers in the reactor room are also well below the occupational annual limits in 10 CFR 20 for a 5-minute exposure. Five minutes is very ample time for workers to evacuate the room if such an accident were to occur.

Table 13-18 Occupational Radiation Doses in the Reactor Room Following a Single Element Failure in Water - Scenario A

Reactor Room Occupancy (minutes)	$CDE_{Thyroid}$ + $DDE_{Thyroid}$ (mrem)	TEDE (mrem)
2	2	<1
5	2	<1

Table 13-19 Radiation Doses to Members of the General Public Following a Single Element Failure in Water - Scenario A

Distance (m)	$CDE_{Thyroid}$ + $DDE_{Thyroid}$ (mrem)	TEDE (mrem)
10	28	6
50	13	3
100	4	1
150	2	<1
200	1	<1
250	1	<1
267	1	<1

Table 13-20 Occupational Radiation Doses in the Reactor Room Following a Single Element Failure in Water - Scenario B

Reactor Room Occupancy (minutes)	$CDE_{Thyroid}$ + $DDE_{Thyroid}$ (mrem)	TEDE (mrem)
2	13	3
5	30	6

Table 13-21 Radiation Doses to Members of the General Public Following a Single Element Failure in Water - Scenario B

Distance (m)	$CDE_{Thyroid}$ + $DDE_{Thyroid}$ (mrem)	TEDE (mrem)
10	26	4
50	12	2
100	4	1
150	2	<1
200	1	<1
250	1	<1
267	1	<1

Table 13-22 Occupational Radiation Doses in the Reactor Room Following a Single Element Failure in Water - Scenario C

Reactor Room Occupancy (minutes)	$CDE_{Thyroid}$ + $DDE_{Thyroid}$ (mrem)	TEDE (mrem)
2	14	3
5	35	7

Table 13-23 Radiation Doses to Members of the General Public Following a Single Element Failure in Water - Scenario C

Distance (m)	$CDE_{Thyroid}$ + $DDE_{Thyroid}$ (mrem)	TEDE (mrem)
10	16	1
50	7	<1
100	3	<1
150	1	<1
200	1	<1
250	0	<1
267	0	<1

Since most of the halogens released from the fuel element will be retained in the primary water, the majority of this activity will end up in the demineralizer tank. The exposure rate from the demineralizer tank can be estimated by:

$$\dot{X} = 6CEN(R\ h^{-1} \text{ at 1 foot}) \qquad (13\text{-}24)$$

where:

C = number of halogen curies retained in the demineralizer tank (Ci);
E = energy of gamma rays (MeV) = 1; and
N = number of gamma rays per disintegration = 1.

From Section 13.2.1.2, the total saturated activity of the halogens is 5,850 Ci. Of this, 1.22E-4 is released to the gap, 0.5 of the gap activity is released to the water, and 0.95 of this remains in the water. Thus, the number of curies retained in the demineralizer tank is 0.339 Ci. The assumption that the average energy of the gamma rays from the halogens is 1 MeV is rather conservative.

Thus,

$$\dot{X} = 2.0\ R\ h^{-1} @\ 1 \text{ foot} \qquad (13\text{-}25)$$

Surrounding the sides of the OSTR demineralizer tank is 6 inches of high-density concrete (no shielding on top). With μ_c for this concrete equal to about 0.20 cm^{-1} for 1-MeV gammas, the overall attenuation factor for the concrete shield is about 4.75E-2. This reduces the exposure rate to about 96 mR h^{-1} at one foot.

13.2.6 Experiment Malfunction

13.2.6.1 Accident Initiating Events and Scenarios

Improperly controlled experiments involving the OSTR could potentially result in damage to the reactor, unnecessary radiation exposure to facility staff and members of the general public, and unnecessary releases of radioactivity into the unrestricted area. Mechanisms for these occurrences include the production of excess amounts of radionuclides with unexpected radiation levels, and the creation of unplanned pressures in irradiated materials. These materials could subsequently vent into the irradiation facilities or into the reactor room causing damage from the pressure release or an uncontrolled release of radioactivity. Other mechanisms for damage, such as large reactivity changes, are also possible.

13.2.6.2 Accident Analysis and Determination of Consequences

There are two main sets of procedural and regulatory requirements that relate to experiment review and approval. These are the Oregon State TRIGA® Operating Procedures (OSTROP) and the OSTR Technical Specifications. These requirements are focused on ensuring that experiments will not fail, and they also incorporate requirements to assure that there is no reactor damage and no radioactivity releases or radiation doses which exceed the limits of 10 CFR 20, should failure occur. For example, the OSTROP contain detailed procedures for the safety review and approval of all reactor experiments.

Safety related reviews of proposed experiments require the performance of specific safety analyses of proposed activities to assess such things as generation of radionuclides and fission products (e.g., radioiodines), and to ensure evaluation of reactivity worth, chemical and physical characteristics of materials under irradiation, corrosive and explosive characteristics of materials, and the need for encapsulation. This process is an important step in ensuring the safety of reactor experiments and has been successfully used for many years at research reactors to help assure the safety of experiments placed in these reactors. Therefore, this process is expected to be an effective measure in assuring experiment safety at the OSTR.

In the OSTR Technical Specifications, a limit of $0.50 has been placed on the reactivity worth of unsecured experiments. This is well below the maximum reactivity limit of $2.30 established in Section 4.7 and would result in fuel temperatures well below the safety limit.

Projected damage to the reactor from experiments involving explosives varies significantly depending on the quantity of explosives being irradiated and where the explosives are placed relative to critical reactor components and safety systems. If in the reactor tank, the OSTR Technical Specification limit the amount of explosive materials, such as gunpowder, TNT, nitroglycerin, or PETN, to quantities less than 25 milligrams. Also, the Technical Specifications state that the pressure produced upon detonation of the explosive must have been calculated and/or experimentally demonstrated to be less than the design pressure of the container. The following discussion shows that the irradiation of explosives up to 25 milligrams could be safely performed if the containment is properly chosen.

A 25-milligram quantity of explosives, upon detonation, releases approximately 25 calories (104.6 joules) of energy, with the creation of 25 cm^3 of gas. For the explosive TNT, the density is 1.654 g cm^{-3}, so that 25 mg represents a volume of 0.015 cm^3. If the assumption is made that the energy release occurs as an instantaneous change in pressure, the total force on the encapsulation material is the sum of the two pressures. For a 1-cm^3 volume, the energy release of 104.2 joules represents a pressure of 1,032 atmospheres. The instantaneous change in pressure due to gas production in the same volume adds another 25 atmospheres. The total pressure within a 1-cm^3 capsule is then 1,057 atmospheres for the complete reaction of 25 mg of explosives.

Typical construction materials of capsules are stainless steel, aluminum, and polyethylene. Table 13-25 lists the mechanical properties of these encapsulation materials.

Table 13-24 Material Strengths

Material	Yield Strength (E3 psi)	Ultimate Strength (E3 psi)	Density (g cm^{-3})
Stainless Steel (type 304)	35	85	7.98
Aluminum (alloy 6061)	40	45	2.739
Polyethylene	1.7	1.4	0.923

Analysis of the encapsulation materials determines the material stress limits that must exist to confine the reactive equivalent of 25 mg of explosives. The stress limit in a cylindrical container with thin walls is one-half the pressure times the ratio of the capsule diameter-to-wall thickness. This is the hoop stress. The hoop stress is 2 times the longitudinal stress, and hence hoop stress is limiting. Thus:

$$\sigma_{\max} = \frac{pd}{2t}, \tag{13-26}$$

where:

σ_{max} = maximum hoop stress in container wall;
p = total pressure within the container;
d = diameter of the container; and
t = wall thickness of the container.

When evaluating an encapsulation material's ability to confine the reactive equivalent of 25 mg of explosives, the maximum stress in the container wall is required to be less than or equal to the yield strength of the material:

$$\frac{pd}{2t} \le \sigma_{yeild}, \tag{13-27}$$

where σ_{yield} is the yield strength. Solving this equation for d/t provides an easy method of evaluating an encapsulation material:

$$\frac{d}{t} \le \frac{2\sigma_{yeild}}{p}. \tag{13-28}$$

Assuming an internal pressure of 1,057 atmospheres (15,538 psi), maximum values of d/t for the encapsulation materials are displayed in Table 13-26. The results indicate that a polyethylene vial is not a practical container since its wall thickness must be at least 4.5 times the diameter. However, both the aluminum and the stainless steel make satisfactory containers.

Table 13-25 Container Diameter-to-Thickness Ratio

Material	d/t
Stainless Steel (type 304)	4.5
Aluminum (alloy 6061)	5.1
Polyethylene (low density)	0.22

As a result of the preceding analysis, a limit of 25 mg of TNT-equivalent explosives is deemed to be a safe limitation on explosives which may be irradiated in facilities located inside the reactor tank, provided that the proper container material with appropriate diameter and wall thickness is used.

13.2.7 Loss of Normal Electrical Power

13.2.7.1 Accident Initiating Events and Scenarios

Loss of electrical power to the OSTR could occur due to many events and scenarios that routinely affect commercial power.

13.2.7.2 Accident Analysis and Determination of Consequences

Since the OSTR does not require emergency backup systems to safely maintain core cooling, there are no credible reactor accidents associated with the loss of electrical power. A backup power system is present at the OSTR that mainly provides conditioned power to the reactor console and the control instrumentation. This backup system consists of a 3-KVA battery-powered inverter system and a 25-kW disel-fueled electrical generator. The system will provide emergency power immediately after the loss of regular electrical power. It will continue to supply power for a period of a few days. This system is maintained and checked on a daily basis to ensure that it is capable of operating properly. Battery-powered emergency lights are also located throughout the facility to allow for inspection of the reactor and for an orderly evacuation of the facility.

13.2.8 External Events

13.2.8.1 Accident Initiating Events and Scenarios

Hurricanes, tornadoes, and floods are virtually nonexistent in the area around the OSTR. Therefore, these events are not considered to be viable causes of accidents for the reactor facility. In addition, seismic activity in the Corvallis area is relatively low compared to other areas in the Pacific Northwest.

13.2.8.2 Accident Analysis and Determination of Consequences

There are no accidents in this category that would have more on-site or off-site consequences than the MHA analyzed in Section 13.2.1, and, therefore, no additional specific accidents are analyzed in this section.

13.2.9 Mishandling or Malfunction of Equipment

13.2.9.1 Accident Initiating Events and Scenarios

No credible accident initiating events were identified for this accident class. Situations involving an operator error at the reactor controls, a malfunction or loss of safety-related instruments or controls, and an electrical fault in the control rod system were anticipated at the reactor design stage. As a result, many safety features, such as control system interlocks and automatic reactor shutdown circuits, were designed into the overall TRIGA® Control System (Chapter 7). RIGA® fuel also incorporates a number of safety features (Chapter 4) which, together with the features designed into the control system, assure safe reactor response, including in some cases reactor shutdown.

Malfunction of confinement or containment systems would have the greatest impact during the MHA, if used to lessen the impact of such an accident. However, as shown in Section 13.2.1, no credit is taken for confinement or containment systems in the analysis of the MHA for the OSTR. Furthermore, no safety considerations at the OSTR depend on confinement or containment systems.

Rapid leaks of liquids have previously been addressed in Section 13.2.3. Although no damage to the reactor occurs as a result of these leaks, the details of the previous analyses provide a more comprehensive explanation.

13.2.9.2 Accident Analysis and Determination of Consequences

Since there were no credible initiating events identified, no accident analysis was performed for this section and no consequences were identified.

13.3 References

13.1 Credible Accident Analyses for TRIGA and TRIGA-fueled Reactors, NUREG/CR-2387, PNL-4028, April 1982.

13.2 Guidelines for Preparing and Reviewing Applications for the Licensing of Non-Power Reactors, Format and Content, NUREG-1537, Part 1, February 1996.

13.3 Safety Analysis Report for the Oregon State University TRIGA Research Reactor, Oregon State University, Corvallis, OR, August 1968.

13.4 Amendment No. 4 to the Safety Analysis Report for the Oregon State University TRIGA Reactor, Oregon State University, Corvallis, OR, Sept. 11, 1975.

13.5 "The Calculations of Distance Factors for Power and Test Reactor Sites," J.J.DiMunno et al, TID-14844, U.S. Atomic Energy Commission, March 1962.

13.6 Regulatory Guide 3.33, "Assumptions Used for Evaluating the Potential Radiological Consequences of Accidental Nuclear Criticality in a Fuel Reprocessing Plant," U.S. Nuclear Regulatory Commission, April 1977.

13.7 Regulatory Guide 3.34, "Assumptions Used for Evaluating the Potential Radiological Consequences of Accidental Nuclear Criticality in a Uranium Fuel Fabrication Plant," U.S. Nuclear Regulatory Commission, July 1979.

13.8 Regulatory Guide 1.5, "Assumptions Used for Evaluating the Potential Radiological Consequences of a Loss of Coolant Accident for Pressurized Water Reactors," U.S. Nuclear Regulatory Commission, June 1974 (Also see Regulatory Guide 1.3 on BWRs).

13.9 "A Guide to Radiological Accident Considerations for Siting and Design of DOE Nonreactor Nuclear Facilities," J.C. Elder et at, LA-10294-MS, Los Alamos National Laboratory, January 1986.

13.10 Nuclear Power Reactor Safety, E.E. Lewis, John Wiley and Sons, 1977, p. 521.

13.11 Nuclear Engineering, Theory and Technology of Commercial Nuclear Power, R.A. Knief, Hemisphere Publishing, 1992, pp. 353, 431.

13.12 "Fuel Elements for Pulsed TRIGA Research Reactors," M.T. Simnad et al, Nuc. Tech. Vol. 28, January 1976

13.13 "The U-ZrH_x Alloy: Its Properties and Use in TRIGA Fuel," M.T. Simnad, General Atomic Report E-117-833, February 1980.

13.14 Regulatory Guide 1.145, "Atmospheric Dispersion Models for Potential Accident Consequence Assessments at Nuclear Power Plants," U.S. Nuclear Regulatory Commission, August 1979.

13.15 "Calculated Atmospheric Radioactivity from the OSU TRIGA Research Reactor Using the Gaussian Plume Diffusion Model," Bright M.K. Wong, Oregon State University Department of Nuclear Engineering Report 7903, August 1979.

13.16 "Internal Dose Conversion Factors for Calculation of Dose to the Public," DOE/EH-0071, U.S. Department of Energy, Washington, D.C., 1988

13.17 "External Dose Rate Conversion Factors for Calculation of Dose to the Public," DOE/EH-0070, U.S. Department of Energy, Washington, D.C., 1988

13.18 "Kinetic Behavior of TRIGA Reactors," G.B. West et al, GA-7882, General Atomics, March 31, 1967.

13.19 Dynamics of Nuclear Reactors, David Hetrick, U. of Chicago Press, 1971.

13.20 "Low Enriched TRIGA Fuel-Water Quench Safety Test," GA-A15413, General Atomics, June 1979.
13.21 Stationary Neutron Radiography System, Final Safety Analysis Report, McClellan Air Force Base, Sacramento, CA, August 1990.
13.22 Safety Analysis Report for the Torrey Pines TRIGA Mark III Reactor, GA-9064, General Atomics, January 5, 1970.
13.23 Safety Analysis Report for the TRIGA Reactor Facility, University of Texas at Austin, May 1991.
13.24 Introduction to Nuclear Engineering, 2nd Edition, John R. Lamarsh, Addison Wesley, 1983, p. 72.
13.25 "Data for Use in Protection Against External Radiation," International Commission on Radiation Protection, ICRP Report No. 51, Pergamon Press, March 1987.
13.26 Safety Analysis Report, Revision 2, McClellan Nuclear Radiation Center, McClellan Air Force Base, Sacramento, CA, April 1998.
13.27 Introduction to Nuclear Engineering, 2nd Edition, Richard Stephenson, McGraw-Hill, 1958, pp. 209-213.
13.28 General Atomics Electronics Systems, Inc. "Safety Analysis for the HEU to LEU Conversion of the Washington State University Reactor," Report TRD 070.01002 RGE 001. August 2007.
13.29 Foushee, F.C. "TRIGA Four-rod Cluster Loss-of-Coolant Accident Analysis," Gulf General Atomics, E-117-196, October, 1972.

CHAPTER 14

TECHNICAL SPECIFICATIONS

(The Technical Specifications are contained in
USNRC Operating License R-106, Appendix A)

CHAPTER 15

FINANCIAL QUALIFICATIONS

Chapter 15 - Valid Pages
Rev. 1 5/1/2012

i	Rev. 1 5/1/2012
ii	Rev. 1 5/1/2012
1	Rev. 1 5/1/2012
2	Rev. 1 5/1/2012

TABLE OF CONTENTS

LIST OF TABLES

THIS PAGE INTENTIONALLY LEFT BLANK

15 Financial Qualifications

15.1 Financial Ability to Construct a Non-Power Reactor

This is not applicable for a renewal application.

15.2 Financial Ability to Operate a Non-Power Reactor

As shown in Table 15-1, the total expenses for the Radiation Center are given. Income is given in Table 15-2. Expenses are projected to increase by 5% for each year. The difference between appropriations and expenses accounted for is from returned overhead, grants, and services charges.

Table 15-1 Current and Projected Expenses for the Radiation Center

Table 15-1 Summary of Expenses						
		FY 08	FY 09	FY 10	FY 11	FY 12
Unclassified Salary	$	232,802	244,442	256,664	269,498	282,973
Classified Salary	$	147,050	154,403	162,123	170,229	178,741
Student Wages	$	6,330	6,646	6,979	7,327	7,694
Payroll Expenses	$	152,015	159,616	167,597	175,976	184,775
Services & Supplies	$	70,822	74,363	78,081	81,985	86,084
Travel	$	277	290	305	320	336
Equipment	$	11,487	12,061	12,664	13,297	13,962
Total	$	620,782	651,821	684,412	718,633	754,565

Table 15-2 Breakdown of Income for the Radiation Center

	FY 08	FY 09	FY 10	FY 11	FY 12
State E&G Funds	$ (763,161)	$ (801,319)	$ (841,385)	$ (883,454)	$ (927,627)
Returned Overhead	$ (30,000)	$ (31,500)	$ (33,075)	$ (34,729)	$ (36,465)
Salary Redistributions	$ (20,000)	$ (21,000)	$ (22,050)	$ (23,153)	$ (24,310)
Grants and Awards	$ (85,000)	$ (89,250)	$ (93,713)	$ (98,398)	$ (103,318)
	$ (898,161)	$ (943,069)	$ (990,223)	$(1,039,734)	$(1,091,720)

The salary numbers given include direct salaries and benefits. These numbers do not include the infrastructure provided by the university such as electrical power, heating, and most building maintenance.

The institutional funding is appropriated by the State of Oregon. None of the provisions of 10 CFR 50.33(d) are applicable. Oregon State University is an entity of the State of Oregon and does not fall into the categories listed in the regulation. OSU is a state institution because the Oregon State Board of Higher Education (OSBHE) conducts and controls the Department of Higher Education [ORS 351.010]. OSBHE has jurisdiction over Oregon University System,

which includes OSU [ORS 352.001(2)]. The OSBHE is an agency of the state [***State ex rel Eckles v. Wooley***, 302 Or 37, 45 (1986), citing ***State ex rel Kleinsorge v. Reid***, 221 Or 558, 570 (1960)]. Since OSBHE is a state agency and it has jurisdiction over OSU, OSU is a state agency.

While the OSTR does perform some commercial irradiation services, this represents only a very small percentage of either expense or income. Commercial activities at this time are limited to isotope production. Assuming that cost is proportional to operating time, then commercial work comprises less than 1% of the cost of owning and operating the facility. In accordance with 10 CFR 50.21, the OSTR should therefore be licensed as a Class 104 facility.

15.3 Financial Ability to Decommission the Facility

Oregon State University is a state institution. Therefore, in accordance with the provisions of 10 CFR 50.75(e)(2)(iv) the funds needed for decommissioning will be requested through appropriate state channels and will be obtained sufficiently in advance of decommissioning to prevent delay of required activities. Oregon State University will likely use the DECON decommissioning method.

The documentation to prove that OSU's financial obligations are backed by the full faith and credit of the state of Oregon. The Legislature has to raise sufficient revenue to pay for the expenses of the State each fiscal year and to pay any interest on debt incurred by the State [Oregon Constitution, Article IX, Section 2]. Every agency receives a state appropriation from the Legislature [Oregon Constitution, Article IX, Section 4]. That appropriation is allotted to each agency by the Department of Administrative Services [ORS 291.234]. Most of the legislative appropriations come from the General Fund [ORS 293.105]. If there is insufficient money available in the General Fund, the Treasurer borrows money to pay expenses. [Oregon Constitution, Article IX, Section 6; ORS 293.165]. The Treasurer can issue bonds to finance current expenses of the state, if the General Fund is insufficient. The bonds are backed by the tax revenues and full faith and credit of the State of Oregon [ORS 293.173(3)(b)].

By the letter dated July 11, 1990, the University estimated the cost of decommissioning at $3 million [Ref. 15.1]. This estimate has been updated annually using data and methodology supplied in NUREG-1307 [Ref. 15.2]. The estimated cost of decommissioning the OSTR in 2011 was $16.4 million.

15.4 References

15.1 Letter to USNRC Document Control Desk from L. Edwin Coate dated July 11, 1990.

15.2 U.S. Nuclear Regulatory Commission, “Report on Waste Burial Charges: Changes in Decommisioning Waste Disposal Costs at Low-Level Waste Burial Facilities,” NUREG-1307, Rev. 10.

CHAPTER 16

OTHER LICENSE CONSIDERATIONS

(There are no other license consideration)

CHAPTER 17

DECOMMISSIONING AND POSSESSION-ONLY LICENSE ADMENDMENTS

(Not Applicable)

CHAPTER 18

HIGHLY ENRICHED TO LOW-ENRICHED URANIUM CONVERSIONS

(Fuel conversion completed in 2008)